FRONTAL POLYMERIZATION: SYNTHESIS OF HOMO AND COPOLYMERS

NARAHARI SHRIKANT PUJARI

POLYMER SCIENCE AND ENGINEERING GROUP

CHEMICAL ENGINEERING & PROCESS DEVELOPMENT DIVISION

NATIONAL CHEMICAL LABORATORY

PUNE 411 008

INDIA

January 2007

FRONTAL POLYMERIZATION: SYNTHESIS OF HOMO AND COPOLYMERS

A THESIS SUBMITTED TO THE

UNIVERSITY OF PUNE

FOR THE DEGREE OF

DOCTOR OF PHILOSOPHY

(IN CHEMISTRY)

BY

NARAHARI SHRIKANT PUJARI

POLYMER SCIENCE AND ENGINEERING GROUP

CHEMICAL ENGINEERING & PROCESS DEVELOPMENT DIVISION

NATIONAL CHEMICAL LABORATORY

PUNE 411 008

INDIA

January 2007

CERTIFICATE

Certified that the work incorporated in this thesis entitled **"Frontal Polymerization: Synthesis of Homo and Copolymers"** submitted by **Narahari S. Pujari** was carried out under my supervision. Such material as obtained from other sources has been duly acknowledged in this thesis.

January 2007
Pune

Dr. S. Ponrathnam
(Research Guide)

DECLARATION

I hereby declare that the thesis entitled **"Frontal Polymerization: Synthesis of Homo and Copolymers"** submitted for Ph. D. degree to the University of Pune has been carried out under the supervision of **Dr. S. Ponrathnam** at the Polymer Science and Engineering, Chemical Engineering & Process Development Division, National Chemical Laboratory, Pune, India. The work is original and has not been submitted in part or full by me for any degree or diploma to this or any other University.

January 2007 (**Narahari S. Pujari)**

Pune

Dedicated to,

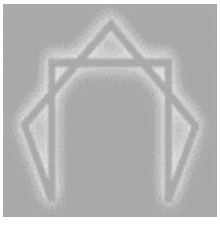

Even then they are smiley….

ACKNOWLEDGEMENT

Sometimes in the misty evening, when I look back, I found myself in a great surprise. "Who are you?" that was the first ever conversation and question asked by my guide, Dr. S. Ponrathnam to me. I am still finding the answer! He molded and trained me to become a researcher. His invaluable guidance and help rendered throughout the course of this investigation, without which I would not have completed this thesis successfully. I express my deep sense of gratitude to him.

I have been fortunate from my prelapsarian childhood as I met really nice people who helped and inspired me time to time. During this research task, apart from my guide, there are four mentors because of whom I feel I can stand and see the firmament.

Dr. C. R. Rajan, I learned all kinds of managemental skills from him. He was always very kind and never said no to me. Dr. S. R. Inamdar, I can't forget hot discussions and arguments which used to end with a cup of coffee and sandwiches. He trained me in chemical engineering. He was there with me throughout the course of this dissertation and am grateful to him for all his help and support. Dr. J. M. Gadgil, my post-graduate college teacher, from whom I learned philosophy of both science and life. I am especially thankful to him for discussions and pedantically proof reading the thesis. I am very much obliged to Dr. B. D. Kulkarni, Deputy Director, National Chemical Laboratory. From his extremely busy schedule, he gave me a time whenever I went to him. He patiently taught me chemical engineering and art of scientific writing.

I am sincerely thankful to Mr. R. K. Tayal and Mr. S. N. Nene for their immense help and encouragement at every stage of my work. I am also grateful to Dr. I. A. Karimi, National University of Singapore for valuable discussions.

The big asset of my stay at NCL is formation of very good friendships. Here I met Ganesh (very hard and neat worker), Rajkumar (very good cook), Pathak (sensitive person), Wasif (soft person), Harikrishna (encyclopedia), Timothy, Abhijit and Sunny (energetic youth), Kumar (calm guy), Dr. N. Chavan (good organic chemist), Dr. Smita Mule (happy go lucky attitude), Supriya (finicky worker), Sarika (we always fought with each other) and Trupti (we never fought), my colleagues and Pratheep, Vivek,

Bhalchandra, Anirudhdha, Amit, Rakesh, C. Gaurshete, Santosh, Aarati, Renuka, Smitha and Jyostna, friends from other research groups. I am very much personally obliged to all my colleagues and friends for their constant help, morale boosting and for keeping a cheerful spirit around.

Apart from laboratory, there is a list of my friends who are well wishers. To mention few are: Ranjit, John, Praveen, Sameer, Sachin Joshi, Rahul Mahashbde, Satish, Prasad, Vinod, Gajanan, Akshay, Ajay, Kuldeep, Bhagyashree, Anjali, Geetanjali, Sharavati, Shubhangi, Prachi etc. I am thankful to all of them.

I wish to thank Dr. K. Guruswamy and Dr. M. Badiger, coordinators of polymer Physics and Chemistry coursework for the help and teaching the subjects. Dr. Varsha Ghadage, Dr. Tanay Seth and Mr. Ambekar from Centre of Materials and Electronics Technology, Pune for SEM facilities and Dr. V. V. Ranade and Mr. Ajay Gorasia for help in high speed CCD camera experiments are duly acknowledged. I thank Dr. O. S. Yemul for sending useful references.

I thank Mr. S. Sathe and L. Giri for their technical help.

I am fortunate for having a great family support. I in particular would like to thank my uncle, Mr. Shripad Pujari, for being a constant source of inspiration. All my cousins, Avadhoot, Mahesh, Amit, Rahul, Kaustubh, Priya and Ashwini were there to give me encouragement and energy. Finally, mere words cannot express my gratitude to my parents and brother for their patience and tremendous support at all the times.

At the end, I would also like to thank Dr. S. Sivaram, Director, National Chemical Laboratory, Pune for permitting me to submit this work in the form of thesis. I take this opportunity to thank Council of Scientific and Industrial Research (CSIR) for the award of fellowship during the period of this work.

Narahari Shirkant Pujari

TABLE OF CONTENTS

CHAPTER VI

FUNCTIONALIZED CROSSLINKED NETWORKS

CHAPTER VII

PATTERN FORMATION

LIST OF FIGURES

Chapter I: INTRODUCTION

Chapter III: HOMOPOLYMERIZATION

Chapter IV: WATER-TRIGGERED FRONTAL POLYMERIZATION

Chapter V: COPOLYMERIZATION

Chapter VI: FUNCTIONALIZED CROSSLNIKED NETWORKS

Chapter VII: PATTERN FORMATION

LIST OF TABLES

Chapter I: INTRODUCTION

Chapter III: HOMOPOLYMERIZATION

Chapter IV: WATER TRIGGERED FRONTAL POLYMERIZATION

Chapter V: COPOLYMERIZATION

Chapter VI: FUNCTIONALIZED CROSSLINKED NETWORKS

LIST OF SCHEMES

Chapter IV: WATER TRIGGERED FRONTAL POLYMERIZATION

Chapter V: COPOLYMERIZATION

ABSTRACT

Frontal Polymerization: Synthesis of Homo and Copolymers

Self-propagating high temperature frontal polymerization (FP) involves the transformation of monomer to polymer in a localized reaction zone. The propagation rate is determined by an interplay of thermal conduction and temperature-dependent reaction rates. The localization of reaction and fast increase in temperature allow for rapid synthesis of a wealth of polymers with spatially controlled microstructures and morphologies. The simplest free radical frontal polymerization consists of a tube filled with monomer and initiator. Under appropriate conditions, when the reactions are initiated at one end of the tube, a thermal front develops and propagates with constant velocity. This apparent simplicity of frontal polymerization has led to this technique being steadily adopted for laboratory scale and possibly industrial polymer syntheses. Indeed, the required technology may be as simple as running a reaction in a test tube or a custom built reactor at ambient temperature and pressure. There is also added benefit of minimum energy consumption, since heat is only needed to start the self-sustained propagation reaction. These factors have, in turn provided the driving force for extensive research efforts directed toward more precisely defining the necessary and sufficient conditions for frontal polymerizations.

Another beauty of FP is the rich nonlinear dynamics involved in the process. The dynamics is present in terms of various instabilities and pattern formations. Instabilities can occur in reactions kinetics due to four reasons: the imbalance between the heat generated in the reaction zone and heat diffused to the cold reaction mixture, dense polymer overlying the monomer, convection, and heat expansion of the medium at reaction zone. A vast literature is devoted to finding causes of instabilities and ways to obviate them. These instabilities may lead to inhomogeneity in the product which may considerably affect its performance in applications.

The thesis consists of seven chapters.

Chapter I deals with current state of knowledge in frontal polymerization and its importance. A review of fundamental and technical information as well as the instabilities occurring during the polymerization was presented.

Chapter II is about aims and objectives of this research work.

Chapter III discusses frontal homopolymerization vinyl monomers. A detailed study of 2-hydroxyethyl methacrylate (HEMA) polymerization was conducted. The study investigated the effect of type and concentration of initiators, solvents and diluents on the existence of front, front velocity as well as front temperature. Products in the form of gels were evaluated for water, cyclohexane gain and porosity. Mechanism of gel formation was discussed. Additionally, the first time observations of various patterns were also presented. Divinly monomer, ethylene dimethacrylate was also frontally polymerised and detailed influencing parametric study was reported.

Chapter IV is divided into two parts. In first part, our totally new mode of frontal polymerization of acrylamide, triggered by mere addition of minute, specific volume of water was demonstrated. Experimental conditions under which this mode of polymerization yields linear and water soluble polyacrylamide were investigated, paving the way to synthesize commercially pertinent homo and copolymers. A detailed study of effects of reaction variables (e.g. type and concentration of redox couple and volume of water) on measurable parameters of FP such as induction period, front velocity, front temperature, shape of front and yield were investigated. The chapter also included the observations such as formation of breath figures and nonplanar frontal regime seen, when few redox couples were used. The causes and physiochemical phenomenon of new patterns i. e. layered and helical are reported. Additionally, micro-phase separation and heterogeneity in the polymer matrix was discussed.

In the second part of the chapter, an analysis of scale-up of a self-propagating water triggered frontal polymerization of acrylamide was investigated. A correlation equation to bring together system size parameters and input parameters was derived and endeavored to understand their effects on induction period and front velocity. Empirical models were derived for rate of polymerization and induction period and those were validated with experimental results.

Chapter V consists of the synthesis of linear copolymers by FP. The compositional drifts that are incompatible and cause phase separation is reported. A series of monomer pairs were evaluated. To name few pairs: acrylamide: potassium methacrylate, acrylamide: potassium acrylate, acrylamide: ammonium methacrylate and acrylamide: ammonium acrylate. Additionally, liquid-solid monomers (such as

acrylamide:styrene) and liquid-liquid monomers (styrene:methyl methacrylate) are also reported. There was a different in reactivity ratio values between Fineman-Ross and Kelen-Tudos method. This was perhaps due to the complex and unconventional mode of frontally prepared copolymers. We could successfully copolymerize few monomers (like potassium methacrylate), homopolymerization of which otherwise cannot be carried by FP.

Chapter VI deals with a complete analysis of frontal copolymerization of functionalized mono and divinyl monomers. A series of copolymers of 2-hydroxyethyl methacrylate (HEMA)/glycidyl methacrylate (GMA) and ethylene dimethacrylate (EGDM) synthesized by frontal polymerization is reported. The study was conducted to investigate effect of crosslink density, type and concentration of initiator, complex initiator system, porogen and diluent on the most relevant parameters of frontal polymerization described above. This chapter also gives the complete physio-chemical characterization (IR, hydroxyl/epoxy number, BET surface area, mercury porosimetry, SEM etc.) for all the copolymers synthesised in this study. The application of these polymers wee evaluated and compared with the conventional suspension polymerization methodology. The chapter presents the first time observations of the exotic patterns observed under microscope. Two basic types of spatial patterns viz. planar and non-planar patterns were observed.

Chapter VII consists of the theory of pattern formation. Patterns are formed on the polymer surface due to presence of various instabilities. Various patterns obtained in systems synthesized by frontal polymerization are mathematically analyzed. These describe the dynamics of spinning waves which propagate during frontal polymerization reaction taking place in a cylindrical reactor tube. It was proposed that the self-organisation of spatio temporal solution of wave equations due to an interplay between thermal diffusion and kinetics gives rise to pattern formation. The analysis of the spinning wave motion near a critical (Hopf) point was derived and a perturbation solution was used to obtain patterns. The analytical solutions are compared with experimental results for a case of preparation of poly(2-hydroxyethyl methacrylate) (PHEMA) and poly(HEMA-EGDM). The models validate the experimental results obtained by instrumental analysis like SEM. These results are reported in open literature for the first

time to our best knowledge. Theory of helical as well as layered pattern formation in case of water triggered frontal polymerization was also developed and discussed.

N. S. Pujari
(Student)

Dr. S. Ponrathnam
(Guide)

Chapter I

INTRODUCTION

1 Introduction

1.1 Frontal Polymerization: General

There are various methods by which polymers are produced from monomers. The most common method uses stirred tank reactors. In this case, due to mixing, both the chemical compounds and temperature are homogeneous in space, so that the polymerization reaction occurs simultaneously at each point in the reactor. Another method exists where in the polymerization reaction zone propagates in an unstirred medium through the monomer mixture converting it into a polymer. This method is termed “frontal polymerization”. It is a new and emerging technique.

Self-propagating high temperature frontal polymerization (FP) involves transformation of monomer to polymer in a localized reaction zone. The propagation rate is determined by interplay of thermal conduction and temperature-dependent reaction rates. The localization of reaction and fast increase in temperature allow for rapid synthesis of a wealth of polymers with spatially controlled microstructures and morphologies, in absence of instabilities. The apparent simplicity of this polymerization is conducive to laboratory scale and possibly industrial syntheses. Indeed, the methodology is as simple as running a reaction in a test tube or in a custom built reactor at ambient temperature and pressure. This has led to rather interesting possibilities such as synthesis of extremely high molecular weight homopolymers, copolymers of any defined composition, block copolymers, filled material etc. Over a period of time, FP has extended into three main branches viz. thermal FP, isothermal FP and UV (photo) initiated FP. Majority of work has been reported in thermal or free radical FP.

This thesis deals with the free radical FP. The mechanism of free radical FP is similar to that in conventional free radical polymerization systems. Initially monomer(s) is/are filled in a test tube along with thermally unstable initiator. On applying heat at the top layer, the initiator decomposes; radicals are formed and begin to combine with the monomers, forming new radicals. The new radicals then bond with other monomers, causing chains to grow. Eventually each chain combines with another radical, terminating the growth and producing a polymer molecule. This sequential set of reactions in an unstirred vessel triggers a wave front of constant velocity. The front is created by coupling the diffusion of the autocatalyst to the chemical reaction. Heat is the autocatalyst in such reactions which diffuses into unreacted regions, stimulating reactions that produce more heat. The reaction travels as a narrow reaction zone creating hot solid polymer as it progresses. Thus, there is a hot reaction zone (over 200^{o}C) with hot, solid polymer above and a cold monomer/initiator mixture below it. This research has many advantages over traditional polymerization such as: (1) reduced waste (2) reduced energy costs and (3) rapid generation of unique morphologies. Fig. 1.1 shows a range of products formed from FP.

In the ensuing sections, we will start with the history of FP and then review the work done in 1970s followed by 1990s. We will analyze in detail various systems studied and parameters affecting FP. We will also give a brief account on various instabilities incurred during FP and at last we will summarize various applications of FP. We will entirely review the work in Russia but restrict ourselves to free radical FP studies from 1990s onwards.

Figure 1.1. Products obtained by frontal polymerization; (Courtesy: http://www.ism.ac.ru/handbook/34front3.htm)

1.2 History

Besides being of technological importance, thermal reaction fronts in condensed media are also very important from the scientific standpoint. In 1967, at the Institute of Chemical Physics in Russia, the process of self propagating high temperature synthesis (SHS) was discovered.[1] A compressed pellet of reactants was ignited at one end, resulting in a self propagating combustion wave (Fig. 1.2). This method has since been used to prepare technologically useful compounds such as ceramics, carbides, borides and nitrides[2-7] and intermetallics such as aluminides, nickelides and germanides.[4,8-11] The advantage of the method is that the initial stimulus is the only energy input required and that superior materials are obtained. A typical temperature profile of the SHS system is shown in Fig. 1.3. The pellet is heated from initial temperature to the ignition temperature at which reaction is initiated. After the combustion front passes, the temperature decreases as the product formed returns to T_o (initial temperature).

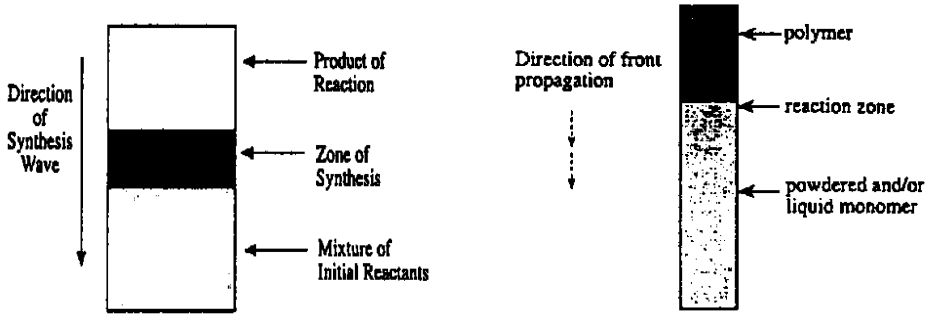

SHS Frontal Polymerization

Figure 1.2. Schematic presentation of synthesis of materials by self-propagating high temperature synthesis (SHS) and frontal polymerization

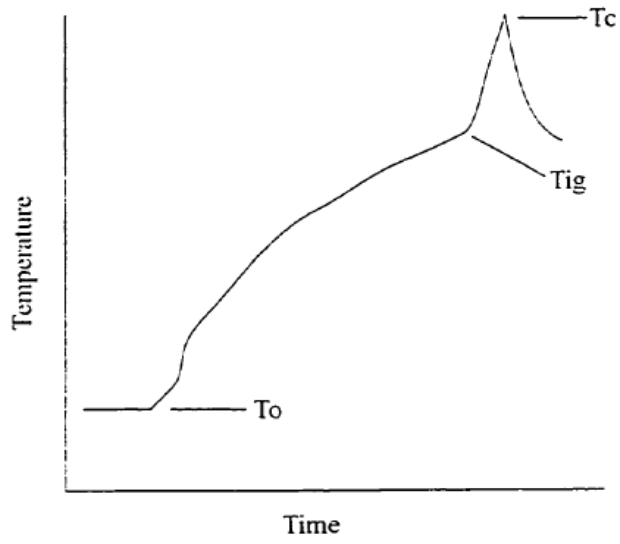

Figure 1.3. Temperature *Vs* Time plot of typical SHS reaction[5]

In 1972, Chechilo et al. applied the same approach to the free radical polymerization of vinyl monomers.[12,13] Using a steel reactor, they studied descending fronts in polymerization of methyl methacrylate (MMA), with benzoyl peroxide as initiator. In 1991, Pojman rediscovered this phenomenon and studied polymerization of methacrylic acid at ambient pressure in standard test tubes, as shown in Fig. 1.2.[14] Frontal

polymerization resembles self propagating high temperature synthesis (SHS) in that both involve a variety of intricate physiochemical processes such as melting, diffusion of the heat and the confinement of reaction in localized region. The reaction mechanism is not well understood. Reaction is triggered at one end of the reactor by ignition and polymerization/SHS self-propagates as a front.[14] In SHS, propagation velocities range from 0.1 to 1500 cm/min and the front temperature is as high as 2000^{o}C.[15] In propagating frontal polymerization, the velocities are of the order of 1 cm/min and front temperatures are about 200^{o}C. We will discuss this in detail in ensuing sections. We will deal with the two eras of FP, in 1970s and 1990s.

1.3 Literature Survey

1.3.1 Work in former Soviet Union

In 1970s, the work was mainly carried out in Russia, which is well reviewed by Davtyan et al.[16] Chechilo and Enikolopyan applied the idea of SHS to the free radical polymerization of vinyl monomers.[12,13] They used steel reactor under high pressure (>3000 atm) and studied the descending fronts of methyl methacrylate with peroxide initiators. Subsequent experimental studies were carried for free radical polymerization of triethylene glycol-γ,ω-dimethacrylate.[16-18] High pressure was necessary to suppress the convective instabilities. It was thought that polymerization wave propagated through the diffusion of radicals through the medium. However, estimations of front velocity through radical diffusion resulted in much smaller velocity than that was experimentally observed. It was concluded that the wavefront propagated by heat diffusion. The heat released by polymerization in the local reaction zone diffuses through the cold mixture to decompose additional initiator and begin further polymerization. The result is a

successive heating of neighbouring regions and a reaction zone that propagates through the cold mixture of monomer and initiator, as seen in Fig. 1.2. Special measurements[16] showed that there is no temperature gradient in the central part of the transverse cross-section of the reaction mixture. This means that under the conditions of the experiment, adiabatic propagation takes place, the front of the polymerization wave is planar and the measured rate of displacement is normal to this plane. The measured values of rate of propagation of the thermal wave lie in 1-3 cm min^{-1}, depending on various parameters of the polymerization mass. The structure of the polymerization wave, the influence of the concentration and the nature of the initiator on the process of polymerization propagation, the role of pressure and the initial temperature were studied extensively.[12,13,16,19-20] It has been shown, in particular, that the stationary rate of propagation of the front of the polymerization wave (v) increases with increase in the initial concentration of initiator (I) according to $v \sim I^{0.38}$.

Almost at the same time in 1970s, the anionic activation of lactams by FP opened up the technological gateway for preparing the construction materials by "chemical forming", directly from monomers. For the first time, Begishev et al. studied anionic non-isothermal FP with ε-caprolactam.[21,22] They mixed monomer with 2,4-toluylene-bis-carbamoyl caprolactam and sodium caprolactam (activator and catalyst) and carried the reaction at 80°C, 11°C above the melting point. They observed that the front did not propagate with a constant velocity because of the significant heterogeneous reaction that occurred at initial temperature. A number of investigators reported a detailed study of the process. This established that under adiabatic conditions, for an initial polymerization temperature of 150°C and above, the polymerization and crystallization take place

separately, whereas below 150°C a combined process is observed. To exclude the influence of crystallization on the kinetics of polymerization, the process was studied either in the initial stage or above 150°C. A number of almost simultaneously published papers[22-24] pointed out this new direction in the study of the kinetics of FP of lactams, mainly ε-caprolactum. These papers describe methods for the separate study of the kinetics of polymerization and crystallization taking place in parallel. The most reliable method proved to be that by Frunze et al.[25] They carried out reactions at two different temperatures and proposed the empirical equation that satisfied the actual temperature of reaction (T):

$$T - T_0 = M_o \frac{\Delta H_P}{c\rho} \alpha$$
$$\frac{T - T_0}{\alpha} = M_o \frac{\Delta H_P}{c\rho} + \frac{\Delta H_{cr}}{c\rho} \eta \qquad 1.1$$

The kinetic curves obtained for polymerization of ε-caprolactam are shown in Fig. 1.4. It can be inferred from the figure that the resulting polyamide displays three regions with increase in temperature: a slow increase, a range corresponding to a high rate of change in temperature and a stage corresponding to the slow completion of crystallization process.

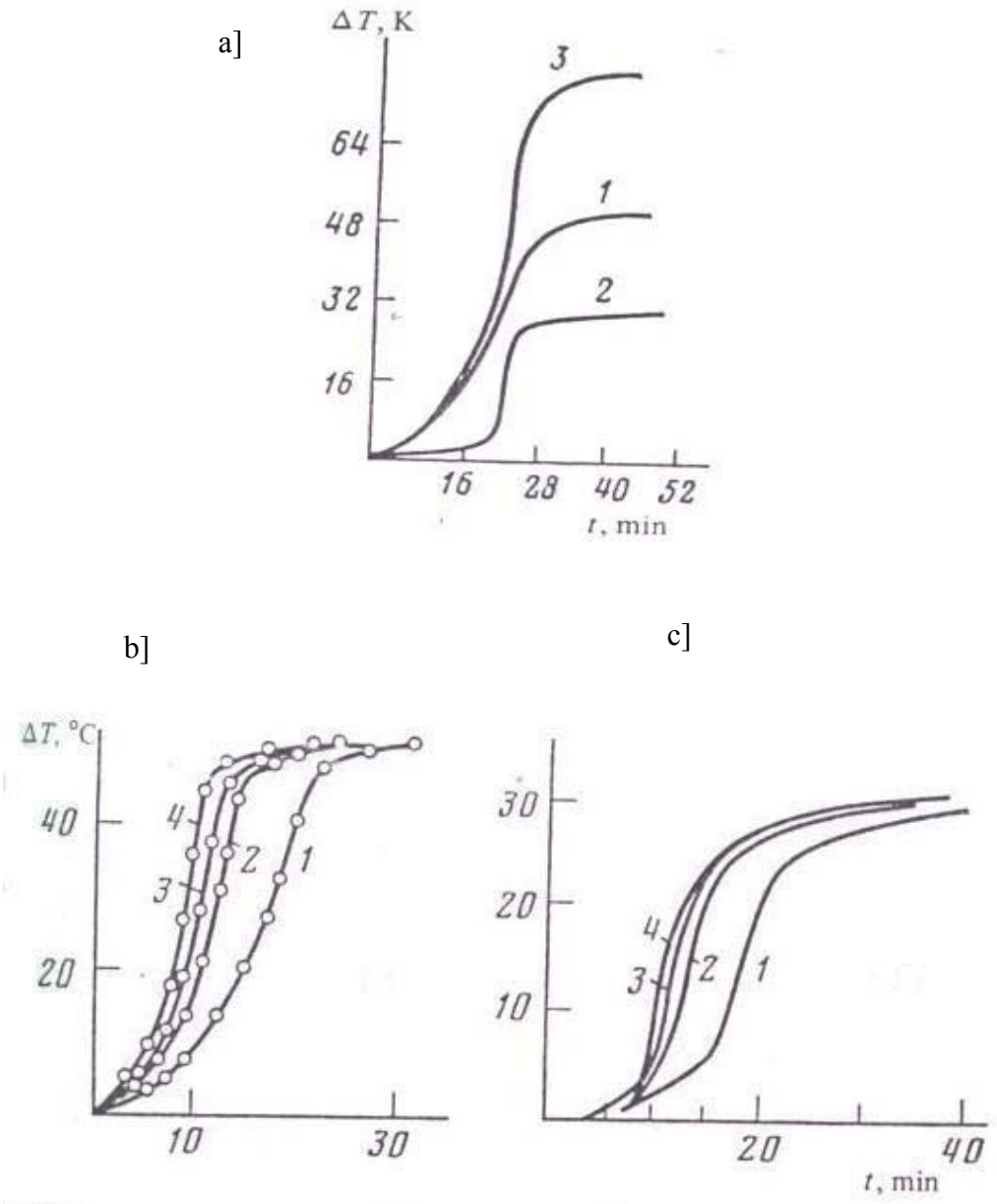

Figure 1.4. Kinetics curves of anionic polymerization of ε-caprolactam. a]: Kinetics of the change in temperature, 1: polymerization, 2: Crystallization, 3: overall curve.; b]: crystallization of polyamide,; c] at different activator concentrations[16]

The existence of three regions are confirmed by the form of the dependence of η on α, due to the sequence of stages involving nucleation, crystal growth, and secondary crystallization, as confirmed by microscopic studies on the morphology of the resulting polymers.[16,21] The methods developed for separating kinetics of polymerization and

crystallization make it possible to carry the quantitative analysis of the kinetics of polymerization and crystallization and to obtain a quantitative description of the complex process. Subsequently studies were conducted on copolymerization of caprolactum with ω-dodecanelactam and the composition in final product was estimated by NMR and elemental analysis.[16]

Another class of monomers extensively studied by Russian researchers was hardening of epoxide oligomers. Arutyunyan et al.[26,27] were the first to study this process in detail. The kinetics of epoxy curing with different molecular masses of epoxy oligomers under the influence of m-phenylenediamine (mPDA) and under adiabatic conditions was studied by conventional methods. The authors used this approach to FP and demonstrated the hardening of epoxy curing under the conditions of reaction front propagation. Fig. 1.5 shows the characteristic profiles of the change in temperature with time in the reaction of epoxide oligomers ED-20 with mPDA and ED-20 with polyethylenepolyamine. It was shown that the front velocity depends on initial concentrations of amines (A_o) and epoxide groups (E_o). The relations obtained was $v \sim A_o^{0.63}$ and $E_o^{0.73}$. It was also found that increase in the initial temperature of the reaction mixture leads to an increase in both the maximum rate and the stationary rate.

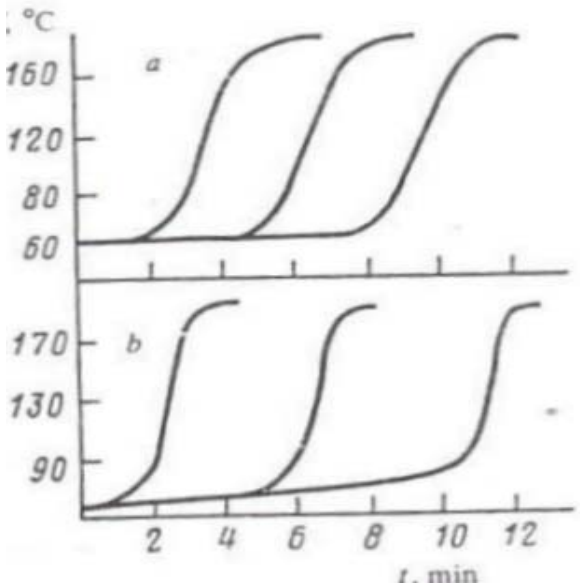

Figure 1.5. Temperature-time profiles for the hardening of epoxide resins in the presence of amines under thermal wave conditions; temperature, a: 60°C, b: 30°C.[16]

Many efforts have also gone into the understanding of the theoretical aspects of FP. This includes the reasons for various assumptions, molecular weight distribution and percent conversion studies, various instabilities and dynamics and theoretical understanding of the instabilities etc. Aleksanyan et al.[28] studied the rules governing the radical vinyl polymerization. They analyzed the extension of front propagation and established the relation between the rate of stationary front propagation, maximum degree of conversion, non-stationary period and monomer and initiator concentration, initial and ignition temperatures and with/without gel formation. They concluded that at high temperature initiator may be "burnt out" and its concentration may come down to zero, and under this condition the polymerization ceases. They derived the formula for maximum degree of conversion:

$$P_{max} = \frac{T_{max} - T}{T_O - T} \qquad 1.2$$

They observed that an increase in monomer initiator concentration increases the mass of polymer formed while the degree of conversion decreases. The effect of parameter, P_a, which characterizes gel formation, on P_{max} u is shown in Fig. 1.6. From the figure it is clear that when P = 0.1-0.2, the degree of conversion reaches to 100 % and any further increase of P reduces the maximum yield of polymer formed.

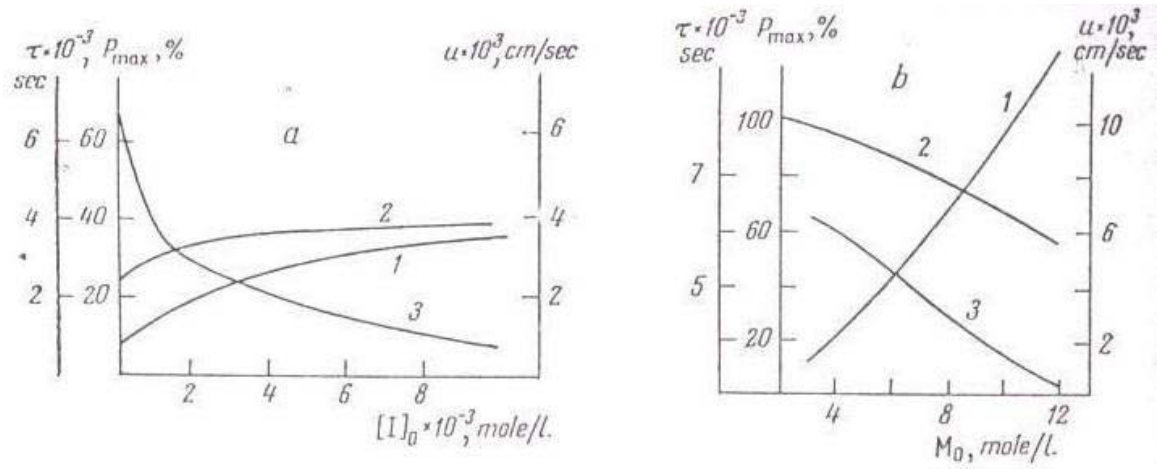

Figure 1.6. Reactions between (1) u (front velocity cm/sec), (2) P_{max}, (3) and the initial concentration of the initiator, I_o (a) and the monomer M_o, (b) $[I_o]$ = 0.15 mole/l with the gel effect; T_o=320 K, T_1 = 380 K[28]

The next important in series was the report by Enikolopyan et al.[29] They considered the problem of the molecular weight distribution analytically when the consumption of initiator was included. They predicted degree of polymerization would be less than 150, with the maximum mass fraction around 30. So, as per the expectation, the distributions were broader than observed in an isothermal polymerization. They did not present any supporting experimental data.

The polymerization process taking place under the non-isothermal conditions shows that the interpretation is complicated by the need to take into account the thermophysical characteristics of the system, the temperature dependence of the parameters, and a number of other factors. Russian workers made important assumptions to understand this complicated process. One of them is the quasi steady state assumption (QSSA) with respect to the macroradicals. This idea was known but they successfully applied it to high temperature free radical frontal polymerization. By making this assumption they could write kinetics of FP and predict the properties like maximum conversion and effect of initiator and monomer concentration on yield. Another unique approximation was the narrow reaction zone.[16] This approximation came from SHS terminology. It is based on the fact that because of the high activation energy of the chemical reaction, most of the transformation takes place in a narrow range at temperatures close to the adiabatic heating of the reaction mixture. This makes it possible to replace the temperature by its maximum value in the equation for the temperature gradient in the reaction zone. The narrow reaction zone made it possible to obtain analytical expressions for the stationary velocity of the polymerization front with consumption of initiator and also for conditions under which its concentration is constant. It also turns out that the non-dimensional parameter, Zeldovich number, which is product of the activation energy of the reaction and difference in temperatures of the cold, unreacted monomer and the temperature in the reaction zone, is responsible for the existence and stability of polymerization wave structure. This is why combustion and polymerization waves have similar structures.

$$Z = \frac{T_m - T_0}{T_m} \frac{E_{eff}}{RT_m} \qquad 1.3$$

where, E_{eff} is the effective activation energy, R is universal gas constant and T_0 is the initial temperature. The width of the reaction zone is inversely proportional to the Zeldovich number. In the limit Z>>1, the reaction zone shrinks to a surface called a front that may move.

The next important assumption was the phenomenon of thermal diffusion rather than chemical diffusion. In polymerization of methyl methacrylate, estimation[12] of velocity front showed that FP phenomenon cannot be attributed to diffusion of active centres from the reaction zone into neighbouring layers with subsequent initiation of the reaction in these layers, since in this case the values of the velocity of the front should have been much lower than the experimental values. This gives grounds for assuming that the propagation of the polymerization front in cold monomer mixture is thermal in character that is similar to normal propagation of flame.

These assumptions were actually utilized in understanding the fundamentals of the process. Khanukaev et al.[30] developed a relation using QSSA and narrow reaction zone as:

$$\frac{k_t}{k_p} >> 1 \; ; \left[\frac{I_o k_t}{k_i} \right]^{1/2} >> 1 \qquad 1.4$$

where, the reaction rate constants are taken at the temperature of adiabatic heating.

In case of caprolactam polymerization, as seen above, authors found another unique observation i.e. presence of hot spot. This is one of the features of FP, also akin to

SHS processes. In the simplest steady state, all of the wave points will move with a constant and ideal velocity. The thermal feedback between the chemical kinetics and the heat diffusion results in the sustainability of a traveling wave. The uniformly propagating wave will become unstable under certain parametric regimes. The dynamics has been studied numerically and analytically in SHS.[15] It is established that heat conduction and diffusion processes determine the structure of the wave front. Here, enthalpy excess concept is also important. When thermal diffusibility exceeds the diffusion coefficient, there is a maximum in the total enthalpy in the preheating zone, and the front may become unstable. The front absorbs the excess energy into itself and thereby enters a generally unstable state. Although the two processes (frontal polymerization and SHS) are similar, because both are thermal waves, they differ in some aspects. It was observed that as crystallization front descends, a "hot spot" propagates helically down the tube, leaving behind the spiral pattern in the product. Volpert et al.[22] developed a model of this two wave systems and analyzed this instability and so the presence of hot spot. They concluded that there is a region of bistability in which uniformly propagating traveling waves and spinning waves coexist. They also conjectured roll of convection of monomer but did not take it into account. This type of crystallization and bistability is absent in SHS.

The first attempts to develop frontal polymerization reactors were carried out by Russian researchers[31] with an aim to design a continuous plug-flow reactor of frontal polymerization. Two types of reactors were tested. The reactors were made of steel and experiments were conducted under pressure. However, researchers could not clearly

resolve the mode of front propagation and the influencing factors; moreover, product was not of very high quality.

1.3.2 Work after 1990

In 1990s, John Pojman and his coworkers from University of Southern Mississippi, USA revisited FP phenomenon and introduced it to the rest of the world. Their remarkable work led into the growth and maturity of the technique. We will review the relevant literature of free radical FP from 1990 onwards with the focus on established theories of FP, experimental findings and observations and detailed account on instabilities observed in FP. At the end we will briefly dwell on applications of the technique in various areas.

1.3.2.1 Review of the mechanism of free radical frontal polymerization

Once frontal polymerization is started by reaction of the initiating species with the monomer functional groups, a chain reaction proceeds very much as in conventional thermal polymerization, except for the control in synthesis temperature and the localized reaction zone. The synthesis of high polymers by free radical methods proceeds by a path involving the repetitive addition of a monomer to growing radicals, generated from a reactive initiator. Propagation ensues as growing transient radicals are continuously regenerated, through a repetitive cycle of bimolecular reactions. The reactive intermediates of the same type, generated in successive steps, differ in molar mass. The π- to σ- bond conversions result in a characteristic heat release. The mechanism of free-radical polymerizations thus consist of three primary steps: (1) initiation, (2) propagation, and (3) termination.[33] Initiation step is characterized by the formation of radical species, $R^{\cdot}$, which is formed upon the decomposition of an initiator species I by heat.

$$\text{Initiation:} \qquad I \rightarrow 2fR^{\bullet} \qquad 1.5$$

In propagation steps, the polymer radical $P_n^{\bullet}$ grows by the consecutive addition of monomer to the active centre.

$$\text{Propagation:} \qquad \left.\begin{array}{l} R^{\bullet} + M \rightarrow P_n^{\bullet} \\ P_n^{\bullet} + M \rightarrow P_{n+1}^{\bullet} \end{array}\right| \qquad 1.6$$

Termination of polymer chain occurs by two mechanisms: combination or coupling, and disproportionation. Combination involves the reaction of two radicals, which destroys the active centres and ends the growth of those chains.

$$\text{Termination:} \qquad P_n^{\bullet} + P_m^{\bullet} \rightarrow P_n + P_m \, or \, (P_{n+m}) \qquad 1.7$$

Disproportionation occurs by the transfer of a *beta* hydrogen to another radical centre causing stabilization of one reactive centre by addition of hydrogen and stabilization of the other by double bond formation, which destroys the active site.

The major heat release in polymerization occurs in the propagation step. However, the propagation reaction does not have a sufficiently high activation energy to provide a frontal regime, i.e. a significant reaction rate difference exists between the reaction and cold zones. Thus, heat cannot be a sufficiently strong and direct activator as it is in SHS reactions. Frontal polymerization autocatalysis takes place through the initiator decomposition step. The initiator radical concentration is the main control for the total polymerization rate. However, the gel effect or direct thermal polymerization that may also be present in the frontal polymerization process. Front velocity therefore, can be affected by the initiator type and concentration but is on the order of a cm/min. The

influence of temperature on the kinetic quantities considered is determined by the activation energies of the appropriate component reactions. The steady-state assumption in the polymerization model gives an approximate relationship between the effective activation energy of the entire polymerization process and activation energy of the initiator decomposition reaction:[33]

$$E_{eff} = 1/2E_i + E_p - 1/2E_t \qquad 1.8$$

where E_p is the activation energy of the propagation step, E_i is that for the initiator decomposition and E_t is that for the termination step. The second term in the right-hand side of eqn. 1.8 depends on the initiator. Because of low E_p and E_t values for most monomers (20-40 KJ/mole) and (8-20 KJ/mole), respectively, homogeneous polymerization are likely to occur. High E_i values are needed in frontal polymerization to prevent homogeneous reaction and allow initiator decomposition at high temperature. Because of this, the initiator plays a significant role in determining if a front will exist and, if so, the temperature profile in the front and how fast the front will propagate.

Thermodynamics can give an indication of whether or not a reaction will occur spontaneously. Although some reactions are endergonic, in which ΔG or change in free energy is positive, we are more concerned with exogornic reaction in which ΔG is negative, and the reaction is spontaneous. The change in free energy can be given as:

$$\Delta G = \Delta H - T\Delta S \qquad 1.9$$

where, ΔG, ΔH and ΔS are changes in free energies, enthalpy and entropy as one mole of monomer is converted into one mole of repeat units, and T is temperature.[33] The change in enthalpy of free-radical polymerization is always negative because the conversion of π-

to σ- bond is always exothermic. The change in entropy, ΔS, is a measure of disorder in a system and thus is usually negative in polymerization reactions because of the decrease in randomness from the conversion of monomer to polymer. Therefore, the change in free energy is negative, and the reaction is spontaneous, when the polymerization is sufficiently exothermic to compensate for the decrease in entropy, which is the case in free radical polymerization.

1.3.2.2 General behaviour

Frontal polymerization works with a wide variety of systems. Highly reactive monomers are preferable in FP as reactive monomers are able to balance the amount of heat needed to sustain polymerization with the heat lost to the environment. Free radical polymerization is ideal because for most peroxide and nitrile initiators the rate of polymerization at ambient temperature is low but is high at elevated temperatures. Remarkable advances have been made in the field of frontal polymerization to synthesize well-defined polymers with predetermined microstructure and morphology. Three classes of monomers are ideal in FP, which differ basically by their physical properties: propagating fronts that result in (1) thermoplastics, (2) phase-separated polymer (the growing polymer is insoluble in its monomer solution), and (3) thermosets.[14]

In the first class, highly reactive liquid monomers, which produce thermoplastics and are molten at front temperature, are included. The advantage of this type is one can polymerize the neat monomers, which otherwise is not possible by any other method. However, the disadvantage is decaying of fronts owing to Taylor instability. A number of reactive neat monomers are reported to polymerize by FP, such as n-butyl acrylate,[34] styrene, methyl methacrylate etc.[14] Although these polymers are soluble in their

monomers, on the timescale of the front the polymer is effectively immiscible with the monomer. Taylor and double diffusive instabilities developed during the system manifest themselves as "fingering" (hot polymer "fingers" into the unreacted cold monomer solution). Addition of inert filler such as CAB-O-SIL, increases the viscosity and stabilizes the front without rate of polymerization getting affected but the homogeneity is greatly compromised. Another problem with monomers like styrene is they boil at front temperature. Russian authors carried the reactions under pressure (20-30 atm) to eliminate monomer boiling. However, researchers have frontally synthesized homogeneous poly(butyl acrylate) under microgravity conditions.[35] Later, the findings that other monomers, such as acrylamide, would polymerize frontally to an uniform product added extra impetus. Furthermore, researchers reported that the synthesis of polyacrylamide can be carried out in organic solvents,[36] without solvents,[37,38] or in water.[36]

The second group of monomers form polymers those are insoluble in the monomer e.g. acrylic and methacrylic acids. The homogeneous systems become heterogeneous due to the insolubility of the growing polymer in the reaction media. The insoluble polymer particles coagulate and adhere to the reactor. This provides a discernible polymer-monomer interface whereby the heat of reaction can easily diffuse into the unreacted zone to proliferate further polymer growth. In these systems, instabilities can occur as well (e.g. convective and Taylor instabilities). In an attempt to suppress convective instabilities, the technique of rotating the reaction around the axis of propagation was devised. The instabilities yielded to the centrifugal force such that stable fronts were established.[39] Microgravity experiments have also generated convection-free

fronts in reactions that under terrestrial conditions are affected by hydrodynamic instabilities.[35]

An immense amount of literature is devoted to the third class, that is crosslinking monomers, (thermosets) such as triethyleneglyco1 dimethacrylate (TGDMA), di(ethylene glycol)dimethacrylate (DGDMA), and divinylbenzene. The free-radical polymerization of these monomers produces rigid crosslinked polymers, which sustain a sharp frontal interface. Some of these monomers are very viscous (e.g. TGDMA) and allow ascending and horizontally propagating fronts because the natural convection is reduced.

Although great strides have been made recently toward a reliable, full experimental analysis of frontal polymerization,[14,37,40,41] the determination of necessary and sufficient conditions to obtain a front has remained a source of frequent experimental and numerical difficulties. A unique combination of initiator, monomer, solvent, and initial temperature must be employed for the FP of each particular monomer. Therefore, understanding the role of each component of FP is crucial to obtaining well-defined polymers and for expanding the scope of FP to other monomers. Several salient aspects of frontal polymerization should be emphasized:[14,41]

1) The monomer must have a boiling point below the front temperature to prevent heat loss from vapourization and bubbles that can obstruct the front.
2) The front temperature should be large. Thus, highly exothermic reactions are the most likely candidates for frontal polymerization because the heat production must exceed the heat losses. The consequent release of thermal energy from the exothermic reaction must be sufficient to sustain a propagating front.

3) Geometry of the system also plays a role. If the surface area to volume ratio is too large even a reactive system will be quenched. For example, at room temperature the only monomer found to propagate in a 3 mm glass tube is acrylamide. No liquid monomer is sufficiently reactive and exothermic.
4) The reaction rate at initial temperature must be ravishingly small but rapid at the front temperature. The front temperature is determined by the enthalpy of the reaction, heat capacity of the product and the amount of heat loss.
5) The polymerization rate should proceed at imperceptible rates at room temperature and increase drastically at the front temperature. In this way, no bulk polymerization exists and polymerization starts only when once perturbed by sufficient thermal energy.

1.3.2.3 Experimental work

Table 1.1 demonstrates the initial study of various monomers homopolymerized by free radical FP. In this section we will review various experimental results and see the effect on front propagation, front velocity, front temperature etc. under the conditions of varying various parameters.

Table 1.1. List of monomers those were homopolymerized in early stage of development of FP technique

Sr. No.	*Monomer*	*Authors*	*Reference*
1.	Methyl methacrylate (MMA)	Chechilo et al.	12,13
2.	Styrene (Sty)	Aleksanyan et al.	28
3.	*n*-Butyl acrylate (BA)	Pojman et al.	14

4.	Methacrylic acid (MA)	Pojman et al.	34
5.	Acrylic acid	Pojman et al.	14
6.	Benzyl acrylate, Hexyl acrylate	Pojman et al.	14,41
7.	Butyl methacrylate	Pojman et al.	14
8.	Tri(ethylene glycol dimethacrylate (TGDMA), di(ethylene glyco1) dimethacrylate (DGDMA), and divinylbenzene (DVB)	Pojman et al.	14,40,42
9.	Acrylamide	Pojman et al.	36,38

Front Propagation

In most of the FP systems, front propagation varies linearly with time. Typical nature of the front propagation is shown in Fig. 1.7.

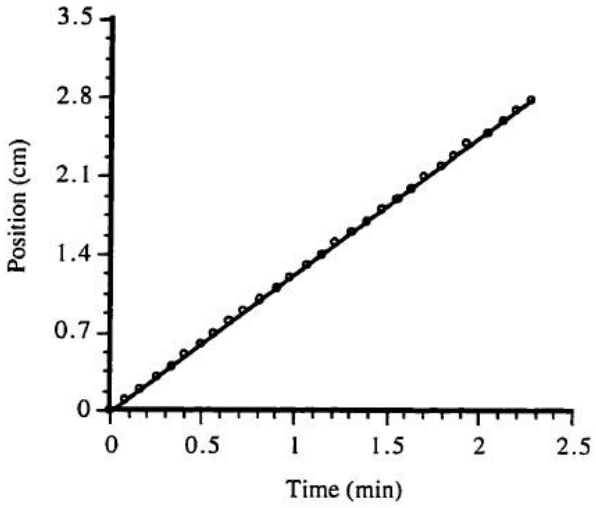

Figure 1.7. Typical linear front propagation behaviour in FP of n-butyl acrylate

Front propagation with third type of monomers produces a sharp frontal interface. These monomers are highly reactive and produce crosslinked polymers. The temperature

is higher at the centre due to the diabatic nature of the reactor tube, front propagation e.g. in TGDMA fronts are, therefore, convex as the higher temperatures at the centre cause faster reaction and a faster front velocity. In propagation of monomers like methacrylic acid, the polymerization front is even and flat. Pojman et al.[42] have found that it is not buoyancy-driven convection that keeps the front flat, but rather the presence of large amounts of bubbles. If the initiator concentration is low with methacrylic acid, the front is actually concave. With low initiator concentration (or in a pressure reactor), a few small bubbles are observed to migrate slowly toward the centre of the front and then disappear into the polymer. In some instances polymerization front gets forced upward due to convection and pressure generated by monomer(s). This happens when thermal expansion exceeds the isothermal contraction, which creates a gap between the polymer and monomer liquid layer resulting in a complete cessation of polymerization process. Many liquid monovinyl monomers from class 1 or 2, at room temperature and ambient temperatures, often lead to the problem of Taylor and convective instabilities as well as bubble formation and therefore their front propagation is uneven and sometimes collapses. As seen above, in styrene or methacrylates, dense polymer drops fingers into the cold monomer solution. This happens because the density of the polymer is higher than the respective monomer (excepting a few cyclic monomers). In some cases it causes the front degeneration and initiates reaction in the bulk. At the front temperature, convective instability appears as a result of the action of gravity. We will discuss the instabilities in ensuing sections.

Change in volume is also an important factor during FP. For mono-acrylates, the volume change during reaction is *ca.* 20%. The higher temperature at the centre causes

faster reaction and therefore a greater rate of conversion. Because the isothermal contraction for the isothermal polymerization of methacrylic acid is much greater than the thermal expansion, the higher converted central region contracts. However, TGDMA is a dimethacrylate and has a small reaction volume, so the front cannot contract upward.

In the experiments performed by Chechilo et al.,[12,13] high pressure (upto 5000 atm) was applied in order to avoid the collapse of front. However, they could not observe the front propagation as they used a metal reactor. Subsequent study by Pojman et al.[14] with n-butyl acrylate and azobisisobutyronitrile (AIBN), at relatively low pressure (34 atm) in a glass reactor, enabled them to observe the front propagation. They found that the bubbles still play a vital role and affect the front propagation nature and front velocity. Bubbles in the system can originate from the thermal decomposition of initiators, such as benzoyl peroxide, AIBN. These initiators produce gases like carbon dioxide and nitrogen respectively. Additionally, trace amount of water present in the monomers, vapours of monomer at front temperature further aid in generating the bubbles. The same workers increased the viscosity of the reaction mixture by adding inert diluents like ultra fine silica gel (CAB-O-SIL) in order to suppress the natural convection. Similarly, Some monomers like styrene and methyl methacrylate required moderate pressure (20-30 atm) to eliminate monomer boiling. Higher-boiling temperature monomers like n-butyl methacrylate and n-butyl acrylate support the frontal regime at ambient pressure in test tubes. Authors observed smooth front propagation.

Nagy and Pojman developed technique to suppress fingering in methacrylic acid fronts.[43] They rotated the tube around the axis of front propagation and found the relation

of rotational frequency with front velocity, and amplitude of front curvature. The relation is as follows:

Front velocity α (rotational frequency)^4 and

Amplitude of front curvature α (rotational frequency)^2

In solvent, frontal propagation was found to be supportive if solvent is a high boiling point liquid. In acrylamide polymerization, in water, dimethyl sulphoxide (DMSO), dimethylformamide (DMF) with several initiators such as sodium peroxydisulfate, potassium peroxydisulfate, ammonium peroxydisulfate, benzoyl peroxide (BPO) etc. front propagation was smooth without instabilities.[36,38] Several other monomers like acrylic acid, sodium methacrylate, zinc dimethacrylate are also capable of undergoing frontal polymerization in such high boiling solvents.[14,41]

Front Velocity, effect of pressure

As seen in section 1.3.1, Russian authors established that the front velocity is highly dependent on initiator concentration. Fig. 1.8 depicts the typical velocity *Vs.* initiator concentration plot which shows exponential behaviour.[44] Pojman et al. worked on n-butyl methacrylate polymerization at five different temperatures and revealed that there was not only a large variation in power function of initiator concentration dependence on rate of front propagation but also the dependency was less than 0.5 unlike steady state kinetic dependence. However, these experiments were carried under pressure.

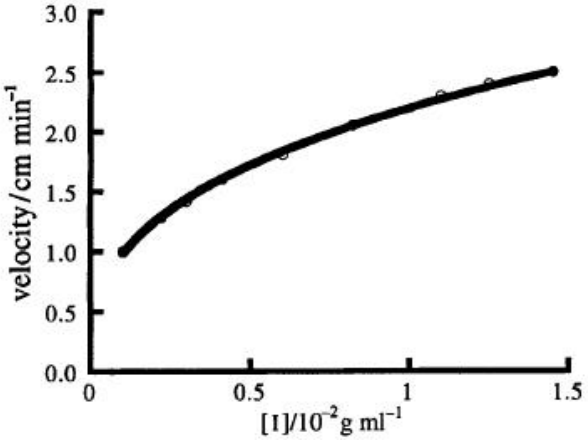

Figure 1.8. Front velocity as a function of benzoyl peroxide concentration for methyl methacrylate polymerization in high pressure steel reactor[44]

Reactions at atmospheric pressures, such as methacrylic acid polymerization, revealed different results.[34] The power function of initiator concentration dependence on front velocity varied from 0.24 to 0.29 depending upon the type of initiator used. It is also proposed that the reactivity of the monomers has a role in determining front velocity.

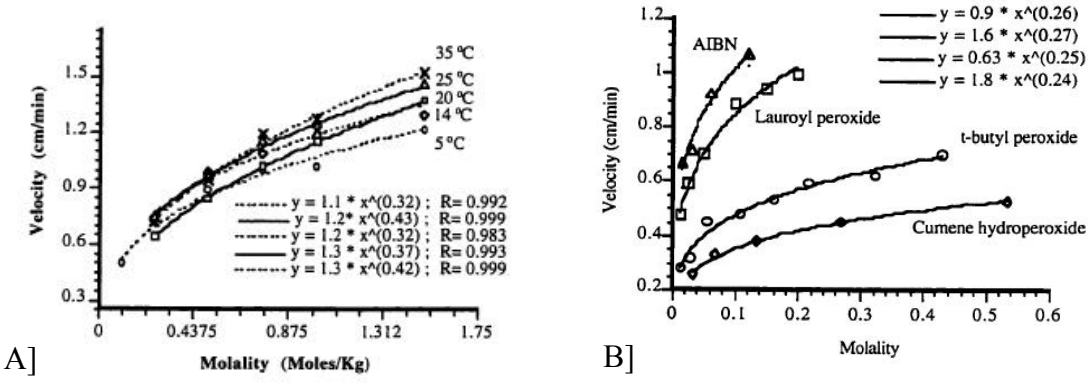

Figure 1.9. Front velocity dependence on initial temperature and type of initiators in n-butyl acrylate polymerization[44]

Pojman et al.[14,45] further demonstrated in case of tri(ethylene glycol) dimethacrylate system that initiator type and concentration has a significant effect on front velocity. They observed that the front velocity increases with increasing

concentration and it is higher for low activation energies. There was a 0.20, 0.23 and 0.31 power-functional dependence for AIBN, benzoyl peroxide and lauroyl peroxide, respectively. The activation energy seems to be a function of initiator concentration; higher the initiator concentration higher was the activation energy. Novozhilov et al.[46] have derived the following equation for the square of the wave velocity for self-propagating reaction fronts in condensed media with the assumption of one step condensation process i.e. the reaction achieves 100 % conversion:

$$u^2 = \frac{R\,T_{max}^2\,k_o\,\kappa}{E_a\,(T_{max} - T_o) - R\,T_{max}}\,\exp\left(-\frac{E_a}{RT_{max}}\right) \qquad 1.10$$

where, u is front velocity, R is gas constant, T_{max} is the maximum temperature of the reaction zone, k_o is the frequency factor, κ is the coefficient of thermal diffusion, T_o is the initial temperature of the reaction mixture, E_a is the effective activation energy. We will deal with the more theoretical models on front velocities in the ensuing sections. This model was first attempt to find the front velocity dependence in activation energy of an initiator. It does not work perfectly in FP but qualitatively gave an approximate estimate of maximum temperature if velocity is known. The estimated front temperature was higher in case of n-butyl acrylate due to two possible reasons: diadiabatic nature of reactor, so the heat losses are more to surroundings and the specific heat value for poly(n-butyl acrylate) is not true for the entire temperature range.

The determination of the true front velocity dependence on initiator concentration requires elimination of the effect of bubbles. These determinations are necessarily limited in their application to developing a numerical model of frontal polymerization. If

TGDMA is partially reacted to produce a gel before front I initiation, no bubbles appear as the front propagates. In ungelled TGDMA, copious bubble production occurs. It seems that the gel prevents nucleation of bubbles before complete crosslinking makes it impossible to form bubbles. Masere et al.[47] synthesized a series of gas-free initiators based on quaternary ammonium peroxydisulfates and addressed this problem. They found that initiators were soluble in organic media, exhibited no gaseous byproducts and polymerization rates were comparable to those with organic peroxides. The initiators worked at ambient pressure.

Front velocity also seemed to be affected by the orientation of reactor tube. Bazile et al.[48] studied the effect of orientation on FP of TGDMA and established that the front velocity depends on $1/(\cos \theta)$ where θ is the angle of the tube. They further derived the relation between the velocity along the axis, U_t and vertical direction U_d with the angle of the tube: $U_t/U_d = 1/\cos \theta$. However, this relation is not universal.

Temperature profile

Temperature profiles in FP give very unique information about true FP mode. If temperature is measured away from the front and it remains constant, it is an indication that no bulk polymerization is occurring simultaneously. Temperature profiles in FP are sharp. In order to characterize the temperature profile along the reaction front, a thermocouple is inserted into the solution, which records the temperature evolution at a particular point of the reaction system. As mentioned earlier, the diffusion of the heat of exothermic polymerization, process coupled with Arrhenius temperature of the initiator decomposition is responsible for the frontal regime. The extreme temperature conditions at the narrow reaction zone are evident from the spatial temperature profile, as shown in

Fig. 1.10a. The temperature profile depicts the temperature history of an arbitrary fixed point in the reaction tube as the wave of frontal polymerization passes through it. After an initial perturbation above the initiation threshold, the reaction begins, followed by a wave propagating at a constant velocity. The temperature reaches a very high point, so the wave propagates at a high velocity (as high as 20 cm/min), corresponding to small residence time in the curing zone. As shown in Fig. 1.10, the temperature at this arbitrary point is ambient when the front is away from this point and raises sharply as front approaches it. Therefore, the reaction zone is narrow with a large temperature gradient. Temperature profile measurements show that the temperature can increase locally from T_o to T_{max} in seconds. According to the constant velocity, c, of the front, the temporal data, $T(t)$, can be converted to spatial temperature profiles (i.e., $T(x)=T(c\ t)$). Consequently, it is found that the reaction zone is localized to a (traveling) infinitesimally small interval.

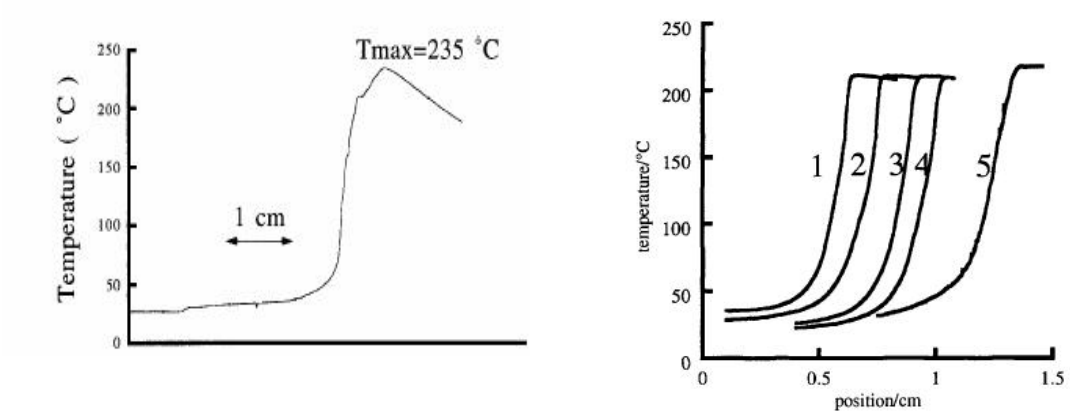

A] B]

Figure 1.10. A] Temperature profile of acrylamide polymerization front with potassium peroxydisulfate (4% w/w)[38]; B] Spatial temperature profiles for methacrylic acid fronts at different initial temperatures: (1)-(4) 2% w/v of BPO, (5) 1.5% v/v of BPO[14]

The maximum temperature mainly depends on the initiator type and concentration and also initial temperature of the reaction mixture. Fig. 1.10b depicts the effect of initial temperature on methacrylic acid polymerization using benzoyl peroxide (BPO) at different initial temperature (profiles 1-4). There is not much of a difference in maximum temperature. Since conversion depends upon the difference between the final and initial temperatures this proves the "burning out of initiator" at front temperature. Profile 5 in the Fig. 1.10b is the reaction carried out using stable initiator, tertiary butyl peroxide (*t*-BPO) which led to the highest conversion and widest heat conductivity zone. The methacrylic acid front with *t*-BPO was significantly slower, inspite of having the highest reaction temperature. This means that the effective activation energy of a polymerization front is directly correlated to the activation energy of the initiator decomposition, as to be expected. The same conclusions with respect to initiator burn out can be drawn for propagating fronts of acrylamide (Fig. 1.4), which was observed at initial reactant temperatures as low as liquid nitrogen. Notice that the conversion is affected by the initial temperature. Temperature profiles are not smooth when instabilities are present.

Product properties

Conversion

Conversion in FP is limited because of rapid increase in temperature and the very fast reaction occurs over a narrow reaction zone. As seen above this causes an incomplete decomposition of the initiator when the reaction is completed.

In exothermic reactions, conversion is inversely proportional to temperature. A relationship between temperature and the equilibrium monomer concentration (assuming

unit activity coefficients) can be derived, in which [M]o is the standard monomer concentration used to calculate the ΔS^o and ΔH^o.[14]

$$T = \frac{\Delta H^0}{\Delta S^0 + R \ln ([\mathrm{M}]_{eq}/[\mathrm{M}]^0)} \qquad 1.11$$

For an adiabatic polymerization, the maximum conversion is uniquely determined by the ΔS^o and ΔH^o of polymerization. As the temperature increases, the equilibrium conversion is reduced and can be related by:

$$\alpha = 1 - \frac{1}{[\mathrm{M}]_{initial}} \exp\left(\frac{\Delta H^0 - T\Delta S^0}{RT}\right) \qquad 1.12$$

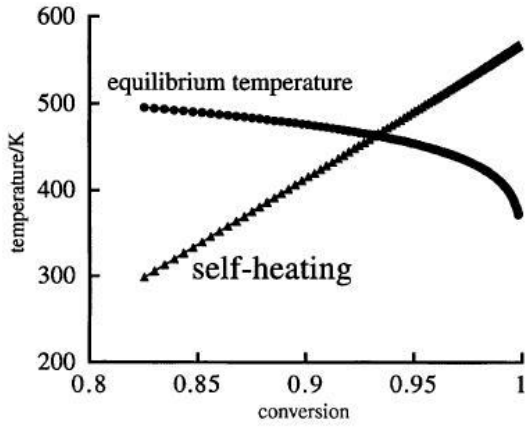

Figure 1.11. Relationship between extent of conversion and ceiling temperature[14]

In adiabatic self-heating reactions such as frontal polymerization, temperature is related to conversion and is given by:

$$T = T_i + \alpha \frac{\Delta H}{Cp} \qquad 1.13$$

where, T is the maximum temperature, T_i is the initial temperature, α is maximum conversion, ΔH is change in enthalpy and C_p is the specific heat of the monomer. Pojman et al.[16] after solving this equation, found that the maximum conversion in methyl methacrylate polymerization would be 0.93 in absence of initiator burnout.

Ceiling temperature of the monomers is also a limiting factor in conversion. Ceiling temperature is the temperature from where the propagation rate and depropagation rates are in equilibrium with each other. Front temperature sometimes may reach to this temperature and depropagation may be triggered resulting in a lowering of conversion. Fig. 1.11 shows the relation between the ceiling temperature and extent of conversion. It can be illustrated for example, zero conversion will be obtained at 310^oC with styrene but α-methylstyrene will not react above 61^oC.

Researchers have addressed the lower conversion problem by couple of ways. One way is to use a greater amount of initiator but the disadvantage of this method is that more initiator results in production of more free radicals, leading to large number of undesirably short polymer chains. A second way is to use a dual initiator system. Two initiators, with variations in activation energies, were used with the idea that the unstable initiator will give the rapid reaction and stable initiator would be responsible for the conversion. Pojman et al.[42] investigated the system of BPO and *t*-BPO dual initiator system. Volpert et al.[49] derived a mathematical model for the complex initiation system and put forward the fact that a combination of stable and unstable initiators tends to make this method of polymerization more viable than that with single initiator. Numerically they derived an equation for front velocity and validated it with experimental results to show that conversion is increased without sacrificing the front velocity.

Molecular weight

Enikolopyan et al.[29] obtained an analytical expression and predicted the broad molecular weight distribution observed in FP. Initially, for MMA polymerization, Pojman et al.[50] observed the molecular weights to be above $>10^5$. However, later the same authors concluded that the higher molecular weight obtained were not exact and resulted perhaps from intermolecular crosslinking due to anhydride formation.[51] By analyzing the samples after anhydride cleavage they found that the molecular weights were significantly lowered (1.0×10^4 g/mol). With n-butyl acrylate fronts, the same authors reported the broader molecular weight distribution with increasing initiator concentration (PWD: 1.7-2.0). The average molecular weight was reduced with increasing initiator concentration.

Effect of inert diluents on MWD was also investigated by carrying the frontal polymerization of butyl acrylate in microgravity.[35] The molecular weights were comparable with a product produced in earth using CAB-O-SIL to suppress the convective instabilities.

Quality

One of the advantages of the FP methodology is that the product is usually obtained in a very short reaction time with unique microstructure and morphology. This has been proved in a variety of systems. A typical example is in the preparation of conductive composites.[52] Authors found that frontally prepared TGDMA and acrylamide copolymers, with embedded graphite/zinc powder and initiated in presence of AIBN, produce unique and homogeneous morphology as compared to the conventional copolymerization technique (see Fig. 1.12).

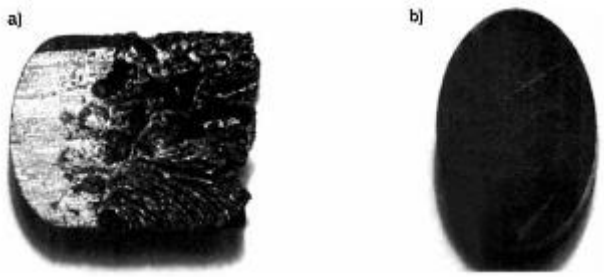

Figure 1.12. Morphology of products: a) synthesis by homogeneous polymerization performed at 60°C**;** b) synthesis by frontal polymerization in a 9.0 mm (i. d.) tube. Initial compositions 54.5 wt.-% acrylamide, 26.7 wt.-Vo TGDMA, 1.1 wt.-% AIBN[52]

The quality of the product formed in FP is, however, sensitive to input parameters such as initial temperature, initiator concentration etc. It works well with solid monomers but with liquid monomers the quality is limited by the various instabilities present during the polymerization. Researchers have tried to overcome this problem and an ultimate solution is still awaited.

Experimental techniques

Experiments under pressure

Russian workers extensively studied the FP process under pressure. They performed the reactions in closed metal reactors under very high pressure. The pressure was up to 5000 atmosphere. By this process they could not observe actual front propagation of the reaction. Pojman et al.[14] later used a custom-built glass chamber reactor. This allowed them to carry the reactions under isobaric and isothermal conditions. The chamber allowed them to perform the reaction under pressure to suppress monomer boiling and to make video observations of reaction. Fig. 1.13 shows the schematic diagram of their study.

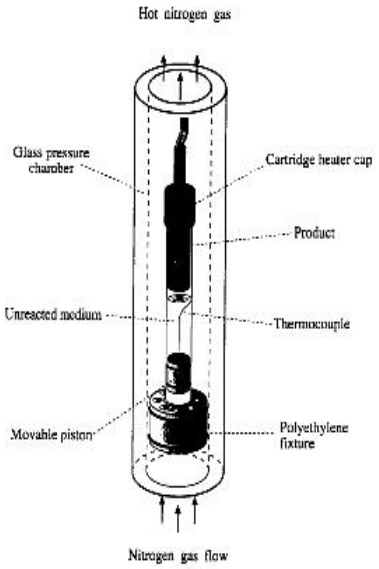

Figure 1.13. Schematic diagram of apparatus used to study FP under pressure[14]

Gill et al.[53] devised a special instrument to synthesize polymer dispersed liquid-crystal materials via FP technique. Schematic diagram shows (Fig. 1.14) the experimental set up where reactor tube is inverted with thermocouple plugged in. Soldering iron is used to ignite the front from the top; the signal from thermocouple is digitized with the use of an analog-to-digital board and personal computer. Video camera is attached to PC which records the reaction as it progresses so as to estimate the time-dependent position of the front. Authors could successfully synthesize polymers based on the formulation of a diglycidyl ether of bisphenol A (DGEBA) monomer and a curing agent (diethylene triamine).

Volpert et al.[54] proposed mathematically that FP in porous media would have technological advantages. They formulated a mathematical model which described FP in porous medium reactor and studied stationary regimes of frontal polymerization as well as their stability.

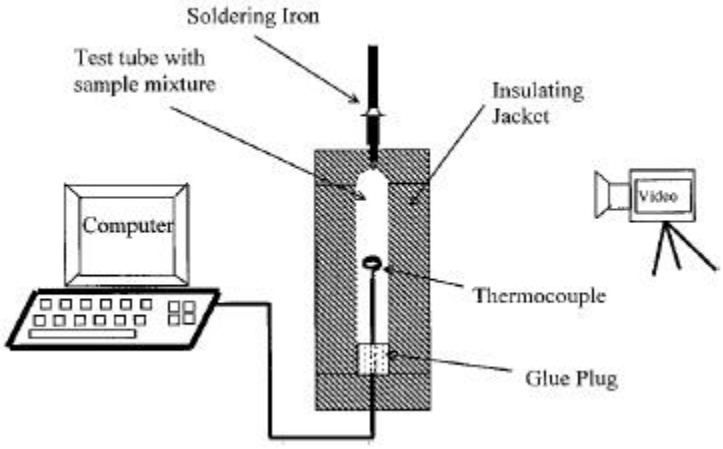

Figure 1.14. Schematic diagram of apparatus used to study the polymer dispersed liquid crystals[53]

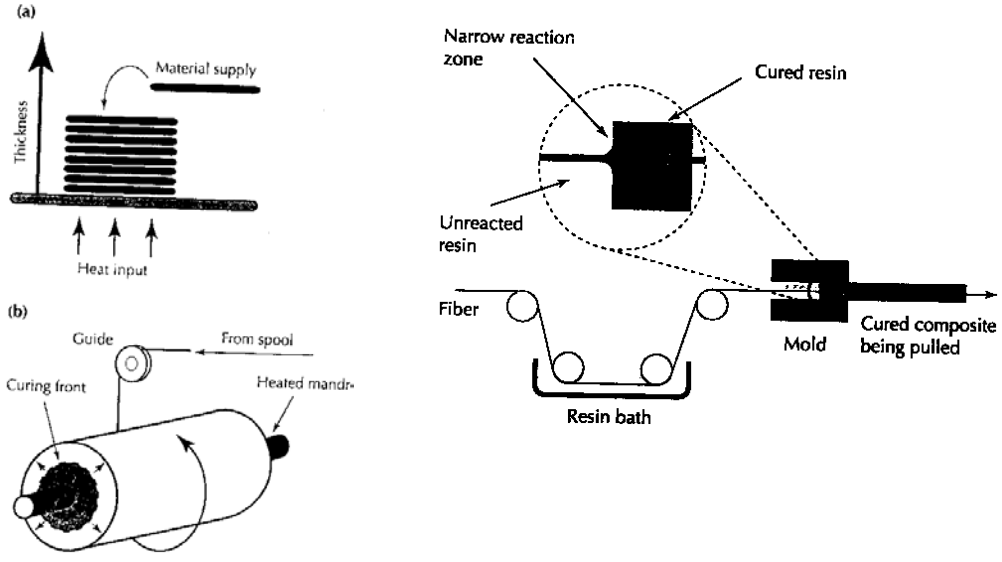

a] b]

Figure 1.15. Schematic diagram of a] frontal curing of epoxides in thick materials via continuous filament winding process for the production of rectangular (a) and cylindrical (b) shaped objects; b] frontal pultrusion process[57]

White and coworkers,[55,56] in developing a promising technology of continuous production of graphite fibre composites, took the step to semi-commercialize the FP process. Although this is not used for free radical FP, we are reviewing it because of its potential application to free radical FP systems as well. They developed two processes: in one, they could form large rectangular shaped objects while in another they prepared cylindrically shaped objects (Fig. 1.15). White showed that the process yields product in less time and with fewer voids. In the first method, layers of prepreg (graphite fibre material impregnated with the epoxy thermoset resin) were placed into a mold heated from below. Pressure (1.7×10^5 Pa) was applied until the front reaches near the top of the mold, at which point the pressure was released and another layer of prepreg was inserted, the process was repeated until the desired thickness was achieved. The second approach is shown in Fig. 1.15a, it was used for production of cylindrical objects, such as energy storing flywheels. A filament winding procedure was developed in which resin impregnated fibres were wound onto a heated mandrel at a rate that matches that of the expanding cure front.

Another technique of FP used is the combination of FP with pultrusion process.[57] The resin impregnated fibres were pulled slowly through a series of heated molds of desired profile shape. Fig. 1.15b shows proposed pultruder with an unheated mold for frontal curing of composite. The front was ignited outside the mold and then a self-sustaining reaction occurred without additional heat input. Front propagated at a velocity equivalent to fibre pull rate.

Some imaging techniques such as IR imaging,[58] NMR resonance technique,[59] dye doping technique[60] etc. were investigated and effectively used to monitor and to study FP. There are some special techniques used to study the instabilities.

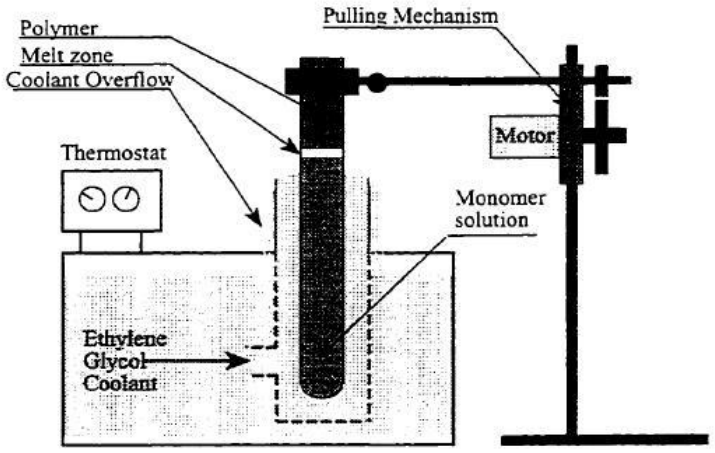

Figure 1.16. Experimental set up to study spin modes at different initial temperature[14]

Figure shown above (1.16) is the set up for studying the hot spots or spin modes. A solution of methacrylic acid and BPO was equilibrated in an ethylene glycol-water bath. The front was initiated and, as it propagated, the tube was withdrawn from the bath to maintain a fixed distance between the front and the coolant. The position of the front could be determined by the narrow melt zone immediately beneath it. Control of heat losses was also realized under free-convective heat exchange conditions by using different cooling liquids and variances in temperatures (temperature measurements were made using unsheathed fine-gauge thermocouples and a Strawberry Tree A/D board on a Macintosh Iicx). Profiles were determined by measuring the temperature at a fixed point as the front propagated down onto a thermocouple that was formed into a spiral parallel

to the front. The spiral decreased the heat flux in the thermocouple. Using the front velocity, the temporal profile was converted to a spatial profile.

Pojman et al.[14] performed experiments on convective instabilities by surrounding the glass tube in which the front was propagating with a reactor. A steady, laminar flow of constant temperature air was passed from the bottom of the tube to the top. Temperature profiles were measured and reaction was videotaped by means described before. Similarly, Pojman et al.[61] in another report used "cylinder-in-cylinder" technique to study the hot spots. They used an out-side tube of dimension 16 mm x 124 mm (capped) and uncapped inside tube (uncapped) of dimension 6 mm x 25 mm. When the reaction was carried out spiral mode was observed in inner cylinder. The polymer rod of the inside tube had to be separated carefully by breaking the glass of the outside tube.

To suppress the convective instabilities, the same authors developed a technique of rotating the reactor tube along the axis.[39]

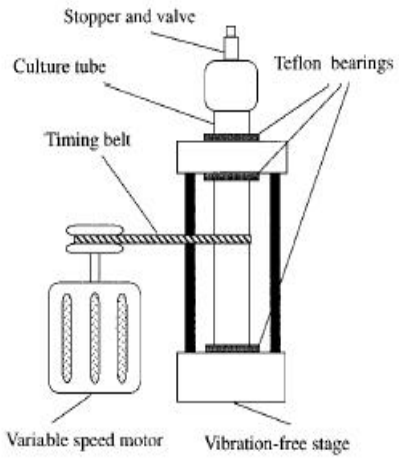

Figure 1.17. Schematic of the devise used to rotate the tube

Reaction mixture (methacrylic acid and redox initiators) was filled in a Kimax culture tube (25 mm x 250 mm, inner diameter 22 mm). The tube then was placed into

the holes of the Teflon bearings of the device shown in Figure 1.17. Bearings were lubricated with a few drops of light mineral oil. A 110 V "60" W motor with a variable speed control between 500 and 7500 rpm rotated the tube via a pulley and belt, which was simply a rubber ring, replaced after each experiment because of mechanical damage. The frequency of the rotation was determined using a stroboscope (Digistrobe, AMETEK) with 20 rpm accuracy. After charging the reaction mixture, the tube was sealed with a thermoplastic sealant ("glue gun" glue) to prevent the liquid from escaping through the porous poly(methacrylic acid). The rotation of the tube was begun only after perfect sealing. Visible images from a Hitachi solid state colour camera equipped with a Cosmicar zoom lens were digitized with a Data Translation board on a Macintosh Quadra 800. Analysis of captured images was performed with Image 1.41 (from NIH). The wave shape evaluation in the case of methacrylic acid polymerization fronts required image enhancement and edge detection using Sobel filtering.

1.3.3 Theoretical predictions

Russian authors developed the theory of FP based on the knowledge of SHS process. Initial attempts, as described in section 1.3.1, revealed that QSSA and narrow reaction zone assumptions are important to model the FP process. Novozhilov first attempted a theoretical model of stability of front in case of SHS process (eqn. 1.10). By using this formula, the effective activation energy of a polymerization could be calculated by measuring the velocity of front propagation at different initial temperatures and assuming the thermal diffusivity to be temperature independent. Classical results concerning nonadiabatic combustion waves with narrow reaction zones and one-step overall idealized kinetics state that, if the heat loss coefficient α exceeds a critical value,

the combustion wave cannot propagate. The propagation velocity u decreases as α increases. At the extinction limit, the propagation velocity was found to satisfy the relation $u_{ext} = e^{-1/2}u_{ad}$, where u_{ad} is the propagation velocity for the adiabatic case. However, this result cannot be directly applied to the frontal polymerization process in which case the kinetics are much more complicated, but are useful for the sake of comparison. Extinction of polymerization waves as well as difficulties with initiating the wave are often encountered in experiments. A number of mathematical models were solved both numerically and analytically.

We will review these models and study the propagation of nonadiabatic free radical polymerization fronts. We will look at the models to examine the structure of the polymerization wave, its propagation velocity, degree of conversion of the monomer, maximum temperature, and how these quantities are affected by changes in initial temperature, concentrations and kinetic parameters. Also, we will review the theoretical results as compared to the experimental data.

In early attempts, Volpert and Volpert[62] studied the traveling wave solutions arising in the process of polymerization with subsequent crystallization of the polymer (ε-caprolactam crystallization waves). But this was not a free radical FP.

Typically, the first step of writing free radical frontal polymerization models is formulating a mathematical model which is based on free radical reaction kinetics. Determination of uniformly propagating planar front solutions is the second step, the third step is analyzing their stability and final step is the discussion and experimental validation of the model.[63-65]

All the models are based on the following assumptions: (a) the reacting mixture is isotropic, (b) the system is adiabatic, (c) the polymerization reaction proceeds by following radical addition chain, (d) mechanism includes depropagation, (e) the rates of the reactions are expressed using the classical long chain approximation, (f) mass diffusion is negligible, (g) the physicochemical properties remain constant, (h) the possible formation of bubbles due to monomer evapouration or initiator decomposition are neglected.

Thermal free radical polymerization involves writing a five-species reaction mechanism. We recall the polymerization kinetic equations 1.5-17:

Initiation: $I \rightarrow 2fR^{\bullet}$

Propagation: $R^{\bullet} + M \rightarrow P_n^{\bullet}$, $P_n^{\bullet} + M \rightarrow P_{n+1}^{\bullet}$

Termination: $P_n^{\bullet} + P_m^{\bullet} \rightarrow P_n + P_m or(P_{n+m})$

Reaction constants are taken in the form of Arrhenius exponentials.

$$K_d = K^o_d \exp(-E_d/R_gT);\ K_t = K^o_t \exp(-E_t/R_gT)$$
$$K_p = K^o_p \exp(-E_p/R_gT) \qquad 1.14$$

where, R_g is the gas constant, T is the temperature of the mixture, and k_d^o, k_p^o , k_t^o and E_d, E_p, E_t are the frequency factors and activation energies of the decomposition, propagation, and termination steps, respectively.

Next step is nondimensionalizing a kinetic model in which the derivative with respect to the traveling wave coordinate (in both the primary radical and polymer radical

concentration equations) is multiplied by a parameter, ε. Thus, the kinetic equations that describe the change in concentrations of the species with time t can be written as shown below (1.15-1.20). Similarly, kinetic equation must be supplemented by the energy balance in the system, which accounts for the thermal diffusion, the net heat release and the heat loss to the surroundings. The heat release during the first propagation step 2 and termination steps 4 and 5 are to be negligible compared to the propagation step 3. Therefore, eqn. 1.20 which is heat balance equation has the following form (1.15-1.20):

$$\frac{d[I]}{dt} = -k_d[I] \qquad 1.15$$

$$\frac{d[R]}{dt} = 2k_d f[I] - k_p[R][M] - k_t[R][P\cdot] - k_t[R]^2 \qquad 1.16$$

$$\frac{d[M]}{dt} = -k_p[R][M] - k_p[M][P\cdot] \qquad 1.17$$

$$\frac{d[P\cdot]}{dt} = k_p[R][M] - k_t[R][P\cdot] - k_t[P\cdot]^2 \qquad 1.18$$

$$\frac{d[P]}{dt} = k_t[R][P\cdot] + k_t[P\cdot]^2 \qquad 1.19$$

$$\frac{\partial T}{\partial t} = \kappa\left(\frac{\partial^2 T}{\partial x^2} + \frac{\partial^2 T}{\partial y^2}\right) - \frac{\Delta H}{\rho c_p} k_p([M][R] + [M][P\cdot]) \qquad 1.20$$

The characteristic scale of the polymerization wave is typically much smaller than the length of the tube, so that traveling wave coordinate (x) may be introduced, and the kinetic equations are rewritten as:

$$uI' + k_d I = 0 \qquad 1.21$$

$$uR' - 2fk_dI + k_pRM + k_tR\dot{P} = 0 \quad 1.22$$

$$uM' + k_pRM + k_pM\dot{P} = 0 \quad 1.23$$

$$u\dot{P}' - k_pRM + k_tR\dot{P} + k_t\dot{P}^2 = 0 \quad 1.24$$

$$uP' - k_tR\dot{P} - k_t\dot{P}^2 = 0 \quad 1.25$$

where, u is the propagation velocity of the wave which must be determined in the course of solution of the problem. Here I, R, M, and P denote the concentrations in mol/L of the corresponding species, $P^{\cdot}$ is the concentration of the polymer radicals, and the prime denotes the derivative with respect to x.

Typically, the front is postulated to have a width that is determined by a small nondimensional parameter. In the presence of an appropriate small, non-dimensional parameter, the reaction zone can be replaced by a propagating front with the chemical reaction approximated by a heat source attached to the front. With the removal of a nonlinear reaction term, the governing equations become significantly simpler but, because the location of the front is not known a priori, the reduced problem is of a free boundary type. The approximate problem is easier to study analytically, especially from the point of view of stability analysis for the traveling wave solutions. Note that, although sharp front approximation is not usually derived via a rigorous asymptotic method, it has been shown to be an effective tool to study SHS and FP problems, yielding qualitatively plausible results. On the negative side, the problems with point-source kinetics are difficult to treat numerically. Then, the characteristic temperature is set as a limit of the temperature in an outer solution instead of prescribing the explicit formula for the

characteristic temperature for a diffuse front, and using a rigorous asymptotic procedure. Since the characteristic temperature for the traveling wave solution is indeed the same as the appropriate outer temperature limit at the interface, this approach successfully captures the stability threshold for the fronts propagating with a constant speed.

Another approach that has been successfully applied in a number of combustion and polymerization studies is to introduce simplified distributed kinetics that is usually combined with the moving front approximation. Within this approach, the Arrhenius temperature dependence is replaced by the step-function with the height equal to the value of a certain predefined characteristic temperature within the reaction zone. The exact choice of the characteristic temperature is determined by the physics of the problem. Although the kinetics function in this setup is very simple, the strong nonlinearity of the Arrhenius kinetics is inherited by making the characteristic temperature dependency on the solution.

The advantage of the step-function kinetics is that the traveling wave solution can generally be found analytically. The stability analysis for this solution is, however, very tedious and the workers have resorted to additional simplifications, in particular via narrow reaction zone type asymptotics that essentially lead back to point-source kinetics. On the other hand, narrow reaction zone approximations of step-function kinetics suffer from the same deficiencies as those for the point-source kinetics.

The analytical treatment includes solutions constructed with the SSA (leading-order outer solution) and without it (leading-order uniform solution). Last step is proceeding to solve for the monomer concentration and temperature profiles, and by

doing so determination of the effect of the farfield breakdown on the final conversion and final temperature of the system.

Goldfeder et al. in 1997[63] solved the free boundary problem and got the expression for front velocity (u) as:

$$u^2 = \frac{\kappa J_0 R_g T_b^2}{E_1(T_b - T_0)} k_{eff}^0 e^{-E_{eff}/R_g T_b} \quad 1.26$$

where, T_b can be replaced by $T_o + qM_o$. If α is sufficiently small, the use of the above asymptotics yields

$$u^2 = \frac{\kappa R_g T_b^2}{2E_1(T_b - T_0)} k_d^0 e^{-E_d/R_g T_b} \quad 1.27$$

Where, T_b was no longer close to $T_o + qM_o$ and was determined by:

$$\left(\frac{2I_0^{1/2} k_p^0}{[k_d^0 k_t^0]^{1/2}}\right) \exp\left[\frac{E_t + E_d - 2E_p}{2R_g T_b}\right] = \ln\left(\frac{qM_0}{T_0 + qM_0 - T_b}\right) \quad 1.28$$

Authors compared their theoretical results with experimental data and representative plots are shown in Fig. 1.18 and 1.19.

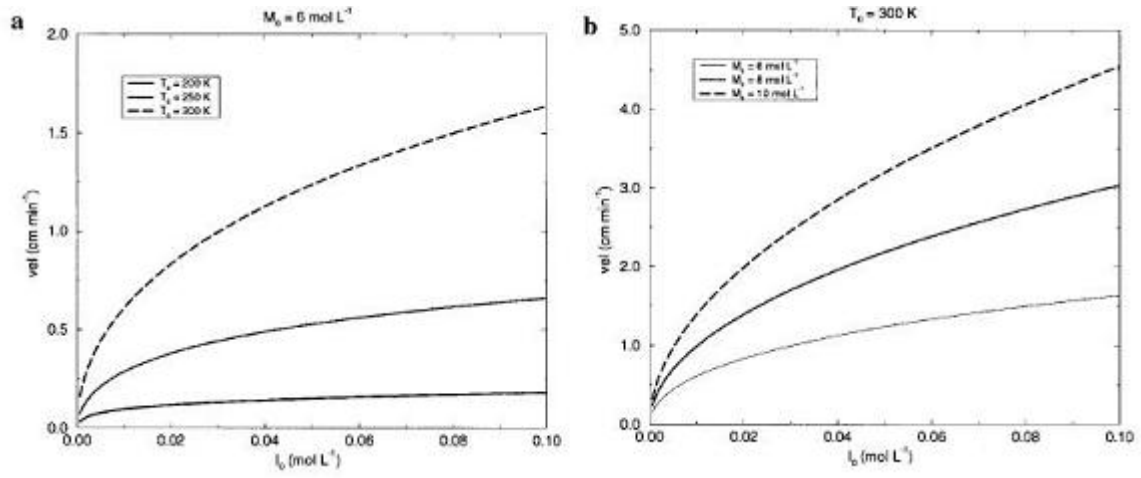

Figure 1.18. Effects of changes in (a) the initial temperature, and (b) the initial amount of monomer present on the propagation velocity[63]

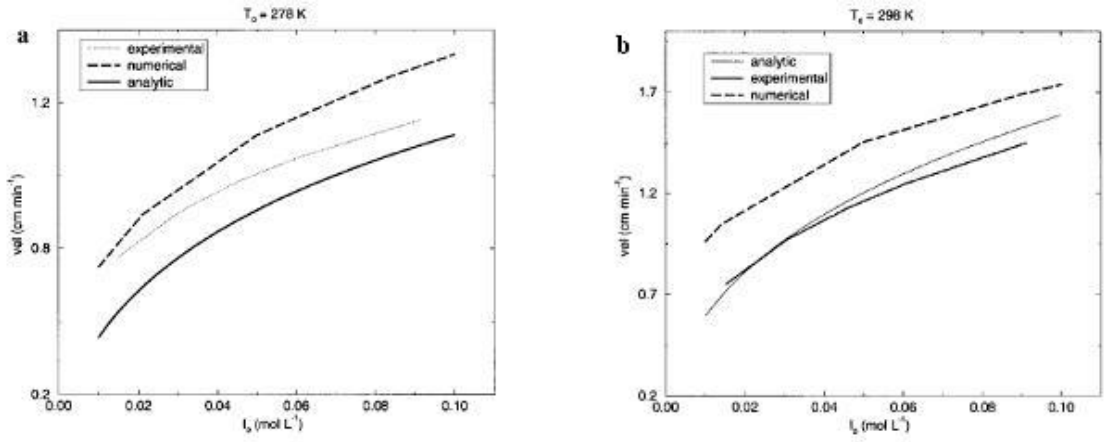

Figure 1.19. Comparison of the velocity curves attained analytically, experimentally, and numerically for initial temperatures of (a) 278 K and (b) 298 K[63]

Spade and Volpert[64] studied two models of free radical, non-adiabatic FP. One was a reduced model which was based on combustion process where polymer kinetics was effectively described by a single reaction. The main drawback of this model was the absence of 'monomer survival'. In other model, multistep model, which consisted of a five step polymerization, reaction kinetics revealed that the monomer was not completely consumed in the reaction zone, which was more practical. They carried a linear stability analysis of the same and investigated extinction limits and stability characteristics of polymerization waves as a function of the system parameters. Front velocity was obtained as:

$$u^2 = \frac{kk_o R_g T_b^2}{M_o q E} \exp\left[\frac{-E}{R_g T_b}\right] \qquad 1.29$$

Linear stability analysis of this front velocity after nondimensionalizing took the following form:

1.30

$$U = \frac{\hat{T}_b^2 P(z_b)}{\hat{T}_a^2 P(z_a)} \exp\left[-\frac{E_1(\hat{T}_a - \hat{T}_b)}{R_g \hat{T}_b \hat{T}_a}\right]$$

$$\beta = \frac{1}{4}\left[\left(\frac{q M_0}{\hat{T}_b - T_0}\right)^2 \left(1 - e^{-z_b}\right)^2 - 1\right] U$$

1.31

Here, both U and β are parametric functions of T_b. β depends on the thermal diffusivity of the system and heat loss. Fig. 1.20 shows the multistep solution curve for four values of initiator concentration and comparison between the single and multistep model. Each curve has a nose like shape and tip of the nose makes the extinction limit of the polymerization wave.

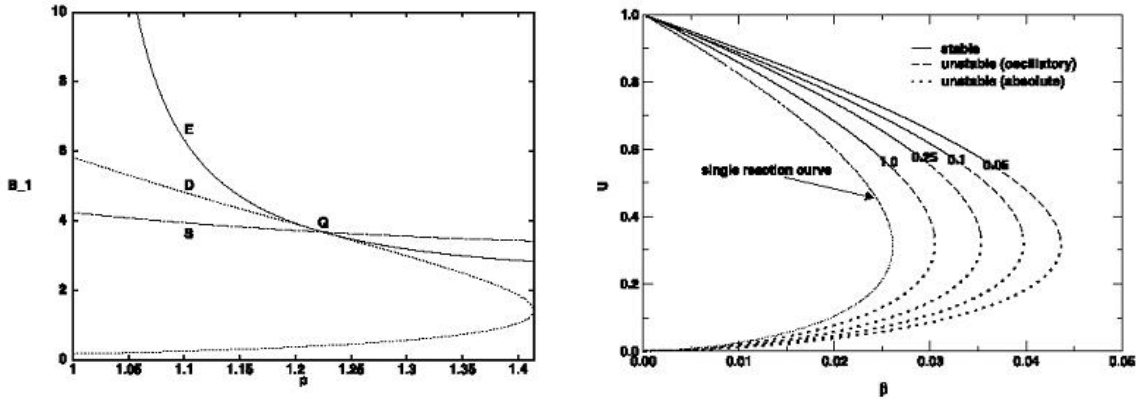

a) b)

Figure 1.20. a) Existence and stability regions of the basic state in the *(p,B1)*-plane; b) The multistep solution curve in the (*β,U*)-plane for four values of the initial initiator concentration I_0. Along each curve the initiator label, given in units of mol L^{-1}, is placed near the point which marks the onset of instability. The thin curve at the far left represents the result for the single-reaction model[64]

Here p of X-axis in Fig. 1.20, is proportional to square root of β.

Solovyov et al. in 1997[65] investigated the role of kinetics on front stability and derived the numerical solutions for the same. They considered a detailed formulation of

mathematical model, including realistic polymerization kinetics, thermal diffusion and appropriate hydrodynamics and developed the mathematical model with three-step polymerization kinetics and heat diffusion, which reproduced the experimental results and also predicted the qualitative system behaviour and some properties of the final product in the absence of convection. Numerical simulations were carried to single step and three step reaction mechanism which demonstrated that the effective activation energy of the polymerization reaction, the Zeldovich number, and the tube diameter are some of the parameters which determine the stability of propagating polymerization fronts and also offer an explanation of the phenomenon of superadiabatic combustion temperature. They also concluded that factors like initiator concentration affect only the front velocity and not its stability.

In 1998, Goldfeder et al.[66] and his coworkers developed a similar model and analyzed the extinction limit of polymerization wave as well as structure of polymerization wave, propagation velocity, degree of conversion, maximum temperature and their dependency on initiator concentration and other kinetic parameters.

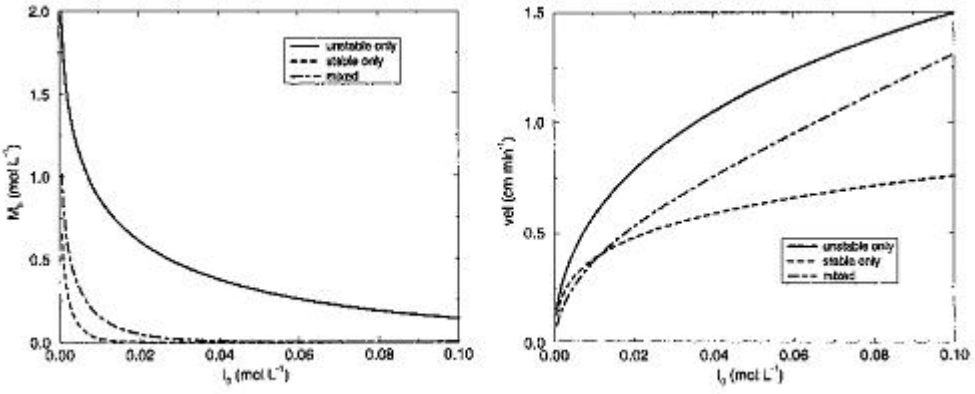

Figure 1.21. Effect of change in initiator type and composition on the amount of unreacted monomer left after the reaction and propagation velocity of the front

Authors also modeled the FP process with complex initiation mode (dual initiator system). There they combined stable and unstable initiator and proved that stable initiator is responsible for a higher maximum temperature, lower propagation velocity and much greater conversion than unstable initiator. Fig. 1.21 depicts effect of change in initiator type and composition on the amount of unreacted monomer and front velocity.

Volpert and Spade[67] further extended their study and solved the problem for FP process both numerically and analytically by considering the steady-state approximation (SSA) and without it, and revealed where the SSA solution breaks down. They found that the non-SSA solution predicts full monomer conversion and an adiabatic final system temperature, whereas the SSA solution predicts a less than adiabatic final temperature and incomplete conversion. The authors further carried an asymptotic analysis which leads to the derivation of an ordinary differential equation of Landau-Stuart type for the slowly varying amplitude of a linearly unstable mode. They classified nonlinear dynamics of the polymerization front by doing a parameter sensitivity study of the amplitude equation. By analyzing the dynamics of Landau-Stuart equation, they identified periodic pulsations of the front for a range of parameter values.

In FP, many times experimental results tend to show a higher degree of conversion than theoretical results. The reason for this discrepancy can be attributed to an autoacceleration of the polymerization rate which occurs when conversion reaches a certain point. This autoacceleration is due to a decrease in the termination rate caused by a phenomenon called ‘gel effect’. Again Volpert et al[68] developed a mathematical model of FP process considering the gel effect and determined its effect on degree of

conversion, maximum temperature and propagation velocity of the system. The additional expression they wrote to take into account the gel effect was:

$$k_t^0 = \begin{cases} k_{t1}^0, & M > M_g \\ k_{t2}^0, & M \leq M_g \end{cases} \qquad 1.32$$

where, M_g is the prescribed amount of monomer remaining when the gel point is reached. k^o_{t1} and k^o_{t2} are the frequency factor for the termination prior to and after gel effect. After solving by usual way, authors showed that as gel effect becomes more pronounced, conversion and maximum temperature increases. Comissiong et al.[69] studied the effect of inert material on FP. They considered one-dimensional frontal polymerization (FP) wave in a sandwich-type two-layer model. One layer is reactive. It contains a mixture of a monomer and initiator. The other layer consists of an inert material. The two layers can exchange heat and thus the presence of the inert layer can significantly affect propagation of the polymerization wave through the reactive layer. Heat exchange was possible between the two layers and thus the presence of the inert layer can significantly affect propagation of the polymerization wave. They proceeded to perform a linear stability analysis of the steady-state solutions. They found that in the case of multiple solutions, the intermediate branch is always unstable. The upper and lower branches can be either stable or unstable depending on the parameter values. Their analysis indicated that the front stability was rather insensitive to the thermo-physical parameters of the problem, except for the heat-exchange parameter in the reactive layer. In general, the overall linear stability of the system was promoted by incomplete monomer conversion by the frontal polymerization process occurring within the reacting layer.

Apostollo et al.[70] gave a physical interpretation of FP phenomenon through a mathematical model that accounts for the depolymerization reaction and was based on the

constant pattern approach. Moreover, the authors proposed an approximate explicit analytic expression for the velocity of propagation of the polymerization front. The theoretical values were compared with those measured experimentally as a function of the initiator concentration for different addition polymerization systems.

Recently, Golovaty[71] looked at frontal polymerization in a different way and suggested a version of a distributed step-function kinetics that can be used to approximate a propagating reaction front in one-dimensional FP. The advantage of this type of kinetics was that the resulting model was amenable to relatively straightforward numerical and analytical computations. The numerical analysis was considerably easier for the step-function kinetics model than for the point-source kinetics model since one does not have to solve for the position of the front. They demonstrated numerically that dynamics of fronts in systems modeled with step-function kinetics and in systems modeled with the Arrhenius kinetics are qualitatively the same at the intermediate time scale. Further, they showed that the stability threshold for step-function kinetics was in excellent agreement with its numerically determined value as well as with other existing kinetics approximations.

Authors extended their study and used numerical simulations to study the influence of reaction kinetics on one-step frontal polymerization in one dimension.[72] They showed that the long time behaviour of systems governed by approximate kinetics (sharp-front, step-function) significantly differs from the long-time behaviour of systems governed by Arrhenius kinetics. The differences are caused by slow bulk reactions in the initial mixture of reagents that influence both the speed and the long time stability of the reaction front. These reactions can play a significant role in FP as their speed are much

slower than SHS. Thus, they showed that for distributed kinetics a “true" FP is only possible for a steadily propagating, traveling-wave reaction front. When a front propagates in a pulsating mode, there is an existence of pockets of unreacted monomer behind the front. These pockets evolve via a bulk polymerization mechanism.

1.3.4 Dynamics and Instabilities

Although frontal polymerization is feasible in a number of systems, there may exist various types of instabilities of reaction fronts which lead either non-uniformity in the product or destroy the front propagation. In the simplest and most important case of steady propagation, all of the wave points move at a constant and identical velocity. When the steadiness is upset, the system may undergo:

a) planar autooscillations in the front velocity (pulsating combustion)
b) localization of reaction in one or several hot spots that move along the spiral trajectory (spinning waves)
c) chaotic motion of numerous hot spots (aperiodic propagation) or
d) in case of strong heat losses (small sample diameter, low adiabatic temperature), wave propagation is not sustained altogether.

The numerical and theoretical analysis of the non-stationary equations describing the thermal reaction wave propagation in condensed media showed a rich variety of dynamical behaviour.[14] We have listed various types of instabilities which occur in FP in section 1.3.2, we will now review each in detail.

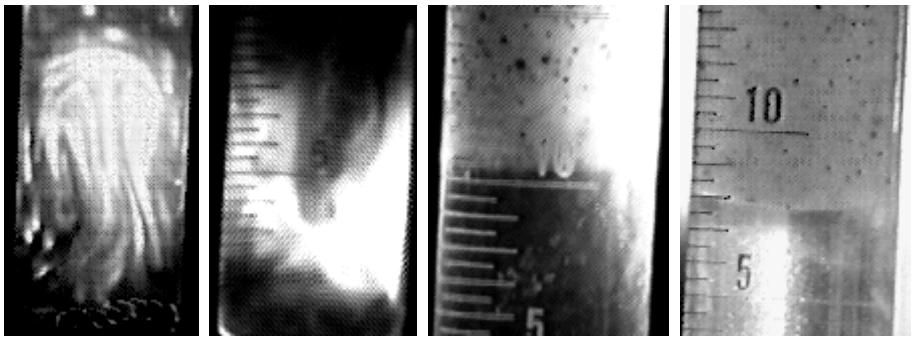

A] B] C] D]

Figure 1.22. Snapshots of the instabilities occurring during the FP (courtesy: www.cpl.usc.edu)

A] Thermal instability

Thermal instability appears because of the competition between the heat production in the reaction zone and the heat diffusion from the reaction zone to the cold reactants. Thermal fronts can travel as flat planar fronts or in more complex modes, including pulsating fronts, spin modes, and chaotic modes. Thermal instability is seen in terms of hot spot(s) or oscillatory modes. These modes are referred to as unstable because they are found beyond the thermal stability boundary of the steady-plan propagating thermal wave. However, these modes are observed experimentally and are reproducible and stable in time. The modes observed are a function of a bifurcation parameter, which is usually the initial temperature, front temperature, or energy of activation. Usually a hot spot follows a helical path along with the front and leaves behind spiral traces on the polymer. Fig. 1.23 shows schematic diagram of the hot spot propagation.

Experimentally it was observed first for the condensed phase combustion and then studied numerically[73-75] and analytically.[9,76,77] It leads to the appearance of periodic modes of propagation such as one-dimensional pulsations or different temporal,

multidimensional structures. Thermal instability of polymerization fronts was also found and studied in a number of works.[14,22,62]

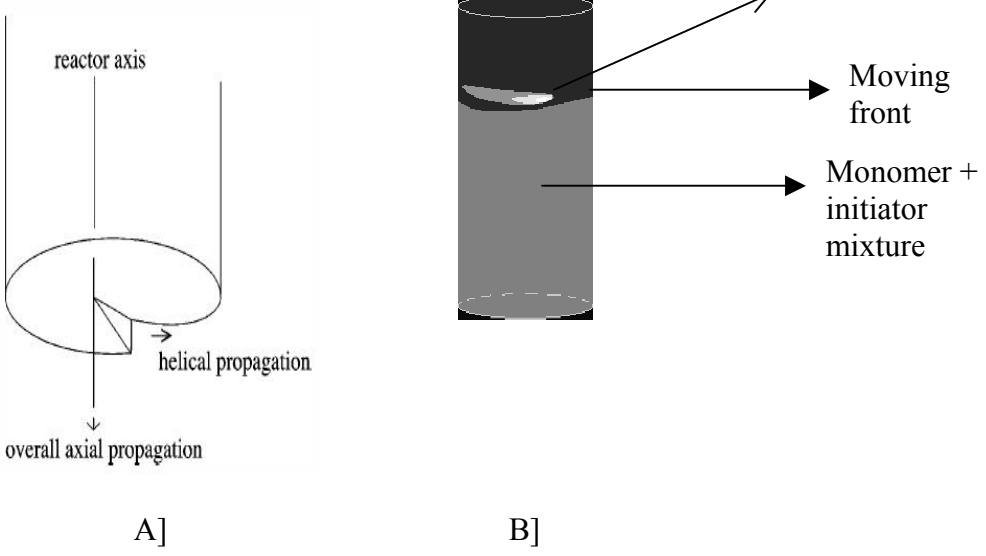

Figure 1.23. An illustration of the spin-head motion that would result in the pattern observed inside the polymer rod

As seen in section 1.3.3, experimentally the loss of steadiness was observed for the first time in anion-activated polymerization of ε-caprolactum in FP.[22] The subsequent study was carried by Pojman in 1995.[78] They studied the free radical frontal polymerization of methacrylic acid with benzoyl peroxide (BPO). Authors reported two types of instabilities. One of them occurred when reaction was carried at room temperature, was due to convection and other was observed when reaction was carried at a initial temperature below the melting point of methacrylic acid (frozen reaction mixture). In latter, spinning modes were observed. Figure 1.24a shows the snapshot of the poly(methacrylic acid) sample which shows the helical patterns on the specimen. This happened due to the presence of a single hot spot. The one head spin mode manifests itself as a small hot hump on the front surface adjacent to the tube wall of the cylindrical

sample. During front propagation, the hump moves along the perimeter of the sample in a spiral fashion. Pojman et al. observed that hot spot propagates around the front with a period of 1.3 min and with velocity 0.66 cm/min. Temperature profiles in the Fig. 1.23b is not smooth and confirms the presence of hot spot. They gave a qualitative mechanism for the process and proposed that initial temperature and the magnitude of heat loss as well as initiator concentration are responsible for the instabilities. In methacrylic acid polymerization loss of up to eight set regimes were revealed, based on the varying initial temperature and heat losses.

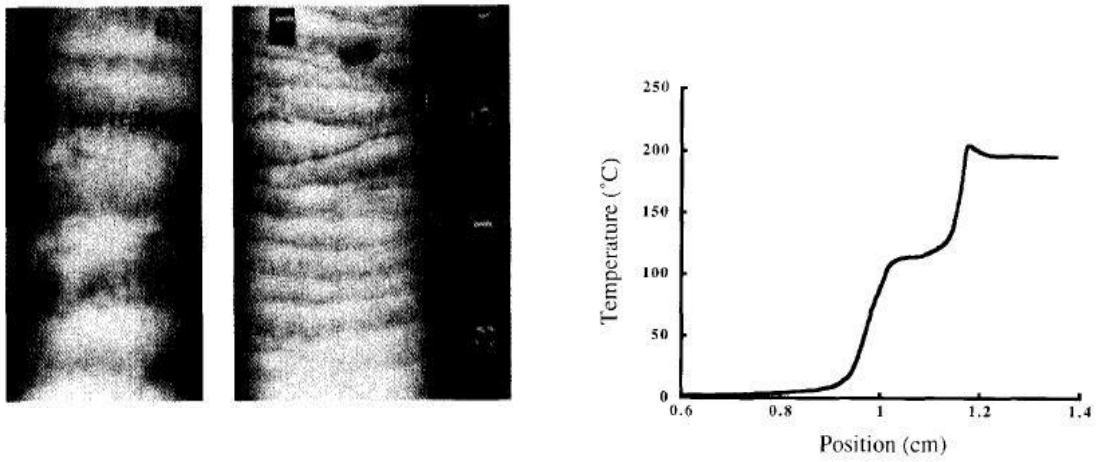

a] B]

Figure 1.24. a] Helical patterns observed on poly(methacrylic acid); b] Temperature profile confirming the presence of hot spot[78]

1,6-Hexanediol diacrylate (HDDA), trimethylolpropane triacrylate and triethylene glycol dimethacrylate were also found to give the single and multi head spin modes.[61,79,80] The reason for an easy formation of spin modes at room temperature in the diacrylate systems is that the effective activation energy of activation of diacrylate is much higher than monoacrylate because it forms a crosslinked network. Mesere and Pojman[60] used dyes that could be bleached by free radicals to accentuate the spirals (Fig. 1.25).

However, when peroxydisulfate salts were used as bubble-free initiators, the dye-bleaching technique did not work. Same authors used magnetic resonance imaging (MRI) technique to monitor the front and analyze the effects of spin modes on the morphology of the polymers.[81] The technique was advantageous over IR or dye method and revealed much complex behaviour of the polymerization process. They confirmed the presence of a single head hot spot by slicing the gels and performing an MRI analysis of each slice followed by a computer-aided reconstruction.

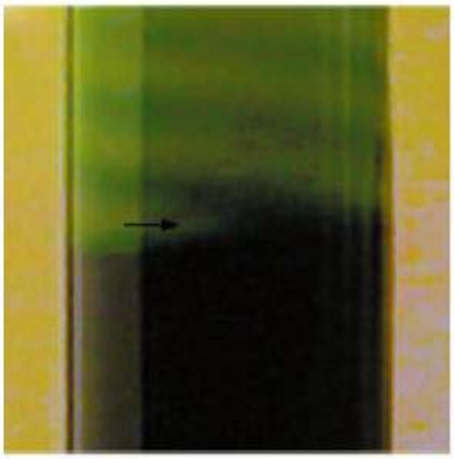

Figure 1.25. Use of bromophenol blue indicator dye in monitoring single head spin mode in HDDA polymerization[60]

Masere et al.[58] used the front temperature as a bifurcation parameter by adding an inert diluent to multifunctional acrylate systems. They also found that varying the ratio of a monoacrylate to a multifunctional acrylate served as a bifurcation parameter for the appearance of the single-head mode, two heads, four heads, and an apparently chaotic mode. They proposed that the energy of activation of the polymerization was a function of the degree of crosslinking, and so increasing the concentration of multifunctional acrylate increased the energy of activation.

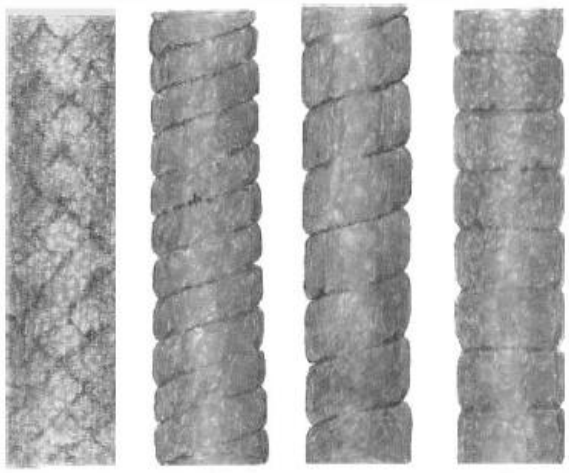

Figure 1.26. Non-linear structures during frontal polymerization of cobalt containing metal-complex monomer. (a) multi-set; (b) two-set; (c) one-set spin regime; (d) self-shortened centre [82]

Table 1.2. The effect of cylindrical tube diameter on the behaviour of the propagating front in the TMPTA frontal polymerization[80]

Volume percentage of TMPTA in DMSO (%)	Tube Diameter (mm)			
	6	8	16	20
28	no propagation	single head	single head	single head
32	no propagation	single head	two heads	two or more heads
35	single head	single head	zig-zag	rippled front
40	single head	single head	flat front	flat front

Various patterns and spiral structures were observed during the polymerization of cobalt nitrate containing metal-complex monomers with acrylamide.[82] Fig. 1.26 shows

nonlinear structures formed during the FP. Authors claimed that a definitive role in the formation of spin regimes, especially for multi-set ones, could be played by the crystallization front propagating at a velocity similar to that of polymerization front.

Pojman et al.[14,61,81] and later Huh et al.[80] studied dependency of solvent and reactor geometry in FP of various multiacrylate monomers. Table 1.2 shows the behaviour of FP under different reaction conditions:

Apart from varying the diameter of the reactors, authors also carried reactions in three different types of reactors viz. cylindrical, two-size tube and conical tube.[80] Authors reported more complex patterns like zig zag patterns in some systems. The new method that is cylinder-in-cylinder revealed the spin heads in the inner cylinder always gave spiral traces on polymer sample. Additionally, in continuously varying diameter reactor tube, hysteresis behaviour of a spin mode, bistability in spin mode was reported.

Pojman et al. looked at the theoretical aspect of the same and derived the expression for reactor radius (b) and number of hot spots, which revealed that increase in b results in the appearance of 2-head, 3-head and 4-head spinning regimes.[61]

$$b_1 = \sigma_{11} / s_* \qquad 1.33$$

Binici et al.[83] recently reported new type of frontal mode, spherically propagating frontal mode that also exhibits spin modes. They used seeded polymerization method. A gel was prepared by the reaction of a trithiol with a triacrylate by an amine-catalyzed Michael addition. A small piece of gel containing a photoinitiator was inserted into the mixture as it gelled. When gelation was complete, fronts were initiated by UV illumination to propagate from the centre. They found that this approach works much better than using a multifunctional acrylate in dimethyl sulfoxide (DMSO) with dissolved

peroxydisulfate, which does not produce bubbles. The thiol–triacrylate gel prevents the appearance of bubbles from the peroxide initiator. Spin modes were observed on the surface of the spherical fronts; this was a novel phenomenon never before observed with thermal fronts in condensed media. With a gel containing a photoinitiator, it was possible to initiate a front under rectangular initial conditions. The gel could be formed in rectangular slabs to observe fronts in quasi-two-dimensional media.

A linear stability analysis of longitudinally propagating fronts in cylindrical adiabatic reactors with one overall reaction predicts that the expected frontal mode for the given reactive medium and diameter of the reactor is governed by the Zeldovich number.[65] The planar mode is stable if $Z < 8.4$ and is unstable if $Z > 8.4$.

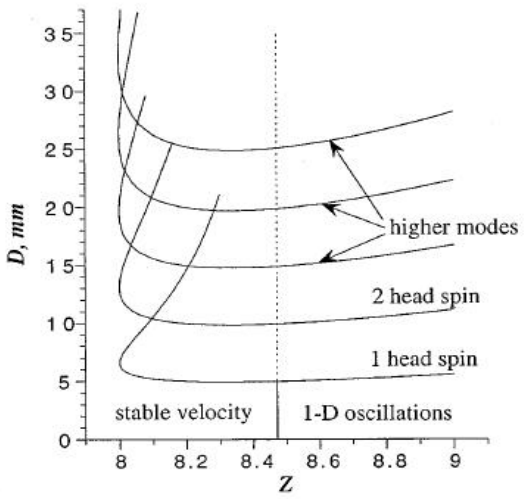

Figure 1.27. Diameter of the reactor tube, D Vs Zeldovich number (D-Z), stability diagram for one-step reaction[65]

Through the variation of Z beyond the stability threshold, more complicated spin mode instabilities can be observed. Polymerization is not a one-step reaction, so the previously shown form of Z does not directly apply. It does indicate that there are three ways to increase the probability of observing spin modes: lower the initial temperature,

raise the front temperature, and increase the energy of activation. The front temperature is limited by the energy released per mass of the monomer, so a lower molecular weight is advantageous.

B,C] Convective and Rayleigh-Taylor instability

Convective instability: By convective instability, we mean that one which appears due to natural convection. It appears as a result of the action of gravity. If the reaction is exothermic and the reactants are in the liquid phase, then natural convection can occur. For ascending fronts there is some analogy with the Rayleigh- Be´nard convection in a layer of a liquid heated from below. The exothermic chemical reaction plays the role of heating the liquid from below and if the Rayleigh number is sufficiently large, the instability occurs.

C] *Rayleigh-Taylor instability:* It is an instability of the interface between two liquids. There are experimental observations of this instability in frontal polymerization.[14,45] It can lead to descending particles/drops of the polymer from the reaction zone, i.e., to fingering. In some cases it causes the front degeneration and initiates reaction in the bulk. Both instabilities are interrelated.

Pojman et al.[45] first reported experimental observations of convective instabilities. They observed three types of convective instabilities: (1) The heat released by the exothermic reaction decreases the density of the reacting solution but changes in the composition tend to increase the density. The net change in density is negative. Simple convection results, which causes a downward propagating front to remain perpendicular to the gravitational vector even as the tube is tilted. (2) Under specific concentration and temperature, however, long slender “fingers” of polymer are observed to sink from the

solid polymer front. The appearance of structures analogous to “salt fingers” in ocean layers of different temperatures and salinity are analyzed in terms of the theory of double-diffusive convection. Similarities with convection in directional solidification are considered. (3) Pulsating fronts have been observed which result in a striated material. The energy of activation of the fronts was determined and used to show that a convective instability instead of a pure thermal one is the cause of the pulsations.

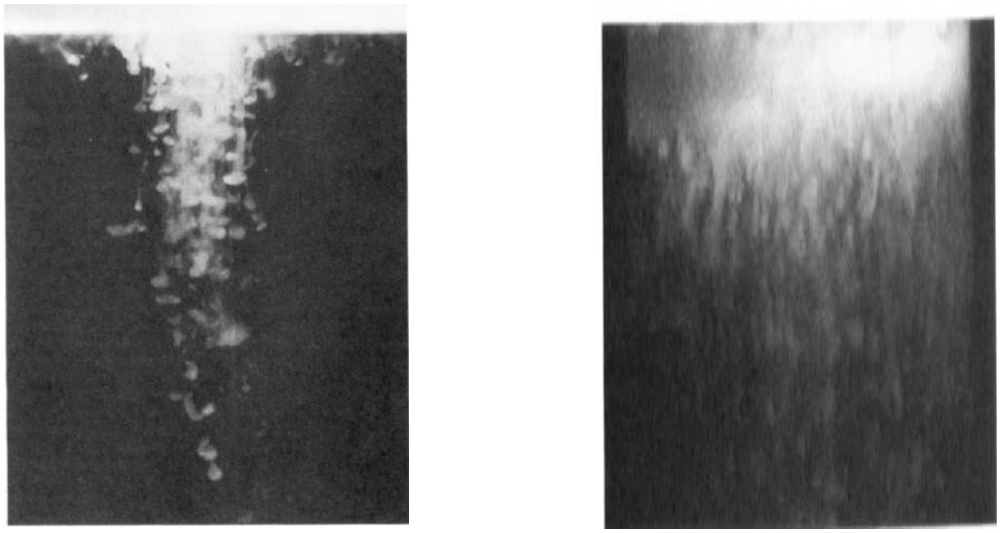

A] B]

Figure 1.28. Fingering of poly(methacrylic acid) drops into the monomer solution[45]

Fronts can exhibit a double-diffusive instability or Rayleigh-Taylor instability resulting in polymer "fingers" analogous to salt fingers in ocean layer mixing and directional solidification because there is a large thermal expansion caused by the exothermicity of the reaction as well as an isothermal contraction during polymerization. Fronts exhibit pulsations that are the result of a convective fluid motion and not a purely thermal instability (Fig. 1.28). The energy of activation of the fronts was determined and shown to be less than the critical value for a pulsating instability in a thermal front. The

authors have suggested a way to obviate the convective instabilities by rotating the reactor tube.[39] This is described in section 1.2.2.3.

Effect of convection on front propagation was carried independently by McCaughey et al.[84] and Bowden et al.[85] McCaughey and coworkers devoted their efforts in descending frontal polymerization of liquid monomer which on polymerization converts to a solid product. They considered a simplified mathematical model which consisted of the heat equation and equation for the depth of conversion for one-step chemical reaction and of the Navier-Stokes equations. Convection instability is usually studied in the pure form if one considers the Boussinesq approximation, *i.e.*, neglecting the change of density everywhere except for the buoyancy term. The Boussinesq approximation was justified and used to study the front stability.[68] The critical conditions of appearance of convection are determined by the frontal Rayleigh number (R),

$$R = \frac{g\beta q\kappa^2}{\nu c^3}, \qquad 1.34$$

where, g is the gravity acceleration, β is the coefficient of thermal expansion, q is the adiabatic heat release, κ is the coefficient of thermal conductivity, ν is the kinematic viscosity, and c is speed of propagation of the front. If the frontal Rayleigh number exceeds a critical value, then convection appears. Depending on values of the parameters, two different convective structures are observed. Based on the Rayleigh number, authors obtained the theoretical stability boundary on the viscosity-velocity plane as:

$$\nu = \frac{g\beta q\kappa^2}{a(2\pi\kappa/L)^2 c + bc^3}. \qquad 1.35$$

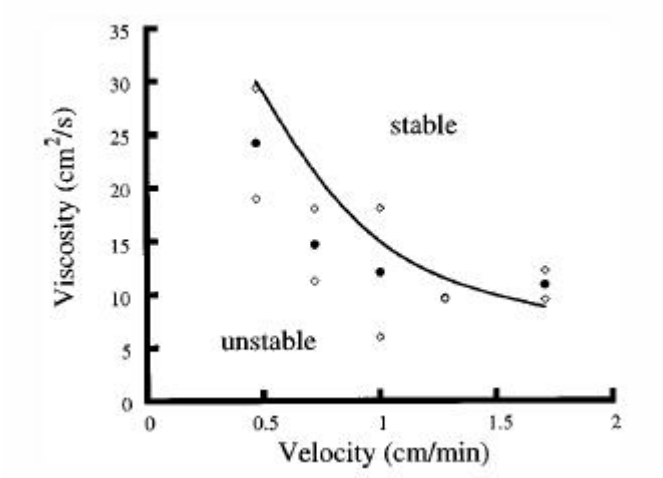

Figure 1.29. Comparison of the experimental and theoretical stability boundary for an ascending front[84]

The authors compared the results with benzyl acrylate polymerization in dimethyl formamide (DMF) and methacrylic acid polymerization (with and without inert diluent). The fact that observed theoretical region is less than experimental (Fig. 1.29) may be explained by the influence of the walls that make the front more stable. The last experimental point at high velocity may not be precise because of the difficulty in eliminating bubbles at the high initiator concentration. The stability conditions depend on the speed of the convection-free front. If the speed is greater, the front is more stable.

Bowden et al.[85] considered the problem of ascending thermal front in which liquid monomer is converted into solid product. They performed acrylamide polymerization in dimethyl sulphoxide (DMSO) in an ascending mode. The heat released by a chemical process can cause the fluid above the front to flow through the interaction of buoyancy, similar to the Rayleigh-Be'nard problem with heating from below. Theoretically, they calculated the stability boundary i.e. the critical viscosity at which an ascending front became unstable as a function of the front velocity. They obtained the following relationship between the critical viscosity and critical velocity:

$$v_c = \frac{g\beta q\kappa^2}{5c^3 + 40(2\pi\kappa/D)^2 c} \quad 1.36$$

$$v_c = g\beta q\kappa^2 \left(\frac{L}{c}\right)^3 \frac{1}{Ra} \quad 1.37$$

Equation 1.37 is arrived after considering the effect of walls. In ascending polymerization mode, it has found that the presence of walls in a two-dimensional system does stabilize the front compared to an infinite plane, but the shape of the boundary is not affected. Experimental fronts exhibited antisymmetric convection for low viscosities and low front velocities, as per their prediction. However, the experimentally determined boundary differed significantly from the calculated ones. The experimental fronts were more stable. It was proposed that the shapes of the boundaries differ due to the temperature dependence of the viscosity, which is not treated in the analysis. Authors used CAB-O-SIL, ultra fine silica gel as a diluent to vary the viscosity of the medium.

Thus, viscosity of a reaction medium has an imparting role in convective instabilities. The same monomer (methacrylic acid) did not perform convective instabilities when reaction carried below its melting temperature of methacrylic acid. This is because at that temperature viscosity of the medium is infinite and convection has no role to play.[58]

Allali et al.[86] took into consideration the influence of vibrations on convective instabilities. Their model consisted of a reaction diffusion equation coupled with the Navier-Stokes equations under Boussinesq approximation. Vibrations were taken into account through the buoyancy term, where gravity acceleration depends periodically on time. They derived an equation similar to that of Rayleigh number, with critical values

based on amplitude and frequency of vibrations. On increasing frequency of vibration, the front stabilized with respect to convective instability (first branch of stability boundary). For larger amplitude another branch of the stability boundary was obtained, which corresponds to parameters instability, and it decreased with amplitude.

D] Hydrodynamical instability

Hydrodynamic instability results from the heat expansion of the medium at the reaction zone. It is well studied for the gaseous combustion. For the frontal polymerization it has been observed experimentally[45] and also studied theoretically.[87-90] A hydrodynamic instability, also called Darrieus-Landau instability, of the reaction front can occur if the density of the medium is variable. Usually it is considered as a given function of the temperature. The instability is caused by heat expansion of the gas or liquid in a neighbourhood of the reaction zone.

Experiments with liquid monomers show the liquid motion under the descending fronts. Volpert et al.[87] considered a model for this hydrodynamic instability, the influence of heat expansion on the front stability in an one dimensional formulation. The thermal expansion decreased the temperature gradient to the right of the reaction zone, so the thermal diffusion from the reaction zone, proportional to the temperature gradient, slows down. Thus, thermal expansion makes the front more unstable. Volpert et al.[88] also analyzed the hydrodynamic stability of a polymerization front. A three dimensional mathematical model consisting of mass and energy balance by usual way, as seen in section 1.3.3, was employed with the additional assumptions of no bubble formation and no pulsating instability. They showed that the eigenvalues of the problem, linearized about the uniformly propagating solution, do not cross the imaginary axis through the

origin, so that that there is no hydrodynamic instability for small heat expansion. If the expansion is more, and if it happens nonuniformly i.e. part of the liquid near the front expands at a greater rate than in surrounding liquid then this part of liquid advances into the cold monomer. As a consequence, heat loss from this part of the liquid increases, which leads to a temperature drop, an increase of the density and consequently to a contraction of the liquid. Thus, the perturbation decays.

1.3.5 Applications

A very advantageous feature of FP is the rapid and uniform conversion of monomer to polymer. Adiabatic polymerization of neat monomer is not possible due to autoacceleration like effects are also is possible in FP. FP however faces problem of instabilities and incomplete monomer conversions. The technique of FP is explored in diverse fields.

1.3.5.1 Interpenetrating polymer networks

Interpenetrating polymerization is a mode of preparing two or more crosslinked polymers to produce a mixture in which phase separation is not as extensive as in normal blending or mixing. Preparations of simultaneous interpenetrating networks (SINs) are carried out by two independent and noninterfering crosslinking mechanisms in bulk, solution, or dispersion. In the simplest case, monomer I is combined with crosslinking and initiator to form network I. Network I is then swollen with monomer II, which is then itself polymerized and/or crosslinked. With highly incompatible polymers, thermodynamics of phase separation occurs before crosslinking takes place. Therefore, there has been a great challenge to synthesize IPN with resolvable domain structures.

Pojman et al.[91] reasoned that the high temperature in the front could make the rates of two reactions nearly equal because of exponential dependence of the rates on temperature. A series of SINs have been developed employing both epoxy (step) and acrylic (chain) polymerizations. The dual curing system of alkylamine (Epicure 3271) and boron trichloride-amine complex was dissolved in an epoxy monomer, diglycidyl ether of bisphenol A. The mixture of tri(ethylene glycol) dimethacrylate and benzoyl peroxide initiator was then added to the solution. A single front propagation, rather than two sequential fronts, was observed and an interesting relationship was obtained. The front velocity was a function of the initial composition of the two components (Fig. 1.30). Contrary to what was observed for frontal copolymerization, the binary frontal polymerization exhibited a minimum at an intermediate composition. The compatibility of IPN was enhanced because the polymers were interlocked in a three-dimensional structure during polymerization before phase separation occurred. The phenomenon was further examined by conducting binary frontal polymerization of two miscible monomers, which polymerize by different mechanisms, in the same reactor tube.[92] The free-radical polymerization of ethylene dimethacrylate (EGDMA) with a peroxide initiator (Luperox 231) was one. The other was the aliphatic-amine curing (using Epicure 3271) of the epoxy resin diglycidyl ether of bisphenol F (DGEBF) and the cationically cured DGEBF with a boron trichloride amine complex. The velocity was weakly dependent on initial monomer concentration, indicating that both mechanisms proceed independent of each other. The dependence was predicted very well using a simple relationship involving the homopolymerization velocities, the reaction orders of each mechanism and the initial composition.

$$\text{velocity}(f) = \text{vel(100\% DGEBF)}\,(1 - f)^2 + \text{vel(100\% EGDMA)}\,f^{3/2} \qquad 1.38$$

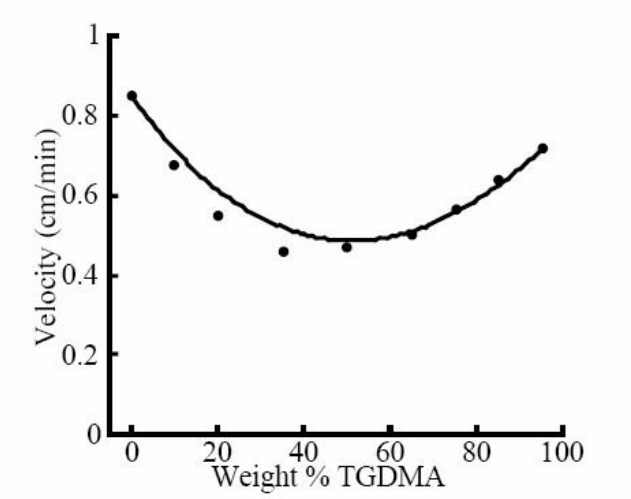

Figure 1.30. The velocity as a function of the fraction of the triethylene glycol dimethacrylate (TGDMA) in binary frontal polymerization with DGEBA cured with a mixture of amine and cationic curing agents[92]

The solid line in Fig. 1.30 is the calculated velocity from Eq. 1.38.[92] Similarly, interpenetrating polydicyclopentadiene/polyacrylate networks were recently reported by Fiori et al.[93] The rapid polymerization in a localized reaction zone allows "homogeneous" SINs for controlled *in situ* frontal polymerization of acrylic/epoxy resins.

1.3.5.2 Copolymer syntheses

Copolymerization reactions involve the simultaneous incorporation of two or more monomers in the same chain during polymerization. In linear copolymerization, the detailed microstructure and compositional heterogeneity of copolymers can have a determining influence on copolymer properties. Through copolymerization, the polymer properties are widely varied from soft, flexible elastomers to hard, stiff thermoplastics and thermoset. However, the composition of the copolymer is generally found to be

different from that in the reactant feed. These compositional drifts are incompatible and cause phase separation in bulk polymerization. To overcome this, researchers have reported the high temperature synthesis of a host of copolymers such that the azeotropic conditions are invoked.[33] This case can be called an "ideal copolymerization". FP may be beneficial as it is proposed that the small finite reaction zone and the accompanied rapid temperature rise reduces compositional drifts, thereby limiting phase separation and produce narrow chain composition distribution.

A number of monomer pairs including methyl methacrylate-methacrylic acid (MMA–MAA), acrylic acid–methacrylic acid (AA–MAA), and methacrylic acid–styrene (MAA–STY) with benzoyl peroxide (BPO) as initiator were copolymerized by Tredici et al.[94] They observed that FP tends to produce rather narrow chain composition distributions with respect to all other conventional techniques. A model was developed to simulate the front propagation process in a copolymerization system and reliability was tested by comparing its predictions, in terms of propagating velocity of polymerization front, with measured data relative to three different systems, under various operating conditions. The additional output was that styrene and MMA could be copolymerized at ambient pressure which otherwise was not possible by homopolymerization using FP.

Szalay et al.[95] took the next step in frontally synthesized copolymers to demonstrate the formation of alternating copolymers of styrene and maleic anhydride (MA). They results revealed that in FP conditions (STY/MA $\leq$1) an alternating copolymer is produced, which explores a facile way of exclusively obtaining an ordered sequence of repeating units.

Unsaturated polyesters (UPE) are widely used as components in composite materials. FP technique was also applied to obtain an unsaturated polyester/styrene resin.[96] Unsaturated polyester was prepared by condensation of MA and 1,2-propane diol (PD). This polyester was copolymerized with styrene with different initiators (AIBN, BPO or aliquat® peroxydisulfate (APS)). Effect of various input parameters was studied. They found that at critical styrene concentration (30 %), true FP exists without phase separation. FP samples had better thermal and mechanical properties over classical batch technique. The yields were also on the higher side. For further increase in mechanical properties of the copolymer styrene was replaced by hydroxyethyl acrylate (HEA) and urethane acrylate (UA).[97] Typical composition was HEA + UA (whole concentration 30 wt. %) + UPE (70 wt. %). A detailed investigation was carried by changing the ratio of the monomer concentration and initator type and concentration. It revealed that UA allows the creation of the homogeneous solution of all the reaction components and had marginal effect on front velocity.

Recently Hu et al.[98] produced urethane–acrylate copolymers using free-radical FP at the ambient pressure. The block copolymer structure of polyurethane (PU), having soft and hard segments, results from the polycondensation reaction of the PU precursor formulation. Properties of PU could be tailored by the variation of these soft/hard segments. The precursors poly(urethane–acrylate) resins are generally prepared by conventional isocyanate-polyol condensation reaction followed by creating terminal unsaturation by reaction of hydroxyethyl acrylate (HEA) with bound isocyanate linkage.[99-101] Prepolymers are either cured by a thermal curing reaction or a UV photochemical method directly from a liquid mixture. These properties are sought by the

aeronautic and automobile industries for composite materials and coatings.[101] They synthesized a urethane–acrylate macromonomer and copolymerized it with 2-hydroxyethyl acrylate (HEA). To avoid bubbles from peroxide or nitrile initiators, they used peroxydisulfate and dimethyl sulphoxide (DMSO) was used as solvent to dissolve all the reaction components. Authors determined the dependence of the front velocity and front temperature on the initiator concentration and discovered that FP could occur even with a low front temperature.

As described above Tredici et al.[94] were the first to model frontal copolymerization. Subsequent analysis was carried by Perry et al.[102] and dependence of the front velocity on the monomer feed composition and reactivity ratios was investigated. Analytical solution was given by analyzing the magnitude of the parameters and using combustion theories. Pertinent parameters of FP like front velocity, front temperature and final concentration were predicted and validated with experimental results. In experiments, monomer pairs like MMA-AAA, acryloyloxyethyltrimethylammonium chloride (AETMA)-acrylamide and AA-acrylamide were copolymerized. The expressions derived in the model matched well with experimental observations. They conjecture a maximum or minimum velocity is obtained when both reactivity ratios are less (greater) than unity. Frontal Homopolymerizaton of AETMA is not possible but its copolymerization was successful.

1.3.5.3 Hydrogels

Hydrogels are network of polymer chains that are water-swellable/soluble. Hydrogels also possess a degree of flexibility very similar to natural tissue, due to their significant water content. Frequently studied thermosensitive hydrogel is based on

solution free-radical crosslinking copolymerization of the monomer N-isopropylacrylamide and the crosslinker N,N-methylene bisacrylamide. Washington and Steinbock[103] reported the frontal synthesis of isopropylacrylamide hydrogels at high monomer and initiator concentrations. In addition to a more rapid synthesis of hydrogels, a substantial increase in the homogeneity of the microstructure of the hydrogel, with respect to the solution polymerization, was obtained. Moreover, large hydrogel samples with similar equilibrium swelling ratio can be readily produced without the effect of microaggregation and phase separation. Recently, Yan et al.[104,105] developed starch graft-poly(acrylic acid) and starch-graft-sodium acrylate/acrylamide hydrogels. The relative amounts of reaction components were varied to determine their influence on the polymerization parameters and polymer properties. Exhaustive characterization has been done. The obtained graft copolymer were better in conversion and water absorbing features than those obtained by classical batch synthesis route. In continuation of their work, they tested effect of reactor geometries on pore properties of hydrogel. The highest degree of swelling for products was obtained when the tube size (30 and 45 mm i.d.) favour the formation of porous microstructure of hydrogel.[106] The unique microstructure of hydrogels produced by FP is critical to the superior absorbing features (Fig. 1.31).

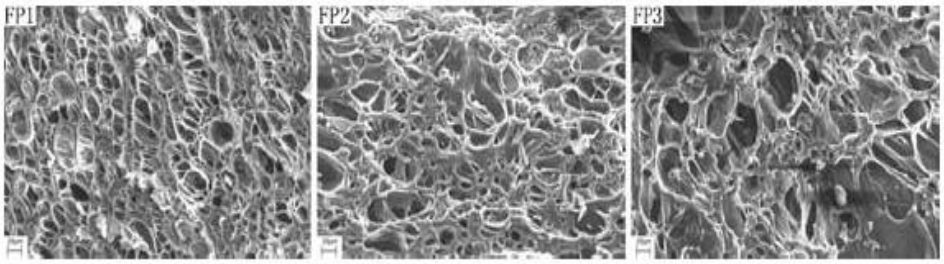

Figure 1.31. Scanning electron micrographs of hydrogels produced by frontal polymerization at different starch/AA ratios: FP1, ratio=0; FP2, ratio=0.1; FP3, ratio=0.3. The scale bar at the bottom left of each image represents 20 mm[104]

To conclude, FP can be exploited as an alternative means of hydrogel synthesis with additional advantages of short reaction times and low cost.

1.3.5.4 Filled materials and composites

Filled materials contain small fibres or particles in polymeric matrix. Interest in inorganic/organic composite materials is due to their possession of vastly diverse of properties associated with either of the separate components.[107,108] The manufacture of thick filled materials is difficult because multicomponent systems often undergo phase separation or sedimentation. At normal processing temperatures, resin viscosity is low and fillers settle causing gradients in composition and properties. This is less of a problem for thermoplastic materials because the filler is added to a viscous melt. However, thermosets formed from crosslinking monomers, require filler to be polymerized *in situ.* If mixing takes place on a lower molecular level and polymerization is swiftly achieved with concomitant crosslinking, phase separation may be kinetically controlled. There are several ways like photopolymerization and thermal curing to do this. Nagy et al.[109,110] prepared a novel material, a thermochromic composite with colour transition from 80 to 140^{o}C. Robust reversible thermosensitive composites were prepared

by uniformly dispersing a cobalt-glycerol solution in acrylamide-triethylene glycol dimethacrylate comonomer solution, supplemented with benzoyl peroxide. The metastable mixture was subjected to frontal polymerization in the form of a viscous pellet at ambient temperature and pressure. In comparison to batch studies, frontal polymerization afforded a superior composite material: batch materials were subjected to phase separation and sedimentation. Composite produced with a propagating front produced an uniform product because of the very fast reaction in the front 'froze in' the non-equilibrium phases. Conductive composite material was prepared by similar technique by FP of TGDMA and acrylamide embedding graphite and zinc powder in presence of AIBN.[52] Products obtained were homogeneous and higher conductive as compared to that prepared by bulk polymerization (Fig. 1.12). Thus, with this synthetic route, engineered multicomponent composite materials of great homogeneity are easily achievable in a shorter time period.

Polymeric products are largely used for consolidation of stone in the field of cultural heritage. Nevertheless, the main problem of polymeric compounds is related to their macromolecular nature, it being difficult for a polymer to penetrate inside the pores which may have a very small diameter. These considerations are the starting points for *in situ* polymerization. Vicini et al.[111] looked at this problem in a different way and used a reversed filled material system in which not the pre-formed polymer, but the monomer was introduced into the stone and polymerized *in situ* in a subsequent step. FP was performed inside the pores of the stone. The monomers employed in the study were fluorinated monomer, 2,2,2-trifluoroethyl methacrylate (TFEMA) because greater stability of C-F bond and water repellence and a crosslinker (HDDA). Two sets of

polymerizations viz. homopolymerization of HDDA and copolymerization of HDDA/TEEMA were conducted. In the technique, initially single monomer (HDDA) or monomer mixture (HDDA/TEEMA) was absorbed in stone due to capillary action and ascending polymerization was facilitated by heating the stone on a hot plate. As soon as ascending polymerization started, filled stone was removed from the plate to nullify the effect of homogeneous polymerization. The results, when compared with identical compositions of batch reactions, led to the conclusion that the hot front is still active in the presence of an inorganic material which partially dissipates the heat released during the polymerization. There is deeper penetration and good absorption of FP technique over the conventional. In this way, the protective and consolidating properties of the stone are improved, in respect to the traditional application method of a pre-formed polymer, which remains confined only into the more external layers.

Davtyan et al.[112] recently, reported the manganese, cobalt, zinc, nickel containing superconducting composites obtained by frontal polymerization. Dynamic mechanical properties (elastic moduli, phase angle) for superconducting (SC) polymer-ceramic composites based on $Y_1Ba_2Cu_3O_{7-x}$ SC oxide ceramic and superhighmolecular polyethylene have been investigated by FP. Work was also devoted to synthesize composites of fiberglass formed frontally with methacrylamide complexes. Solid phase FP was conducted and the transformation process was analyzed by thermal analysis and product gaseous product analysis. Periodic modes of propagation and the bistability between a polymerization mode and a combustion mode, depending on the initiating temperature, were observed. Above a critical loading of a fiberglass as a filler, front stabilized and propagated in a planar mode.

1.3.5.5 Polymer blends

Mixing two or more polymers together to produce a blend (or 'alloy') is one well established strategy to achieve a specified portfolio of physical properties, without the need to synthesize specialized polymer systems.[113] The subject is vast and has been the focus of much work, both theoretical and experimental.[114,115] Several different approaches have been used to prepare polymer blends such as melting, mixing, casting from common solvents, and template polymerization.[114] There are a few reports on blends synthesized by FP technique. Tredici et al.[116] devised a method of improving the miscibility of the polymers by freezing in the metastable state of the monomer/polymer mixture before phase separation of the two polymers could occur. The researchers reported the frontal preparation of a series of polystyrene (PSTY)-poly(methyl methacrylate) (MMA) blends from a mixture of MMA and PSTY. SEM micrographs of the PSTY-MMA blends showed spherical PSTY composition dispersed in the PMMA matrix with an average particle size of 1 μm and uniform distribution. This was attributed to the rapid reaction in the localized reaction zone of the self-propagating front. The shifts in properties also accompany the changes in molecular arrangements produced by the rise in temperature. With rapid heating, low molecular weight polymers may compatibilize on a molecular length scale. This metastable state is subsequently fossilized by crosslinking. In contrast, conventional preparation is too slow to arrest phase separation, and thereby leads to samples that separate into two distinct phases of the individual components.

1.4 Concluding Remarks

Significant advances in polymer synthesis techniques have opened the way to the development of polymers with tailored molecular architectures and physical properties.

By carefully controlling polymerization reactions, synthetically well-known polymers and crosslinked networks can be produced with novel microstructures and morphologies. Synthetic schemes are partly aimed at the development of new approaches and methods for the preparation of large molecules with defined architecture and shape. Frontal polymerization provides a versatile and facile methodology for the preparation of polymers with control of the major variables that affect polymer properties. For diverse monomer and initiator systems, well-defined polymers can be prepared with low degrees of compositional or morphological heterogeneity. Selective technologically advanced examples of various polymers are presented to authorize the adaptability and the scope of frontal polymerization.

We have so far reviewed the work of free radical or thermal frontal polymerization. However, these are not the only systems. There are two other branches, isothermal and photo or UV initiated FP, which also have matured. Apart, from these the frontal curing of epoxy resins has been investigated.[14,117] Frontal ring-opening metathesis polymerization has been successfully achieved with dicyclopentadiene and has been applied to make interpenetrating networks.[118] Mariani and coworkers[119,120] prepared polyurethanes (PUs) frontally with 1,6-hexamethylene diisocyanate and ethylene glycol and prepared interpenetrating polydicyclopentadiene–polyacrylate networks via FP. Fiori et al.[121] synthesized polyacrylate/poly(dicyclopentadiene) networks frontally. Frontal atom transfer radical polymerization has also been achieved.[122] Polyurethane acrylate-nanocomposites were also developed.[123,124] There are many potential application of the FP technique but the significant chemical and dynamical issues need to be solved.

Chapter II

AIMS & OBJECTIVES

2 Aim and Objectives

2.1 Origin and importance of task

Chapter I outlined that frontal polymerization (FP) allows syntheses of novel materials. Although an exhaustive work has been carried out in free radical FP, there is a lot of scope to explore the FP technique for a variety of systems and applications. In this work, we investigated and optimized the conditions for frontal polymerization for synthesis of various homopolymers. We also evolved a new mode called as water triggered frontal polymerization. Linear copolymers and nano/micro/macro-porous functionalized copolymer networks were also synthesized. There is either no literature or very little work reported in these areas. Investigations and optimization of frontal polymerization conditions of above synthesized products may potentially give an alternative route to the conventional synthesis. As yet there is no reported work on the effect of various parameters and nonlinear frontal regime in free-radical crosslinking copolmymerization in FP. Water triggered frontal polymerization is a novel methodology and is reported for the first time. We feel to enrich the fundamental understanding of FP process, investigations on the above mentioned types are necessary and certainly helpful.

We also observed a rich non-linear dynamics while studying our systems. Nonlinear dynamical systems are described either by a set of first order ordinary or partial differential equations, and singularities are inherently found in parameter space. These are the main causes for giving rise to branching of solutions across the parameter point. Furthermore, if we combine mass, momentum and energy transport

equations, adding reaction terms to mass balance equation gives rise to a very complex problem. The nature of wave solutions produced needs to be investigated in detail to reveal many more characteristic features of the system.

We began with experimental observations of various instabilities and pattern formation and later provided theoretical analysis to explain the same. Instabilities occurring in reaction dynamics affect the quality of polymers leading the inhomogeneity in nano, micro as well as macro structures. Inhomogeneities in polymer structures considerably affect its performance in applications. A few examples are non-porosity in the copolymer matrix used in column chromatography for metal chelation and chiral separation and imidization in acrylamide polymerization. Analysis will be useful in establishing the causes of instabilities to obtain product with uniform microstructure and morphology. Determining the conditions for occurrence of instabilities to identification of regions in parameter space where inhomogeneities can be present will make frontal polymerization more technologically sound. Understanding the causes of the same will lead to the synthesis of FP products with uniform microstructure, in a reproducible manner. The study of nonlinear dynamics itself is a fascinating field and understanding the theory of pattern formation would certainly aid in getting better insights into FP technique.

2.2. Objectives

In this chapter we intend to outline and justify the goals of this research in context of producing homo and copolymers via frontal polymerization technique and understand the fundamentals as well as instabilities involved during the process:

2.2.1 Homopolymers

This is a third chapter of the task. Although the free radical FP has been explored in a variety of systems, there is still insufficient data and results on monomers that can undergo homopolymerization. In this chapter we present the investigation on the traveling fronts of 2-hydroxyethyl methacrylate homopolymerization. The effect of various input parameters (initiator type and concentration, solvent, diluent type and concentration etc.) on. front velocity, front temperature and conversion were investigated. The polymers formed were tested for water swellability and DMF uptake. The reaction conditions for freez-thaw technique and presence of instability, if any, were studied. Similar study was aimed to conduct homopolymerization of ethylene dimethacrylate by FP technique.

2.2.2 Water triggered frontal polymerization

Hitherto, FP of acrylamide has produced imidized product. Another aim was to evolve a FP methodology to generate linear, commercially important polyacrylamide. The search for the solution yielded a new branch in FP, water triggered FP. After initiating this new branch, the task was to search for the conditions under which reaction can be triggered and to investigate the effect of various parameters, as mentioned earlier (section 2.2.1), as well as reaction variables such as type and concentration of redox couple and volume of water on measurable parameters of FP such as front velocity, front temperature, shape of front and yield.

Nonplanar frontal regime was observed with the use of few redox couples. We set our goal to see reducibility and to analyze patterns i.e. visually observed helical and

microscopically observable layered patterns. Our aim therefore was to understand the reasons for these pattern formation as well as the physio-chemical phenomenon behind it. Possibility of the scale up of the process was then investigated. We derived the empirical equations and investigated the effect of reactor geometries on scale-up of water triggered FP.

2.2.3 Copolymers

There is no report on solid state copolymerization via FP technique. The monomer pairs studied in frontally synthesized copolymers have been either liquid-liquid or liquid-solid. The composition of the copolymer is generally found to be different from that in the reactant feed. Different models have been put forth to visualize the mechanism of addition of growing chains and the factors influencing them. We aspire to investigate the validity of the reactivity ratio concept in frontal copolymerization. Monomer pairs such as i) acrylamide-potassium methacrylate, ii) acrylamide-potassium acrylate, iii) acrylamide-ammonium methacrylate, iv) acrylamide-ammonium acrylate and also some conventional pairs like styrene-methyl methacrylate, styrene-butyl acrylate, methyl methacrylate-butyl acrylate etc were copolymerized.

2.2.4 Functionalized crosslinked networks

Functionalized networks are typically synthesized as spherical beads by suspension polymerization using a combination of vinyl monomer with a high relative concentration of crosslinking multivinyl comonomer. The macroporous structure results from phase separation of an inert organic solvent (porogen) from the

discontinuous polymerizing droplet. These materials find commercial use in catalysts, enzyme immobilization, as HPLC supports, drug delivery systems, adsorbents, etc. There are no reports to produce functionalized networks by FP. Synthesis of micro/macroporous functionalized copolymer networks was investigated to obtain the conditions for the front's sustainability. The effect of varying parameters such as comonomer pairs, crosslink density, type and concentration of initiators, type and volume of porogens, type and concentration of diluents, on the FP technique parameters (mentioned earlier) were studied. The features of the polymers thus synthesized were compared with that prepared by suspension method. Divinyl monomers lead to the spin head instability under specific conditions. Another objective was to identify any instability and pattern formation, and to present the physio-chemical explanation for the same. We, for the first time, observed new types of patterns (layered patterns), observable under a microscope.

2.2.5 Characterization

Polymers synthesized by FP, and also by suspension and solution polymerization were well characterized by physical (IR, DSC, GPC, mercury porosimetry, BET surface area measurements, TG, SEM etc.) as well as chemical methods (titration, elemental analysis, solvent, non-solvent regain, picnometry etc.).

2.2.6 Pattern formation

A beauty of FP is the rich nonlinear dynamics involved in the process. The dynamics of the system is revealed as various instabilities and pattern formations. As seen in chapter I, instabilities can occur in reactions kinetics due to four reasons: the

imbalance between the heat generated in the reaction zone and heat diffused to the cold reaction mixture, dense polymer overlying the monomer, convection, and heat expansion of the medium at reaction zone. In our frontal polymerization experiments, we obtained unique helical and layered patterns. The investigation of theory of pattern formation is presented in Chapter VII. Additional motive was to develop mathematical model and to validate them with the experimentation as well as to explain the physio-chemical phenomenon of the process.

2.3 Work Method

1) Prototype laboratory scale reactor tubes were fabricated to perform the experiments. CCD camera (Nikkon Motionpro) was used to make for visual observations. For temperature measurements, thermocouples with temperature indicators were fabricated (Hitech India Ltd.).

2) Homopolymerization were carried in graduated test tubes and visual observations of front propagation were made. The reactions were initiated by heating from the top of the reactor tube.

3) Water Triggered Frontal Polymerization: Methodology for the experimental condition was same as that for the homopolymerization reactions excepting that a heat source was not used. Reactions were triggered by addition of specific trace volume of water.

4) Copolymerization experiments were carried by charging the monomers in a known quantity and freezing the reaction after the front has initiated and propagated for 50 % of the column length. By carrying this synthesis methodology, copolymer reactivity ratios were be calculated using Fineman-Ross and extended Kelen-Tudos models.

5) Functionalized copolymer networks based on glycidyl methacrylate-ethylene dimethacrylate (GMA-EGDM), 2-hydroxy ethylmethacrylate-ethylene dimethacrylate (HEMA-EGDM) were synthesized, characterized and screened for their properties (intruded pore volume, pore size and its distribution, specific surface area, morphology etc.). The systems were made progressively more complex by the inclusion of porogens, diluents and additives.

6) In every set of reaction (mentioned in 2-5) parameters such as, effect of initiator type and concentration, porogen type and volume, diluent type and weight, geometry and diameter of the reactor, initial temperature etc. were investigated. A series of reactions were thus performed for every set. Additionally, few special experiments were also performed with novel techniques (freezing, kinetic study etc.).

7) Polymers were exhaustively characterized by analytical (e.g. IR, DSC, GPC, mercury porosimetry, BET surface area measurements, TG, SEM etc.) as well as chemical methods (titration, elemental analysis, solvent, non-solvent regain, picnometry etc.).

8) Experiments on homopolymerization and later copolymerization were performed to find out temperature profile, along the axis as well as radial directions. Pattern formation phenomenon was studied mainly by optical microscopy and scanning electron microscopy. Polymer samples were carefully taken from the different parts of the rod and mounted on the stubs and sputter coated with gold. Layered patterns were analyzed for nearly 10 pieces of each sample. Helical patterns were observed by naked eyes and dimension analysis of the same was observed by the CCD camera, coupled by an image analyzing software. The simultaneous occurrence of singularities in mass,

momentum and energy transport equations in spatial direction and in parameter space gave rise to complex wave patterns which we intended to analyze using bifurcation theory and RPM and the solution were obtained using MATHEMATICA. The results give us an idea on pitch of a spiral and phenomenon of formation of spatio-temporal patterns.

In water triggered frontal polymerization, the scale-up relation was developed based on the redox polymerization kinetics and appropriate energy balance equations. Empirical models were developed and validated using experimental data points.

Chapter III

HOMOPOLYMERIZATION

3 Homopolymerization

3.1 Introduction

The hydroxyl group in poly(2-hydroxyethyl methacrylate) (PHEMA) can be derivatized to produce a wide range of polymeric reagents suited to pharmaceutical, chromatographic applications as well as to immobilize biopolymers (enzymes, antibodies, cells), encapsulate mammalian cells and other sensitive compounds.[125-133] In the form of beads, in the size of hundreds of micrometers, these are utilized as reactive supports and carriers, fillings of chromatographic columns, and in diagnostics.[125-127] Spherical particles are typically produced in an aqueous medium by the suspension radical polymerization (a major disadvantage of which is the formation of broad size distribution) or by multistep seeded polymerization.[134] The main disadvantage of these techniques is that they are highly sensitive to small changes in the numerous reaction parameters involved in the process, such as the initial solubility parameter of the system, composition of monomer mixture, type and concentration of stabilizer and initiator, temperature, etc.[125,134]

Transparent PHEMA, prepared by bulk polymerization, forms gels by entrapping water or other liquids. Polymerization in presence of a liquid diluent, below a critical concentration, leads to transparent gels. On equilibrium swelling, PHEMA attains a three dimensional rubbery state. In swollen crosslinked gels, termed ‘fishnet gels’, the crosslinks are separated by large zones of flexible polymer strands, structurally akin to typical rubber-like networks. Crosslinked PHEMA displays rubber like behaviour above the glass transition temperatures (~70-90^{o}C) or when swollen with water or polar diluents.[134]

Monomers like styrene, MMA, methacrylic acid etc. has been investigated by FP. Homopolymerization of HEMA has hitherto remained unexamined. The effect of type and concentration of the initiators, type and volume of porogens as well as diluents on sustainability of the front, front velocity and front temperature were investigated relative to percent yield, gel formation, T_g and porosity in the PHEMA formed. Additionally, instability studies reactions were conducted by freezing and supercooling the reaction mixture.

3.2 Experimental

3.2.1 Materials

Analytical grade 2-hydroxyethyl methacrylate (HEMA) was obtained from Sartomer, USA and used as received. Azobisisobutyronitrile [AIBN], (M/S SISCO, India) was recrystallized from methanol before use. Benzoyl peroxide [BPO], dicumyl peroxide [DCP], β-cyclodextrin (CD), 2-ethoxy ethyl acetate (EEA), silica gel (SG) (100-400 μm), silica sol (SS) and dimethyl formamide (DMF) were obtained from Aldrich Chemicals Ltd. and used as received.

3.2.2 Polymerization

To synthesize poly(2-hydroxyethyl methacrylate), HEMA was mixed with initiator (varying mol %) in a thick walled test tube marked in 1 mm units. Polymerization was initiated by means of solder gun till the propagation of front. Velocity, distance traveled by front per unit time (1 minute), was timed. Temperature profile was measured by inserting a K-type thermocouple in the reaction mixture (2 cm

from top and monitoring the temperature by digital thermocouple reader from Hi-Tech Scientific, India) (Table 3.1). Few reactions were performed by adding inert diluents.

To investigate the presence of instability, two special types of experiments were carried: in first, HEMA and initiator mixture was frozen using liquid nitrogen. This solid matrix was initiated via frontal polymerization by usual means. In second, HEMA was cooled at 0^{o}C for four days and then FP was carried out.

3.2.3 Purification and isolation

Homopolymers were incompletely soluble in reported solvents for PHEMA. Dimethyl formamide was used repeatedly to extract unreacted monomer, linear polymer, additives (cyclodextrin, silica gel, silica sol) and initiators at room temperature. The crude gel(s) were cut, placed in an excess of DMF containing a small amount of 1,4-benzoquinone as inhibitor, and the solvent was replaced every other day over a one week until no further extractables could be detected. The networks, after extraction, were carefully deswollen in a series of DMF-methanol mixtures of progressively increasing methanol content. They were washed several times with methanol and dried at room temperature under vacuum to constant weight. The amount of soluble polymer was determined gravimetrically by precipitating it in an excess of methanol followed by vacuum drying. The weight fraction of gel W_g was calculated as:[134]

$$W_g = \frac{g}{g + s} \qquad 3.1$$

Where, g and s are the weights of extracted network and soluble polymer, respectively.

3.2.4 Swelling measurements

The swelling measurements were carried out in water at room temperature. In order to reach the equilibrium degree of swelling, the networks were immersed in water for at least one week; the swelling equilibrium was tested by weighing the samples. To achieve a good precision, three measurements were carried out on samples of differing weights taken from the same gel. The networks were then weighed in the swollen state and dried, after a solvent exchange with methanol, as described in section 3.2.3, under vacuum to constant weight. The extent of swelling was characterized by 'q_v', the volume swelling ratio, which was calculated as:[134]

$$q_v = 1 + \frac{(q_w - 1)d_p}{d_s} \qquad 3.2$$

where, q_w is the ratio of weights of the gel in the swollen and the dry state, d_p and d_s are the densities of polymer and solvent, respectively.

3.2.5 Characterization

The pore volume was determined from water and cyclohexane regain (g/g).[139] Mercury intrusion porosimetry (Quantachrome Corp., USA) was used to estimate pore volume and pore size distribution. The equilibrium water content was determined by fully drying the samples in a vacuum oven to constant weights followed by reswelling in water. The equilibrium water content (EWC) was defined as:[137]

$$EWC\ (\%) = \frac{W_w - W_d}{W_w} X\ 100 \qquad 3.3$$

where, W_w and W_d are the weights of the fully hydrated and dry polymer gel, respectively.

Glass transition temperature of PHEMA samples, both homo and gel polymers, were measured by differential scanning calorimetry (DSC) (Mettler-4000 thermal analyzer coupled to a DSC-30S cell).

Table 3.1. Experimental conditions and observations in frontal polymerization of 2-hydroxyethyl methacrylate

Sr. No.	HEMA mol g	Initiator mol % g)	Solvent g	Test tube size mm	Front temp. °C	Front velocity cm/min	Remarks
HH1	0.077 (10.0)	1[a] (0.13)	-	12 x 150	130	0.44	Front was observed, less bubbling
HH2	0.077 (10.0)	2[a] (0.25)	-	12 x 150	127	0.63	Front ceased after propagating 30 % of the column length
HH3	0.077 (10.0)	4[a] (0.51)	-	12 x 150	128	0.92	Front ceased after propagating 30 % of the column length
HH4	0.077 (10.0)	6[a] (0.76)	-	12 x 150	-	-	Initiator was not soluble in the monomer
HH5	0.046 (6.0)	4[a] (0.30)	4.00[1]	12 x 150	121	-	No front was observed, only bubbling and homopolymerization
HH6	0.039 (5.0)	4[a] (0.27)	5.00[1]	12 x 150	120	-	No front was observed, only bubbling and homopolymerization
HH7	0.046 (6.0)	4[a] (0.30)	4.00[2]	12 x 150	39	-	Front collapsed after propagation to 0.5 cm due to extensive fingering and less bubbling
HH8	0.039 (5.0)	4[a] (0.27)	5.00[2]	12 x 150	37	-	Front collapsed after propagation to 0.5 cm due to extensive fingering and less

							bubbling
HH9	0.030 (3.85)	4[a] (0.20)	6.16[2]	12 x 150	36	-	Front collapsed after propagation to 1 cm due to extensive fingering and less bubbling
HH10	0.077 (10.0)	1[b] (0.18)	-	12 x 150	152	varying	No front was observed, extensive fingering
HH11	0.077 (10.0)	2[b] (0.37)	-	12 x 150	153	varying	No front was observed, extensive fingering
HH12	0.046 (6.0)	4[b] (0.45)	4.00[1]	12 x 150	140	varying	Extensive fingering
HH13	0.046 (6.0)	4[b] (0.45)	4.00[2]	12 x 150	148	varying	Front was collapsed after propagating 0.5 cm due to extensive fingering
HH14	0.039 (5.0)	4[b] (0.38)	5.00[2]	12 x 150	147	varying	Front was collapsed after propagating 0.5 cm due to extensive fingering
HH15	0.030 (3.85)	4[b] (0.29)	6.16[2]	12 x 150	142	varying	Front was collapsed after propagating 0.5 cm due to extensive fingering
HH16	0.077 (10.0)	1[c] (0.21)	-	12 x 150	150	varying	No front was observed, hompolymerization
HH17	0.077 (10.0)	2[c] (0.42)	-	12 x 150	180	varying	No front was observed, clear fingering was observed, hompolymerization
HH18	0.046 (6.0)	4[c] (0.50)	4.00[1]	12 x 150	152	varying	No front was observed, only extensive fingering
HH19	0.077 (10.0)	1[a] (0.13)	1[3]	12 x 150	-	-	No sustainable front
HH20	0.077 (10.0)	1[a] (0.13)	1[4]	12 x 150	169	-	Lot of fingering followed by sustaining a front till it meets polymer settled at the bottom.
HH21	0.077 (10.0)	1[a] (0.13)	1[5]	12 x 150	-	-	Front was collapsed after propagating 0.5 cm due to extensive fingering

HH22	0.077 (10.0)	1[a] (0.13)	1[3]	16 x 150	131	0.51	Slow front propagation went till completion
HH23	0.077 (10.0)	1[a] (0.13)	1[4]	16 x 150	144	0.63	Little Fingering and bubbling at the top after that clear front was seen
HH24	0.077 (10.0)	1[a] (0.13)	1[3]	18 x 150	140	0.50	Slow front propagation went till completion
HH25	0.077 (10.0)	1[a] (0.13)	1[4]	18 x 150	175	-	Front was ceased due to extensive fingering after propagating 0.5 cm.
HH26	0.14 (20.0)	1[a] (0.26)	3[3]	25 x 150	153	0.5	Slow front propagation went till completion.
HH27	0.14 (20.0)	1[a] (0.26)	3[4]	25 x 150	173	0.23	After initial bubbling and fingering, front propagates till end .
HH28	0.15 (20.0)	1[a] (0.26)	3[5]	25 x 150	128	0.25	After little localized homopolymerization, clear front was seen which went till completion
HH29	0.077 (10.0)	1[a] (0.13)	-	25 x 150	170	1.13	Front sustained after initial fingering and bubbling
HH30	0.077 (10.0)	2[a] (0.25)	-	25 x 150	171	1.12	Front sustained after initial fingering and bubbling
HH31	0.146 (19)	4[a] (0.24)	1.00[2]	25 x 150	170	0.31	Front sustained after initial fingering and bubbling
HH32	0.138 (18)	4[a] (0.22)	2[2]	25 x 150	120	0.31	Extensive bubbling but front was observed to propagate till its completion
HH33	0.15 (20.0)	1[c] (0.42)	-	25 x 150	169	-	No front was seen .Localized homopolymerization
HH34	0.15 (20.0)	1[a] + 1[b] (0.26 + 0.36)	-	25 x 150	171	0.31	Front was clearly seen but ceased after 85 % conversion

HH35	0.15 (20.0)	1[a] + 1[c] (0.26 + 0.42)	-	25 x 150	-		No FP
HH36	0.15 (20.0	1[a] (0.25)	6[6]	25 x 150	-		No front, only fingering
HH37	0.15 (20.0	1[a] (0.25)	3[7]	25 x 150	-		No reaction

HEMA: 2-hydroxyethyl methacrylate, a: Azobisisobutyronitrile [AIBN], 1: cyclohexanol, 2: 2-ethoxy ethyl acetate, b: benzoyl peroxide, c: dicumyl peroxide, 3: β-cyclodextrin, 4: silica gel, 5: silica sol (40 % silica), 6: poly(ethylene glycol) mol. Wt. 200, 7: poly(ethylene glycol) mol. Wt. 650.

3.3 Results and discussion

3.3.1 Initiator effects

The use of benzoyl peroxide (BPO) and dicumyl peroxide (DCP), as initiators, did not yield a sustainable front, but for differing reasons. BPO was studied at 1, 2, 4 mol % concentration relative to HEMA (HH10-15; Table 3.1). Fig. 3.1 shows that the front temperature, as sensed by the thermocouple, increased with BPO concentration. Front temperature is known to be dependent on initiator concentration.[14,41] However, front did not propagate due to extensive bubbling and fingering over the entire composition. Repetitive experiments at each BPO concentration indicated a 5-10 % fluctuation in the sensed temperatures. This means that thermal fluctuations exceed the temperature variations relative to BPO concentration. Benzoyl peroxide decomposes at 55^{o}C. This decomposition in viscous medium into benzoyl radical predominantly liberates carbon dioxide which is followed by coupling with the other benzoyl radical to obtain phenyl benzoate.[135]

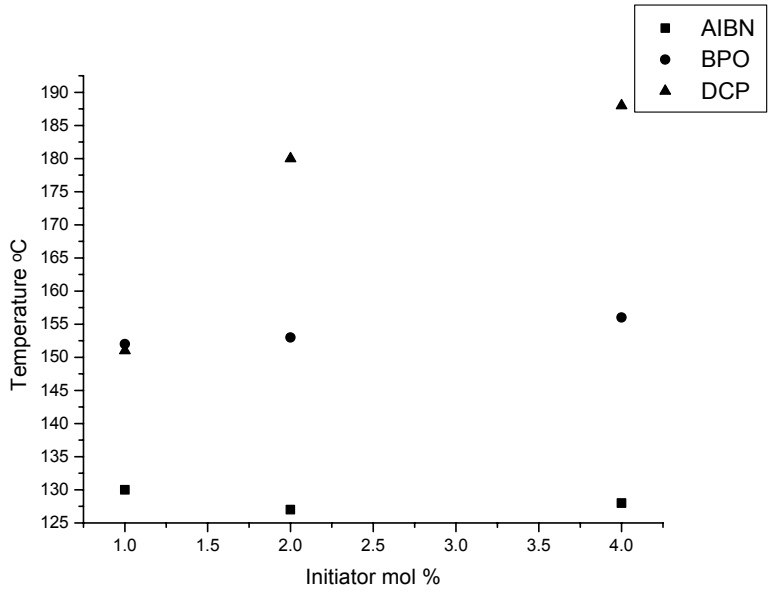

Figure 3.1. Effect of initiator concentration on front temperature

Bubble expansion causes more convection under a descending front than in a buoyancy-driven flow.[51] Total increase in pressure is twice the initial value. Another source of bubbles is the trace water invariably present in the monomer. 1 mg of water produces 2 cm^3 water vapour at front temperature (~150^oC) at 1 atmospheric pressure, which causes extensive bubbling. Further front distortion arises from convective fingering[36] (to be discussed later, 3.3.7.1). One way to eliminate these difficulties is to perform the reactions under pressure. We did not conduct the reactions under pressure because it is difficult to manage a temperature control in a pressure reactor.

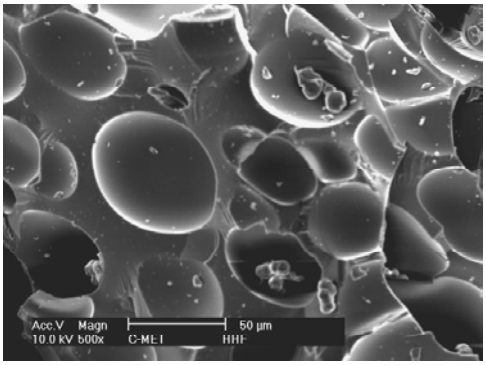

Figure 3.2. Surface morphology of polyHEMA sample observed by SEM shows the fossilized imprinting of the bubbles in the polymer sample

Excessive bubble formation is seen as poke marks (molecular imprinting) in the polymer sample. They sometime form a breath like structure. Fig. 3.2 clearly shows this kind of structures. The reason for the observed morphology is that the pressure generated during the process forces the bubble to expand and at the same time monomer tries to force from below and this causes the bubbles to burst out from the polymer matrix leaving the imprint at the surface.

The decomposition temperature of DCP is 110^{o}C. Front sustainability (activation energy of a polymerization front) depends upon the decomposition activation energy of the initiator. Only localized homopolymerization were observed at all DCP concentrations (HH16-HH18). At higher DCP concentrations fingering, with localized homopolymerization, was observed. The temperature profile however indicated an enhancement in front temperature with increasing DCP concentration (Fig. 3.1). The reason for this is that DCP, having greater thermal stability, gave a wider heat conductivity zone.[49,136] In frontal polymerization thermal wave will no longer propagate if heat loss exceeds a critical value (extinction limit). With stable initiator, front velocities

are much lower. This allows for greater amount of heat loss. This is termed as "wider heat conductivity zone".

A self sustaining front was observed when AIBN was used as initiator. The activation energy for decomposition of AIBN is the lowest amongst the three initiators investigated. An uniform, clear front was observable only at 1 mol % AIBN concentration (HH1). At higher concentrations (2 and 4 mol%), front ceased around 50 % conversion because large bubbles were formed by excessive bubbling at the front, as a result of increased nitrogen evolution. This led to a discontinuous liquid phase, thereby preventing propagation by thermal conduction (HH2-HH4). Fig. 3.1 shows that the front temperature at different concentrations of AIBN was within a narrow band in the range 127-130^{o}C. Literature reports indicate that bubble formation increases the velocity of the front at ambient pressure by as much as 25 % as compared to the fronts in identical polymerizations under the pressure.[42] Here, front velocity increased with the AIBN concentration (0.44, 0.62, 0.92 cm/min for 1, 2 and 4 mol % AIBN, respectively). At all compositions, front propagated in the form of small bubbles which migrated to the central region of front before disappearing within the polymer.

There are literature reports that mixed initiators increase the efficiency of FP.[14] AIBN: DCP and AIBN: BPO (1: 1 mol/mol) dual initiator systems were studied with HEMA (HH34-HH35). While the first combination did not yield FP, propagation was observed with the latter till 85 % of the overall run (column length).

3.3.2 Solvent effects

Frontal polymerization was investigated in presence of high boiling solvents such as cyclohexanol (160^{o}C) and 2-ethoxy ethyl acetate (156^{o}C) (EEA) using 2 and 4 mol %

AIBN. No frontal polymerization was observable at the three HEMA: cyclohexanol V/V ratio compositions investigated (HEMA: cyclohexanol: 1:1.6, 1: 0.8, 1: 0.4). Only extensive fingering was noticed (HH5-HH9; Table 3.1). At identical compositions with EEA, the front propagated very marginally prior to its collapse. This is discussed in ensuing section.

3.3.3 Effect of reactor diameter

Experiments were conducted in two test tubes of differing diameter, 18 and 25 mm, respectively. No discernable differences were noticed with BPO and DCP. With AIBN, at 1 mol % concentration (HH29), the front temperature increased with increasing diameter of the test tube (130, 135, 170^{o}C for 15, 18 and 25 mm test tubes, respectively). In the widest test tube the front propagated with bubbling and fingering.

3.3.4 Diluents

The effect of inert diluents on FP was investigated in test tubes of identical dimensions (25 x 150 mm) with AIBN at 1 mol % concentration (HH26-HH28, HH36-HH37; Table 3.1). With viscous diluents, like poly(ethylene glycol) no reaction took place as all heat was absorbed by the high specific heat viscous, inert diluent. We then evaluated the three diluents: silica gel (SG) (100-400 mesh), β-cyclodextrin (CD) and silica sol (SS) (40 % wt/v silica in water) (7 % wt/v of monomer). Diluents increase the viscosity of the medium which suppresses the instabilities.[14] Clear FPs were observed with all three diluents. It is known that increasing viscosity of the medium triggers gelation and that simultaneously the polymerization front flattens.[61] While these phenomenon were observed in the present system, an initial diminutive fingering and bubbling was noticed with silica gel.

Maximum front temperatures of 173, 153, 128^{o}C were recorded with silica gel, β-cyclodextrin and silica sol, respectively (Table 3.1). The front temperature was suppressed by silica sol due to the 60 % water. Front velocities were 0.50, 0.23 and 0.25 cm/min, respectively.

The data presented in Table 3.2 indicate maximum gel formation (W_g: 0.42) in presence of SS, due to the water. It is imperative to study the behaviour of PHEMA beads in water, for applications as implants which come in contact with blood. Thus, porous structure was characterized by water regain (g H_2O/g dry material). The water regain of PHEMA formed in presence of SG was 0.42 g/g, corresponding to an equilibrium water content (EWC) of 29.57 %. Thus, the polymers possess only gel-type microporosity (swelling porosity) and not a permanent pore structure. The particles are glassy when dry. Obviously, no phase separation occurs in glassy particles during polymerization. With CD as diluent, water regain was 1.93 g/g. This corresponds to an overall porosity of 65.87 %. We could find no explanation to describe this anomalous behaviour excepting that the large sized cyclodextrin with specific hydrophilic and hydrophobic regions generates some thing akin to a memory effect.

Table. 3.2. Effect of diluents on synthesis of poly(2-hydroxyethyl methacrylate) by FP

Diluent	Yield in %	W_g[a]	Water regain g/g	Cyclohexane regain mL/g	PV[b] mL/g	EWC[c] in %
CD	86.2	0.14	1.93	0.00	0.025	65.87
SG	87.3	0.17	0.42	0.01	0.024	29.57
SS	84.0	0.42	1.60	0.01	0.027	61.53

a: weight fraction of gel; b: pore volume by mercury porosimetry (MP); c: equilibrium water content

In contrast, in presence of SS, FP results in phase separation. The continuous medium (water) did not remain in the network, but boiled off during the polymerization and the purified and dried polymer exhibited permanent pores or holes on loss of porogen. However, the higher FP temperature resulted in smaller pores and hence larger surface area. These particles showed a water regain of 1.6 g/g, which corresponds to an overall porosity of 61.53 %. The swelling porosity is over and above the permanent porosity in the dry state.

The water absorbency ability of the all synthesized polymers in the absence of the crosslinking agent, is higher than those reported with the crosslinking agent because the former contained both soluble and insoluble parts with poor gel strength. The noncrosslinked portion dissolves in water. The insolubility of the polymer may possibly be explained by the following side reactions: a] Chain transfer to polymer may occur during the polymerization,[135] c] The occurrence of intermolecular reactions (cyclization of pendent -OH group of two molecules) that usually takes place in the polymerization of HEMA at high temperature and pH.8.

These results are interesting. The maximum reported equilibrium swelling content (EWC) of PHEMA is 39 %. The conventional approach to boost the EWC is to copolymerize HEMA with a more hydrophilic comonomer, N-vinyl-2-pyrrolidone. FP methodology is advantageous, as it directly yields a better swelling PHEMA. This is crucial to contact lens applications, since the oxygen permeability of any lens is solely governed by EWC.[137]

Internal pore volume of the three samples (synthesized using diluents) were measured by mercury intrusion porosimetry and by cyclohexane regain. Mercury

porosimetry identifies the presence of meso and macropores. The low volumes obtained (0.025-0.027 mL/g) indicate that the pores in PHEMA are not of this dimension. Gel formation in PHEMA is a consequence of the inter and intramolecular crosslinking, arising from chain transfer to the hydroxy hydrogen. This is well recorded in FP of acrylamide and is ascribed to imidization.[38] The high temperature and radical concentration causes intermolecular crosslinking due to a relative increase in the chain transfer to polymer. Porosity is a consequence of the osmotic pressure of the monomer and the gaseous products evolved during polymerization. Fig. 3.3, a graph of dV/d log P *Vs* radius (r in nm), shows the pore size distribution in PHEMA prepared using SS as diluent. Smaller pores (<15 nm) are generated. Initiator also plays a vital role in forming smaller pores. The decomposition rate of initiator increases with temperature. More free radicals are produced at higher front temperature which results in a large number of nuclei and globules. Since the monomer concentration is very nearly the same in each polymerization, the increase in number of globules translates into a decrease in pore size, at a given polymerization (front) temperature. In absence of porogen, only the void space between macromolecular chains is available for the transfer of solute molecules. The pore diameter is therefore within the range of molecular dimensions, not larger than a few nanometers. Since mercury porosimetry typically recognizes pores only in the range 10000 to 35 nm,[133] actual pore volume will be higher than that recorded, due to presence of smaller pores.

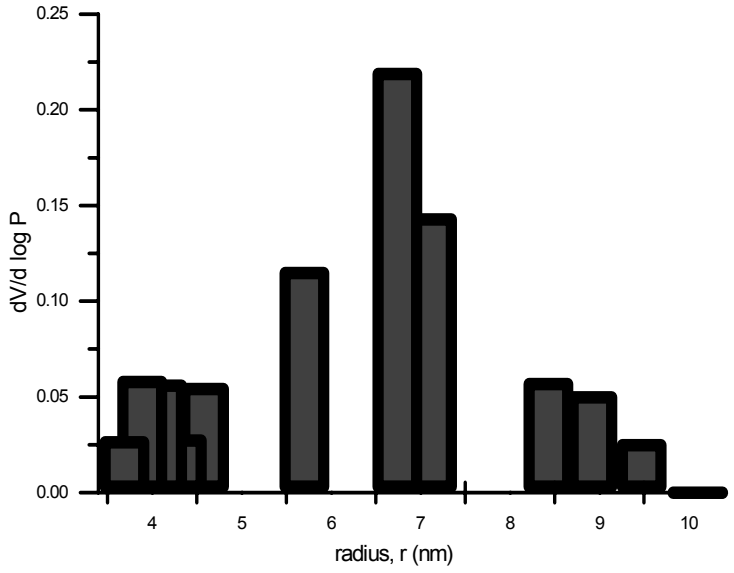

Figure 3.3. Differential pore size distribution in PHEMA gel synthesized using (40 % wt/V) silica sol as diluent

Dry porosity of PHEMA networks bears no correspondence to the swollen-state porosity. Water regain of PHEMA networks is thus always significantly higher than cyclohexane regain or the pore volume obtained from mercury porosimetry. Mercury porosimetry estimates porosity in bone-dry samples. The removal of diluent and drying collapses the expanded networks, but this is reversible and the network regains the original size on addition of water.[138] Thus, the pore volume measured by mercury porosimetry is lower than that estimated from water regain but is equivalent to the pore volume obtained from cyclohexane regain (Table 3.2).

Fig. 3.4 represents a plot of q_v *Vs* time. The swelling is governed by two separate processes: 1) water filling pores as determined by volume of the diluent, which separates from the network phase during the polymerization and 2) solvation of network chains, as

determined by volume of the diluent remaining in network structure during polymerization. The solvation depends on interaction between water molecules and segments in the polymer network. This process is characterized by the equilibrium volume swelling ratio, q_v of the network in water, if isotropic swelling is assumed the pore volume remains constant on swelling. Thus, q_v includes only the amount of water taken up by the gel portion of the network. Kinetic study shows that the gels attain equilibrium swelling in 4 hours (Fig. 3.4). The maximum equilibrium volume swelling ratio was obtained in presence of CD. The higher q_v value also indicates that the instantaneous phase separation occur at interface during the reaction.

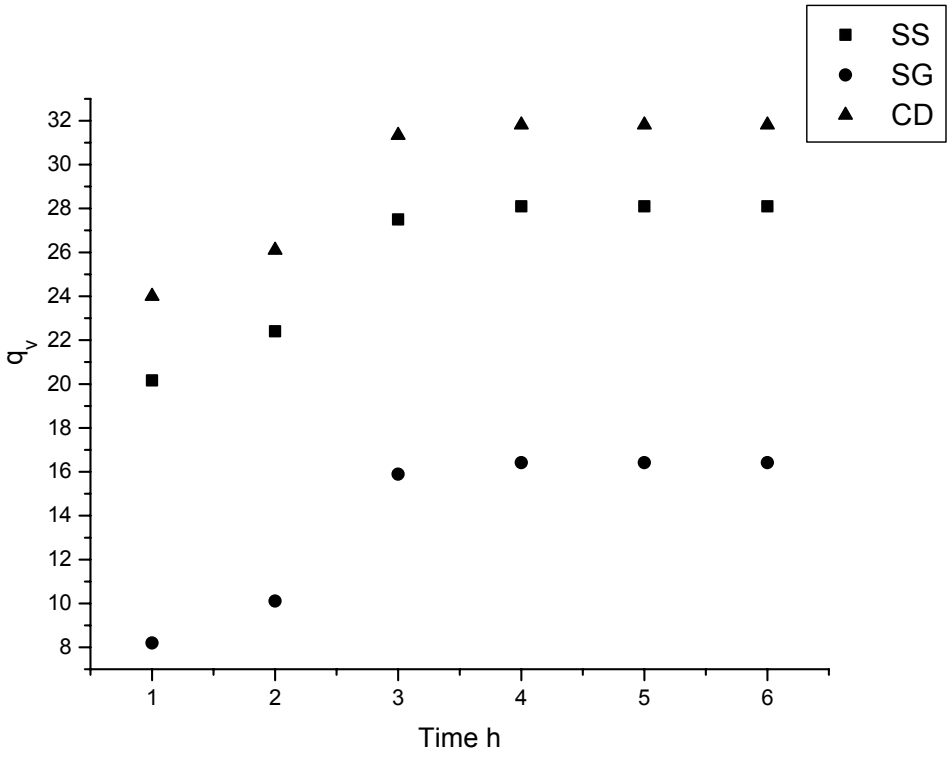

Figure 3.4. Equilibrium volume swelling ratio of PHEMA gels, formed using cyclodextrin (CD), silica gel (SG) and silica sol (SS) as diluents, as a function of time

3.3.5 Reactions at lower temperature

Reactions were attempted at lower temperatures to obtain homopolymer free from gelation. Two sets of reactions of identical compositions (1 mol % AIBN, 25 x 150 mm test tube) were conducted. In the first, polymerizing mixture was maintained at 0^oC for 4 days and in the second reaction, mixture was frozen to liquid nitrogen temperature to yield a solid matrix (freeze-thaw technique). In the former, front went to completion with bubbling. In the latter, FP was successfully triggered to yield a front propagation without fingering and extensive bubbling. Starting temperature was approximately -100^oC. Interestingly, the thermocouple recorded two maxima, one at the front temperature, 57^oC and other at 104^oC. The higher temperature is indicative that inter and probably intramolecular reactions, which are responsible for the gel formation, occurred due to instabilities. Front velocity was uneven and slow (0.5 cm/min). Small bubbles arose continuously from the bottom of the test tube. PHEMA obtained in both cases comprised of ~25-30 % gel. These results indicate that it is difficult to circumvent the facile inter and intramolecular chain transfer reactions that occur in the bulk polymerization of HEMA.

3.3.6 Other characterization

PHEMA gels synthesized using crosslinker (ethylene dimethacrylate) show higher glass transition temperature, as compared to the homopolymer. The T_g of PHEMA is quite similar to that noted for PHEMA gels prepared in the present investigation (77 *vs.* 79^oC). We did not measure the molecular weights of the homopolymers, since there is a high probability of obtaining inaccurate results due intramolecular reactions, as observed with poly(methacrylic acid).[51]

3.3.7 Instabilities

We observed two types of instabilities in polymerization of HEMA, viz. fingering and pattern formation. Fingering was first observed in FP of methacrylic acid.[45] The formation of layered patterns have been observed for the first time in this study.

3.3.7.1 Fingering

As seen in first chapter, fingering is the instability which occurs when dense polymer drops 'fingers' into the solution of cold monomer solution.[45] Pojman and Epstein[140] postulated that any exothermic traveling reaction front could cause conditions for double-diffusive (multicomponent) convection if the sum of the partial molar volumes of the products was less than the sum of the partial molar volumes of the reactants; i.e. the product solution is denser than the reactant solution. Or, it was also thought that having a thermal expansion ($\Delta_{pT} < 0$) greater than an isothermal contraction ($\Delta_{pc} > 0$) will lead to double diffusive instabilities.[45] Free radical polymerizations are exothermic and form products that are denser than the monomer. Thus, double-diffusive convection should occur in traveling fronts in a polymerization reaction. In our system, fingering was observed only when solvents were used. It was extensive with higher volume of solvent (cyclohexanol). The appearance of fingering is a function of the temperature (both of the unreacted solution and the front), density, and viscosity of the polymer solution at the front as well as the rate of front propagation. The initiator can affect all of these except the initial temperature of the solution. The fact that fingering occurs only in solvents and not in neat system is indicative that side reactions occur, increasing the activation energy and thus reducing the double diffusive instabilities. Fingering did not occur during the entire propagation**.** It would often appear immediately after a marginal propagation of

front and then fingers into the cold solution like drizzling. Fingering never occurs all the way until the front reaches the bottom of the tube. The thermal autocatalysis for the frontal polymerization takes place in the initiator decomposition step because the radical concentration primarily controls the polymerization rate. In liquid monomers, with initiators having low activation energy and at lower concentration, solvents considerably reduce the viscosity of the medium and the heat of polymerization is not sufficient to sustain the front. The dense polymer descends from the top as drizzles, destroying the 'autocatalytic action' needed to sustain and propagate the front (Fig. 3.5).

Figure 3.5. Fingering in frontal polymerization of 2-hydroxyethyl methacrylate in presence of cyclohexanol

3.3.7.2 Pattern formation

The unique observation of this study is the pattern formation. When the initial temperature was low and reactions were carried (freeze-thaw technique), clear patterns were observed for the first time (Fig. 3.6). We will give a detailed explanation of the same in the seventh chapter.

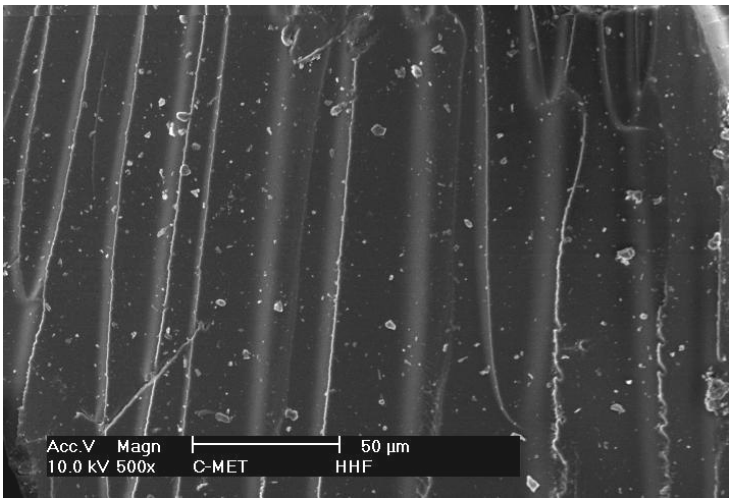

Figure 3.6. Patterns observed in FP of 2-hydroxyethyl methacrylate carried by freezing the reaction mixture

3.4 Homopolymerization of ethylene dimethacrylate (EGDM)

Ethylene dimethylacrylate is a diester formed by condensation of two equivalents of methacrylic acid and one equivalent of ethylene glycol and has the structural formula: $CH_2=C(CH_3)$-CO-O-CH_2-CH_2-O-CO-$C(CH_3)=CH_2$. This monomer is a widely used crosslinker and its polymerization leads to the formation of three-dimensional, crosslinked and insoluble structures. The main application of this monomer is also in contact lens application.[141,142]

Homopolymerization of ethylene dimethacrylate (EGDM) was carried as per the procedure given in 3.1.5. Effect of initiator type and concentration and porogen type and concentration as well as dual initiator system was evaluated on the most relevant parameters of the frontal polymerization (percent yield, front velocity, front temperature, nature of front etc.). Results are summarized in Table 3.3.

Table 3.3. Synthesis of Poly(EGDM)

Code No.	EGDM mol (mL)	Porogen mL	Initiator mol %	FV cm/min	FT ^{0}C	Yield %	Remarks
E1	0.04347 (8.2)	-	2[a] (0.14)	1.5	174	93.04	Steady and smooth front
E2	0.04347 (8.2)	-	2[b] (0.21)	1.40	167	82.60	Steady and smooth front
E3	0.04347 (8.2)	-	2[c] (0.24)	-	181	-	Slow front took long time to initiate; showed decreasing velocity and finally ceased after 60 % of column length
E4	0.04347 (8.2)	-	4[a] (0.28)	1.7	182	85.6	Steady and smooth front
E5	0.04347 (8.2)	-	4[b] (0.42)	1.52	185	89.1	Steady and smooth front
E6	0.04347 (8.2)	-	4[c] (0.46)	1.24	169	81.9	Slow front propagation;
			AIBN :DCP				
E7	0.04347 (8.2)	-	4 (0.21:0.12))	1.46	193	97.88	At the start uneven and bubbles. It flattened afterwards.
E8	0.02946 (5.84)	2.36[1]	4 (0.17:0.09)	0.51	129	94.46	In the form of small bubble propagation, varying velocity
E9	0.02946 (5.84)	2.36[2]	4 (0.17:0.09)	0.65	163	96.05	Uneven at start, flattened afterwards; no evolution of vapours or gases from the sides of the walls. Smooth reaction

a: AIBN; b: BPO; c: DCP; 1: cyclohexanol; 2: 2-ethoxy ethyl acetate

To avoid the effect of bubbles observed in homopolymerization of HEMA, we used the divinyl monomer. The idea behind using the divinyl monomer is due to the higher reactivity of this monomer at room temperature, the nucleation of bubbles is suppressed. From the Table 3.2, it is clear that we observed flat fronts in all systems. The simultaneous crosslinking reaction helps in avoiding the bubbling. With stable initiator (DCP), reaction did not go the completion due to excessive heat losses. However, with complex initiation (AIBN +DCP) reactions went smoothly and the percent yields were also very high.

3.5 Conclusion

Traveling fronts in polymerization of 2-hydroxyethyl methacrylate were studied. Series of polymerizations were conducted varying parameters such as type and concentration of initiator, solvent, test tube size, diluents etc. Only AIBN among AIBN, BPO and DCP as well as dual initiator system (AIBN: BPO and AIBN: DCP) could sustain the frontal polymerization. Cyclohexanol and 2-ethoxy ethyl acetate triggered double diffusive instabilities which distorted the front. Frontal polymerization of HEMA yielded gels. Diluents were effective in suppressing instabilities. Gels formed were characterized by water and cyclohexane regain and mercury porosimetry. Water regain was significantly higher than cyclohexane regain or pore volume as measured by mercury porosimetry. The effective water content (EWC) was much higher than that observed hitherto for PHEMA by conventional polymerization, which is advantageous in applications like contact lens. The study also revealed the first time observations of patterns at granular level. These results are discussed further in chapter VII.

Ethylene dimethacrylate was also frontally polymerized. The propagation of this monomer was more stable with less bubble formation than HEMA. This is because the highly reactive double bonds which are responsible for crosslinked structures. The crosslinked structures reduce the nucleation of bubbles. The percent yield of these polymers was also high.

Chapter IV

WATER TRIGGERED FRONTAL POLYMERIZATION

4 Water Triggered Frontal Polymerization

4.1 Introduction

Here we report a totally new mode of frontal polymerization which is triggered by simple addition of minute, specific volume of water. This experimental method paves the way to synthesize commercially pertinent homo and copolymers. New redox couple was identified to circumvent the imidization and the ensuing gelation, hitherto associated with frontal polymerization (FP) of acrylamide. Effects of reaction variables such as (i) type, (ii) concentration of redox couple and (iii) volume of water on measurable parameters of FP such as front velocity, front temperature, shape of front and yield have been studied. Two types of redox couples are reported.

Redox reactions are well documented.[143-146] Activation energies of redox polymerization reactions are typically 15 kcal/mole. The mode of attack in redox reaction are usually highly selective to form specific primary radical species.[145,146] In this way, radicals can often be produced from peroxides, at temperatures lower than those at which they thermally decompose at a convenient rate. Redox systems can be carried in aqueous solutions, suspensions and emulsions.[148-150] The special significance of redox reactions in aqueous solutions is that they proceed at high rates at relatively low temperatures, whereby high molecular weight polymers are obtained. Moreover, transfer and branching reactions are less prominent. Number of organic redox processes are useful initiators in non-aqueous media. The best known are amine-peroxide systems; particularly N,N-dimethyl aniline and benzoyl peroxide.[148-159] The main limitations in amine-peroxide systems are low polymerization efficiency and limited range of effectiveness of amines.[153,157]

Redox polymerization has not been exhaustively explored in FP. Pojman et al. demonstrated polymerization of methacrylic acid using dimethyl aniline as activator.[34] Same authors, for acrylamide polymerization, reported oxidizers and/or redox couples such as ceric ammonium nitrate, ceric ammonium sulfate, bromate/malonic acid, lead dioxide and lithium nitrate.[37]

In this chapter, we introduce redox FP of acrylamide triggered at ambient temperature and pressure by traces of water. The present work is the first report of FP using potassium peroxydisulfate in combination with a number of activators (reducing agents). Imidization is a problem in FP of acrylamide. Fortenberry and Pojman have tried to solve this problem by adding fillers (barium carbonate) to the reaction mixture.[38] We have come up with a new method for prevention of imidization, to yield commercially pertinent soluble, linear polyacrylamide.

Nonplanar frontal regime was observed in few redox couples. We could visually observe helical patterns with naked eyes, while layered patterns were observable under SEM. Additionally, micro-phase separation and heterogeneity in the polymer matrix was observed due to unreacted pockets of monomer which evolve via bulk mode. This nonlinear phenomenon is presented.

Exotic patterns formed in FP can be investigated as nonlinear phenomena. This was reviewed in Chapter I. In our experimental systems, two types of patterns were observed for the first time: (i) clearly visible helical pattern along axial direction, and (ii) the layered pattern, observed predominantly along radial direction under scanning electron microscope (SEM). Helical patterns are formed due to nonplanar front propagation (spin modes). Experimental evidence and rigorous mathematical analysis of

causes of helical patterns and factors affecting it have been well recorded in the literature.[61,62,65-71] Volpert and Spade, especially, have explained the stability of steady state reaction front propagation. They have also discussed the bifurcations of stable and unstable solutions, which can occur if interface dynamics is analyzed to determine stability of steady state spatial propagation.[62,64] On the other hand, layered pattern formation in FP has not been explored. In reaction diffusion system, Winfree[160] explained the spiral pattern formation as self-organization phenomena. Our observations also revealed the formation of complex patterns, micro-phase separation and formation of porous networks under specific conditions. Clearly, variations in reaction chemistry, that is, rate and transport parameters give rise to differing modes of spatio-temporal spin motion.

4.2 Experimental

4.2.1 Experimental part

4.2.1.1 Materials used

Analytical grade acrylamide and potassium peroxydisulfate (S. D. Chemicals, India) were recrystallized in methanol before use. Ammonium formate, potassium formate, sodium formate, sodium bisulphite, sodium thiosulfate, sodium dithionite (all from Fluka Chemicals Ltd.) were used without further purification. Potassium peroxydisulfate was purified by crystallization from methanol.

4.2.1.2 Polymerization

Potassium peroxydisulfate and reducing agent were powdered, and intimately mixed with acrylamide (recrystallized in methanol and dried) and loaded in thick-walled

test tubes (11 mm x 145 mm) marked in 1 mm units. Polymerization was triggered by addition of deionized water (25-500 μL/11.5 g reaction mixture) at room temperature ($31\pm1^{o}C$). After specific induction period (IP), dictated by concentration of redox pair and volume of water, a descending front of solid polymer formation was observable. The formation and propagation of fronts in these experiments were video taped (Red Lake Imaging; Motionpro model, 50-400 frames/s). The front velocity (rate of propagation, cm/min) and temperature profiles were measured. Effects of activator and oxidant concentration, diameter of tube and volume of water on parameters of FP such as shape of front, front velocity, temperature profile, yield were investigated.

4.3 Characterization

4.3.1 Velocity of front

A stopwatch was used to time the rate of movement of the front. A high speed CCD camera was also used to measure the distance traveled by the moving front. We related number of frames per second to the distance traveled by the front.

4.3.2 Temperature profiles

A hole (one centimeter deep) was drilled at the top of the cylindrical monomer feed with a 0.125 mm drill bit to insert a thermocouple, of diameter 0.125 mm (Hi-Tech Scientific, India). Temperature was measured as a function of time with programmable temperature controller (Hi-Tech scientific, India). The maximum temperature was averaged by taking temperatures at three different points. (top, middle and at the bottom of the test tube).

4.3.3 Percent conversions

Polyacrylamide was formed either in imidized or in unimidized state depending upon the reaction condition. Polymers presented in Tables 4.1-4.3 are the imidized one. These were crushed to a fine powder and extracted repeatedly with acetone to completely remove unreacted monomer(s). After washing, the samples were dried to a constant weight in a vacuum oven at 40^{o}C and weight of each sample was recorded.

Polymers presented in Tables 4.4-4.5 and 4.7-4.8 were completely soluble in water. These were purified by repetitive dissolution in water followed by precipitation from methanol. Percent conversions were calculated from the weights obtained after drying in a vacuum oven at 45^{o}C.

4.3.4 Elemental analysis

Elemental analysis for carbon and nitrogen were performed by Elemental Analyser, Model Elementar, Vario EL (Germany). Percentage of carbon and nitrogen were found with a precision of ± 0.02%.

4.3.5 Infra-red (IR) spectra

IR spectra of the samples were taken on a *Shimatzu* model *470* spectrometer. The samples were run in KBr pellets. The sample was milled, mixed with potassium bromide, and pressed into a solid disk of 1.2 cm diameter prior to the IR measurement.

4.3.6 Differential scanning calorimetry (DSC)

DSC analysis of polymer samples was conducted using Mettler-4000 thermal analyzer coupled to a DSC-30S cell. The sample mass was kept between 9-11 mg. Empty pans were weighed to match within a deviation of $\pm$ 0.002 mg. All samples were heated

to 200°C at 10°C/min so as to erase previous thermal history. Samples were reheated at 10°C/minute up to decomposition temperature.

Temperature calibration was made by using Indium-Lead-Zinc standard and that of heat flow by using indium standard. The thermal transitions are reported as the maxima and minima of their endothermic or exothermic peaks, respectively.

4.3.7 Determination of water content

Water content of the samples was evaluated by Karl Fisher titration coupled with an oven (Lab India Ltd., India). Samples were heated to 175°C and the moisture flushed out by nitrogen was determined using Karl Fisher reagent.

4.3.8 Gel permeation chromatography (GPC)

Molecular weights of the soluble (unimidized) polymers were determined by GPC on model Waters, Alliance in water using column TSK gel PW on polyacrylamide standards.

4.3.9 Observations

Following tables give the detailed observations of the reactions carried.

Table 4.1. Water triggered frontal polymerization of acrylamide using peroxydisulfate-dithionite redox pair

Polymer code no.	AA Mol, (g)	PP Mol, (g)	SD Mol, (g)	DI water (μL)	IP Sec	FT °C	FV cm/min	% conversion
A 1	0.1610 (11.5)	0.0016 (0.43)	0.0016 (0.32)	100	105	232	1.28	81.51
A 2	0.1610	0.0011	0.0011	100	129	207	1.21	66.02

	(11.5)	(0.31)	(0.21)					
A 3	0.1610 (11.5)	0.0008 (0.22)	0.0008 (0.16)	100	167	224	1.06	81.81
A 4	0.1610 (11.5)	0.0005 (0.13)	0.0005 (0.09)	100	164	219	0.73	78.51
A 5	0.1610 (11.5)	0.0002 (0.04)	0.0002 (0.03)	100	394	235	0.67	70.30
A 6	0.1610 (11.5)	0.0002 (0.04)	0.0005 (0.03)	75	85	240	0.78	76.20
A 7	0.1610 (11.5)	0.0002 (0.04)	0.0005 (0.03)	50	164	245	0.95	70.03
A 8	0.1610 (11.5)	0.0002 (0.04)	0.0005 (0.03)	25	117	240	0.80	84.10

AA=acrylamide; PP=potassium peroxydisulfate; SD=sodium dithionite; DI=deionized water; FT= front temperature; FV= front velocity. Reactions were conducted in 11 mm i.d. reactor tubes.

Table 4.2 Water triggered frontal polymerization of acrylamide using peroxydisulfate-thiosulfate redox pair

Polymer code no.	AA Mol, (g)	PP Mol, (g)	ST Mol, (g)	DI (μL)	IP Sec	FT °C	FV cm/min	Conversion %
A 9	0.1610 (11.5)	0.0016 (0.43)	0.0016 (0.41)	100	259	218	0.81	90.01
A 10	0.1610 (11.5)	0.0019 (0.52)	0.0019 (0.49)	100	389	205	1.33	68.4
A 11	0.1610 (11.5)	0.0013 (0.34)	0.0013 (0.32)	100	398	215	0.94	78.89
A 12	0.1610	0.0010	0.0010	100	-	-	-	No FP

	(11.5)	(0.27)	(0.25)					
A 13	0.1610 (11.5)	0.0016 (0.43)	0.0016 (0.41)	75	252	221	0.84	74.12
A 14	0.1610 (11.5)	0.0016 (0.43)	0.0016 (0.41)	50	298	235	0.85	79.54
A 15	0.1610 (11.5)	0.0016 (0.43)	0.0016 (0.41)	25	242	216	0.8	68.50

AA=acrylamide; PP=potassium peroxydisulfate; ST=sodium thiosulfate; DI=deionized water; FT= front temperature; FV= front velocity. Reactions were conducted in 11 mm i.d. reactor tubes.

Table 4.3. Water triggered frontal polymerization of acrylamide using peroxydisulfate-bisulfite redox pair

Polymer code no.	AA Mol, (g)	PP Mol, (g)	SB Mol, (g)	DI (μL)	IP Sec	FT °C	FV cm/min	conversion %
A 16	0.1610 (11.5)	0.0016 (0.43)	0.0016 (0.17)	100	47	249	1.28	84.21
A 17	0.1610 (11.5)	0.0011 (0.31)	0.0011 (0.12)	100	105	221	1.10	80.1
A 18	0.1610 (11.5)	0.0008 (0.22)	0.0008 (0.09)	100	18.56	247	1.20	80
A 19	0.1610 (11.5)	0.0005 (0.13)	0.0005 (0.05)	100	56.32	225	0.76	75.21
A 20	0.1610 (11.5)	0.0002 (0.04)	0.0002 (0.02)	100	256	248	1.09	76.10
A 21	0.1610 (11.5)	0.0002 (0.04)	0.0005 (0.02)	75	125	233	0.84	76.50
A 22	0.1610 (11.5)	0.0002 (0.04)	0.0005 (0.02)	50	397	192	0.74	69.25

A 23	0.1610 (11.5)	0.0002 (0.04)	0.0005 (0.02)	25	171	216	1.00	68.02

AA=acrylamide; PP=potassium peroxydisulfate; SB=sodium bisulfite; DI=deionized water; FT= front temperature; FV= front velocity. Reactions were conducted in 11 mm i.d. reactor tubes.

Table 4.4. Water triggered frontal polymerization of acrylamide using ammonium formate-potassium peroxydisulfate redox pair

Poly. No.	AM mol, g	AF mol, g	PP mol %, g	DI μL	Observation
A 24	0.126 (8.95)	0.021 (1.32)	0.6 (0.20)	200	IP: 8.0 min, Propagation: even Velocity: 1.8 cm/min; FT= 177°C
A 25	0.126 (8.95)	0.028 (1.76)	0.6 (0.2)	200	IP: 7.5 min, propagation: even Velocity: 1.4 cm/min.
A 26	0.126 (8.95)	0.042 (2.64)	0.6 (0.2)	200	IP: 9.0 min, propagation: even, velocity: 1.19 cm/min
A 27	0.126 (8.95)	0.084 (5.294))	0.6 (0.2)	200	IP: 16.2 min, propagation: even, velocity: 0.94 cm/min
A 28	0.126 (8.95)	0.126 (7.94)	0.6 (0.2)	200	IP: 22.0 min, propagation: even, velocity: 0.76 cm/min
A 29	0.126 (8.95)	0.126 (7.94)	1.0 (034)	500	IP: 10.0 min, propagation: even, velocity: 1.50 cm/min

AA=acrylamide; AMF=ammonium formate; PP=potassium peroxydisulfate; DI=deionised water. Reactions were conducted in 11 mm i.d. reactor tubes.

Table 4.5. Parametric studies of other reducing agent from Set II

Poly. No.	AA mol, g	RA mol, g	PP mol %, g	DI μL	IP min	Observation
A 30	0.161, (11.5)	SF, 0.027, (1.40)	0.6, (0.26)	200	32	Vigorous reaction FV= 2.8cm/min FT= 171°C
A 31	0.161 (11.5)	PF, 0.027, (1.86)	0.6, (0.26)	200	41	Vigorous reaction FV= 3.2cm/min FT= 174°C
A 32	0.028 (6.0)	AO, 0.036, (6.0)	0.3 (0.13)	200	38	Vigorous reaction FV= 1.9cm/min FT= 166°C
A 33	0.028 (6.0)	AO, 0.018 (3.0)	0.3 (0.13)	200	40	Vigorous reaction FV= 2.1cm/min FT= 174°C
A 34	0.028, (6.0)	AO, 0.009 (1.5)	0.3 (0.13)	200	42	Vigorous reaction FV= 2.4cm/min FT= 175°C

AA=acrylamide; RA=reducing agent; PP=potassium peroxydisulfate; SF= sodium formate; PF= potassium formate; DI= deionised water; IP= induction period; FV= front velocity; FT= front temperature. Reactions were conducted in 11mm i.d. reactor tubes.

4.4 Results and Discussion

The well-established classical sequential initiation, propagation and termination processes are all not exactly applicable to FP due to fast reaction rates and high reaction temperature. Additionally, quite unlike in conventional free-radical FP, the present methodology is seen to have an induction period (IP) prior to the onset of polymerization. When trace, measured quantity of water is added (25-300 μL) from the top of the reactor, temperature drops down marginally (by ~0.5°C) and is followed by an IP when

temperature is constant. Once radicals are formed (initiation), the temperature increases quite rapidly, and within 30-60 sec reaches in excess of 150^{o}C, triggering a front (propagation) by heat diffusion. The polymerization has thus two clearly discernible regions: first is IP and initiation and second is, propagation of front. The frontal polymerization experiments were conducted using oxyacids of sulfur (thiosulfate/bisulfite/dithionite) in conjunction with peroxydisulfate. These experiments were grouped together as Set I (Tables 4.1-4.3). In the other set of experiments, salts of formic acid (ammonium formate, potassium formate, and sodium formate) with peroxydisulfate redox couple was used and experiments were termed as Set II (Tables 4.4-4.5). We also simply illustrate the efficacy of potassium peroxydisulfate: ammonium oxalate as redox pair in water triggered FP, but do not provide the detailed analysis. Amongst the several pairs studied by us, we illustrate using the data observed for potassium peroxydisulfate: sodium dithionite (Set I) and potassium peroxydisulfate: ammonium formate (Set II) systems as model water triggered FP. The similar trend and reaction mechanism and effect of input parameters are valid for other systems as well.

4.4.1 IP and initiation

Aqueous peroxydisulfate solutions are known to be photosensitive and decompose into sulfate free radicals, in presence of actinic light.[144,145] In our experiments we could not trigger front formation when experiments were conducted in the dark. This indicates the need for actinic light in the initiation step. Overall, the initiation step is a complex one and consists of a series of reactions (Eqn 4.1-4.6). Transfer of electron followed by number of chemical steps is well known and follow free radical mechanism.[144] First step is decomposition of free radical at much lower temperature than its decomposition

temperature and forming a redox pair with reducing agent. Radicals are generated in this step.

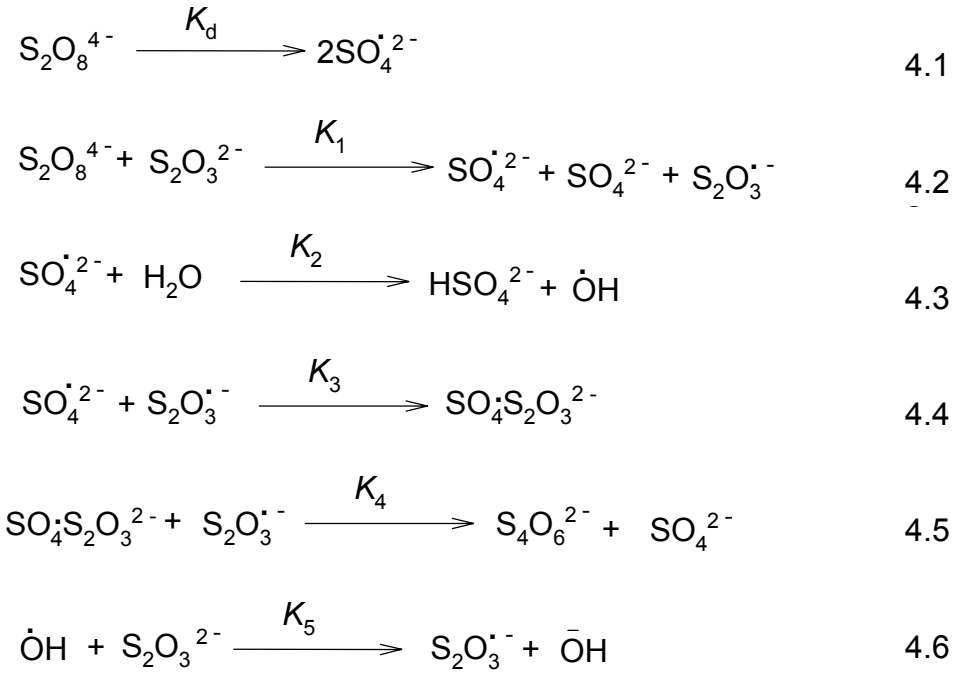

$$S_2O_8^{4-} \xrightarrow{K_d} 2SO_4^{\bullet 2-} \quad 4.1$$

$$S_2O_8^{4-} + S_2O_3^{2-} \xrightarrow{K_1} SO_4^{\bullet 2-} + SO_4^{2-} + S_2O_3^{\bullet -} \quad 4.2$$

$$SO_4^{\bullet 2-} + H_2O \xrightarrow{K_2} HSO_4^{2-} + \dot{O}H \quad 4.3$$

$$SO_4^{\bullet 2-} + S_2O_3^{\bullet -} \xrightarrow{K_3} SO_4{:}S_2O_3^{2-} \quad 4.4$$

$$SO_4{:}S_2O_3^{2-} + S_2O_3^{\bullet -} \xrightarrow{K_4} S_4O_6^{2-} + SO_4^{2-} \quad 4.5$$

$$\dot{O}H + S_2O_3^{2-} \xrightarrow{K_5} S_2O_3^{\bullet -} + \bar{O}H \quad 4.6$$

Two radicals formed can then combine with a monomer to initiate polymerization. This is the initiation step.

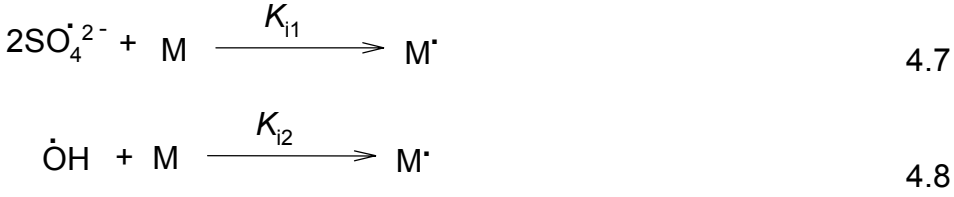

$$2SO_4^{\bullet 2-} + M \xrightarrow{K_{i1}} M^{\bullet} \quad 4.7$$

$$\dot{O}H + M \xrightarrow{K_{i2}} M^{\bullet} \quad 4.8$$

Propagation step involves addition of monomer radical to another monomer to form growing chain.

$$M^{\bullet} + M \xrightarrow{K_p} M_1^{\bullet} \qquad 4.9$$

$$M_{n-1}^{\bullet} + M \xrightarrow{K_p} M_n^{\bullet} \qquad 4.9a$$

Here n is number of monomer molecules. Propagation step continues until a termination occurs either by direct combination of two polymer radicals (4.10) or by the reaction with other radical(s) (4.10a).

$$M_n^{\bullet} + M_m^{\bullet} \xrightarrow{K_t} M_{m+n} \qquad 4.10$$

$$M_n^{\bullet} + R^{\cdot} \xrightarrow{K_t} \text{Polymer} \qquad 4.10a$$

Polymer (4.10a) is a polymer molecule, termed as dead/ inactive polymer.

The basic assumption embodied in this scheme is that thiosulfate radical ion is unreactive in initiating polymerization and this assumption is well supported by our experiments.[159] Considering steady-state principles and imposing the assumptions, thermal decomposition of thiosulfate is considered negligible hence the rate of polymerization R_p is:

i $K_4[S_2O_3^{-}] >> K_3[S\dot{O}_4^{2-}]$

ii $K_3[S_2O_3^{\bullet -}] >> K_2 + K_{i1}[M]$

iii $K_{i2}[M] >> K_5[S_2O_3^{2-}]$

iv $K_1[S_2O_8^{4-}] >> K_5[\dot{O}H]$

With these assumptions,

$$R_p = K_p (K_2/K_3)(K_1K_4)^{1/2} \frac{[S_2O_8^{4-}]^{1/2}}{[S_2O_3^{2-}]^{1/2}} [M] \qquad 4.11$$

Also applying Arrhenius Reaction kinetics,

$$K_d = K^o_d \exp(-E_d/R_gT);\ K_t = K^o_t \exp(-E_t/R_gT)$$

$$K_p = K^o_p \exp(-E_p/R_gT)$$

where R_g is the gas constant, T is the temperature of the mixture, K^o_d, K^o_p, K^o_t are the frequency factors and E_d E_p, E_t are activation energies of decomposition, propagation and termination steps, respectively.

Thus, after the primary step, sulfate free radicals react with water to produce hydroxyl free radicals. These in turn rapidly decompose the oxidizing ions. The activation energy of the reaction is 15.5 Kcal mole^{-1}.[144,145] The general mechanism is:[145]

$$S_2O_8^{2-} + S_xO_y^{n-} \longrightarrow SO_4^{-\cdot} + SO_4^{2-} + \dot{S}_xO_y^{(n-1)-} \qquad 4.12$$

$$SO_4^{-\cdot} + HOH \longrightarrow \dot{O}H + HSO_4^- \qquad 4.13$$

All three $SO_4^{-\cdot}$, $S_x^{\bullet}O_y^{(n-1)-}$ and OH radicals can initiate polymerization. But as reducing sulfoxy compounds or radicals derived from them are very good scavengers of OH radicals, polymerization is mainly initiated by sulfate radicals rather than OH or $S_x^{\bullet}O_y^{(n-1)-}$ radicals.[145] For acrylamide polymerization, Riggs and Rodriguez[149] have suggested that as acrylamide is highly reactive towards the OH radicals, initiation takes place with both sulfate and OH radicals. In our reaction, traces of water are present at the top layer (microliter). Therefore, the OH radical concentration is much lower than that of sulfate radicals.

Rate of solution polymerization of acrylamide (in tetrahydrofuran or carbon tetrachloride) has been shown to increase by addition of water but no explanation has been offered.[161] When top layer of reaction mixture is exposed to air is wetted by water, oxygen acts as cocatalyst and facilitates peroxydisulfate decomposition, which in turn triggers further redox initiation. After the IP, the exothermicity of redox initiated polymerization induces the front propagation. We confirmed catalytic action of reductant and water. In absence of water, polymerization could not be initiated. Polymerization had a very long IP (~80 min) in absence of reductant and could be triggered only at higher water volumes (>300 μL). Similarly, along expected lines, the induction time decreased with an increase in concentration of redox pair (Fig. 4.1). IP was typically between 1-6 min, depending on the composition. IP was invariant beyond 500 μL of water but displayed an oscillating behavior, in the volume range 25-300 μL. IP was least for 25 and 200 μL of water. This indicates that water acts only as an accelerator and that it evaporates/boils off during the reaction. If wetting generates the required critical radical concentration, reaction is triggered. The mechanism of radical formation in FP is measurable only indirectly by investigating the effects due to added radical scavengers. Temperature did not rise beyond 45^{o}C and propagation did not occur in reactions conducted in presence of radical scavenger (Tinuvin 770 from Ciba-Geigy).

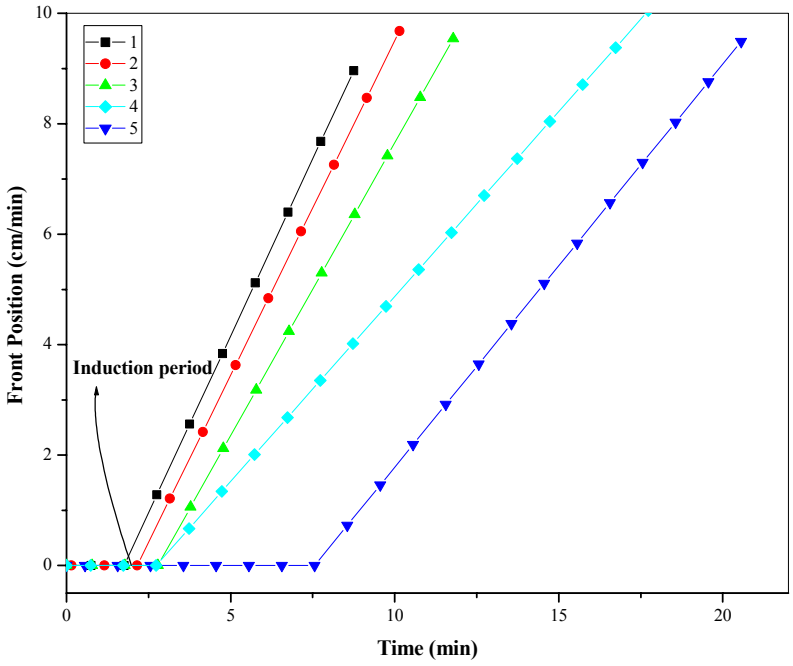

Figure 4.1. Typical plot of front position *versus* time for water triggered frontal polymerization of acrylamide (Set I; water: 100 μL, acrylamide: 0.161 mol, varying concentration of potassium peroxydisulfate: sodium dithionite redox pair. Potassium peroxydisulfate and sodium dithionite are in equimolar concentration); Concentrations of sodium dithionite (or potassium peroxydisulfate) are (in mmol): 1-1.6; 2-1.1; 3-0.8; 4-0.5; 5-0.2

With Set II redox system, the initiation step was a more complex one. The published literature is very scanty as well as contradictory. Ours is the first report of peroxydisulfate: ammonium formate as a redox pair. Shrivastava and Ghosh[162] and Kapanna[163] have investigated kinetics of the reaction between peroxydisulfate and formate ions. The activation energy was estimated to be 8.93 and 21.3 kcal mol^{-1} (for formic acid and potassium formate, respectively). The two papers express divergent views regarding the order of reaction with respect to formate ion. The peroxydisulfate decomposition is dependent on pH since hydrogen ion produces the ion and radical as follows:

$$S_2O_8^{2-} + H^+ \longrightarrow SO_4^{-\cdot} + HSO_4^- \qquad 4.14$$

Here, we may conjecture that after actinic light triggers the production of SO_4 radicals, reaction is further catalyzed by the presence of H^+ ions derived from ammonium formate. Further, oxygen from atmosphere and from decomposition of peroxydisulfate under such conditions[10a] accelerates the reaction by considerably increasing the generation of reactive radical species, thereby decreasing IP. Here also oxygen acts a cocatalyst, thereby reducing rather than increasing the IP.[146] IP varied in Set II from 6-22 min, depending on ammonium formate concentration (Fig. 4.2). IP showed a minima with respect to ammonium formate concentration. At high and at very low concentration, ammonium formate was seen to inhibit polymerization (see later). The reaction could not be triggered at lower concentration of ammonium formate. The threshold concentration for initiation of frontal polymerization was established as 0.16:1 mol/mol with acrylamide. Other reducing agents (potassium and sodium formate) in this set had IP in the range of 30-40 min (Table 4.5). This data also supports hydrogen transfer mechanism of ammonium formate, which underlies the higher catalytic efficiency of the same.

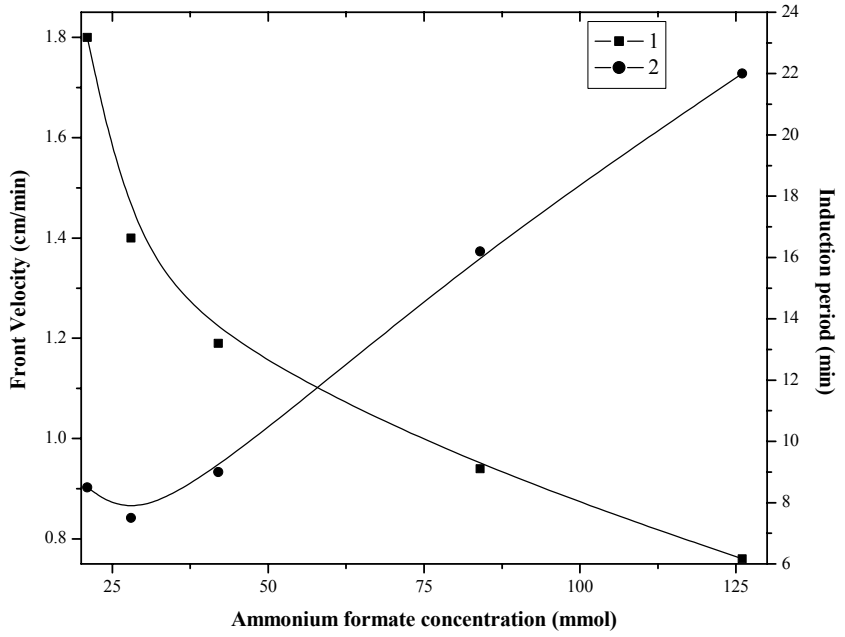

Figure 4.2. Effect of ammonium formate concentration on front velocity and induction period (Set II, water: 200 μL, acrylamide concentration varying such as total feed of the reaction mixture is 11.5 g, potassium peroxydisulfate: 0.5 mol % of acrylamide)

4.4.2 Front Propagation

Thermal decomposition of peroxydisulfate is predominant at front temperature. Rapid propagating reaction zone is followed by an ignition delay (due to heterogeneity of reaction mixture) during the preheating of the neighbouring layer. The heat is transported by conduction through gaseous and solid phases, convection through the gas phase and by radiation heat transfer. Varma et al.[164] showed that wave propagation in heterogeneous media such as combustion depends upon *local* heat transfer and kinetics. In FP, the heat wave structure is described by constant propagation of wave points (in steady state). If the particles are big and packing density is lower, water penetrates unevenly and the structure of the heat wave may get disturbed. Here, the polymerization heat wave is

dependent on the type of activator (reductant). In steady front propagation, while Set I system produced a sharp front, with liberation of ammonia (litmus test), Set II redox systems produced molten monomer region followed by a polymer solidification front (Fig. 4.3).

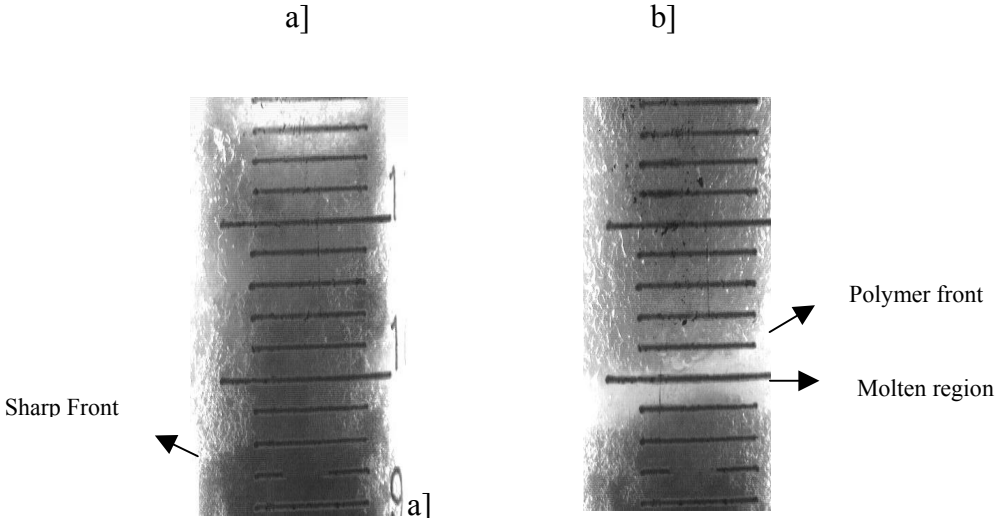

Figure 4.3. Snapshots showing the difference in nature of propagation of front between the two types of activators: a] potassium peroxydisulfate-sodium dithionite couple (water: 200 μL, acrylamide: 0.161 mol; potassium peroxydisulfate and strong activator, sodium dithionite: 0.5 mol % of acrylamide each) and b] potassium peroxydisulfate:ammonium formate redox couple (water: 200 μL, acrylamide: 0.161 mol, ammonium formate: 0.027 mol, potassium peroxydisulfate: 0.5 mol % of acrylamide)

In Set II, the front temperature recorded was around 180^{o}C. Ammonium formate decomposed at this temperature to give ammonia. Polymer front propagated in the form of small bubbles. It was observed that bubbles give little pulsation to the front. These bubbles are gases released due to higher concentration of ammonium formate. The released gases are water vapor, ammonia, carbon dioxide and the vaporized monomer. As the concentration of ammonium formate is higher than that of oxidant, the heat is partially utilized to decompose ammonium formate. As shown later, ammonium formate has a retarding effect and acrylamide melts at this temperature. The reaction rate therefore

reduces and front propagates in the form of molten layer followed by a polymerization solidification front. The width of the propagating molten monomer region was ~1 mm. This molten region penetrates into crystalline monomer. The penetration occurs either by gravitation or surface tension energy of the crystallization monomer. It is determined by the heat transfer of the media and the penetration intensity of the melted monomer into free volume occupied by air vials.[82] Due to very low activation energy required for initiation, concentration of free radicals is high in Set I system. Polymerization is, thereby very rapid and polymerization advances as a sharp front even before acrylamide can melt.

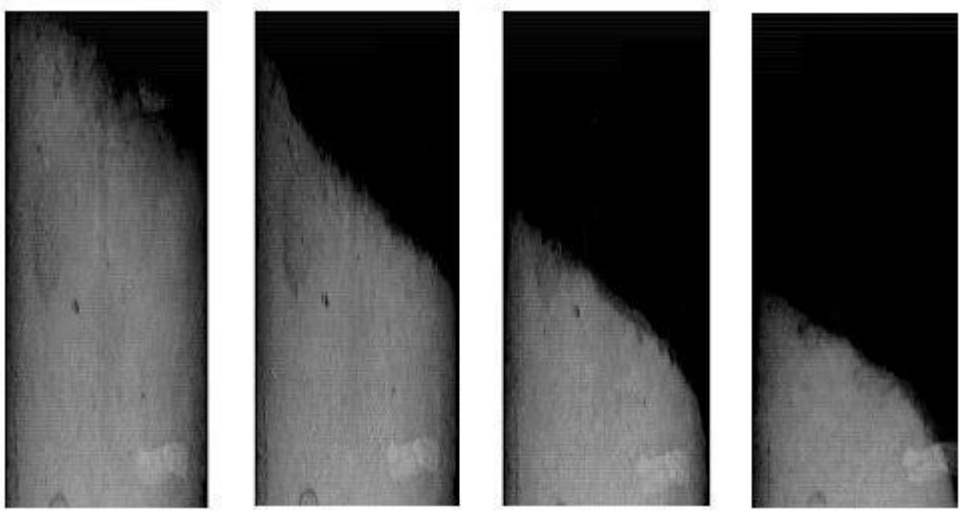

Figure 4.4. Effect of water added on front propagation. Snapshots were taken after every 2 seconds

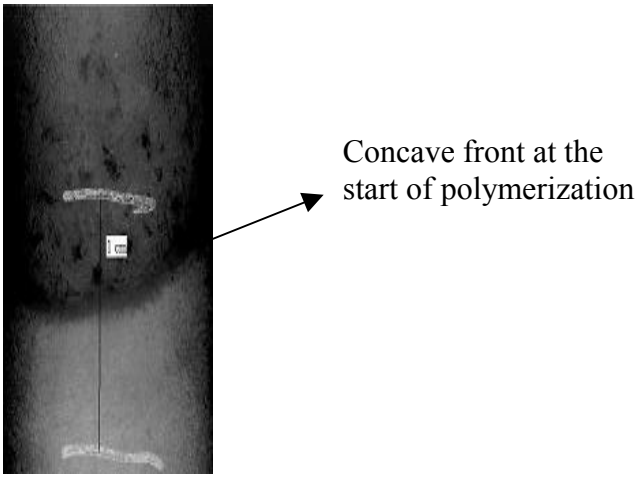

Figure 4.5. Initial concave front propagation observed in Set II polymerization systems

At the start of polymerization, the propagation of front is oscillatory and sensitive to the volume of water added as well as manner in which it is added. The packing density and pore size of the sample also play a role. Illustrative Figure 4.4 demonstrates that if higher volume of water (500 μL) is added in loosely packed monomer (0.9 g/cm^3) from the sidewalls of the tube, the front propagates in a tilted form. From figure it is clear that the tilted angle goes on reducing (from 45 to 23 ^{o}) and front attains a planar motion if the reactor length is sufficiently long. In Set II, at the start of the reaction it was observed that front propagation is actually concave (Fig. 4.5). This happens because water penetrates more at the centre if added from top of the tube at the centre. The radical concentration therefore builds up across the concave direction and front at the start becomes concave. This may or may not get stabilized, which is dependent on the packing density of the reaction mixture.

4.4.3 Front velocity and temperature

In FP, front velocity and temperature are dictated by initiator and subsequently by the concentration of free radicals.[14] In the present case, it is dependent on concentrations of oxidant and activator. An uniform velocity was observed after the IP (see Fig. 4.1 and 4.2). In both sets, front velocity were in the range 0.76 to 2.0 cm/min, dependent only on concentration of redox couple. Reactions were vigorous with very low IP. In Set II, front velocity decreased exponentially with increase in ammonium formate concentration. Other formates in Set II showed a similar behavior, but the velocities were marginally higher.

Temperature profiles were sharp in both sets but differences were noted in maximum front temperatures (Fig. 4.6). With Set I system, it was in the range 220-250^{o}C, while in Set II, it was in the range 150-180^{o}C. This temperature difference of 50-70^{o}C leads to interchain imidization in Set I polymers (scheme 4.1).

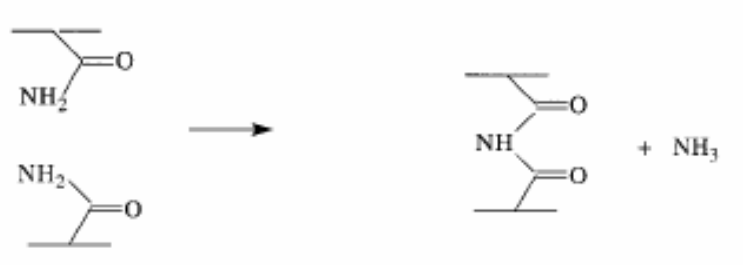

Scheme 4.1. Intermolecular imidization reaction that results in a crosslinked product

In Set I, two radicals are produced per molecule of peroxydisulfate. The energy of activation is low and rate constants are high. For this reason, the reaction has higher front velocity and temperature. This lowers selectivity and increases side reactions such as chain transfer and imidization. In Set II, ammonia has a catalytic effect while formate ion has an inhibitory effect.[162]

$$S_2O_8^{2-} + HCOO^- \longrightarrow HSO_4^- + SO_4^{2-} + CO_2 \qquad 4.15$$

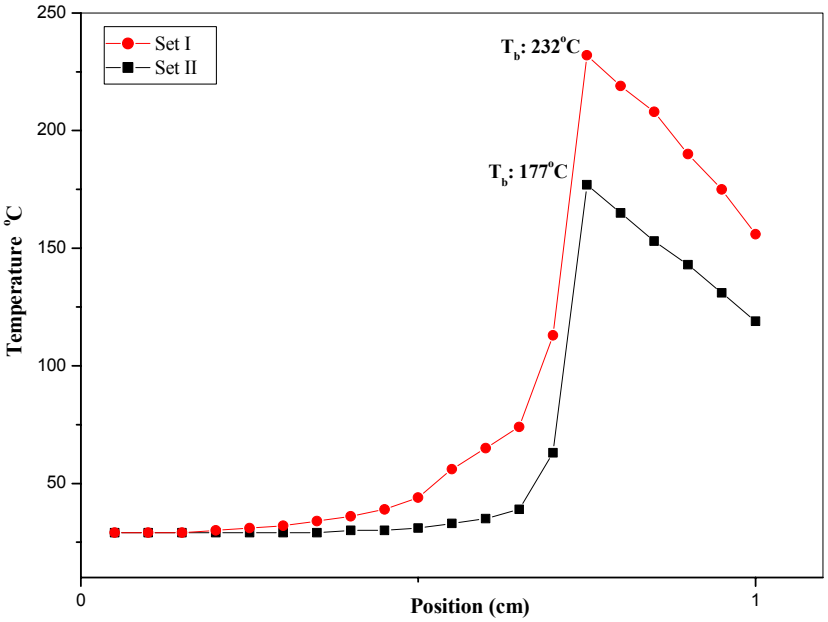

Figure 4.6. Temperature profiles of acrylamide polymerization triggered by water (water: 200 μL, acrylamide: 0.161 mol, potassium peroxydisulfate 0.5 mol % of acrylamide). Set I: reducing agent, sodium dithionite (0.0016 mol); Set II: reducing agent, ammonium formate (concentration: 0.028 mol)

One of the products in reaction 4.15, either SO_4^{2-} or HSO_4^-, is also known to inhibit the reaction to the same extent as the parent formate ion.[163] Thus, radical concentration in ammonium formate system is much lower than that in dithionite system. Moreover, ammonium formate was used in excess and thus acts as reacting diluent, adding further to the high retarding effect. All these factors suppress the concentration of reactive centres; depress the front temperature, thereby effectively preventing imidization.

We reconfirmed this by conducting the following experiment: We packed a mixture comprised of acrylamide, potassium peroxydisulfate and ammonium formate atop (2 cm) column of acrylamide and potassium peroxydisulfate. We successfully triggered polymerization with water. Polymer formed in the top 2-3 cm of the reactor was water soluble while the polymer formed below was water insoluble (due to imidization) (Fig. 4.7). This is an important observation as it reveals that it is possible to play around with concentration of ammonium formate to get the desired quality of product. This is also important in that in same reaction we could form the gradient in microstructure of polymer.

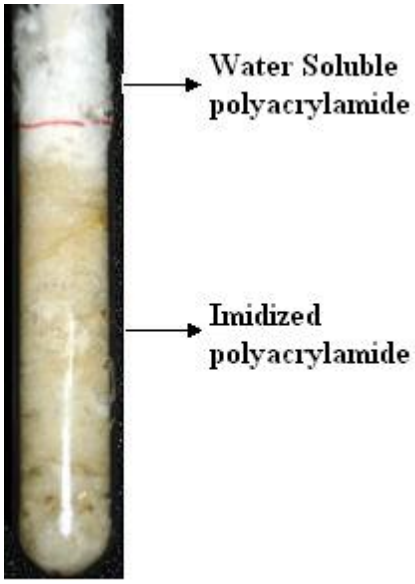

Figure 4.7. Use of ammonium formate to avoid imidization. Ammonium formate: potassium peroxydisulfate redox pair was filled along with acrylamide atop on the column of acrylamide and potassium peroxydisulfate: sodium dithionite redox pair. Gradient in microstructure of polymer formed was observed. Top portion was water soluble while bottom part was water insoluble due to imidization

4.4.4 Product

In all polymerizations of Set I, polymer rods were significantly yellowed in the centre indicating imidization. It also had an outer white skin that is formed by the evolving monomer vapors escaping at the walls of the reactor and getting polymerized there (Fig. 4.8). In a few reactions, the central core was nearly charred due to very high temperature there. Extent of imidization was noted to be 6-8%, confirming that reported by Pojman et al.[38] Elemental analysis showed the presence of sulfur in traces indicating that termination is through disproportionation.[149]

Figure 4.8. Snapshot of polyacrylamide sample showing the formation of yellowed core (due to imidization) and outer polymer skin formed due to polymerization of evaporating monomer vapors

Polymer yields were 75±10 % and 85±5 % in Set I and Set II (Table 4.1-4.6), respectively. Molar mass of polyacrylamide formed using ammonium formate:potassium peroxydisulfate system was estimated by GPC (polyacrylamide standards) to be M_w: 1.25±0.03 x 10^4 g/mol with PDI: 3±0.5. At all compositions, molar masses were

relatively independent of experimental parameters. A rise in the rate of active centre formation and chain propagation increases the overall rate of conversion of monomer to polymer. Contrary to this, an increase in the rate of termination retards this process, shortens the kinetic chain length and decreases the molecular weight of polymer. Oxygen is known to play the dual role as catalyst and inhibitor.[145,146] After initiation, oxygen acts as an inhibitor. The possible reaction mechanism is given below (scheme 4.2**)**. Additionally, there is a "burning out" effect of radicals at high temperature.[14,16] The lower conversions and molar masses observed are therefore along expected lines.

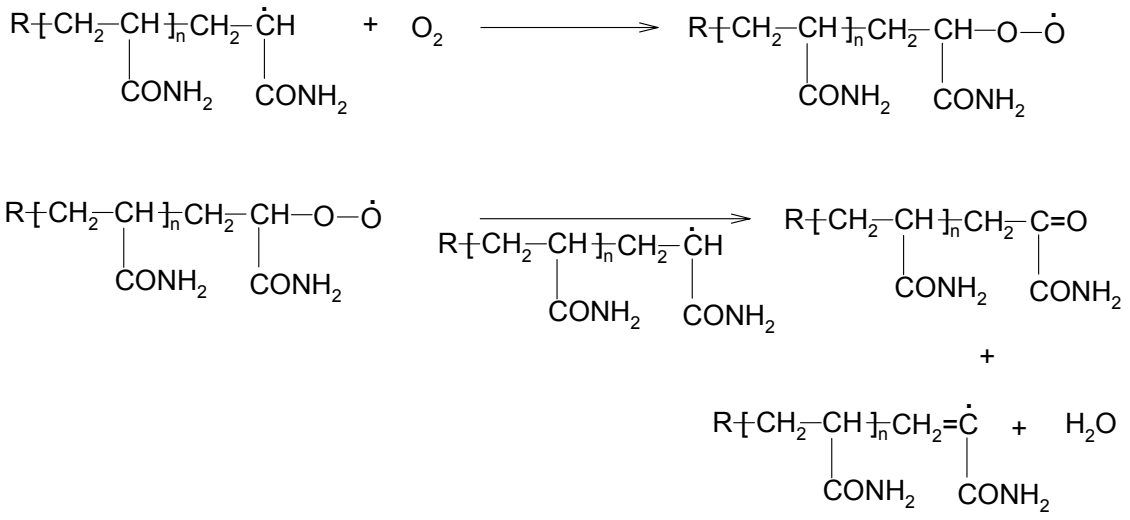

Scheme 4.2. Possible reaction mechanism of oxygen as inhibitor for growing polymer chain

4.4.5 Dynamics

As seen previously, in Set II, the propagating homogeneous molten layer was followed by a polymerization front. Further, front propagated with small bubbles, which do not allow the generation of spin modes as it reduces heat conduction in the

propagating layer. No visible instabilities were observed in set II polymers. However, slow speed of polymerization and undulation due to bubbles present at the interface of the reaction zone, gave the opportunity to form the breath like structures. Fig. 4.9 is the typical example of the breath like structure formed during the FP of acrylamide when high concentration of ammonium formate is used as a reducing agent (acrylamide: ammonium formate, 1:0.32 mol/mol).

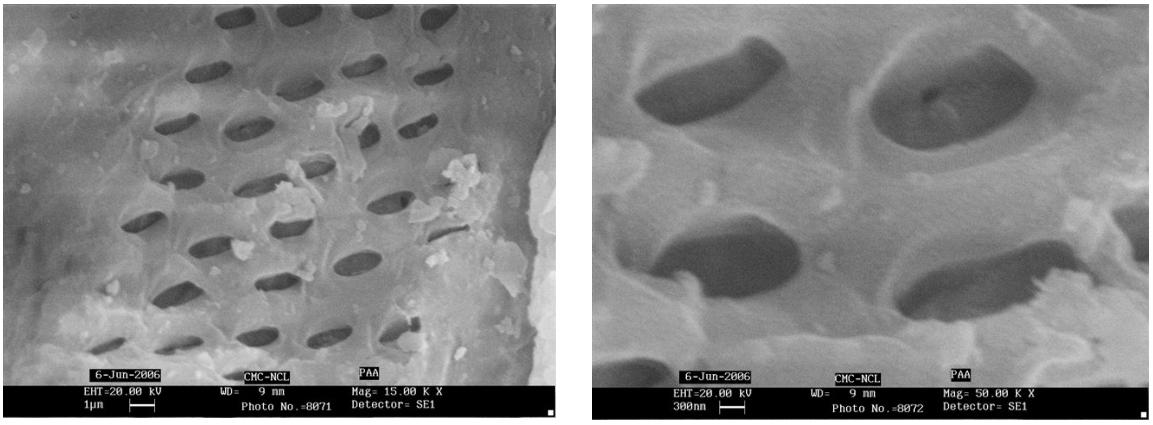

A] B]

Figure 4.9. Formation of breath figure in FP of polyacrylamide in potassium peroxydisulfate:ammonium formate redox pair

Breath figures form when a cold solid or a liquid surface is brought in contact with moist air. Moisture then condenses on the cold surface to form water droplets that grow with time, giving rise to distinct patterns on the surface.[165] The formation of spherical cavities, or 'breath figures' made by the condensation of micrometer-sized water droplets on the surface of a polymer solution that self-assemble into a well-ordered array. When moist air is in contact with cold surface (solid or liquid), moisture condenses forming water droplets that grow with time generating ordered patterns on the surface.

The hole size and the polydispersity are controlled by the solvent type, the flow rate of the condensing vapor, and the polymer concentration. Breath figures have been studied since the early 20th century by Lord Rayleigh,[166,167] Aitken,[168] and Baker[169] who reported qualitative differences in water condensation on substrates with various chemical or physical treatments. Many of the fundamental principles of breath figure nucleation and growth kinetics on solid and immiscible fluid surfaces are now relatively well understood, largely based on the work of Knobler, Beysens, and co-workers in the 1980s and early 1990s.[170-172] In the initial stages of the growth process of breath figures, the droplets grow as isolated objects with no interaction between droplets, and in the later stages growth occurs by coalescence, leading to polydispersity in their size. Beysens, Knobler, and co-workers[170,172] showed that it was possible to form an ordered array of water droplets on a liquid surface during the initial stages of the condensation. The condensed water formed arrays, or "breath figures," that evaporated to create opalescent films containing three-dimensional ordered arrays of holes. The hole size could be tuned by changing the airflow over the surface. This effect may also contribute to nanoporosity in more complex patterning schemes that also rely on evaporative drying in air.[165] Within the past decade, materials scientists have had relatively good success in utilizing breath figure structures as *self-organized templates* to build ordered macroporous films of polymers and nanocrystals.[165,173-176]

In our system, the picture is different. When the front propagates downward the gel column weight is balanced by the buoyant pressure exerted by reactant mixture below it. Front has bubbles which consists of water and monomer vapors. This front has spatial periodicity and between two periodic turns we find a small gap. Here, the bubbles come

in contact with molten monomer layer, which is a relatively cold layer. This is conducive to the growth of bubbles as it captures the moisture coming in contact with it. At the same time next helical turn is formed. Here, a polymer layer begins to emanate from helical path upon which the bubbles coming in contact leave an imprint. The decoupled motion will not have reached far enough, and hence the imprints appear upon a small helical strip (of dimensions approximately 10 micron in width) and when solidification is complete we see the breath figure formation upon samples of polymer (Fig. 4.9). We note that when heat wave traverses along helical path the bubbles on the strip ruptures and leaves behind an imprint. Since the dent, and depth of this imprint (averaging about 5 micron) is not conforming to a perfect spherical cavity we confirm that it is a rupture of bubble that caused an imprint at that site. We do not know the mechanistic details of rupture of bubbles but the imprint does have an identifiable geometric shape as described by Srinivasarao et al.[165] We feel that further study of this process is beyond the scope of present work and we limit ourselves here to giving a physico-chemical explanation. The following things need to be done in due course of time:

1] A detailed investigation on effect of various input parameters on formation of breath figures

2] The density of these structures is low. We need to formulate a system in which these structures can be formed over the entire wake of polymer.

3] To understand the dynamics of the process

4] To propose a detailed mathematical model for the system

4.4.6 Pattern formation

In Set I polymers, helical (seen by naked eyes) and layered (observed under SEM) patterns were noted and in few reactions weak and complex patterns, micro-phase separation and porosity were also noted.

Uniform helical pattern formation indicates the presence of spin modes (Fig. 4.10). The observed helical patterns along axial direction and layered pattern along radial direction (but slightly inclined to axis of motion) (Fig. 4.11) are due to nonplanar front propagation (spin modes). The detailed physico-chemical explanation of pattern formation is given in Chapter VII.

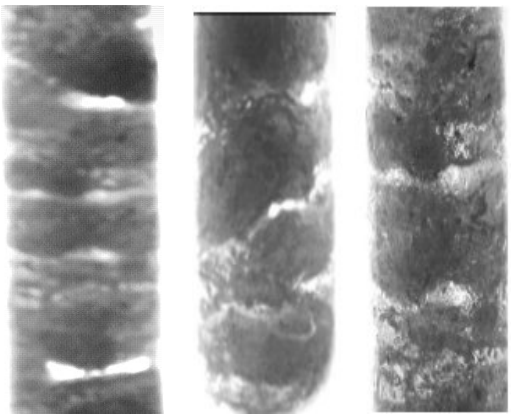

Figure 4.10. Snapshots showing helical patterns on the polyacrylamide surface (dimensions: 12 x 50 mm) in Set I redox systems

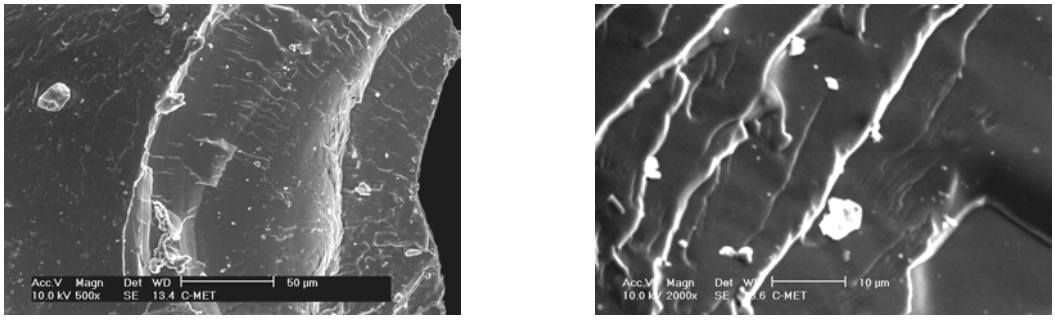

Figure 4.11. SEM surface morphology showing layered patterns on the polyacrylamide surface (dimensions: 12 x 50 mm) in Set I redox systems

With increase in reactor diameter, number of hot spots increases and front wave motion becomes more complex.[61] This was observed in our experiments. With an increase in reactor diameter and/or loose packing, additional features such as weak, complex patterns (Fig. 4.12) and micro-phase separation (Fig. 4.13a) were seen, which resulted in a porous and heterogeneous polymer matrix. This effect was extensive with excess of water (≥500 μL). When the irregularity in packed solid increases water penetrates unevenly through the crevices at the beginning and heat is easily transferred to neighboring solid layers due to conduction. The simultaneous generation of radicals at adjacent layers leads to discontinuities in spatio-temporal motion, introducing irregularities in the pattern formation. This results in unreacted micro cavities (monomer pockets), and the ensuing microphase separation may evolve via a partial bulk polymerization mode.[71]

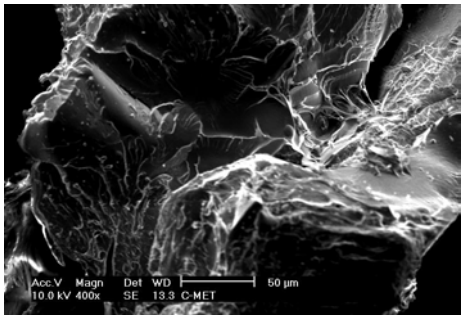

Figure 4.12. Complex pattern formation of observed in Set I polymerization with increasing diameter and loose packing

Gases released tend to escape upward creating irregular pathways and further contribute to porosity in the polymer formed. SEM photograph (Fig. 4.13b) shows the formation of interconnected porous structure in Set I polymer. Interestingly, this porosity is developed in the matrix without the use of a multi-vinyl crosslinker. The swelling ratio in water was estimated as 5.62 g/g polymer. These polymers have potential in applications like hydrogels.

a] b]

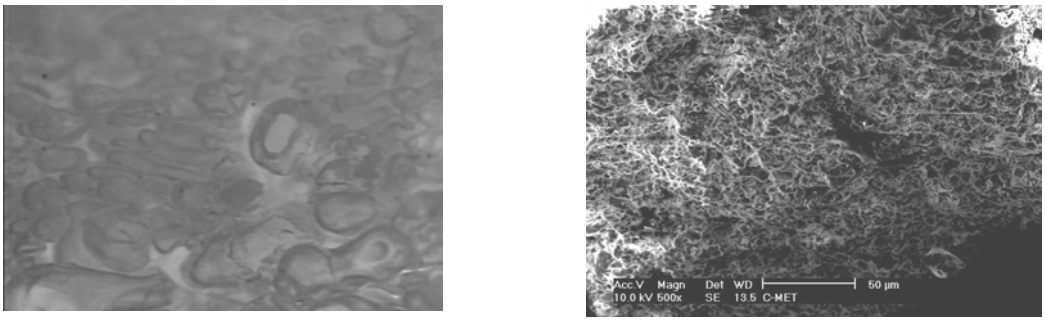

Figure 4.13. a] Micro-phase separation observed under Optical Microscopy (Olympus BX 500 image analyzer, resolution 40 X; dimensions 1 mm) (potassium peroxydisulfate:sodium thiosulfate, 8 x 10^{-4} mol each, reaction triggered by 500 µL water in a loosely packed reaction mixture); b) Representative SEM photograph of imidized polyacrylamide showing the formation of porous structure (potassium peroxydisulfate:sodium thiosulfate, 8 x 10^{-4} mol each, reaction triggered by 200 µL water)

4.5 Scale-up Criterion

There have not been very many attempts made in scaling up the frontal polymerization process. The main reason for this is the occurrence of various instabilities. As we discussed in chapter I, although instabilities are a fascinating topic of research, and vast literature is devoted to this problem, they are not desirable in polymerization. However, under given experimental conditions they are inevitable and cause steady state spatial pattern formation. As seen previously, currently four types of instabilities viz. i] thermal, ii] convective, iii] fingering (Rayleigh-Taylor) and iv] hydrodynamic instabilities have been identified in FP which severely affect the quality of polymer.[65]

The scale-up of a polymerization reaction is a step to take laboratory preparation recipe to an industrial scale for the purpose of large-scale production. As a physico-chemical phenomenon, the frontal polymerization reaction is an interfacial chemical reaction occurring as a free boundary problem. In this reaction system the mixture of monomer and initiator is transformed into a polymer gel and gaseous products try to escape through the formed gel at the interface of liquid and gel. When we devise an apparatus as a laboratory scale reaction system for the purpose of scale-up, we have to take note of the following things. The reactor is operated in a batch mode. Unlike other conventional reactors, in FP, there is no velocity effect experienced by reacting chemical species, as there are no inflow of reactants and outflow of products across the open boundaries of reaction system. However, as reactant mixture gets transformed into polymer gel the reaction front propagates at a constant velocity as is evident from experimental observations. Its effect upon scale-up should be analyzed. We are motivated by the objective of studying the role of experimentally determined rate of polymerization,

induction period and steady state, described by constant front velocity, in scaling up the reaction for commercial production of the polymeric material.

Additionally, certain facts of the physico-chemical nature are also to be noted. Since there is no velocity effect across system boundaries, problem of dispersion does not arise. Further, effect of material parameter such as surface tension is not considered here as experimental observations indicate a flat profile of front; although there is undulation of front due to gases released during reaction. It is evident from past work[14] that the front temperature, which remains constant for the reaction zone and the constant front velocity, give us the steady state of front propagating along axial direction. The steady state front velocity and temperature vary with system size and other input parameters of reaction system (e.g. initiator concentration). The system size is expressed in terms of tube length and tube diameter. But as the system size varies the steady state varies as a function of input parameters, thereby changing the performance of reaction system. This forms the basis for experimental investigation for scale-up of frontal polymerization reaction. Clearly experiments are needed to study effects of input parameters and reactor geometries. We also compare our results with laboratory scale reactor (11 x 125 mm).

As seen above, polymers from Set II, synthesized using “weak reducing agent” (ammonium formate), yielded water soluble, unimidized and pattern free polymers. Therefore, we used this system for the scale-up analysis. In first part we will increase the length of the reactor tube keeping other parameter constant and in second part, we will increase the diameter of the reactor tube. Pojman et al.[61] studied the instability in term of number of spin modes as radius of tube is varied. However, there are no reports we could find in open literature regarding its dependence up to reactor diameter to scale up the

reactor. So we experimentally studied the dependence on diameter for water triggered frontal polymerization system. Our efforts are directed towards comparing the scale up results in terms of front velocity, IP and conversion as well as molecular weight.

4.5.1 Effect of reactor length

4.5.1.1 Results

In first part we kept the diameter of the reactor constant and carried the reactions changing the parameters as per Table 4.6. Note that all reactions were performed in ~50 g batch size in 60 cm long reactor tube (i.d. 11 mm). From Fig. 4.14 we see that keeping concentration of reducing agent and volume of water added to trigger the reaction constant, as concentration of oxidizing agent is increased, at low concentrations we have higher induction time and slower front velocity (A35-A38; Table 4.6). While at higher concentrations of oxidizing agent, after attaining a low value at around 0.4 moles, the front velocity increases almost linearly from 1.06 to 1.8 cm/min and, the induction period, which does not follow the trend of front velocity, increases only marginally. This is due to the fact that induction period is a function of concentration of reducing agent and volume of water added as well as atmospheric oxygen. In this case, volume of water added is 200 μL, which causes atmospheric oxygen to dissolve in upper layer generating oxygen-induced decomposition of peroxydisulfate generating free radicals. At low concentrations of oxidizing agents the concentration of free radicals is not enough to start the front propagation. The activation energy of redox process is around 9 kcal/mol[162] which leads to specific and well defined kinetic chain lengths. At higher concentrations of potassium peroxydisulfate (oxidizing agent) higher concentrations of free radicals are generated, which are responsible for higher rates of polymerization. Induction time,

however, remains unaffected after certain concentrations. If we compare these results with laboratory scale reactor, we can find that the front velocity is increased in scaled-up process and IP is decreased marginally.

Table 4.6. Scale-up-I: water triggered frontal polymerization of acrylamide with potassium peroxydisulfate:ammonium formate pair: Effect of input parameters

Polymer code no.	AA Mol, (g)	AF Mol, (g)	PP Mol %, (g)	DI water µL	Observation
A 35	0.63 (44.75)	0.11 (6.52)	0.6 (1.0)	200	IP= 6.10 min; FV= 1.8 cm/min; FT= 177^{o}C
A 36	0.63 (44.75)	0.11 (6.52)	0.4 (0.7)	200	IP= 3.51 min; FV= 1.06 cm/min; FT= 172^{o}C
A 37	0.63 (44.75)	0.11 (6.52)	0.1 (0.4)	200	IP= 5.12 min; FV= 1.7 cm/min; FT= 162^{o}C
A 38	0.63 (44.75)	0.11 (6.52)	0.06 (0.1)	200	IP= 8.08 min; FV= 1.29 cm/min; FT= 148^{o}C
A 39	0.63 (44.75)	0.11 (6.52)	0.6 (1.0)	50	IP= 18.4 min; FV= 1.10 cm/min; FT= 143^{o}C
A 40	0.63 (44.75)	0.11 (6.52)	0.6 (1.0)	100	IP= 3.11 min; FV= 1.16 cm/min; FT= 149^{o}C
A 41	0.63 (44.75)	0.11 (6.52)	0.6 (1.0)	300	IP= 8.44 min; FV= 1.06 cm/min; FT= 151^{o}C
A 42	0.63 (44.75)	0.11 (6.52)	0.6 (1.0))	500	IP= 3.07 min; FV= 1.08 cm/min; FT= 155^{o}C
A 43	0.57	0.19	0.6	200	IP= 5.20 min; FV= 1.08 cm/min; FT= 149^{o}C

	(39.63)	(11.59)	(0.77)		
A 44	0.38 (28.15)	0.38 (23.11)	0.6 (0.51)	200	IP= 6.11 min; FV= 0.83 cm/min; FT= 124^{o}C
A 45	0.20 (14.02)	0.60 (37.80)	0.6 (0.32)	200	IP= 10.11 min; FV= 0.58 cm/min; FT= 120^{o}C; reaction ceased after propagating 80 % of the column length.

AA=acrylamide; AF=ammonium formate; PP=potassium peroxydisulfate; DI=deionised water; IP= induction period; FV=front velocity; FT=front temperature. Reactions were conducted in 11x 600 mm i.d. reactor tubes.

When we studied the effect of water addition upon steady state of front motion while keeping concentration of oxidizing and reducing agent constant (A35, A39-A38; Table 4.6), we found that the front velocity is almost constant, irrespective of water added. This confirms that role of water is only to catalyze the reaction in the initial step. This is shown in Figure 4.15. The water added does not have any effect on rate of polymerization and it only catalyzes the reaction initially and boils off during the reaction. Also, we note that the induction time and front velocity remain constant when the volume of water added exceeds 500 μL. At very low volumes (50 to 80 μL) of water, the induction time is very high. This can be attributed to inadequate wetting of upper layer causing no dissolution of atmospheric oxygen.

Figure 4.16 and A35, A42-A45 in Table 4.6 show effect of ammonium formate concentration. The melting point of ammonium formate is 119^{o}C. So, at front temperature it releases ammonia (confirmed by litmus test) and formic acid is left behind in the monomer mixture. The ammonium formate has a labile hydrogen atom. Therefore, although the reaction gets catalyzed as per the reaction mechanism shown in Eqn. 4.14 it has retarding effect. Figure 4.16 confirms this retarding effect, the perpetual increase in

IP with increase in concentration of ammonium formate. The IP was very high and the front was extinguished at 90% of column length, when the concentration was very high (0.6 mol) (A45). Similarly, as expected, front velocity decreased exponentially with ammonium formate concentration. This trend is similar to the laboratory scale reactor.

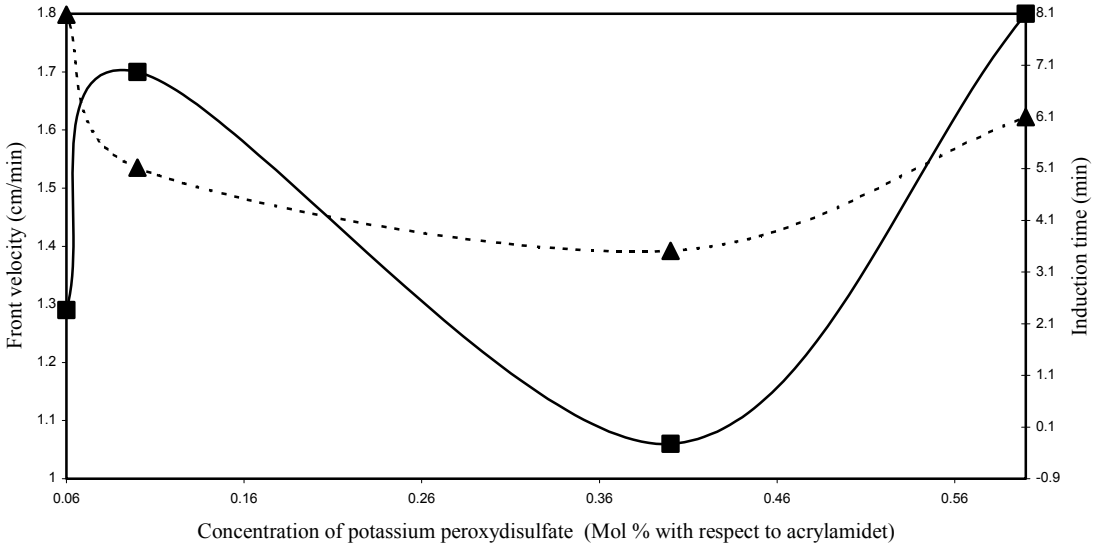

Figure 4.14. Effect of change in concentration of oxidant on induction time and front velocity

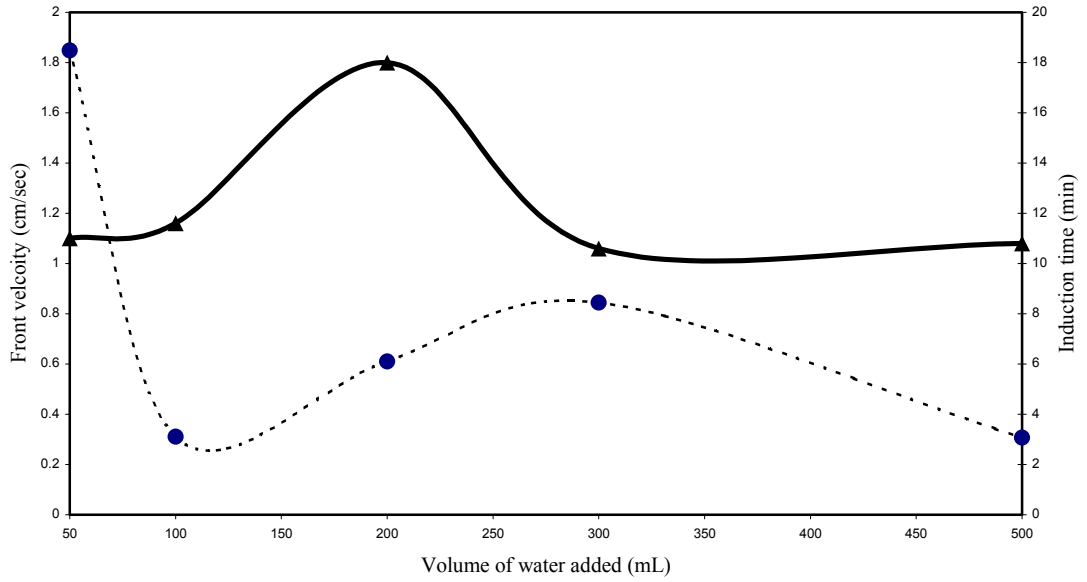

Figure 4.15.. Effect of volume of water added on front velocity and induction time

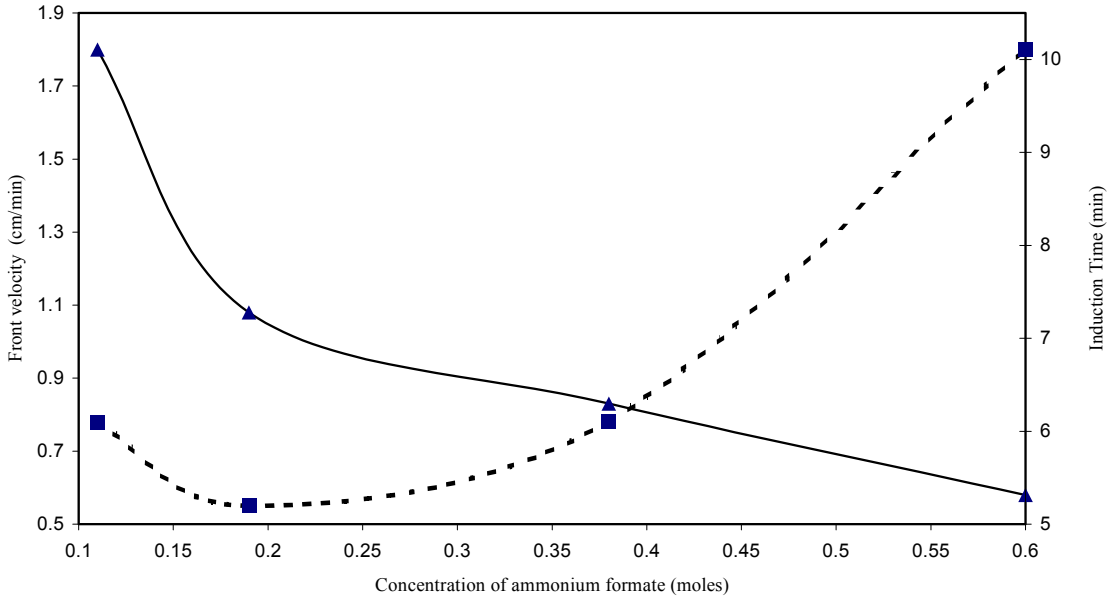

Figure 4.16. Effect of concentration of ammonium formate on front velocity and induction time

4.5.1.2 Yield and molecular weight

Percent conversion in large scaled reactor tube were marginally high (Table 4.7). All lie around ~85±5 %. The GPC analysis shows much lower polydispersity index in the scaled-up reactor. In other words, the length of the reactor has an influence on PDI. The higher PDI in laboratory reactor may be due to improper dissipation of heat leading to the shortening and branching of chains**.**

Table 4.7. Molecular weights by GPC using polyacrylamide standards

Polymer Code No.	Mn g/mol	Mw g/mol	PDI	Conversion %
A 35	6,503	11,013	1.693	88.10
A 36	6,660	11,122	1.670	89.20
A 37	6,880	10,942	1.590	81.44
A 38	6,274	10,089	1.608	88.32
A 39	9,658	14,331	1.769	79.8
A 40	9,359	12,654	1.658	81.40
A 41	6,449	11,410	1.769	88.91
A 42	6,216	11,122	1.789	86.43
A 43	7,018	12,310	1.754	84.64
A 44	10,787	14,521	1.761	86.52
A 45	-	-	-	-

Mn= no. avg. molecular weight; Mw= wt. Avg. molecular weight; PDI= polydispersity index

Thus, the increase in the length of reactor increases front velocity and reduces IP. Other factors remain same as that of laboratory scale reactions. The reason for this is

perhaps that once front attains a steady state, it becomes independent of the length it travels. Until it has a supply of radicals from the next layer it propagates. This also gives us an important inference that the rate of polymerization is pseudo zeroth order with respect to initial monomer concentration. In terms of conversion, the length of the reactor tube may be beneficial as the yields were on the higher side. Also, the length has a marked effect on PDI of polymer. In the scaled-up process, PDI came down drastically and was in the range 1.6-1.7.

Although it is difficult to correlate the above inferences leading to an actual reactor design, we note that FP can be conducive at semi scaled reactor and we conceive that virtually, at any reactor length, water triggered FP will sustain the front.

In next part, we report experiments conducted by varying the reactor diameter (Table 4.8).

4.5.2 Effect of reactor diameter

Table 4.8. Scale-up-II water frontal polymerization of acrylamide with potassium peroxydisulfate:ammonium formate pair: effect of reactor geometry

Code. No.	AA Mol (g)	AF Mol (g)	PP Mol x 10^{-3} (g)	TT mm	Observations
A 46	0.04 (3.0)	0.006 (0.37)	0.25 (0.07)	8	IP= 6.0 min; FV= 1.56 cm/min FT= 139^{o}C; % yield =86.41
A 47	0.05 (3.80)	0.009 (0.57)	0.32 (0.87)	11	IP= 10.25 min; FV= 1.66 cm/min FT= 147^{o}C; % yield =71.73

A 48	0.11 (7.93)	0.019 (1.20)	0.67 (0.18)	14	IP= 11.20; FV= 1.8 cm/min FT= 175 ^{o}C; % yield =81.66
A 49	0.20 (14.46)	0.035 (2.18)	1.22 (0.33)	16	IP= 12.00; FV= 2.22; FT= 170 ^{o}C; % yield =85.63
A 50	0.33 (23.19)	0.0555 (3.50)	1.95 (0.53)	25	IP= 47 min; FV= 3.32cm/min; FT= 169^{o}C; % yield = 88.56
A 51	0.65 (46.38)	0.11 (7.00)	3.9 (1.05)	50*	Non-reproducible results. Lot of smoking. Could not see the front propagation

AA=acrylamide; AF=ammonium formate; PP=potassium peroxydisulfate; TT=test tube inner diameter; IP=induction period; FV=front velocity; FT=front temperature. In all reactions the ratio of acrylamide to ammonium formate was kept constant i.e. 1:0.17 mol/mol. The potassium peroxydisulfate concentration was also 0.6 mol % with respect to acrylamide. All reactions were triggered by addition of 200 μL water at 31±2^{o}C.

* In this experiment, addition of 200 μL water did not yield polymerization due to insufficient wetting. Therefore, the reaction was conducted by adding 700 μL of water.

From the table (Table 4.8) and figure (4.17), it is clear that reactor diameter considerably affects the polymerization process. It was observed that both front velocity and IP increase nonlinearly with reactor diameter. Front temperature did not seem to have changed much. The reason for this is with increasing diameter, the ratio of width to length increases which increases the volume for the quantity of water added. We kept volume of water added constant (200 μL). Therefore in larger reactor diameter the inadequate wetting was obvious. When we conducted the experiments in 50 mm inner diameter tube, 200 μL of water could not initiate the reaction. Only after addition of 700 μL water, the front was initiated with a touch of smoke. We could not see the front propagation due to the dense smoke. Moreover the reaction was not reproducible and IP was inconsistent. The percent conversion and quality of product were poor (A 51).

Now, we will deal with the mathematical modeling of the process. First using the steady state assumption and known literature results, we formulate the empirical relation between the front velocity and reactor diameter. Then, using this relation we will go to the IP and solve the problem to predict the same.

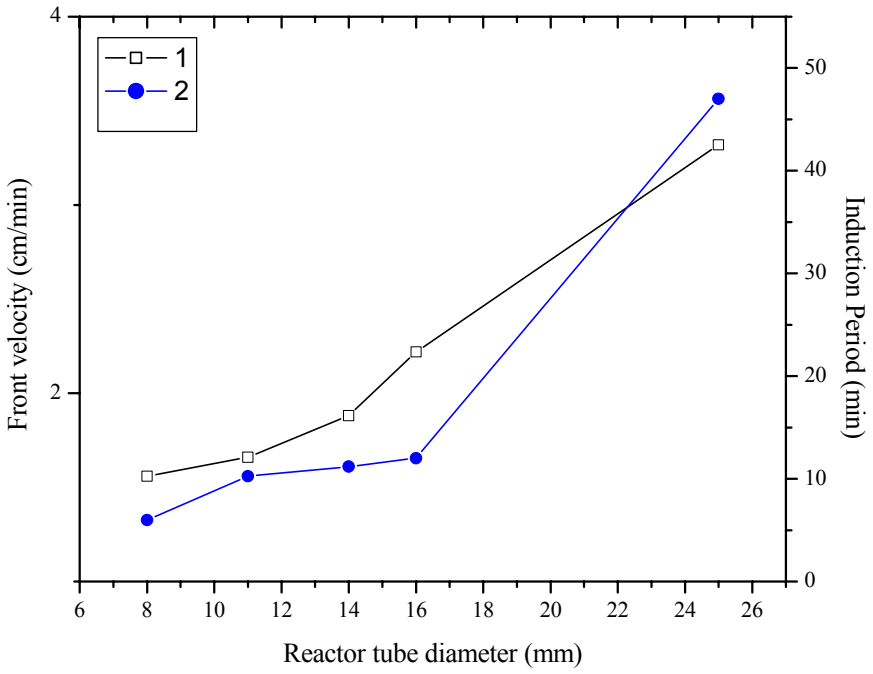

Figure 4.17. Effect of change reactor diameter on front velocity and induction period. 1: front velocity (cm/min); 2: induction period (min)

4.5.3 Mathematical model

4.5.3.1 Kinetics

In open literature no reference was found to the scale-up of this type of reaction system and reactor. Thus, we start by raising various questions and try to answer them based upon existing literature on basic mathematical models, experimental results and our

own experience related to experimental analysis of several types of FP reactions. Then, we will explain how we devised a number of experiments to obtain useful results. This will throw some light on difficulties that may be faced during scale-up and how experimental runs on a semi-pilot scale reactor can be used to strengthen our conclusions.

This reaction system has a linear kinetics and gives rise to unimidized acrylamide without any non-planar frontal regime.

The simplified kinetic model of redox polymerization has the following form:

Initiation

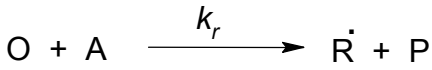

4.16

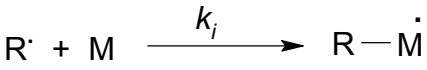

4.17

Propagation

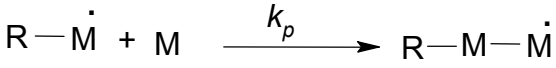

4.18

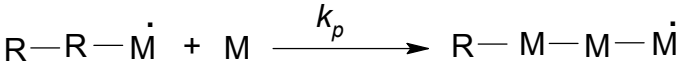

4.19

Termination

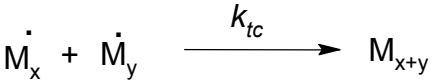

4.20

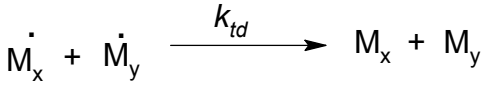

4.21

where, O and A are oxidant and reductant, respectively. $R^{\cdot}$ and $RM^{\cdot}$ are primary and secondary radicals while k_r and k_i are the rate constants for the redox reaction and

initiation steps. R-M-M$^{\cdot}$ and R-M-M-M$^{\cdot}$ etc. are the growing macroradicals, k_p is the rate constant for the propagation step, k_{tc} and k_{td} are the rate constants for the termination by combination and disproportionation, respectively.

We assume that the heat release during the first propagation step 2 and termination steps 4 and 5 are negligible, as compared to that in the propagation step 3. Then, the nonstationary two-dimensional equations describing the kinetics of the process and the heat balance for the system 4.16-4.21 take the following form:

$$\frac{d\,[R]}{dt} = K_r\,[O]\,[A] \qquad 4.22$$

$$\frac{d\,[M]}{dt} = K_p[M]\,[R\dot{M}] \qquad 4.23$$

$$\frac{d[P\,]}{dt} = K_t[RM^{\cdot}] + K_t\,[M^{\cdot}] \qquad 4.24$$

Making usual assumptions of steady state equations, we get the rate of polymerization, R_p,

$$R_p = -d[M]]/dt = k_p\left[\frac{k_r}{2k_{tc} + 2k_{td}}\right]^{0.5} [O]^{0.5}\,[A]^{0.5}\,[M] \qquad 4.25$$

The simplest model reflecting basic transport and dynamical behavior of adiabatic thermal fronts in the cylindrical geometry can be written as a heat conductivity equation with a reaction heat source along with the equation of first order reaction kinetics. Hence the energy balance is given as:[63]

$$\frac{\partial T}{\partial t} = \kappa\left(\frac{\partial^2 T}{\partial x^2} + \frac{\partial^2 T}{\partial y^2}\right) - \frac{\Delta H}{\rho c_p} k_p([M][R] + [M][P\cdot]). \qquad 4.26$$

Here, the ΔH is reaction enthalpy, ρ is the monomer density, C_p is the monomer heat capacity, k the thermal diffusivity and all concentrations are in mol L^{-1}. The Eqn. 4.26 defines a moving boundary value problem. Using a moving boundary coordinate transformation,

$$\xi = z - \phi(r, \theta, t) \qquad 4.27$$

The boundary conditions are given as:

$$\left.\begin{array}{ll} \xi \to +\infty, & T = T_0, \quad M = M_0 \\ \xi \to -\infty, & \frac{\partial T}{\partial \xi} = 0 \end{array}\right\} \qquad 4.28$$

The details can be found out in ref. 63 and detailed explanation is given in Chapter VII.

As seen earlier, water triggered FP has two distinct regions viz. IP and steady front propagation. We, therefore, formulate our problem in two regions. In the first part we derive the empirical equation of steady state front propagation and then using these results we qualitatively propose the model for IP.

4.5.3.2 Model for front velocity

As we seen earlier, the FP methodology has an IP which is determined by type of the reducing agent. However, once the front motion begins it is the thermal decomposition of peroxydisulfate that dominates the process. Ammonium formate acts as reacting diluent. So, the situation may be considered to be with two state variables. As done in the work of Spade and Volpert,[64] it is useful to consider certain limiting cases in

which the multi-step reactions scheme reduces to one-step effective kinetics, because much is known about such waves from combustion. One such limiting situation is when appreciable consumption of initiator occurs in the wake of polymerization wave and therefore does not affect the wave propagation. This is the case, for example, if the decomposition rate constant is sufficiently small. We, therefore, adopt the equation for initiator and analyze the kinetics as a two variable system. Further, we say that multiplicity due to kinetics is absent.

Apostollo and Varma[70] presented a mathematical model describing frontal polymerization as a one-step kinetic process. The model included macroscopic equations giving rate of change of concentrations of initiator, monomer and a heat energy balance with Laplacian operator term multiplied by thermal diffusivity. This spatial dependence plays the key role in giving rise to constant spatial pattern, which descends at a constant velocity. We found that the generic elementary reactions in his work are identical to our reaction scheme assuming that the reducing agent is retarder or inert, the production of radicals and the oxidant assumes the role of initiator for further polymerization reaction. Hence, we used the steady state equation in their work to predict the front velocity given experimental data on initiator concentration, kinetic data, and reaction conditions.

$$V_f = \left[\frac{2RT_{AD}^2 \lambda k_P^0 \sqrt{\frac{k_I^0}{k_T^0}} \sqrt{2I_0}}{(-\Delta H_P) M_0 (2E_P - E_T + E_I) \times \exp\left(\frac{2E_P - E_T + E_I}{2RT_{AD}}\right)} \right]^{1/2} \qquad 4.29$$

In our first numerical calculations, we kept the diameter of reactor tube (system size) constant, varied other input parameters (Table 4.6) and calculated the front velocity.

The data used for the calculation is given in Tables 4.9 and 4.10. These computed values were compared with the experimental values. We found that the prediction by steady state model is satisfactory. From the Table 4.8, where we conducted the experiments with varying the diameter of the reactor tube, we found that the steady state model in Eqn. 4.29 was not able to account for effect of change in diameter of reactor tube. Therefore, we assume a power law variation[177] with respect to (w.r.t.) radius of reactor tube as a multiplying factor to right hand side of Eqn. 4.29. This implies that we have adopted an empirical approach.[177] as a standard data fitting model to study variation of a variable w.r.t. a parameter. According to power law model the correlated velocity is given by a product of predicted velocity (as in Eqn. 4.29) and scaling factor, which is a power law model.

$$\text{Correlated velocity} = \text{predicted velocity (Eq. 4.27)} \times a \times R^{b} \qquad 4.30$$

Where R is the radius of reactor tube and a, b are constants in power law model. Using nonlinear fitting tool in symbolic manipulator (MATHEMATICA) we obtained the constants in power law model as, a= 2.6754, b= 1.2328. Now using the scaled model we see that prediction is satisfactory as seen from Fig. 4.18. However, the results are not satisfactory at smaller diameter reactor tube (8 mm) because of the excessive and unpredictable radiational and convective heat losses.

We thus conclude that the scaled steady state model prediction varies with power law exponent as 1.2328. In next phase of analysis, we try to predict the induction time before temperature rises steeply and polymerization reaction begins and front propagates. So, we use simple scale-up analysis. The exponent in power law model (1.2328) is close to 1 indicating a weak nonlinear variation w.r.t. radius of reactor tube.

Table 4.9. Parameter values used for numerical calculations[70,178]

Parameter	Values
C_p (j/g k) at 298 K	1.20
ρ (g/cm^3)	1.14
λ (J/s cm K)	1.96 e^{-3}
C_M (at 298 K)	0.12 e^4
$(-\Delta H_p)$ (J/mol)	81.50 e^3
E_p (J/mol)	18.80 e^3
k_p (mol/s) at 298 K	6 e^3
k_t (mol/s) at 298K	3.3
k^o_p (cm^3/mol s)	6.20 e^8
E_t (J/mol)	12.50 e^3
E_{ove} (J/mol)	70 e^3
k^o_t (cm^3/mol s)	9.50 e^{11}
T_{AD} (K)	696
T_C (K)	712
R_g (J/mol-K)	8.314

Table 4.10 Parameter values for potassium peroxydisulfate[178]

Parameter	Values
K_d (s^{-1}) at 298 K	3 e^{-4}
K^o_I (l/s)	3.2 e^{16}
E_I (J/mol) at 298 K	140.2 e^3

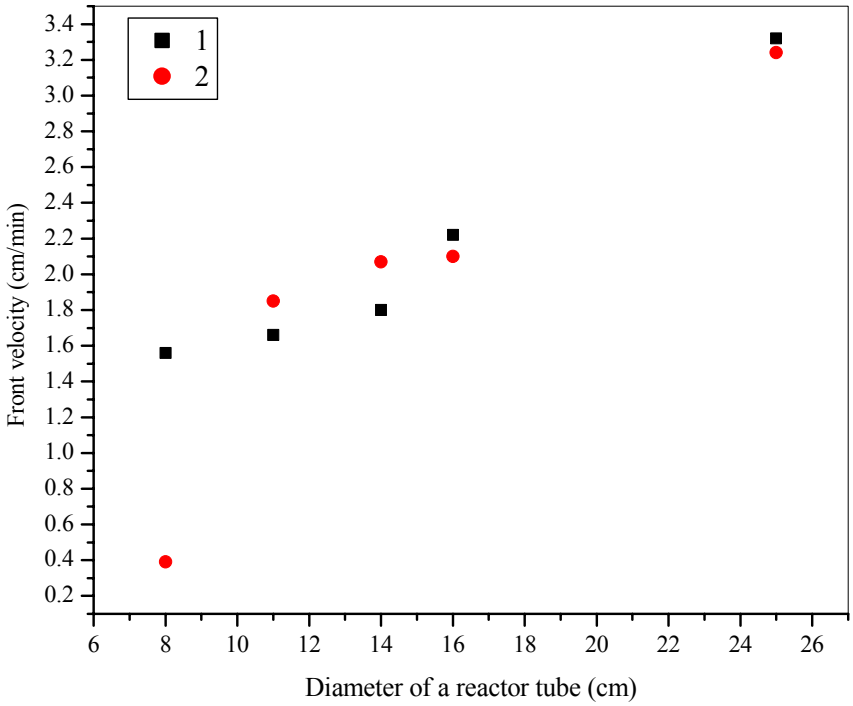

Figure 4.18. Comparison of experimental and numerical values of front velocities with variation in reactor diameter. 1: Experimental results; 2: predicted numerical results

4.5.3.3 Model for induction period

It is thought that the radicals produced from the reducing agent induces the peroxydisulfate decomposition and the mechanism is a free radical one, as we noted earlier. Induction period is the time required to establish a steady state concentration

(equilibrium) of free radicals. Polymerization starts only after reaching redox equilibrium intermediate (REI). The time constant is a function of a few reaction system parameters. These parameters are concentration of oxidant and reducing agent, thickness of reaction zone, radius of reactor tube, rate constant of limiting kinetics and concentration of atmospheric oxygen. The IP in FP can be depicted as follows:

Reaction mixture consisting of monomer and redox pair (potassium peroxydisulfate and ammonium formate) is packed in a cylindrical reactor tube. Unlike conventional polymerization, this mixture is exposed to atmospheric oxygen, as the tubes are not sealed. The reaction is initiated by adding traces of water. Now, as seen above, the peroxydisulfate is sensitive to actinic light. When water is added to the reaction system, it penetrates through the top layer. We observed this penetration zone using high speed camera and found that it decreases with reactor diameter at addition of constant volume of water in each reactor tube. Actinic light, water and atmospheric oxygen catalyze the redox reaction and radicals are generated. Water may presumably permit diffusion of oxygen and allow decomposition of oxidizing agent to occur more rapidly. On the other hand, water may also be effective in reducing the activation energy of the reaction between radical and monomer.[179] We note that the concentration of radicals is limited to only the penetration zone and volume of reactor. Apart from chemical species, the IP is therefore highly sensitive to the water penetration depth (ζ) and volume of reaction zone (V_R). Here, we define the volume of reaction zone as a product of area of cross section of the reactor tube and water penetration depth. Thus, $V_R = A \times \Delta\zeta$. To predict the induction period for the polymerization reaction, using the scaling factor in previous scaling relation, we postulate an empirical relation for scaling induction time as radius of reactor

tube is varied as (this follows the elementary Buckingham's π theorem in fluid dynamics used to derive empirical equations and also for general scale-up principles see Bisio and Kabel[180]):

$$\left[\frac{T_i \times k \times R_t}{\Delta\zeta}\right] = \alpha_o \left[\frac{[O]}{[A]}\right]^{\alpha_1} \left[\frac{V_{H2O}}{V_R}\right]^{\alpha_2} R_t^b \qquad 4.31$$

Here α_0, α_1 and α_2 are the constants. The basic assumptions subject to which this scaling relation holds are that the oxygen is present in large excess at every layer, for all possible values of temperature and intensity of actinic light and thus is treated as constant (which is fairly a good assumption). Also as we saw previously the reaction is psuedo zeroth order with respect to front velocity or rate of polymerization.

Using the values from Tables 4.8 and 4.11, and using NONLINEARFIT command from STATISTICS module of MATHEMATICA symbolic processing software package we fitted the data using Eqn. 4.31. The constants in the empirical equation came out to be α_o= 56.5447, α_1 = 1.75548, α_2 = -1.34757. We found out b = 1.2328 as a power law exponent previously. Now predicting the induction time using above empirical equation, we plot them together with experimental results in order to compare the two as shown in Figure 4.19.

Table 4.11. Numerical values for modeling of induction period

V_{H2O} (Lit)	200 x 10^{-6}
k (min^{-1})*	7.39 x 10^{-3}
$\Delta\zeta$ (cm)	1.8, 1.5, 1.2, 1.0 (for 0.8, 1.1, 1.4, and 1.6 cm id reactor tubes respectively)
b	1.2328

* from ref 144

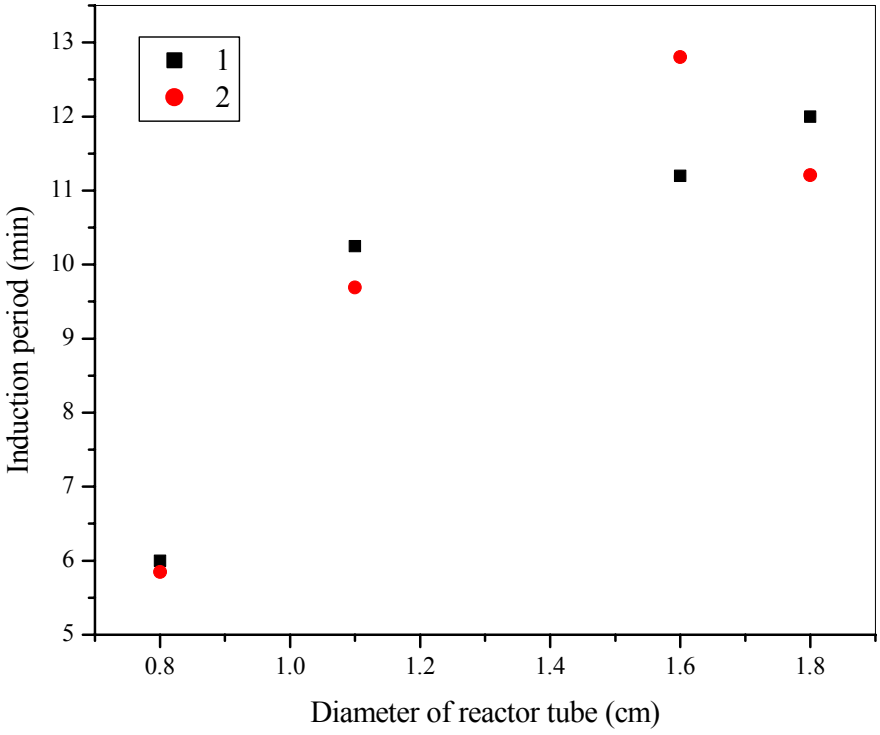

Figure 4.19. Comparison of observed and numerically calculated induction period values. 1: Experimental results; 2: numerical results

It is clear from the plot that the values are fairly in agreement with each other. Induction period was found to increase with reactor diameter. There are however, still limitations, as the reactions in larger diameter like 2.5 cm could not be predicted correctly by the numerical calculations. It was also difficult to consider the inadequate wetting of reaction mixture in 5.0 cm i.d. reactor. Model could not predict the IP under these conditions.

We developed an empirical mathematical model for the propagation of water triggered frontal polymerization fronts. We did this by examining the kinetic equations and energy balance in order to analytically determine the structure of the polymerization wave then we adopted the results by Apostollo to determine the effect of reactor geometry on front velocity. The scale-up analysis revealed the 1.2328 power dependency of reactor diameter on front velocity. Using this result, we derived another empirical formula for the induction period which is crucial and determines the wave structure and polymerization process. We numerically calculated the IP, which was in agreement with the experimental findings.

4.6. Conclusion

We could start a new sub-branch in FP, water triggered FP. New redox pairs were investigated and the mechanism of the water triggered polymerization was proposed. Conditions under which reaction can be triggered and effect of various parameters as well as reaction variables such as type and concentration of redox couple and volume of water on measurable parameters of FP such as front velocity, front temperature, shape of front and yield were investigated.

The methodology also yielded a rich dynamics. We observed some unique features like breath structures with “weak redox couple” and nonplanar frontal regime with “strong redox couples”. For the first time helical and layered patterns were obtained. Possibility of the scale up of the process was also investigated. For this, effect of reactor length and geometry was investigated on rate of polymerization and induction period. A detailed mechanism of the water triggered frontal polymerization was modeled and empirical equations were derived for rate of polymerization and induction period. The expressions were validated using experimental data. It was found that FP method is rapid and can be scaled-up easily and effectively.

We could also trigger copolymerization of acrylamide and N,N-methylenebisacrylamide using ceric ammonium nitrate (reductant) and water.

Chapter V

COPOLYMERIZATION

5 Copolymerization

5.1 Introduction

Copolymerization is the most useful method for tailor making a polymer product with specially desired properties. Copolymerization modifies the symmetry of the polymer chain and modulates both intermolecular and intramolecular forces, so properties such as lower critical solution temperature (LCST), solubility, etc. of the smart polymer may vary within the wide limits. Free-radical binary copolymerization reactions are important from both practical and theoretical point of view. Theoretically, it is interesting to focus on the effect of the chemical structure on the reactivity of monomers and radicals. Practically, radical copolymerization is the most recommendable process to prepare an unlimited number of polymer compounds by changing the nature and relative proportions of monomers in the reaction medium.

The kinetics and mechanisms involved in the free-radical binary copolymerization of vinyl monomers have been a research topic of interest for many years. The copolymerization of two monomers, A and B, give rise to the formation of a copolymer chain having composition and sequence distribution, which are dependent on the relative proportion of applied monomers as well as the monomers and radical reactivities.[33] The composition of a copolymer produced by simultaneous polymerization of two monomers is usually different from the composition of the comonomer feed from which it is produced. This shows that different monomers have different tendencies to undergo copolymerization. These tendencies often have little or no resemblance to their behaviour in homopolymerization. Different models have been put forth to visualize the mechanism of addition of growing chains and the factors influencing them.

Copolymerization reactivity ratios were originally measured for the purpose of describing the relative reactivties of various monomers towards various radicals. Nowadays they are being treated as a quantitative data and so the need to accurately measure it arises. Several methods have been developed to estimate reactivity ratios. Some of these methods require laborious calculation procedures and so the digital computer can be put to use in an efficient manner to estimate reactivity ratios

The copolymerization equation

The differential form of the binary copolymerization equation is given as:[33,181-183]

$$dM_1/dM_2 = (r_1M_1^2 + M_1M_2) / (r_2M_2^2 + M_1M_2) \qquad 5.1$$

where r_1 and r_2 are the monomer reactivity ratios and dM_1/dM_2 is the relative rate of addition of the two monomers to the chain. Only for low conversions this may be approximated to be equal to the mole ratio the respective monomer in the copolymer. If the estimation methods used for calculating the reactivity ratios are based on the differential equation of the copolymerization equation then the reaction should always be stopped at low conversions (below 60%).

Methods of estimation[182,183]

There are several methods to estimate the copolymer reactivity ratios. They may fall into one of the following categories:

- The intersection method
- The curve fitting method
- The linearisation method

The different methods of evaluation are

- The Mayo Lewis method

- The Joshi and Joshi method
- Finemann and Ross method
- Tidwell and Mortimer method
- Kelen Tudos method
- The extended Kelen Tudos method
- The Kuo Chen method
- The YBR method

We will quickly review few of them which are still importance in today's context.

1] The Mayo and Lewis method[184]

The differential form of the binary copolymerization equation was rearranged to be linear in terms of r_1 and r_2. The value of the copolymer and comonomer composition of each experiment yields a linear equation in terms of r_1 and r_2. The intersection of all the straight line gives the value of the reactivity ratios.

In practice though all the straight lines do not have a single intersection point due to the errors inherent in the system and so the best point of intersection is located in the probable area confined by the straight lines. This choosing of this point has no mathematical significance and depends only on the judgment of the investigator. This is also a source of error.

2] Joshi and Joshi method[185,186]

This method is actually an improvement of the Mayo Lewis intersection method. The best point of intersection was given a mathematical significance in this method. The best point of intersection was defined as the one which was statistically closest to all experimental lines and which if it were not for experimental errors would lie on every

line of the Mayo Lewis plot, resulting ideally in a unique intersection point. A condition was set up to make the sum of the squares of the perpendicular distances from the all lines to the best point of intersection minimum. This method does not suffer from the errors of reindexing the monomers.

3] Finemann and Ross method[182,187]

This method offers a simple graphical method of evaluating reactivity ratios. A simpler method involves carrying out the copolymerizations to low conversions and using the approximate form of differential copolymerization equation to estimate the reactivity ratios. However, a simpler technique, which permits the use of data in the intermediate concentration regions and reduces the uncertainties in the r values, is possible. f = (m_l/m_2) and F = (M_1/M_2), then the differential equation 5.1 can be rewritten as:

$$\frac{F(1 - f)}{f} = r_2 - \frac{F^2}{f} r_1 \qquad 5.2$$

A plot of (f -1)/F as ordinate and f/F^2 as abscissa is a straight line whose slope is $-r_1$ and whose intercept is r_1. The method of least squares can be employed to find the line of best fit. The slope of the line of best fit is influenced very much by the points which are nearer the origin. So it does not give an uniform weightage to the points and so if it suffers from errors of reindexing the monomers.

4] Tidwell and Mortimer[188,189]

The Tidwell and Mortimer method employs the nonlinear least squares procedure to estimate the reactivity ratios. Briefly the method consists of the following: given initial estimates of r_1 and r_2 a set of computations is performed which on repetition rapidly leads

to a pair of values of the reactivity ratios which yields the minimum value of the sum of the squares of the differences between the observed and computed polymer composition.

This method has a disadvantage. If the initial estimates are very much different from the actual values of r_1 and r_2, the value of the sum of square of deviations does not reach a minimum. In order to get rid of this problem the Gauss Newton nonlinear least square procedure was subject to modifications suggested by Box. If the initial estimates are very good then the number of iterations required for the value of the sum of square of deviations to converge is less.

5] The Extended Kelen Tudos method[190,191]

This is probably the most useful and widely accepted method these days. If copolymerizations are carried to higher conversions the determination of copolymerization parameters involves laborious calculations because the integrated equation must be applied. The Extended Kelen Tudos method is used to estimate reactivity ratios with data even at high conversions

$$\eta = \xi \left(r_1 + r_2/\alpha \right) - r_2/\alpha \qquad 5.3$$

η and ξ are functions of the compositions of the monomers in the feed and in the copolymer. They are estimated based on the procedures given in the reference.

Binary copolymerization models are used to predict the overall propagation rate coefficients of a copolymerization, and the composition and sequence distribution of the resulting copolymer, as a function of the feed ratio of the comonomers and a small set of characteristic constants. In order to derive these models it is necessary to make simplifying assumptions as to the factors influencing the rate of the propagation step, and

the types of side-reactions that may occur. If the models are to be meaningful then they should reflect the physical chemistry of the copolymerization reaction.

As seen above, one of the simplest models is the terminal (or Mayo–Lewis) model, in which it is assumed that side reactions are not significant, and that the reactivity of the propagation reaction is governed only by the nature of the monomer and the terminal unit of the polymer radical. For many years it was thought that this model could describe the many of the copolymerization systems and it was thus considered the basis of copolymerization kinetics. Those systems, which did not obey the terminal model, were thus regarded as exceptions, with the failure of the model being attributed to the particular chemical properties of these monomers, which rendered them susceptible to additional system-specific influences. For these 'exceptional' systems, alternative models were proposed. These took into account the influence of additional units of the polymer radical and/or the interference of side reactions (such as complex formation, monomer partitioning and depropagation). Fukuda et al.[192] used these characteristic parameters to predict the terminal model propagation rate for the system styrene with methyl methacrylate, they found that the predicted and their measured values were completely different. They proposed a penultimate model in which it is assumed that both the terminal and penultimate units of the polymer radical affect its reactivity, but only the terminal unit affects its selectivity.

Acrylamide itself is by far the most important monomer of amides of acrylic and methacrylic acid groups. Acrylamide polymers and copolymers have found applications in a wide variety of fields, such as adhesives, dispersants, flocculants, printing plates, viscosity modifiers and thickeners, leather, paper sizing, protective colloids in

photographic emulsions, surface coatings, textile treatments, gels for electrophoresis, improvement of cements, water purification, paper treatment, soil stabilization, well drilling, boiler water treatment, hair sprays, ion-exchange resins, pigment binders, and polyester-binding resins.[193] Interest in water-soluble acrylamide copolymers with acrylic/methacrylic acid salts, which can be prepared by various methods including the alkali hydrolysis of polyacrylonitrile fibers, has greatly increased in recent years.[193-196] To a considerable extent, this interest is due to the fact that such copolymers upon radiation crosslinking can produce polyelectrolyte hydrogels capable of absorbing up to 1000 g of water per gram of dry polymer.[197,198] Additionally, the copolymers of acrylamide and acrylic/methacrylic acid salts are being widely used as friction reducers in the oil recovery. Most preparations of this additives involve emulsion polymerizations and copolymers are available as emulsions. The composition of the copolymer is important with regard to the application and performance. The carboxyl salt moiety of the copolymer increases solubility in aqueous solvents and amide group may enhance the viscosifying property of the copolymer.

As seen in Chapter I, there are examples of various copolymers prepared by FP. However, the area still demands a deep insight and understanding of the process. There are no reports of solid-solid monomer pair synthesized by FP. There is also a lack of data of reactivity ratios and its validity in FP. Most of the efforts have been gone in understanding the wave structure and velocity determination. Tredici et al.[94] have shown that although producing large conversion values, FP is not subject to compositional drift like other polymerization processes and tends to produce narrow chain composition distributions.

Focus of this study was to investigate the validity of concept of reactivity ratio in solventless FP system. It was also intended to investigate the copolymerization beahaviour of "sluggish monomers" that cannot be otherwise homopolymerize by FP. Different sets of solid-solid, solid-liquid and liquid-liquid comonomer pairs were used and conducted the experiments by varying the mol ratios of individual monomers with respect to each other. The underlying frontal copolymerization mechanism was investigated to find if there exists any copolymer composition drift in FP.

5.2 Experimental

5.2.1 Synthesis of salts

5.2.1.1 Preparation of potassium acrylate (KA)

Potassium acrylate: A three neck round bottom flask was charged with anhydrous potassium carbonate (0.50 mol, 70 g) and 50 mL pet-ether. The flask was fitted on a magnetic stirrer and one neck was joined to the vacuum liner. 72 g of acrylic acid (1.0 mol) was charged in a dropping funnel and added drop-wise to the flask containing potassium carbonate within a 30 min. Evolution of carbon dioxide was observed. Reaction was continued for another 60 min. Supernatant pet-ether was decanted off and product was purified by giving washings of pet-ether.

Recrystallisation: In a conical flask 0.013 g (200 ppm) of phenothiazine was dissolved in ethanol and this solution was poured into the potassium acrylate formed in reaction (potassium acrylate is sparingly soluble in ethanol). This solution was heated in a thermostat at 70^{o}C and hot solution was filtered through cotton plug. The procedure was repeated for 4-5 times till all potassium acrylate dissolves in ethanol. The filtered solution

was cooled and transparent, brittle crystals of potassium acrylate were formed. It was dried and kept in a desicator as it is hygroscopic. It was characterized by melting point and IR spectroscopy.

$2CH_2CHCOOH + K_2CO_3 \longrightarrow 2CH_2CHCOOK + H_2O + CO_2aq$

The IR analysis of the potassium acrylate showed the peaks at 1857 cm^{-1} (_C"O of acrylate unit), 294l cm^{-1} (-CH- stretching of acrylate unit), 1234 and 1035 cm^{-1} (-C-O-C- stretching coupling interactions of ester group).[198]

Similarly, ammonium acrylate, potassium methacrylate and ammonium methacrylate were synthesized.

5.2.2 Poly(acrylamide-co-potassium methacrylate)

Acrylamide and potassium methacrylate (mole ratio 9:1) were blended and 1 M% of potassium peroxydisulfate was added to it (Table 5.1). The mixture was ground and packed by applying pressure of 1.8 x 10^3 kg. The cylinder was dropped in 11 x 125 mm thick walled test tube that had been marked in 1 mm units. The reaction was initiated by means of solder gun. Propagation of front was started. The reaction was chilled using liquid nitrogen when the front reached to the 50 % of the column length. The product was isolated and purified by giving repetitive washings of acetone.

Similarly other comonomer pairs like acrylamide:ammonium methacrylate, acrylamide: ammonium acrylate, acrylamide:potassium acrylate were synthesized (Tables 5.1-5.4).

All other pairs were also copolymerized by similar way (Table 5.5).

Table 5.1. Copolymer feed composition of acrylamide (M_1): potassium acrylate (M_2) comonomer pair

Code no.	Mole ratio M_1:M_2	Mol of M_1 in the feed	Mol of M_2 in the feed	Monomer feed		Initiator ($K_2S_2O_8$)
				M_1 g	M_2 g	g
AKA1	0.9:0.1	0.1380	0.0153	9.811	1.689	0.2
AKA2	0.8:0.2	0.1126	0.0283	8.051	3.119	0.2
AKA3	0.7:0.3	0.0972	0.0416	6.909	4.589	0.2
AKA4	0.6:0.4	0.079	0.0530	5.656	5.83	0.2
AKA5	0.5:0.5	0.0635	0.0635	4.510	6.989	0.2
AKA6	0.4:0.6	0.0487	0.0779	3.459	8.040	0.2
AKA7	0.3:0.7	0.0350	0.0818	2.491	9.008	0.2
AKA8	0.2:0.8	0.0224	0.0899	1.598	9.902	0.2
AKA9	0.1:0.9	0.0108	0.0974	0.077	10.73	0.2

Polymerizations were stopped at 50 % conversion

Table 5.2. Copolymer feed composition of acrylamide (M_1): potassium methacrylate (M_3) comonomer pair

Code no.	Mole ratio M_1:M_4	Mol of M_1 in the feed	Mol of M_4 in the feed	Monomer feed		Initiator ($K_2S_2O_8$)
				M_1 g	M_4 g	g
AKM1	0.9:0.1	0.1354	0.0151	9.630	1.869	0.2
AKM2	0.8:0.2	0.1126	0.0281	8.004	3.495	0.2
AKM3	0.7:0.3	0.0925	0.0397	6.576	4.923	0.2
AKM4	0.6:0.4	0.0748	0.0498	5.313	6.187	0.2
AKM5	0.5:0.5	0.0588	0.0588	4.183	7.307	0.2

AKM6	0.4:0.6	0.0447	0.0669	3.174	8.318	0.2
AKM7	0.3:0.7	0.0319	0.0735	2.265	9.231	0.2
AKM8	0.2:0.8	0.0202	0.0810	1.439	10.06	0.2
AKM9	0.1:0.9	0.0097	0.0870	0.688	10.81	0.2

Polymerizations were stopped at 50 % conversion

Table 5.3. Copolymer feed composition of acrylamide (M_1): ammonium acrylate (M_4) comonomer pair

Code no.	Mole ratio M_1:M_3	Mol of M_1 in the feed	Mol of M_3 in the feed	Monomer feed M_1 g	M_3 g	Initiator ($K_2S_2O_8$) g
AAA1	0.9:0.1	0.1420	0.0158	10.04	1.406	0.2
AAA2	0.8:0.2	0.1231	0.0308	8.756	2.744	0.2
AAA3	0.7:0.3	0.1053	0.0452	7.848	4.025	0.2
AAA4	0.6:0.4	0.0880	0.0587	6.256	5.227	0.2
AAA5	0.5:0.5	0.0718	0.0718	5.103	6.396	0.2
AAA6	0.4:0.6	0.0562	0.0843	3.992	7.506	0.2
AAA7	0.3:0.7	0.0421	0.0961	2.930	8.569	0.2
AAA8	0.2:0.8	0.0269	0.1076	1.912	9.588	0.2
AAA9	0.1:0.9	0.0132	0.1186	0.936	10.563	0.2

Polymerizations were stopped at 50 % conversion

Table 5.4. Copolymer feed composition of acrylamide (M_1): ammonium methacrylate (M_5) comonomer pair

Code no.	Mole ratio M_1:M_5	Mol of M_1 in the feed	Mol of M_5 in the feed	Monomer feed		Initiator ($K_2S_2O_8$)
				M_1 g	M_5 g	g
AAM1	0.9:0.1	0.1393	0.0154	9.903	1.590	0.2
AAM2	0.8:0.2	0.1187	0.0297	8.440	3.060	0.2
AAM3	0.7:0.3	0.0998	0.0427	7.091	4.408	0.2
AAM4	0.6:0.4	0.0823	0.0548	5.847	5.653	0.2
AAM5	0.5:0.5	0.0660	0.0641	4.693	6.687	0.2
AAM6	0.4:0.6	0.0510	0.0764	3.621	7.879	0.2
AAM7	0.3:0.7	0.0369	0.0861	2.623	8.877	0.2
AAM8	0.2:0.8	0.0237	0.0958	1.690	9.809	0.2
AAM9	0.1:0.9	0.0115	0.1036	0.818	10.68	0.2

Polymerizations were stopped at 50 % conversion

Table 5.5. Various other monomer pairs used in copolymer synthesis by FP

Sr. No.	Comonomers pairs	Composition range mol: mol	Remarks on FP
1	Styrene: butyl acrylate	0.1-0.9	No FP when styrene content was more
2	Styrene: methyl methacrylate	0.1-0.9	No FP observed
3	Acrylamide: styrene	0.1-.09	No FP when styrene content was more;
4	t-butyl styrene: divinyl benzene	0.1-.09	No FP
5	Glycidyl methacrylate: N-vinyl pyrillodone	0.1-.09	No FP

5.2.3 Characterization

Front velocity, front temperature measurements and IR were conducted as given in Chapter III. Potassium salt containing copolymers were characterized by thermal analysis (TGA) and atomic absorption spectroscopy (AAS). The analysis was also supported by IR spectroscopy. Ammonium salt containing copolymers were characterized by pH meter.

A Perkin-Elmer thermogravimetric system was employed. The samples were studied in dynamic nitrogen atmosphere at a flow rate of 50 cm^3/min at heating rate of 10^oC/min. Before each test system was purged with nitrogen for 15 min at a flow rate of 100 cm^3/min. Samples were heated from room temperature to 900^oC. The composition was estimated from the derivative graph and area under the curve.[199]

Atomic absorption (AA) spectroscopy uses the absorption of light to measure the concentration of gas-phase atoms. Since samples are usually liquids or solids, the analyte atoms or ions must be vaporized in a flame or graphite furnace. The atoms absorb ultraviolet or visible light and make transitions to higher electronic energy levels. The analyte concentration is determined from the amount of absorption. Potassium lamp was used to detect the K concentration in the sample (Varian AA100 Atomic Absorption Spectrometer).

pHmetric titration were performed using pH-meter, equipped with a glass electrode. Ammonium salt containing copolymer (0.1 g), poly(accrylamide-*co*ammonium methacrylate) was dissolved in 10 mL water and 0.093 N NaOH was added to it. Solution was kept for shaking on a shaker for 30 h and was titrated against 0.113 N HCl (pH metry). pH was recorded per 0.2 mL addition of HCl. First standardization was done by

the titration of homopolymer of methacrylic acid. Similarly, all other titrations were conducted.

5.3 Results and discussion

5.3.1 Front propagation, front velocity and front temperature

A series of copolymers were synthesized by FP. FP method was especially useful for synthesizing the copolymers, homopolymer of which (e.g. potassium methacrylate) is not otherwise possible. Copolymerization of both liquid-solid and solid-solid monomer pairs using FP technique was attempted. In liquid-liquid pairs, fronts were extinguished either due to excessive fingering or heat losses. Efforts in synthesizing copolymers from styrene-n-butyl acrylate, styrene-MMA, *t*-butyl styrene-divinyl benzene, glycidyl methacrylate-N-vinyl pyrrolidone monomer pairs were therefore not successful. In the solid-liquid system like acrylamide-styrene, the reactions were possible only at lower concentration of styrene in the feed. At higher concentration, reactions were again extinguished and sometime even could not be started. Typically, the FP reactions were possible only when the styrene content was less than 40 % in the feed.

We then focused our work in complete analysis of solid-soilid monomer pairs. These types of systems have not been evaluated in FP. The aim of the synthesis was to perceive the effect of high temperature and localized reaction zone if any on the copolymer which we think would help in study of frontal polymerization reactions which normally take place at high temperature. We suspected that this will give the proof for inter or intramolecular bonding between the copolymer synthesized by frontal polymerization. It was observed that IR signals (see later) were not enough to distinguish the difference between the closely spaced peaks. Therefore, to study the effect of high

temperature on copolymer structure, isothermal heating method was applied. In this method, 100 mg of copolymer samples was compressed into 2 x 1 mm disc which was mounted on specially designed isothermal heating plate with adjustable heating rate and conditions. Disc was heated at 20°C/min to 190°C (front temperature) and kept isothermally for 15 min. After cooling, disc was removed, polymer sample was washed and was given to the potassium ion content analysis. Analysis yielded no difference between the K content of room temperature copolymer sample and that of heated copolymer indicating the fact of no anhydride formation during the frontal polymerization.

A separate set of experiments of all four pairs was conducted allowing the completion of reaction to have a better understanding of front velocity and temperature data and to avoid localized fluctuations in low conversion reactions. There was a difference between the front velocities of acrylate and methacrylate salts. The comparative velocity data copolymerization of potassium/ammonium salts of acrylic/methacrylic acid with acrylamide shown in Tables 5.6 and 5.7.

Table 5.6. Front velocity and front temperature data of copolymerization reactions carried as per Table 5.1 and 5.2

Code no	Mol ratio AA-KA	FV cm/min	FT °C
AKA1	0.9: 0.1	2.8	235
AKA2	0.8: 0.2	2.5	227
AKA3	0.7: 0.3	2.6	247
AKA4	0.6: 0.4	2.9	217

Code no	Mol ratio AA-KM	FV cm/min	FT °C
AKM1	0.9: 0.1	2.1	177
AKM2	0.8: 0.2	1.9	188
AKM3	0.7: 0.3	1.82	168
AKM4	0.6: 0.4	1.86	169

AKA5	0.5: 0.5	3	214	AKM5	0.5: 0.5	1.9	171
AKA6	0.4: 0.6	3.1	211	AKM6	0.4: 0.6	1.81	147
AKA7	0.3: 0.7	3.2	189	AKM7	0.3: 0.7	1.8	151
AKA8	0.2: 0.8	2.9	164	AKM8	0.2: 0.8	1.7	129
AKA9	0.1: 0.9	No FP		AKM9	0.1:0.9	No FP	

AA=acrylamide; KA=potassium acrylate; KM=potassium methacrylate; FV=front velocity; FT=front temperature

Table 5.7. Front velocity and front temperature data of copolymerization reactions carried as per Table 5.3 and 5.4

Code no	Mol ratio AA-A	FV cm/min	FT ^{o}C	Code no	Mol ratio AA-KA	FV cm/min	FT ^{o}C
AAA1	0.9:0.1	2.21	181	AAM1	0.9: 0.1	1.84	178
AAA2	0.8:0.2	1.96	194	AAM2	0.8: 0.2	1.78	181
AAA3	0.7:0.3	1.95	178	AAM3	0.7: 0.3	1.81	165
AAA4	0.6: 0.4	1.86	174	AAM4	0.6: 0.4	1.69	174
AAA5	0.5: 0.5	1.94	168	AAM5	0.5: 0.5	1.75	172
AAA6	0.4: 0.6	1.74	159	AAM6	0.4: 0.6	1.66	179
AAA7	0.3: 0.7	1.79	164	AAM7	0.3: 0.7	1.51	169
AAA8	0.2: 0.8	1.80	174	AAM8	0.2: 0.8	1.49	156
AAA9	0.1: 0.9	1.40	156	AAM9	0.1: 0.9	No FP	

AA=acrylamide; A=ammonium acrylate; AM=ammonium methacrylate; FV=front velocity; FT=front temperature

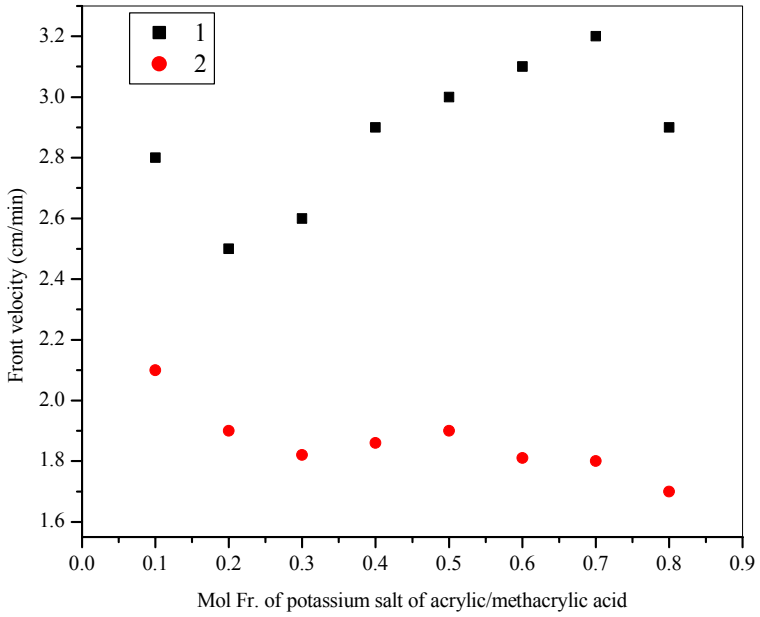

Figure 5.1. Comparison of front velocity data of potassium salts of acrylic/methacrylic acid. 1: acrylamide:potassium acrylate system, 2: acrylamide:potassium methacrylate system

All three pairs except AKA behaved similarly. The reactions with potassium acrylates were very fast and vigorous. Usually, acrylates reacts faster than their methacrylates. From graph (Fig. 5.1), it is clear that the rate of polymerization is much higher in AA copolymerization system than AKM. With acrylate content in the monomer feed the rate was increased in AKA while the front velocities were almost constant in AKM system. There was no trend in front temperature but it was higher in AKA system. This higher temperature leads to the partial crosslinking in the AKA copolymers. At higher temperatures the life span of radical reduces, the stability decreases and thus gives rise to the radical transfers. Thus it could be intra molecular radical transfer leading to grafting on the main chain leading to crosslinking. The intermolecular radical transfer could initiate graft and chain transfer reactions. Due to intermolecular grafting the

polymer crosslinks and becomes swellable due to intramolecular transfers overall molecular weights are brought down. Polymers were not soluble in water but highly swellable. As given in section 3.3.4 of Chapter I, here also the water absorbency ability of the all synthesized copolymers was higher than those with the crosslinking agent for the same reasons. In addition to chain transfer, here following side reactions take place: autocrosslinking through a hydrogen abstraction from the polymer backbone followed by radical combination and the occurrence of imidization that usually takes place in the polymerization of acrylamide at high temperature (as seen in Chapter IV) and pH 8. The imidization of the amide pendants in the copolymer is shown in scheme 5.1.

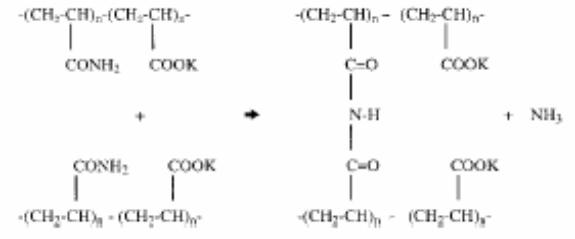

Scheme 5.1. Intermolecualar crosslinking in acrylamide:potassium acrylate copolymerization

While polymerization of AKA system, gaps in a helical fashion leading to the heterogeneity in the product was observed. It might be due to the combined effect of spin mode, nonplanar front regime and pressure exerted by the monomer column due to the release of gases. Other copolymers were linear and soluble in water. There was also a difference in the nature of product. With AKA polymer rods that were formed flexible and the stiffness increased with increase in KA concentration. With AKM rods were of identical quality and not flexible.

In case of ammonium salts, the copolymerization shows a similar trend. With AAM reactions were rapid and vigorous with liberation of ammonia and with AAM reactions were relatively slower. Front velocities were more or less constant (Table 5.7).

The IR spectra of the copolymers were recorded in FTIR using KBr pellet. Representative IR spectrum (Fig. 5.2) of the copolymer (AKM-5) shows the peaks corresponding to the functional groups attached to the monomer units. The peaks observed are 3404 cm^{-1} corresponding to the NH stretching of acrylamide unit, 1570 cm^{-1} corresponding to C=O of (meth)acrylate unit, and 1691 cm^{-1} corresponding to the carbonyl group of the acrylamide unit. In addition to the above peaks, peaks are also observed at 1306 and 1059 cm^{-1} corresponding to C-O-C stretching interactions of ester groups. This IR analysis indicates that all of the monomeric units; that is, acrylamide and potassium methacrylate are incorporated in the copolymer backbone.

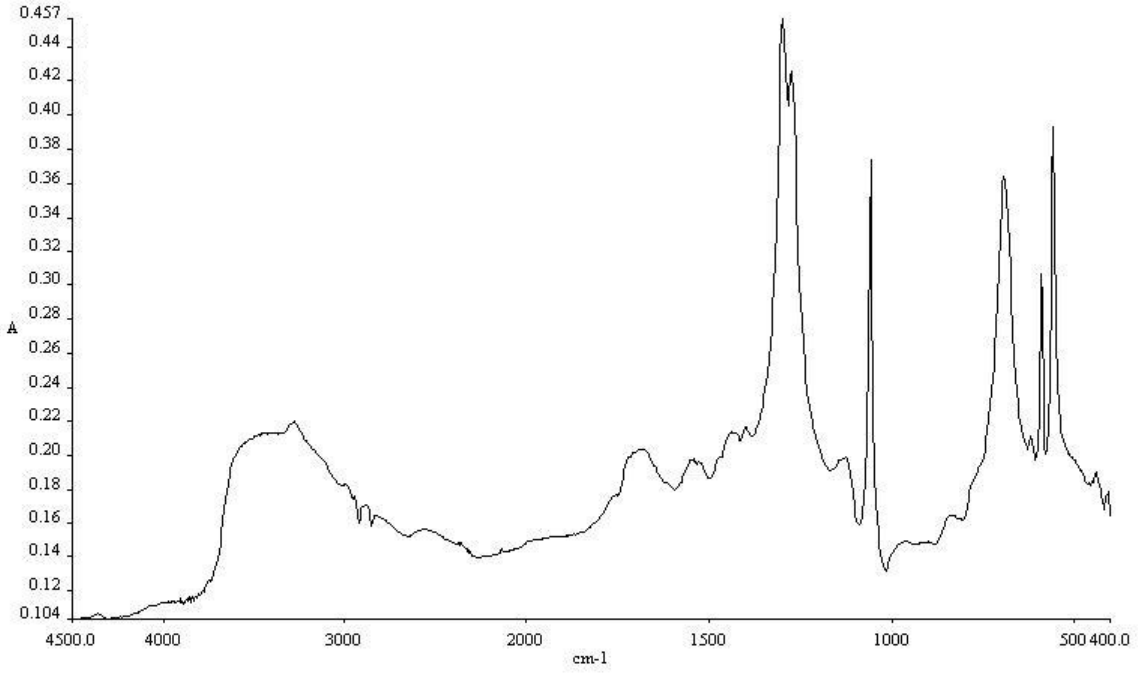

Figure. 5.2. Representative IR spectrum of AA-KM at 5:5 composition (AKM5). From the ratio of the peaks at 1449 and 1410 cm^{-1} we get the composition of individual monomer in the composition

5.3.2 Copolymer composition analysis

5.3.2.1 Poly(acrylamide-potassium methacrylate)

Methods based on quantitative determination of nitrogen according to Kjeldahl are most popular for establishing the copolymer compositions; these methods, however, are not applicable to copolymers containing ammonium acrylate and to technical samples contaminated by impurities containing nitrogen. For salts of ammonia even thermogravimetric method is not that useful as ammonium salts also release ammonia along with acrylamide when heated. For determination of copolymer compositions of acrylic salts of alkali metals and acrylamide, thermogravimetric and AAS was used which was further supported by IR technique. And for ammonium salts the pHmetric method was used.

Thermal analysis

Thermostability of the dry sample was performed using a Perkin Elmer Thermogravimetric Analyzer (TGA) Instrument. The temperature range in the experiment covered 50–900^{o}C at a heating rate of 10^{o}C/min using a dry nitrogen at a flow rate of 50 mL/min. Representative TGA/DTG thermograms are of copolymers (AKM2 and AKM4) are presented in Fig. 5.3. The sample shows a very small weight loss below, at 100^{o}C, implying loss of moisture. The initial weight loss of the sample started at 181.24^{o}C. The sample had significant weight loss at 210^{o}C (14.35%) and 300^{o}C (9.12%) and continued to lose weight up to 500^{o}C, with a weight loss of 41.27%. The first step is attributed to loss of bound water, second corresponds to loss of ammonia by imidization (inter and intra molecular) and water by dehydration and third step (>340^{o}C). Therefore, this particular sample had an initial decomposition temperature of 181.24^{o}C.

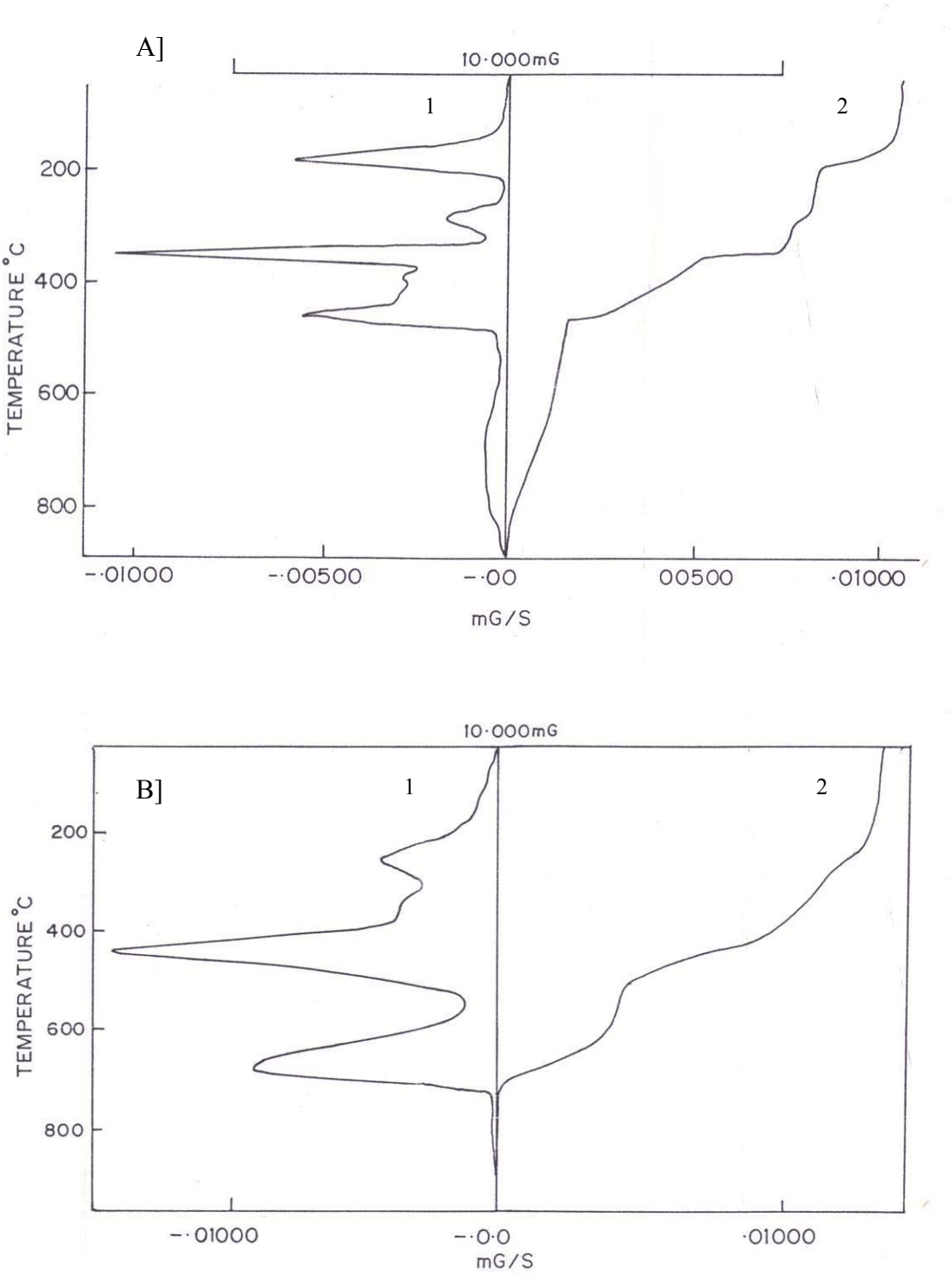

Figure 5.3. Thermogravimetric curve of an acrylamide/potassium methacrylate copolymer pyrolyzed to 900°C. 1] first derivative of the temperature-weight change curve (DTG), 2] temperature-weight change curve (TG). A] AKM2 and B] AKM4

The third region (>340^{o}C) represents substantial weight loss, and is normally attributed to main chain breakdown of polyacrylamide.

The controlled pyrolysis of polymer samples to give characteristic degradation products has been extensively studied.[200] The method uses the observation that, C-N bonds are weaker bonds than C-O bonds (C-N, 69.5 kcal/mol; C-O, 84 kcal/mol). Other factors such as the formation of products with higher bond energies, e.g. ammonia, hydrogen chloride and water, may in addition to the bond dissociation energies, increase reaction rates and therefore reduce pyrolysis temperature. Dassanayake and Phillips[199] reported that analysis of residue by infrared spectrophotometry reveals the disappearance of both amide carbonyl and the amide $-NH_2$ absorption peak beyond 492^{o}C in thermal analysis of the acylamide-sodium acrylate copolymer. Therefore, the cumulative loss upto 488^{o}C should indicate the presence of the amide fraction of the copolymer. The residue remaining after that 488^{o}C pyrolysis should represent the present by weight of the carboxylate fraction in the copolymer. We also obtained similar results and when we analyzed the residue for energy-dispersion X-ray analysis (EDAX), presence of potassium ion (Fig. 5.4) was found.

The weight loss data of two regions (before 500^{o}C and after 500^{o}C) was used to estimate the copolymer composition. Second thermogram (Fig. 5.3) shows a similar behaviour. The higher weight loss above 500^{o}C indicates a higher weight fraction of potassium methacrylate. After correcting the weight loss due to moisture by results obtained from Karl-Fischer analysis, the copolymer composition was estimated. The results are tabulated below (Table 5.8). The results are compared with AAS and the two matched within ±5 % (except for AKM8).

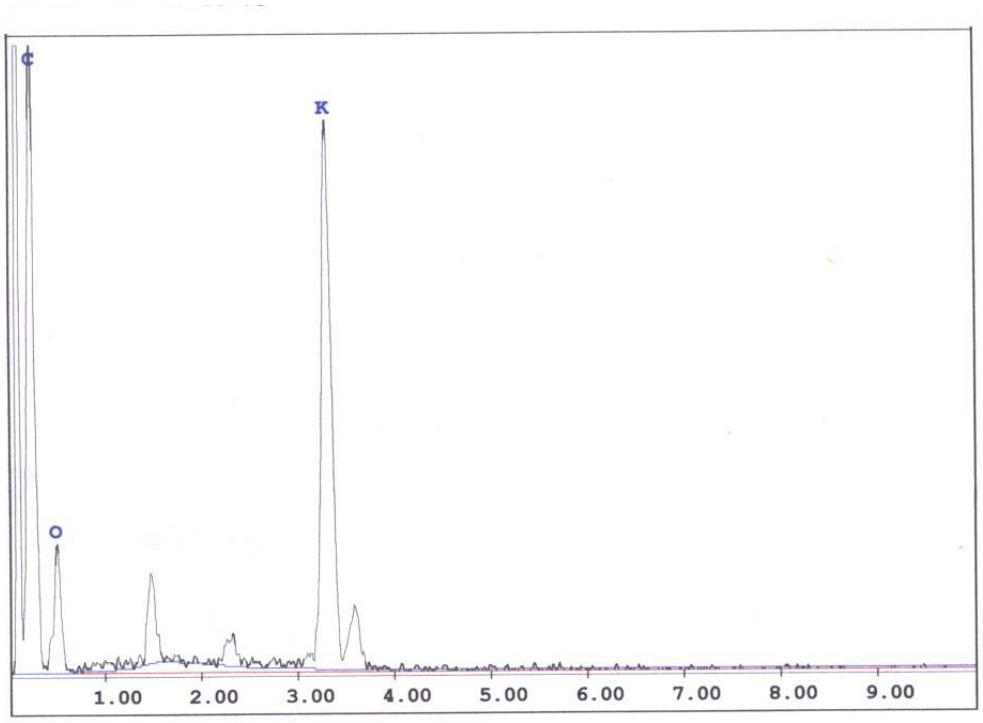

Figure 5.4. EDAX micrograph of the copolymer sample showing the content of potassium (AKM3)

Table 5.8. The tabulated data of the results from thermal analysis and the AAS analysis of acrylamide/potassium methacrylate copolymer

Code no	Mol fr AA	Mol fr KM	Method
AKM1	0.95	0.05	TA
	0.96	0.04	AAS
AKM2	0.93	0.07	TA
	0.96	0.04	AAS
AKM3	0.71	0.29	TA
	0.73	0.27	AAS
AKM4	0.68	0.32	TA
	0.69	0.31	AAS

AKM5	0.82	0.18	TA
	0.84	0.16	AAS
AKM6	0.77	0.21	TA
	0.86	0.18	AAS
AKM7	0.76	0.24	TA
	0.77	0.23	AAS
AKM8	0.51	0.49	TA
	0.69	0.32	AAS

AA=acrylamide; KM=potassium methacrylate; TA=thermogravimetric analysis; AAS=atomic absorption spectroscopy

IR spectrophotometric analysis

The amide carbonyl group absorbs near 1650 cm^{-1} and the carboxylate carbonyl group absorbs near 1570 cm^{-1}. The ratio of the area of amide absorption to that of the carboxylate absorption should give the relative amounts of the two components present in the copolymer. If the polymer spectrum can be easily obtained and the carbonyl absorptions of the two moieties are well resolved, the infrared spectrophotometric method gives accurate results. Additionally, Shaglyayeva et al.[201] have proposed another IR based method to compute the copolymer composition of the acrylamide/alkali metal acrylate copolymers. Analytical bonds at 1410 and 1448 cm^{-1} corresponding to bond stretching vibrations of COO^- and deformation vibrations of methylene group respectively was used. The dependence of the optical density ratio of these absorption bands on the ratio of acrylate and acrylamide units in mixture of polyacrylamide with alkali metal polyacrylates takes form,

$$x_2 = 151.33y_2 - 125.39 \; ; s= 0.004, R = 0.998 \qquad 5.4$$

where, x_2 is the content of acrylate unit in wt %, s is correction coefficient, R is dispersion, and $y_2 = D_{1410}/D_{1448}$.

Here, the optical density ratio of absorption bands at 1440 and 1448 cm^{-1} is independent of the number of acrylamide and acrylic acid units. From the IR spectrum shown in Fig. 5.2 we calculated the composition of each monomer in the copolymer composition and found that acrylamide to K-methacrylate composition for 5:5 mol/mol ratio was 0.86:0.14 which is very close to the predicted values from TGA and AAS.

5.3.2.2 Poly(acrylamide-ammonium acrylate/methacrylate)

It is very difficult to determine the copolymer compositions in ammonium salt containing copolymers by nitrogen estimation or IR studies. Ammonium from both acrylate and acrylamide group interferes in the analysis. The known method is the potentiometric/pHmetric titration in such cases.[202] We also adopted the same to estimate the copolymer composition. The samples were dissolved in excess of ~0.1 M NaOH; the excess NaOH and the blank sample were titrated with ~0.1 M HCl. The mole percent of acrylate/methacrylate in the samples was determined from the titration data. pH was recorded per 0.2 mL addition of HCl. Pure polymer in the form of ammonium salt, when dissolved in water, shows an extended chain due to the dissociation phenomenon. Hydrolyzed polyacrylamide is a polyelectrolyte whose properties depend on the degree of purity, hydrolysis, and neutralization. Leyte and Mandell[203] have described how a strong micromolecular electrolyte can screen the polyelectrolytic character of the poly(acrylic acid) solution. This can be explained by the steric structure of the dissolved polymer, which presents a varied number of water dipoles around the carboxylic groups. The more chain is charged (the carboxylic groups are more dissociated), more are the water dipoles

around the polymer. If the concentration of a micromolecular electrolyte increases, the number of water dipoles around the carboxylic groups decreases, which leads to screening the polyelectrolytic character. This feature appears at potentiometric or pHmetric titration, obtainable only at low electrolyte levels.

Copolymer can be considered as a hydrolyzed PAA that has a weak-acid character and theoretically can be titrated. To obtain an accurate titration the reagents were added gradually in the smallest quantities possible. After one addition the relaxation time is 5-10 min. The longest time was observed when the carboxylic groups were transformed into acid form. This length of time makes necessary a steady current source. The titration was done from alkaline to acid to avoid hydrolysis. If the polymer is alkaline, titration yielded the release of ammonia and formation of acid. Titration with an acid gives the neutralization level. To ensure that the obtained value will represent the total quantity of the carboxylic groups or only the neutralization level, the titration was done with an alkaline solution in the opposite direction. The representation of a full determination is given in Fig. 5.5. From the titration curve and the copolymer composition may be computed as follows: The solutions used: 0.113 N HCl and 0.092 N NaOH; used segment weights: M_1 = 71 for acrylamide units, M_2 = 89.09 and M_3 = 103.09 for ammonium acrylate and methacrylate respectively. First the standard polyacrylamide and poly(acrylic acid) and poly(methacrylic acid) solutions in NaOH were titrated using HCl. By doing this, we get the idea of end points of respective acids. Copolymer composition was then estimated by following method: By definition, the degree of hydrolysis gives the percentage of acrylamide groups in the PAA chain that are transformed into acrylic acid groups. Typical titration curve is shown in Fig. 5.5**.** In first step the moles of NaOH

were calculated in 10 mL. This was original moles of NaOH (0.959 mmol). As seen from the titration curve, there are two end points. Usually the first end point was observed in between 7-8 pH and assigned for the unreacted sodium hydroxide. Second end point was observed in acidic range and was assigned to the moles of NH_4^+ replaced by sodium hydroxide. From this, g and mol fraction of individual monomer segment in a given copolymer was estimated. The detailed data is presented below in Tables 5.8-5.10.

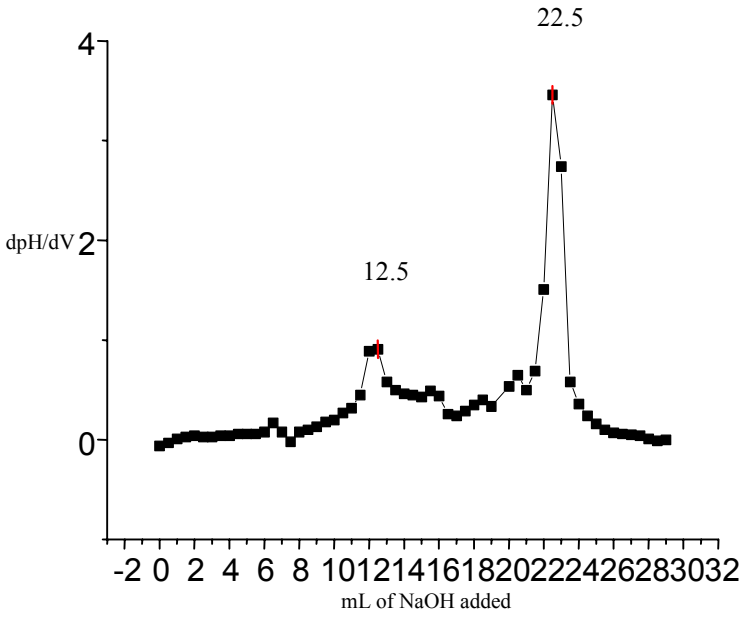

A]

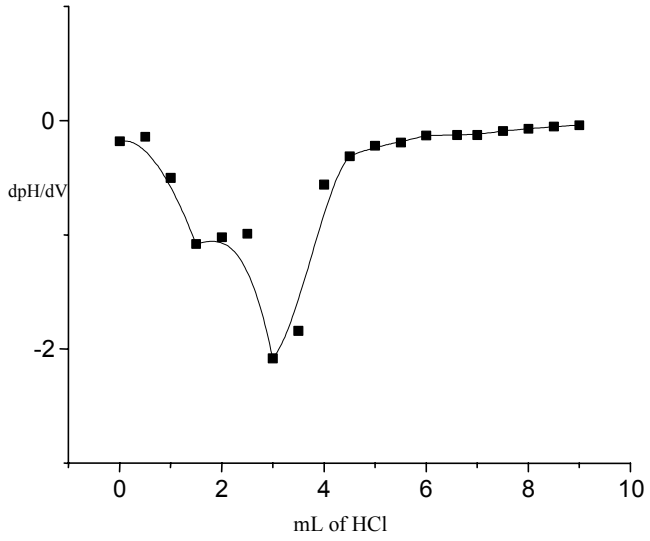

B]

Figure 5.5. Typical first derivative plots in titration of copolymer against A] NaOH and B] HCl. It gives the two end points

Table 5.9. Copolymer composition data of poly(acrylamide-*co*-potassium methacrylate) based on thermal analysis

Code no.	Mole Fr. M_1:M_4	Wt. of copolymer g	Wt. Fr. Conversion	Mol Fr. M_1 in the copolymet	Mol Fr. M_3 in the copolymer	conversion
AKM1	0.9:0.1	5.72	0.761	0.95	0.05	0.4973
AKM2	0.8:0.2	5.51	0.890	0.91	0.09	0.4791
AKM3	0.7:0.3	4.82	0.676	0.71	0.29	0.4191
AKM4	0.6:0.4	5.50	0.774	0.68	0.26	0.4831
AKM5	0.5:0.5	6.44	0.814	0.80	0.20	0.56
AKM6	0.4:0.6	5.68	0.870	0.77	0.21	0.4939
AKM7	0.3:0.7	3.98	0.662	0.76	0.24	0.3553
AKM8	0.2:0.8	4.14	0.702	0.59	0.41	0.36
AKM9	0.1:0.9	-		-	-	-

*Weight fraction conversion: weight of purified copolymer/weight of formed polymer

Table 5.10. Copolymer composition data of poly(acrylamide-*co*-ammonium acrylate) based on pHmetric method

Code no.	Mole ratio M_1:M_3	Wt. of copolymer g	Wt. Fr. of copoylemer g	Mol Fr. of M_1 in the copolymer	Mol of M_4 in the copolymer
AAA1	0.9:0.1	7.74	0.936	0.863	0.137
AAA2	0.8:0.2	7.72	0.941	0.737	0.272
AAA3	0.7:0.3	7.75	0.937	0.712	0.288
AAA4	0.6:0.4	7.76	0.931	0.701	0.299
AAA5	0.5:0.5	7.81	0.935	0.692	0.307
AAA6	0.4:0.6	7.01	0.930	0.681	0.319
AAA7	0.3:0.7	7.97	0.951	0.675	0.325
AAA8	0.2:0.8	7.56	0.942	0.664	0.334
AAA9	0.1:0.9	7.99	0.939	0.657	0.343

Table 5.11. Copolymer composition data of poly(acrylamide-*co*-ammonium methacrylate) based on pHmetric method

Code no.	Mole ratio M_1:M_5	Wt. of copolymer (w1)	Wt. Fr. conv.	Mole of M_1 in copolymer	Mol of M_5 in copolymer
AAM1	0.9:0.1	5.72	0.847	0.909	0.091
AAM2	0.8:0.2	9.83	0.942	0.840	0.140
AAM3	0.7:0.3	5.88	0.947	0.716	0.284
AAM4	0.6:0.4	4.11	0.931	0.575	0.425
AAM5	0.5:0.5	3.22	0.870	0.636	0.364
AAM6	0.4:0.6	6.84	0.929	0.596	0.404
AAM7	0.3:0.7	4.13	0.886	0.57	0.43
AAM8	0.2:0.8	4.64	0.892	0.530	0.470
AAM9	0.1:0.9	3.26	0.860	0.450	0.550

5.3.3 Reactivity ratio

The copolymerization reactions are characterized by the monomer reactivity ratios of the reacting monomers. It is interesting to check the concept of reactivity ratio in FP. The next goal was therefore, to estimate the reactivity ratio values for the monomers and check its effect on relative rates of copolymerization. While estimating the reactivity ratio values following assumptions were made:

1] Long Chain assumption i.e. initiation and termination reactions can be ignored in the calculation of copolymer composition

2] Equal reactivity i.e. rate is independent of chain size

3] Reactivity ratios are independent of rate and conversion

4] Reactivity ratios are independent of inhibitors, retarder etc.

5] The mixture is homogeneous (the comonomers are uniformly distributed). The monomers were powdered using tumblers for 72 h to get a fine powder. So even at micro level the heterogeneities are present, at gross level they are absent and mixture can be treated as homogeneous mixture

6] Reaction is stochastic at front temperature. Therefore, the penultimate effects are neglected and terminal models are used

7] Reaction is psuedo zeroth order w.r.t. monomer. Therefore, even if the reactions were freezed at 50% conversion, the percent yields were not 50 % but the difference between the weight of copolymer formed and weight of copolymer remained after washings

8] The composition and temperature waves travel along the system without changing their shape following QSSA

The experimental data of the present work were treated by the terminal models. Two such methods Fineman-Ross (FR) and extended Kelen-Tudos (KT) equation in the following form were used:

Fineman-Ross model:

$$\frac{F(1-f)}{f} = r_2 - \frac{F^2}{f} r_1 \qquad 5.2$$

$$F_1 = 1 - F_2 = \frac{d[M_1]}{d[M_1] + d[M_2]}$$

$$f_1 = 1 - f_2 = \frac{[M_1]}{[M_1] + [M_2]}$$

Extended Kelen-Tudos Model:

$$\eta = [\, r_1 + (r_2 / \alpha)\,]\, \xi - (r_2 / \alpha) \qquad 5.3$$

$$\eta = G / (\alpha + F)$$
$$\xi = F / (\alpha + F)$$
$$\alpha = (F_{min} * F_{max})^{1/2}$$

Here, G is defined as:

$$X = \frac{[M_1]_0}{[M_2]_0} \qquad Y = \frac{d[M_1]_t}{d[M_2]_t} \qquad G = X(Y-1)/Y;\ F = X^2/Y;$$

and α is fit parameter come from max and min F values. Here, η is plotted against ξ to yield a straight line and from the intercept and slope, r_2 and r_2 can be calculated respectively.

5.3.3.1 Fineman Ross method

Fineman and Ross method is a common method to linearize the copolymer composition equation (Eqn. 5.2). F and f were calculated from the monomer feed and copolymer composition data respectively (Tables 5.9-5.11). Plot of F(1-f)/f *Vs* F^2/f was a straight line with a negative slope. The reactivity ratio values r_1 (acrylamide) and r_2 (potassium methacrylate, ammonium methacrylate or ammonium acrylate) were computed from the graph as a slope and intercept respectively. The main disadvantage of this method is that this method is unsymmetrical with respect to r_1 and r_2 and the experimental data is unequally weighed. Plot of each monomer pair studied is given below (Figs. 5.6-5.8). When the graph for Fineman-Ross method is observed, except, AKM system, AAM and AAA systems showed linearity. Potassium salts based system was nonuniform indicating its scattered nature. The r_1 and r_2 values obtained are presented in Table 5.12.

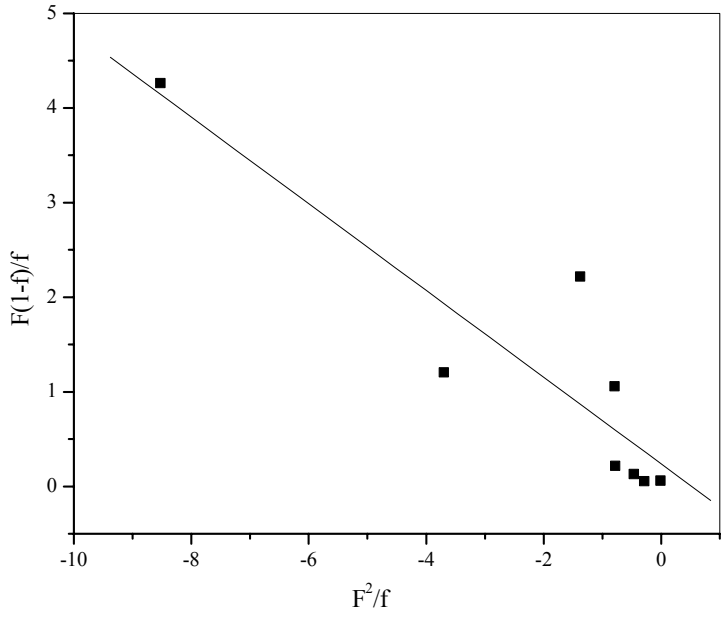

Figure 5.6. Estimation of reactivity ratio by Fineman-Ross method for poly(acrylamide-co-potassium methacrylate) system. r_1= 0.46±0.09 and r_2=0.24±0.30

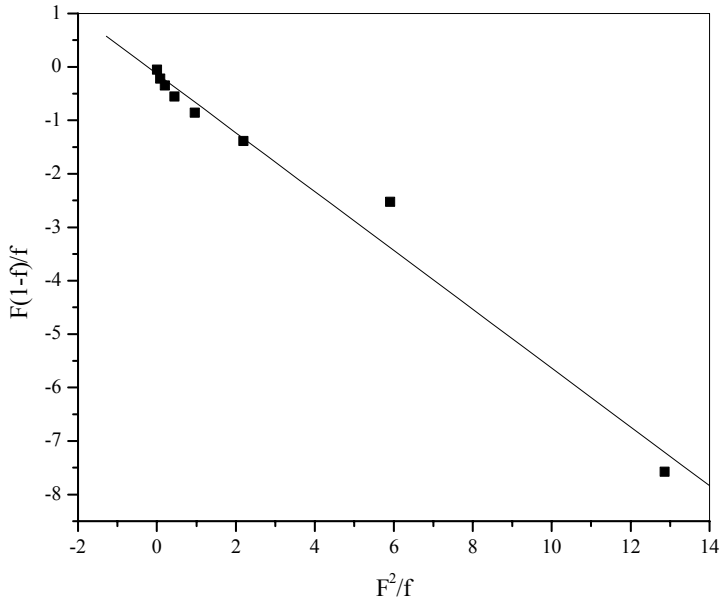

Figure 5.7. Estimation of reactivity ratio by Fineman-Ross method for poly(acrylamide-co-ammonium methacrylate) system. r_1 = 0.55 ±0.03; r_2 = -0.13±0.17

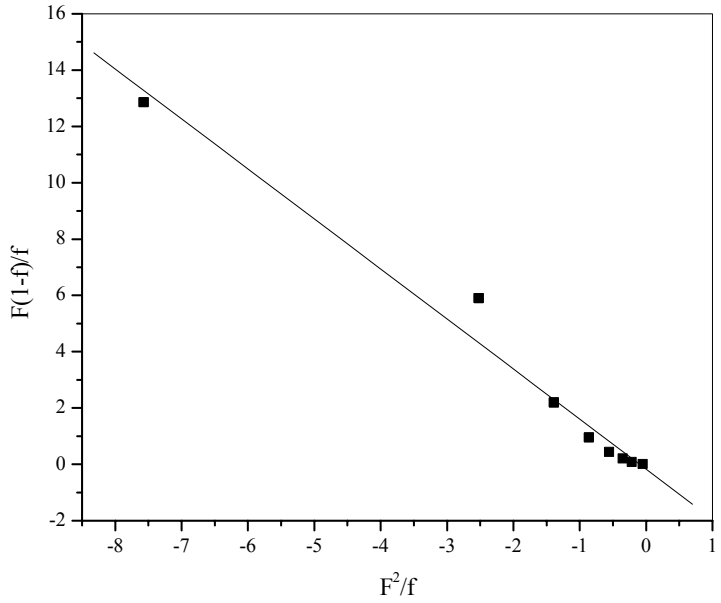

Figure 5.8. Estimation of reactivity ratio by Fineman-Ross method for poly(acrylamide-co-ammonium acrylate) system. $r_1 = 1.77 \pm 0.10$; $r_2 = 0.17 \pm 0.31$

5.3.3.2 Extended Kelen-Tudos method

Kelen-Tudos method is a graphical semi-empirical procedure generally used to overcome the shortcomings of Fineman-Ross linearization. This provides accurate values of r_1 and r_2 by analytical solution. A large number of binary copolymerization systems have been predicted by this method. A straight line is obtained by plotting η as a function of ξ. This linearity testifies to the applicability of copolymer composition equation and the simple two parameter model implicit in it. Extrapolation to $\eta=0$ yield $-r_2/\alpha$ and r_1 as respective slope and intercept. The proper choice of α can be chosen such as 1 for a monomer pair with nearly identical ratios. When reactivities of two monomers are markedly different or data is not uniformly distributed, then α is chosen considering the entire experimental range of composition for both polymer and comonomers, if F_{min} and F_{max} are lowest and highest values of F, $\alpha = (F_{min} \times F_{max})^{1/2}$. The procedure does not suffer

from reindexing error. This modification can be used for relatively high conversion. It gives the data symmetrically located along the interval of the independent variable and gives a visual evaluation of the applicability. The confidence limit for this method is a function of student's distribution for n experiments at n-2 degrees of freedom and at the desired probability level. For all three sets, the graphs were plotted using the experimental data (Tables 5.9-5.11 and Figs. 5.9-5.11). The r_1 and r_2 values obtained are presented in Table 5.12.

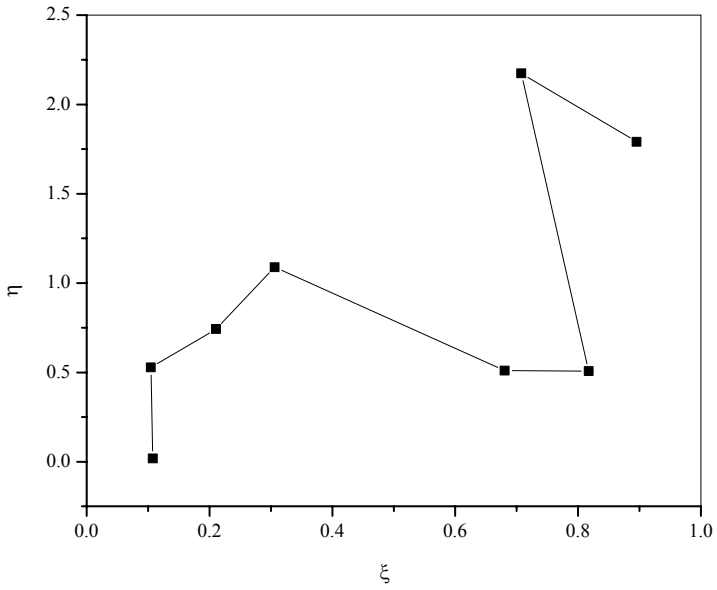

Figure 5.9. Estimation of reactivity ratio by extended Kelen and Tudos method for poly(acrylamide-potassium methacrylate) system. This plot does not have any physical meaning and no estimation of r_1 and r_2 value can be obtained

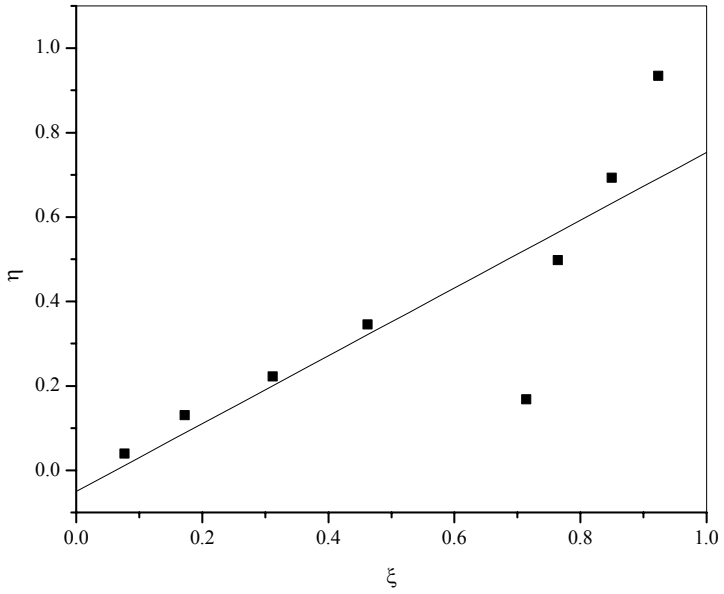

Figure 5.10. Estimation of reactivity ratio by extended Kelen and Tudos method for poly(acrylamide-ammonium methacrylate) system. r_1= 0.85±0.21 and r_2=0.03±0.13

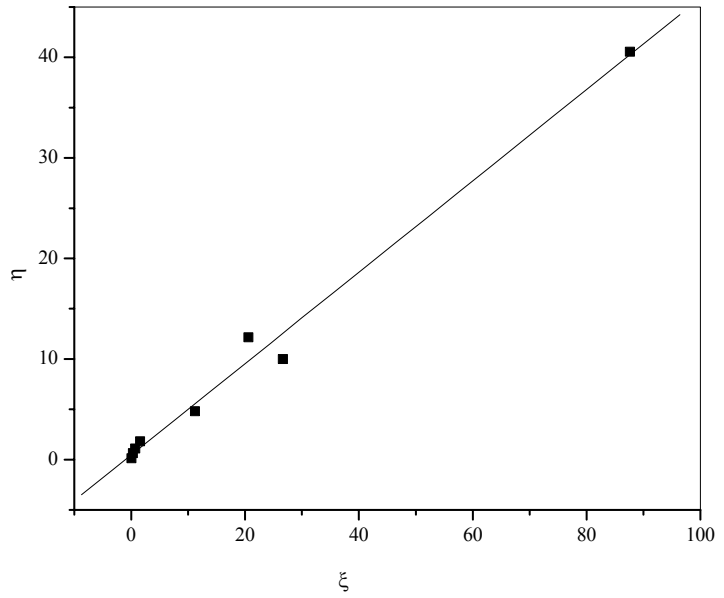

Figure 5.11. Estimation of reactivity ratio by extended Kelen and Tudos method for poly(acrylamide-ammonium acrylate) system. r_1= 0.85±0.01 and r_2=0.39±0.40

5.3.3.3 Discussion

It is believed that the reactivity ratios approach unity as temperature increases. Typical expression of the reactivity ratio as a function of temperature and assume that the pre-exponential factors are of the same order of magnitude, i.e. K^{o}_{ii} /K^{o}_{ij} (Eqn. 5.4). It is then apparent that if E_{ii} is smaller than E_{ij}, the reactivity ratio is larger than 1 and it decreases toward 1 as the temperature increases. On the other hand, if E_{ii} is greater than E_{ij}, r_i is smaller than 1 and it increases toward 1 as the temperature increases. Thus in both cases the reactivity ratio approaches one as the temperature increases.[94]

$$r_i = \frac{K^0_{ii}\exp(-E_{ii}/RT)}{K^0_{ij}\exp(-E_{ij}/RT)} \qquad 5.4$$

In our case the situation seems to be different. Linearization methods were used to analyze the data and estimate the reactivity ratio values. In Fineman-Ross model, for AKM system, the points were not linear. Points did not show any trend but were scattered in a plane. The calculated reactivity ratio values were $r_1 = 0.46\pm0.09$ and $r_2 = 0.24\pm0.30$. The high error bar, ±0.30 indicates the scattered nature of the plot. In case of acrylamide-ammonium acrylate/methacrylate, $r_1 > 1$ and $r_2 << 1$. This means both acrylamide and carboxylate radicals preferentially add to acrylamide until it is exhausted. Carboxylate radical would subsequently homopolymerize but as AM is a sluggish monomer and the reactions are very fast and chilled at 50%, homopolymerization was not possible.

The data which showed linearity in Fineman-Ross model when subjected to Kelen-Tudos method, showed nonlinearity in which two different linear regions were observed. This means the data cannot be interpreted by conventional means. In case of AKM system, points were scattered for both the systems. And for r_2, again the error bar

was high. In AAM system, r_1 and r_2 values by Fineman-Ross method were 0.55±0.03 and -0.13±0.17 and by Kelen-Tudos method, 0.85±0.21 and 0.03±0.13 respectively. The r_1 by different methods are different and in addition to this difference in r_2 values, as seen above, the error bar was high. Similar trend was observed in AKA system. The r_1 and r_2 values by Fineman-Ross method are 1.77±0.10 and -0.171±0.31 and by Kelen-Tudos method, 0.64±0.01 and 0.19±0.88 respectively. The values confirm points do not fall in the conventional copolymerization behaviour.

It was curious to see the plausible reasons for the nonlinear behaviour of these systems and for AKM system in particular. Data of analysis was checked for consistency. It can be inferred from the Table 5.8, all the values obtained from different analytical techniques (TGA, AAS, IR, EDAX) were in good agreement which mean analytical inconsistency is not the source of nonlinearity. This behaviour could be inherent.

When data was analyzed carefully, it was observed that after a critical concentration, the carboxylate salts do not enter in the copolymer or enter at marginal rate. In all three sets, after the 6:4 (mol/mol acrylamide:carboxylate salt) composition, the incorporation rate was decreased and the copolymer composition did not reflect the true values. Sometimes it showed higher mol fraction of acrylamide than present initially in the feed!! Surely, this has to be taken into the account when we analyze the system. Carboxylate salts are not very much prone for frontal homopolymerization so when they are present at low concentration along with reactive monomer, acrylamide, they tend to get copolymerized easily. When their concentration in the feed increases, they act as a heat sink, removing the exothermic heat. Reduction in front temperature with increase in carboxylate concentration in the feed supports this fact. Rate of polymerization is also

affected. At front temperature and in the reaction zone, copolymerization takes place stochastically. Reaction time for polymerization to take place is very less. Relatively inert material like salts at higher concentration could not polymerize in this short period and thus act as diluent. A critical concentration come beyond which salt cannot be entered into the copolymer or the rate of incorporation trims down drastically. Typically, it was observed that above 6:4 mol/mol (M_1:M_2) composition, salt cannot be entered into the copolymer or very low amount is incorporated in case of reactive monomer like ammonium acrylate.

Therefore, the compositions above 4:6 can be discarded in order to minimize error bar and nonlinearity. Fineman-Ross model was reapplied using compositions upto 0.6:0.4 (M_1:M_2) (Figs. 5.12-5.14). It was observed that in case of potassium methacrylate, the confidence region was still less. However, the reactivity of carboxylate radical was found to increase. With ammonium salts, the reactivity ratio values did not change and confidence region was high with minimum standard deviation. This may tend to conclude that the incorporation of higher concentration of carboxylate salts in the monomer feed could be responsible for the inconsistency.

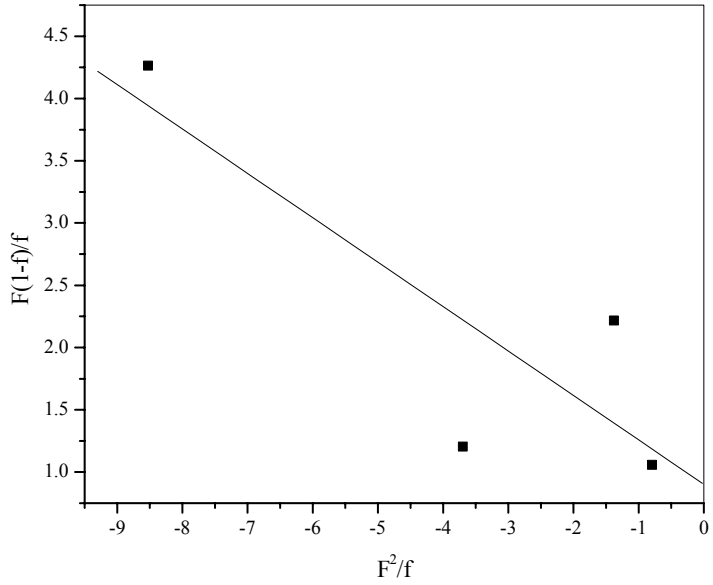

Figure 5.12. Estimation of reactivity ratio by Fineman-Ross method for poly(acrylamide-co-potassium methacrylate) system. $r_1 = 0.36 \pm 0.16$; $r_2 = 0.90 \pm 0.74$

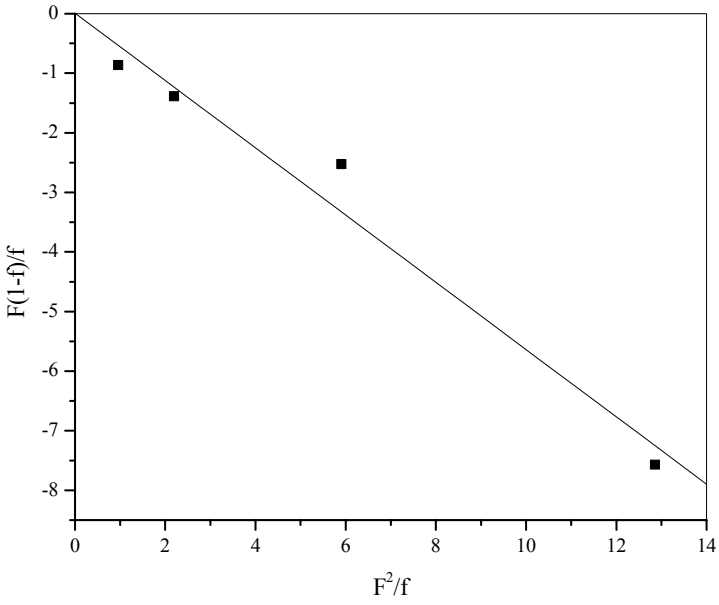

Figure 5.13. Estimation of reactivity ratio by Fineman-Ross method for poly(acrylamide-co-ammonium methacrylate) system. $r_1 = 0.56 \pm 0.01$; $r_2 = 0.01 \pm 0.11$)

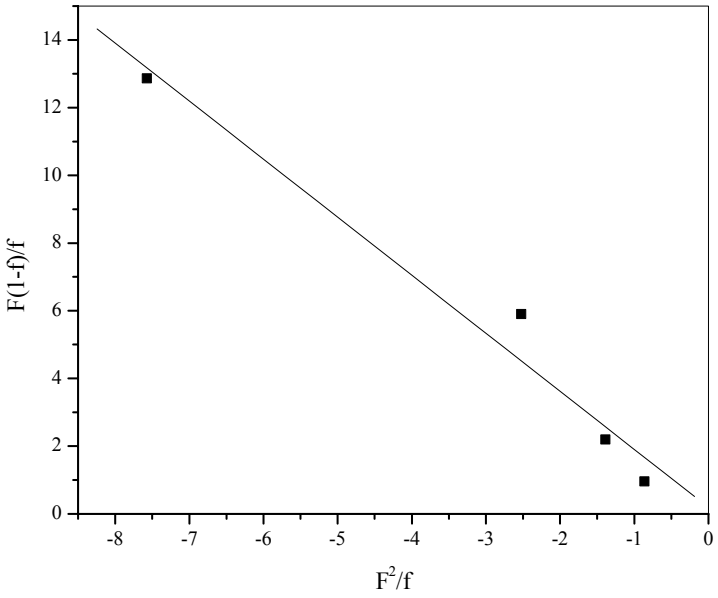

Figure 5.14. Estimation of reactivity ratio by Fineman-Ross method for poly(acrylamide-co-ammonium acrylate) system. $r_1 = 1.72 \pm 0.21$; $r_2 = 0.19 \pm 0.28$)

However, Kelen-Tudos method did not support this conclusion. The plots of the same data when plotted by Kelen-Tudos method (Fig. 5.15), showed positive intercept in case of AKM system, while ammonium salts based systems showed linearity (Figs. 5.16, 5.17). However, the slopes of the plots and hence the reactivity ratio values increased drastically. The rate of incorporation of carboxylate salts in the copolymerization was increased. It can be seen that both the reactivity ratio values in each set were above 1 indicating the tendency towards the block copolymer formation. However, this is not supported by experimental values. In those systems, incorporation of carboxylate salts is not consistent with reactivity ratio more than 1.

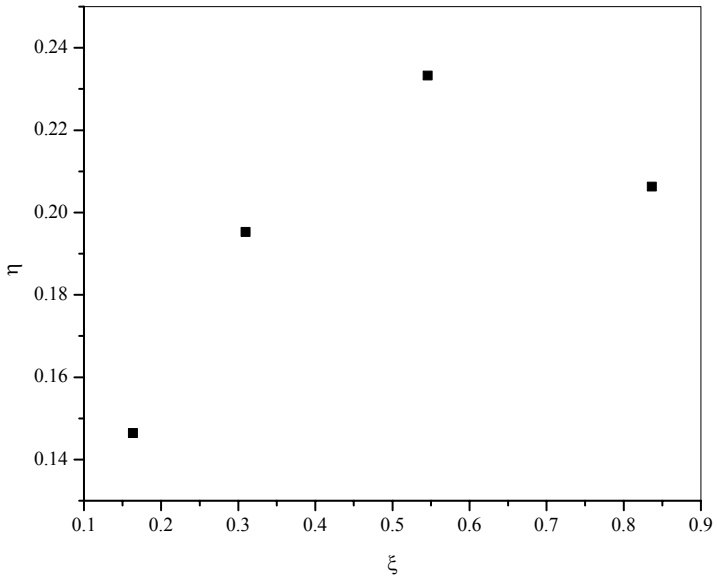

Figure 5.15. Estimation of reactivity ratio by extended Kelen and Tudos method for poly(acrylamide-co-potassium methacrylate) system. $r_1 = 1.97 \pm 0.13$; $r_2 = 1.42 \pm 0.06$

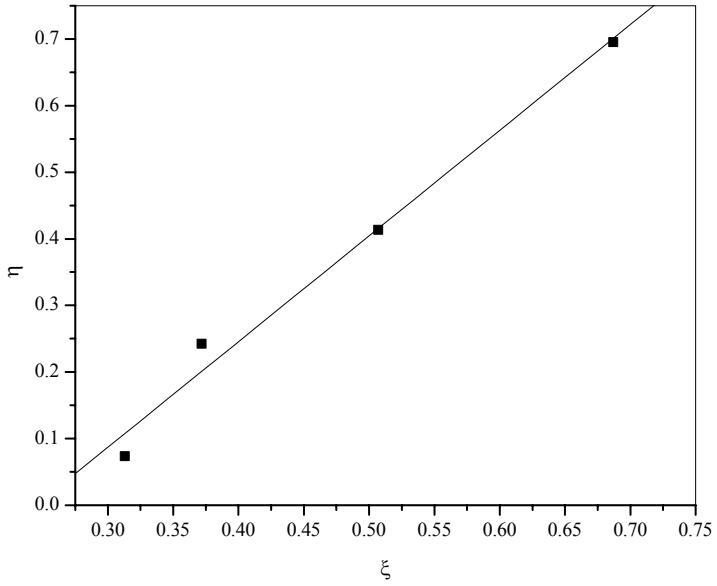

Figure 5.16. Estimation of reactivity ratio by extended Kelen and Tudos method for poly(acrylamide-co-ammonium methacrylate) system. $r_1 = 1.97 \pm 0.13$; $r_2 = 1.42 \pm 0.06$

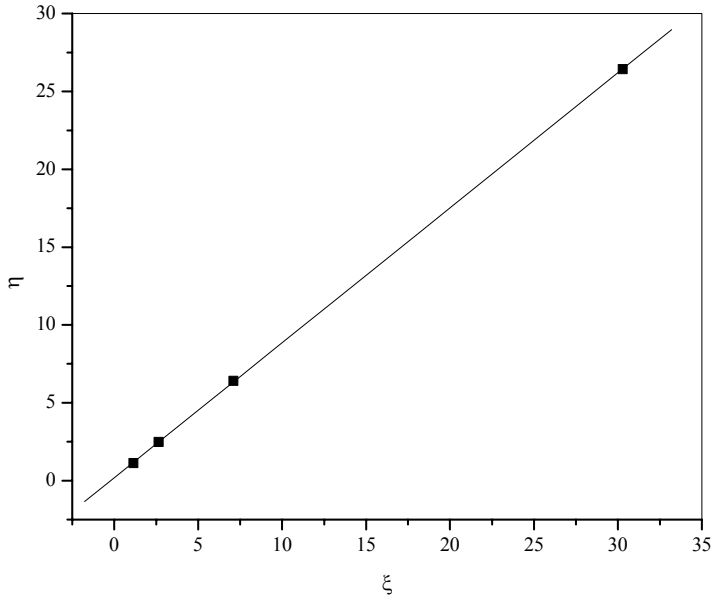

Figure 5.17. Estimation of reactivity ratio by extended Kelen and Tudos method for poly(acrylamide-co-ammonium acrylate) system. $r_1 = 1.06 \pm 0.01$; $r_2 = 0.93 \pm 0.04$

5.3.3.4 Comparisons and analysis of nonlinear behaviour

Table 5.12. Reactivity values from Fineman-Ross and Kelen-Tudos methods obtained from graphs

	Fineman-Ross		Extended Kelen-Tudos	
	All points	First four points	All points	First four points
Poly(AKM)				
r_1	0.46±0.09	0.36±0.16	No physical meaning	1.97 ±0.13
r_2	0.24±0.30	0.90±0.74		1.42±0.06
Poly(AAM)				
r_1	0.55±0.03	0.56±0.01	0.85±0.21	1.97±0.13
r_2	-0.13±0.17	0.01±0.11	0.03±0.13	1.42±0.06

Poly(AAA)				
r_1	1.78±0.10	1.72±0.21	0.85±0.01	1.06±0.01
r_2	0.17±0.31	0.19±0.88	0.39±0.40	0.93±0.02

r_1 is the reactivity ratio of acrylamide and r_2 is reactivity ratio of potassium methacrylate, ammonium methacrylate or ammonium acrylate

When we tried to find the validity of reactivity ratio concept in FP, it was indeed observed that less reactive monomer reacts slowly even at high temperature. The r_1 value (acrylamide) was always much higher than its comonomer r_2 values (e.g. potassium methacrylate). Reactivity ratios were calculated by taking the entire data range and first four data points. From the Table 5.12, it is clear that, in Fineman-Ross method, there is no change in reactivity ratio values of the two plots. This means that the comonomer incorporation is highly effective initially and determines relative rates of addition. Comonomer then acts as inert diluent. In Kelen-Tudos method, the r_1 and r_2 values for both regions markedly differed. When the entire data range is taken, the values are comparable with Fineman-Ross method but for the initial four points plot, unexceptional rise in r_2 values was observed. The data revealed the tendencies of formation of block copolymers. However, as seen above, this was not true and copolymers were random.

When the values obtained by Fineman-Ross and Kelen-Tudos were compared, they differed. For example, in case of AKM system, the r_1 changed from 0.36±0.16 to 1.97 ±0.13 and r_2 from 0.90±0.74 to 1.42±0.06 (Table 5.12). This means that frontal copolymerization does not follow trivial ways of copolymerization. Hence the system may not behave as per the assumptions of the models on more than one point.

Following are the probable explanations for anomalous behaviour of the frontal copolymerization systems:

1] The copolymer analysis and comparison with feed indicates noncomparable reactivities. The simple model is based on the assumption of comparable reactivities which yields copolymer composition equations. The methods of estimation of reactivity ratios are based on copolymer composition equation. In such cases, the validity of the steady state assumption is questionable and may not be applicable.[194]

2] The reactions were conducted in solid phase. Although homogeneity is assumed, it may not be true at molecular level and this assumption may be violated. This may affect collision frequency of the monomers minimizing the randomization.

3] The reaction temperatures were high (>170^{o}C) and the rate of polymerization was rapid at localized level. Although at high temperature the activation energy difference should be minimum between two monomers, other competing reactions such as grafting, cyclization etc. dominate. Moreover, at high temperature, premature termination rates are also high which is supported by the molecular weights of the copolymer. The molecular weights were in between 1.3±0.03 x 10^4 g/mol with high PDI 3.5±0.5 (on polyacrylamide standards). Thus, in kinetic sense, the system contains more than two monomers and/or more than two active centres.

4] As seen above, carboxylate salts act as reacting diluents. The concentrations of these diluents vary through out the feed composition. This effect might be one of the reasons for inconsistent data.

Therefore, the system cannot be treated by simple models and various complexities involved in the polymerization need to be taken into account. A different model is required to explain this behaviour.

5.4 Conclusion

The possibility of using frontal polymerization to produce copolymers has been investigated. Amongst several pairs tested, solid-solid monomer pairs yielded clear front propagation. With liquid-liquid monomer pairs, fronts were extinguished due to various instabilities. With solid-liquid pairs, front propagation was possible only at low concentration of liquid monomer. An exhaustive analysis of four pairs viz. acrylamide-potassium acrylate, acrylamide-potassium methacrylate, acrylamide-ammonium acrylate and acrylamide-ammonium methacrylate was carried out. It was observed that with acrylate salts the rate of polymerization was always higher than respective methacrylate salts. In methacrylate salts, the rate of polymerization was relatively unaffected by the molar composition in the feed. Front temperature was also higher in acrylates.

The high front temperature in acrylamide-potassium acrylate system triggeres in imidization and yields copolymers which are not water soluble but are partially crosslinked. Three remaining pairs were characterized for the monomer composition in the copolymer. Copolymers containing potassium salts were analyzed by TGA, AAS and IR. The results were in good agreement with both techniques. Ammonium containing salts were estimated for monomer composition by pHmetric technique. The data obtained was used to estimate the reactivity ratio values.

Copolymer reactivity ratios were estimated by Fineman-Ross and Kelen-Tudos methods. It was observed that carboxylate group does not incorporate into the copolymer or incorporated marginally after a critical value. Graphs were plotted by taking the entire data range points and first four points (upto 0.6:0.6 mol/mol M_1/M_2). It was observed that acrylamide always yield higher reactivity ratio values than corresponding carboxylate

salt. There was difference in reactivity ratio values for Kelen-Tudos method when calculated by taking four points. Here, both r_1 and r_2 values in all three sets were greater than 1. The reactivity ratio values by both methods do not match because of the complex and unconventional mode of frontally prepared copolymers.

Finally, one of the unique outcomings of this process was, we could successfully copolymerize carboxylate salts, homopolymerization of which otherwise is not possible by FP.

Chapter VI

FUNCTIONALIZED COPOLYMER NETWORKS

6 Functionalized crosslinked networks

6.1 General

Macroporous polymers,[125,127,204-210] known since 1950's, have internal porosity in both swollen and dry states. These are typically synthesized as spherical beads by suspension polymerization using a combination of vinyl monomer with a high relative concentration of crosslinking multivinyl comonomer. Beaded poly(glycidyl methacrylate-*co*-ethylene dimethacrylate) [poly(GMA-EGDM)] and poly(2-hydroxyethyl methacrylate-*co*-ethylene dimethacrylate) [poly(HEMA-EGDM)] have a reactive epoxide ring and hydroxyl group in the side chain, respectively, which are useful in the design of a whole range of compounds with various functional groups.[125,127,210] Optimal morphological porous structure of these crosslinked network copolymers has been demonstrated for applications as catalysts, chromatographic materials, separation and adsorbent media, immobilization matrices for enzymes and in clinical fields.[210-216]

In suspension polymerization, the reaction occurs in the discontinuous phase as droplets comprised of monomers, initiator and porogen. Nuclei are formed at very early stage of the copolymerization and the size depends on the chosen relative concentrations of the crosslinking divinyl monomer such as ethylene dimethacrylate, and porogen. The polymer formed also phase separates, being crosslinked and insoluble in the mixed solvent composed of monomer and porogen. Porous properties are generally controlled by the type of porogen, the crosslinker and their relative volumes.[127,133] The porogen is a low molar mass compound/ polymer that is miscible with the monomers, does not take part in copolymerization and at the end of the reaction can be easily removed from the copolymer.[133,217-219] The nuclei develop into globules during polymerization, and fuse

together to form microspheres, which associate to form particles. The development of microspheres and particles, which constitute clusters, depends on the porogen.

As seen in chapter I, in case of FP of monovinyl and multivinyl system (crosslinking agent), a sharp front propagates through the reaction media, as polymerization and crosslinking occur simultaneously. The mechanism of this reaction is similar to that in the conventional free radical polymerization systems. Initially monomer(s) is filled in a test tube along with thermally unstable initiator. After applying heat source, initiator decomposes, radicals form and begin to combine with the monomers, forming new radicals. The new radicals then bond with other monomers, causing chains to grow. Eventually each chain combines with a second radical, terminating the growth and producing a polymeric structure. Crosslinking in FP yields rigid thermosets, with novel microstructures and morphologies capable of withstanding high temperatures.[41] Detailed experimental observations and theoretical aspects were presented in chapter I.

In the present study a comprehensive analysis of FP of monovinyl functionalized monomers, HEMA and GMA with divinyl monomer, EGDM is reported. In first part of this study, effect of type and concentration of the initiators and solvents as well as complex initiation and mode of FP (descending and ascending) system on sustainability and shape of the front, front velocity, front temperature and percent yield were investigated. Polymers were exhaustively characterized for micro/macroporosity in the matrix, gel formation and surface morphology as well as compared with identical compositions prepared by suspension polymerization (SP). Later, we present a detailed account of the first experimental observations using SEM photographs which showed

formation of spinning modes in the FP. The propagation of spin modes gives rise to layered pattern in solidified polymer material. The physico-chemical phenomenon of the pattern formation is also discussed.

6.2 Experimental

6.2.1 Materials

Glycidyl methacrylate (GMA), 2-hydroxyethyl methacrylate (HEMA) and ethylene dimethacrylate (EGDM) obtained from Sartomer, USA were used as received to prepare the copolymers. Azobisisobutyronitrile [AIBN], (SISCO, India) was recrystallized from methanol before use as initiator. All other reagents were used as received.

6.2.2 Polymerization

Thick walled test tubes, graduated in 1 mm intervals (12 (i.d.) x 125 mm), were used for the experiments. Polymerization was triggered with soldering iron. Progress of polymerizing front was monitored visually. Rate of propagation of front was timed with a stopwatch and reported as velocity of front (cm/min). A thermocouple, 0.125 mm diameter (Hi-Tech Scientific, India), was inserted after monomers and initiator (benzoyl peroxide (BPO), azobisisobutyronitrile (AIBN), dicumyl peroxide (DCP) or complex initiators DCP:AIBN) were charged into the test tube. Temperature was measured relative to time with programmable temperature controller (Hi-Tech Scientific, India). Monomer feed ratios as well as copolymer composition are indicated as percent crosslink density (% CLD), the mole percent of the crosslinking divinyl monomer, ethylene dimethacrylate, relative to the functional monovinyl monomer, HEMA or GMA. Reactions were videotaped at 50-400 frames/s using Red Lake Imaging, Motionpro

model attached with AF micro Nikkor 105 mm lens CCD camera. Few experiments were triggered by giving the heat source at the bottom (Ascending FP). Copolymers formed were ground using a blender, purified by washing several times with methanol, water and dried in vacuum oven at 50^{o}C for 36 h.

Suspension polymerization: The synthesis was conducted in double walled cylindrical reactor fitted with eight bladed Ruston turbine stirrer and nitrogen inlet. The continuous phase comprised of one weight percent aqueous solution of poly(vinyl pyrrollidone) (PVP). The discontinuous organic phase consisted of GMA, crosslinking divinyl monomer (EGDM) and polymerization initiator [AIBN]. The discontinuous organic phase was introduced into the aqueous phase, stirring was set at 300 rotations per minute and the temperature was maintained at 70^{o}C by circulating hot water. The reactant compositions were identical to those used in FP. The polymerization was continued for 3 h. The copolymer obtained in beaded form was separated by decantation, washed with water, methanol and dried at room temperature under reduced pressure.

Both the sets of copolymers from frontal and suspension were sieved using Kumar test sieves (Mumbai, India), to obtain uniform particles of similar size range (80-100 mesh), used for characterization.

6.2.3 Characterization

6.2.3.1 Velocity of the front and temperature profile

Thick walled test tubes graduated every 1 mm were used for experiments. Movement of polymerizing front was monitored visually (as melting) or thermally. The rate of propagation of front was timed with a stopwatch. A thermocouple, 0.125 mm diameter (Hi-Tech Scientific, India), was inserted after the monomers and initiator were

charged into the test tube. Temperature was measured relative to time with programmable temperature controller (Hi-Tech Scientific, India).

6.2.3.2 Functional group analysis

Surface epoxy/hydroxy functional groups of copolymers were estimated titrimetrically.[220] Millimole of epoxide/hydroxy per gram of polymer was estimated by end group analysis. A brief procedure for expoxy content determination is as follows: a known weight of poly(GMA-EGDM) sample (0.1 g) was taken in a 50 mL conical flask with 25 mL 0.2 N hydrochloric acid solution in 1,4-dioxane. The flask was warmed for 2 hours in an oil bath set at 70^{o}C. Then, 25 mL cresol red (diluted in 50 % ethanol) was added to the mixture and kept in a dark place for 30 min. The mixture was finally titrated against 0.1 N alcoholic potassium hydroxide solution. Similarly blank titration was also performed and the difference followed by numerical calculations yielded the surface epoxy groups of the polymer matrix.

Additionally, for functional group analysis, IR study was implemented. A Shimadzu 8300-Fourier transform infrared spectrophotometer (FTIR) with a resolution of 1 cm^{-1} in the transmission mode was used. The copolymers were milled (2 mg each), mixed with potassium bromide (100 mg), and pressed into a solid disk of 1.2 cm diameter prior to the infra-red measurement.

6.2.3.3 Mercury porosimetry

The pore structure in the copolymers was investigated using mercury intrusion porosimetry in the pressure range 0 – 33000 PSIG (Autoscan, 60 mercury porosimeter, Quantachrome, USA). The mercury contact angle was 140^{o}.

6.2.3.4 Specific surface area

The specific surface area of the polymers was measured using the single point Brauner-Emmett-Teller method. The adsorption of nitrogen at liquid nitrogen temperature was measured at the nitrogen concentration of 30 mol% (balance helium), using a monosorb surface area analyzer (Quantachrome Corp., USA). Before carrying out the measurements using this dynamic adsorption/desorption technique, the instrument (analyzer) was calibrated by injecting a known amount of air and the polymer (0.2-1.5 g) was pretreated *in situ* in the sample cell at 100^{o}C for two hours under the flow (30 cm^3 min^{-1}) of moisture free helium, to remove moisture completely.

6.2.3.5 Scanning electron microscopy

General morphological elucidations of poly(HEMA-EGDM) and poly(GMA-EGDM) beads/particles, using scanning electron microscopy (SEM) was carried out as follows: Dried sample were mounted on stubs and sputter-coated with gold, in order to visualize the bead. Micrographs were taken on a JEOL JSM-5200 SEM instrument. For the study of pattern formation, samples from different parts and depth of the polymer rod were taken carefully and observed for patterns.

6.2.3.6 Porosity

The skeletal density (d_b) and the apparent density (d_a) of polymers were measured by picnometry with mercury as the confining fluid. The copolymers were degassed in a picnometer and filled with mercury under vacuum at 25°C. From the density measurements, total porosity in the matrix was estimated as:

$$\% \text{ porosity} = (1 - d_s/d_p) \times 100 \qquad 6.1$$

6.2.3.7 Solvent-nonsolvent regain

The equilibrium dimethyl formamide (DMF) (g/g) content (EDC) was found out by fully drying the samples in a vacuum oven to constant weights followed by reswelling in DMF. It was defined as:[221]

$$\text{EDC (\%)} = \frac{W_w - W_d}{W_w} \text{ X } 100 \qquad 6.2$$

where, W_w and W_d are the weights of the fully swollen and dry polymer gel, respectively.

Kinetics of EDC was studied by weighing gels after regular time intervals. Similarly water uptake was estimated.

6.3 Results and discussion

6.3.1 Phenomenon

It is well established that free radical frontal polymerization is triggered by the thermal decomposition of initiator.[14] The heat of polymerization induces the initiator in the immediate neighbourhood to decompose into radicals and this sequential reaction propagates as a front. Schemes 6.1 shows the copolymerization of mono and divinyl monomers by FP and SP.

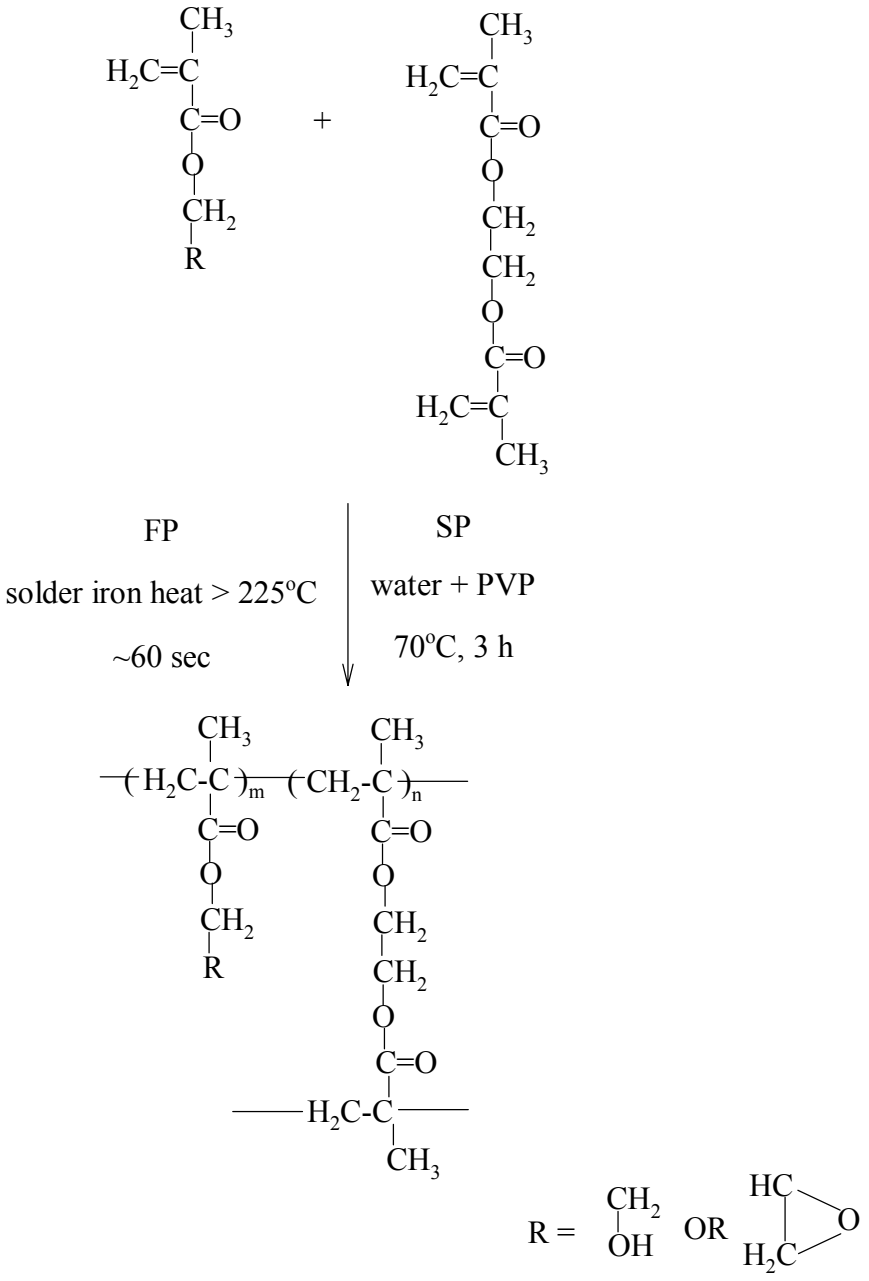

Scheme 6.1. Reaction scheme of frontal and suspension polymerization of HEMA-EGDM and GMA-EGDM

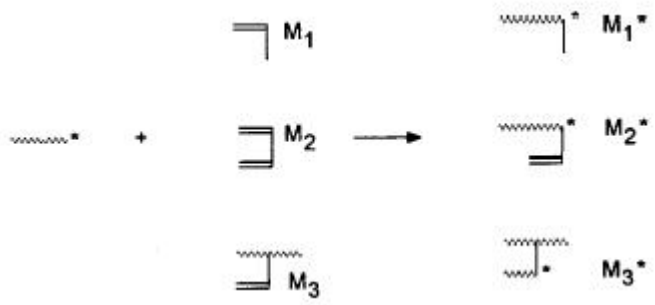

Scheme 6.2. Types of vinyl groups and radical centers in mono and divinyl functionalized copolymerization[205]

Free radical frontal copolymerization between a monovinyl and multi-vinyl comonomer forms a thermoset. Three types of vinyl group exist in free radical crosslinking copolymerization of vinyl/divinyl monomers, namely those on monovinyl (M_1), on divinyl monomer (M_2) and on polymer chains i.e. pendent vinyl (M_3) (scheme 6.2). Crosslinking and ultimately gel formation takes place when M_3 takes part in the reaction. In the present system, ethylene dimethacrylate is the difunctional monomer. The reactivity ratios, r_1 and r_2 for GMA and EGDM system are 0.98 and 1.00 respectively[127] while in HEMA and EGDM system it is 0.84 (±0.20) and 6.2, respectively.[222] When r_1 and r_2 are close to unity and front temperature of polymerization is quite high, the composition of copolymer is expected to mirror the monomer feed ratios. For the copolymerization of HEMA with EGDMA, $r_2 >> r_1$ which means that both types of radicals react preferentially with EGDMA. There is a tendency for successive homopolymerization of the two monomers. Therefore, a heterogeneous network is expected to form. However, during FP, the situation is rather complicated and reactivity ratio concept may get violated because of high front temperature and rapid reaction rates. Due to high temperature and oxygen being present in the system, side reactions and premature termination is expected to takes place leading to a complex crosslinked

structure. All reactions are instantaneous in the narrow reaction zone and probably pseudo zeroth order with respect to monomers. The conditions for preparing heterogeneously crosslinked copolymers from GMA-EGDM and HEMA-EGDM are shown in Tables 6.1 and 6.3.

6.3.2 Front shape, propagation and bubbles

In all reactions, small and big bubbles were generated at the beginning and the front was uneven, and propagated randomly (Fig. 6.1). Bubble layer may act as an insulating layer for heat transfer, and it causes a slow pulsation of moving front. After such an uneven propagation for 2-3 cm, the front attains stability. This stability depends on the amount of crosslinker, initiator type and its concentration. The diffusion of heat through bubble to the adjacent layer is critical. Bubbles are formed due to the liberation of gaseous products due to initiator decomposition, monomer vapors and traces of moisture present in monomers. As bubble grows, it pushes monomer out of its path. At front temperature (FT), there is a rolling motion of low viscosity polymer and monomer. As monomer reacts, it rapidly heats up and thereby increases its volume. Because bubbles are coming down, it can only swell and push down.[45] There is a competition now between descending bubbles and expanding monomer. In this process, generally, bubbles find their way down and monomer goes up, where it polymerizes, triggering a repetition of this process. If convection is higher and bubbles are in large excess, heat is removed in the process and the front ceases. In some instances polymerization front was forced upward due to convection and pressure generated by monomer(s). This happens when thermal expansion exceeds the isothermal contraction, which creates a gap between the polymer and monomer liquid layer resulting in a complete cessation of polymerization

Table 6.1. Experimental variables used for copolymerization of HEMA-EGDM and GMA-EGDM: Effect of variation in initiator type and concentration

Code No.	Crosslink density %	AIBN mol %	BPO mol %	Code No.
H1	25	-	2	G1
H2	50	-	2	G2
H3	100	-	2	G3
H4	200	-	2	G4
H5	400	-	2	G5
H6	25	-	4	G6
H7	50	-	4	G7
H8	100	-	4	G8
H9	200	-	4	G9
H10	400	-	4	G10
H11	25	2	-	G11
H12	50	2	-	G12
H13	100	2	-	G13
H14	200	2	-	G14
H15	400	2	-	G15
H16	25	4	-	G16
H17	50	4	-	G17
H18	100	4	-	G18
H19	200	4	-	G19
H20	400	4	-	G20

[a] H1-20 & G1-20: Frontal copolymerization reactions using 2-hydroxyethyl methacrylate (HEMA)-ethylene dimethacrylate (EGDM) and glycidyl methacrylate (GMA)-ethylene dimethacrylate (EGDM), respectively.; [b] CLD: crosslink density {mol of EGDM/[mol of HEMA/GMA + mol of EGDM] x 100}; [c] AIBN: Azobisisobutyronitrile; [d] BPO: benzoyl peroxide; [e] For FP: heating time: ~60 sec. Total reactants volume was 8.2 mL; [f] Identical compositions were synthesized by suspension polymerization (SP). For SP: temperature- 70^{o}C, stirring speed- 300 rpm, reaction time- 3 h.

process (Fig. 6.2). This was predominant in presence of solvent (e.g. G20-43). We also encountered velocity lag for which we had to give an additional heat impetus for 2-5 sec (e.g. H3, G3).

Table 6.2. Front velocity, front temperature and percent yield data of the reactions performed, as in Table 6.1

Code No.	FV Cm/min	FT ^{o}C	Yield %	Code No.	FV cm/min	FT ^{o}C	Yield %
H1	1.37	175	85.81	G1	0.71	177	86.22
H2	1.10	182	92.71	G2	0.87	187	88.23
H3	1.19	185	94.54	G3	0.94	190	91.25
H4	1.09	185	89.38	G4	0.95	199	90.35
H5	1.42	187	92.26	G5	1.01	198	92.55
H6	0.89	192	84.12	G6	0.76	186	86.70
H7	0.95	196	90.21	G7	0.92	196	85.60
H8	1.06	198	92.45	G8	0.97	183	83.60
H9	1.16	200	91.12	G9	1.03	187	89.41
H10	1.2	203	94.45	G10	1.11	191	95.10
H11	0.87	175	89.12	G11	0.81	189	80.32
H12	0.95	169	87.35	G12	0.86	197	80.67
H13	0.83	172	96.02	G13	0.88	194	81.23
H14	0.85	162	86.10	G14	0.92	179	83.88
H15	0.87	158	97.40	G15	0.94	181	81.16
H16	0.82	181	85.56	G16	0.83	184	82.10
H17	0.92	190	86.12	G17	0.88	187	79.24
H18	0.93	193	94.51	G18	0.9	191	87.10
H19	1.08	198	84.94	G19	0.97	167	92.70
H20	1.2	198	95.53	G20	1.22	178	86.25

[a] FV: front velocity; [b] FT: front temperature; [c] yield: percent yield of the polymer of crosslinker, initiator type and its concentration.

Set I

a **b** **c**

Set II

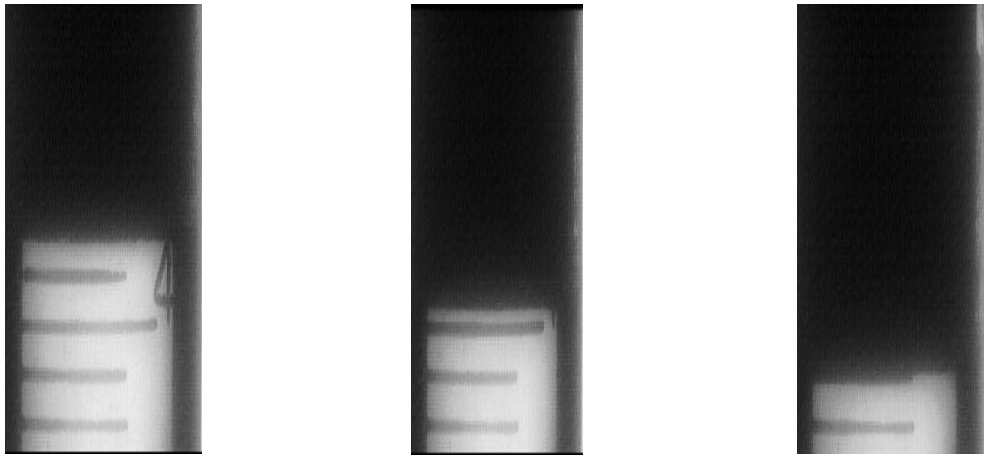

d **e** **f**

Figure 6.1. Snapshots of front propagation in complex initiation system (GMA-EGDM 100 % CLD; 2 mol % AIBN + DCP; a-c: front propagation is uneven and in the form of bubbles; d-f: front stabilized and even propagation without bubbles; images were taken by high speed CCD camera (Motionpro) at a speed of 50 frames/s; Above montages are the images obtained after every 5 sec in each set)

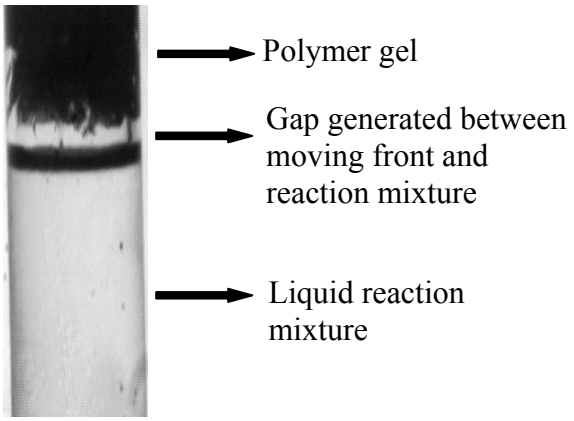

Figure 6.2. Front extinguishes due to the gap created between monomer and propagating polymerization front (code no. G27; reactor size: 12 x 125 mm; BPO:4 mol %; EGDM: 100 % CLD; 1:0.4 v/v monomer:porogen ratio)

6.3.3 Initiator effects

Front velocity is intricately related to initiator concentration and crosslink density.[14,41] Copolymerization reactions were evaluated at 2 and 4 mol % concentration of AIBN and BPO (Table 6.1; H1-H20 and G1-G20) as well with DCP (not shown in Table). For AIBN and BPO, in both HEMA-EGDM and GMA-EGDM systems, clear fronts were observed at 2 and 4 mol % concentration (sometimes additional 5-10 s impetus had to be given at lower CLDs), which went through, forming polymeric product, taking the shape of the reactor (cylindrical). No double diffusive instabilities were observed. Table 6.2 summarizes the details of front velocity, temperature and percent yield. No specific trend was observed at low initiator concentration for HEMA-EGDM system. Representative Fig. 6.3 depicts the front velocity (cm/min) as a function of crosslink density at the two concentrations (2 and 4 mol %) of AIBN and BPO in GMA-EGDM system. It is clear that front velocities are higher at 4 mol % initiator concentration for all monomer feed compositions (CLD %). The increase in radical concentration increases the rate of heat generation and thus the velocity of frontal

polymerization. It was also seen that front velocity increases with the crosslink density. With high crosslink density, rate of termination decreases which in turn increases activation energy of the reaction. In other words, multifunctional vinyl compounds react faster at room temperature than monovinyl monomers.[58] Relative increase in divinyl monomer concentration (EGDM) leads to more inter and intramolecular crosslinking reactions. A comparison between the two initiators indicates that AIBN produces slightly faster fronts than BPO.

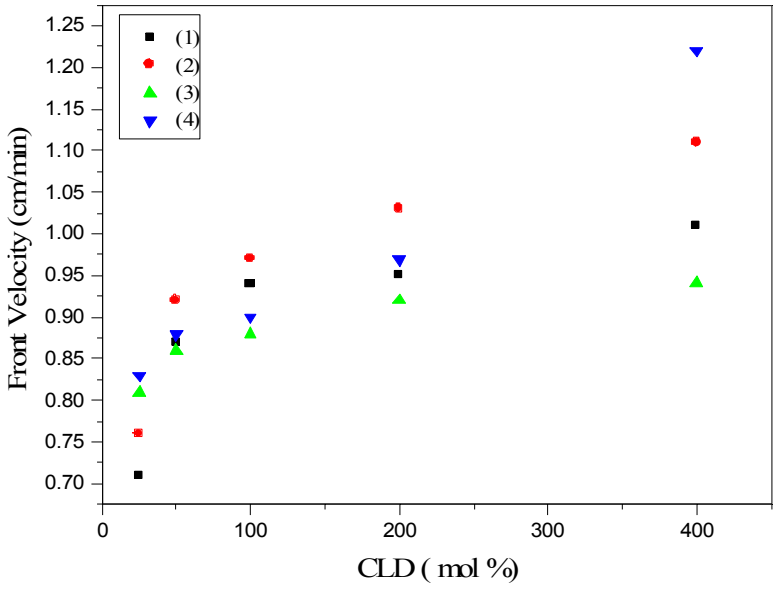

Figure 6.3. Representative graph of front velocity (cm/min) *Vs* CLD (mol %) of poly(GMA-EGDM). Poly(GMA-EGDM) synthesized using (1): 2 mol % BPO; (2): 4 mol % BPO; (3): 2 mol % AIBN and (4): 4 mol % AIBN

Results with DCP, however, were different. The decomposition temperature of DCP at which the first order rate constant exceeds 10^{-5} sec^{-1} is 110°C (activation energy: 147.2 KJ/mol). Front sustainability (activation energy of the polymerization front) depends upon the decomposition activation energy of the initiator. At low DCP

concentration (2 mol %), due to its high decomposition activation energy, a front propagation was initiated but ceased after propagating for a short distance (50-80 % of the column length) for both copolymerization systems (GMA-EGDM and HEMA-EGDM). The radiational and convective heat loss could bring the front temperature below that required to sustain the front. At 4 mol % concentration, sharp transparent front propagation was observed. In both sets, at 25 and 50 mol % CLD, a long trail of bubbles could be seen during the polymerization or on the specimen after the polymerization (Fig. 6.4). At 100 mol % CLD a transparent front propagation was observed. However, the front could not be sustained at higher CLDs perhaps due to increase in activation energy with CLD needed to sustain the front. Greater the stability of the initiator, higher is the overall energy of activation of the front, slower is the front velocity.

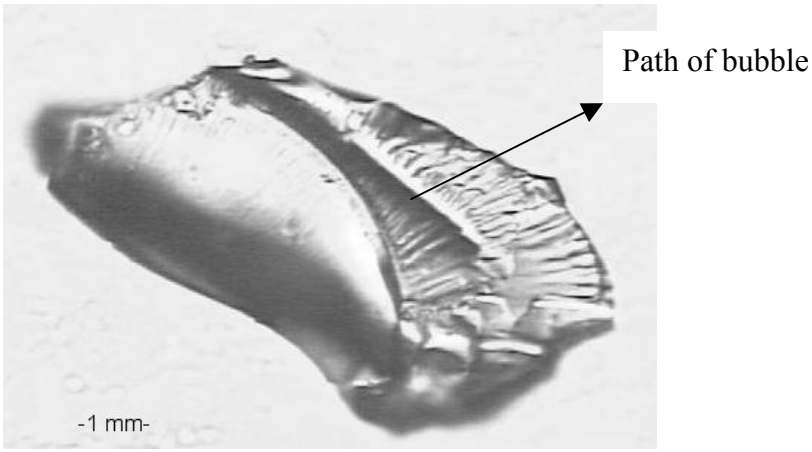

Figure 6.4. A path of bubble observed in 4 mol % DCP initiated system poly(GMA-EGDM); CLD 50%

Therefore, in both sets, front velocities were low and in the range 0.4-0.6 cm/min. With AIBN, a velocity lag was observed at higher CLD due to a density gradient between polymer and monomer reaction mixture. This was circumvented by adding diluents like

silica gel to increase the viscosity of the medium or by giving additional heat impetus for 5 seconds.

Front temperature is dictated by the combination of factors such as enthalpy of the reaction, the heat capacity of the product and the heat lost to the surroundings. Table 6.2 shows that the front temperature varies within $\pm 10^{o}$C for all polymerizations of identical compositions. Also, at all compositions, front temperature was generally high at higher CLDs (100, 200 and 400 % (180 ± 10^{o}C). Front temperature was lower with 2 mol % AIBN in HEMA-EGDM set. As a general trend, the data revealed that the front temperature oscillates with monomer feed composition, with maxima in the CLD range 50-100%, and then a minima at 200% CLD followed by a gradual raise till 400% CLD, at both 2 and 4 mol % initiator concentration. Temperature drift, however, was not very high and was in the range where thermal fluctuations exceed the variations in the temperature. With DCP, as expected, in the reactions which ceased, the temperature was lower (153 ± 5^{o}C); otherwise it was 180 ± 3^{o}C.

Initially, the problem in FP was the lower conversions because of high front temperature, which is responsible for rapid initiator decomposition or 'burning out'. Gel formation in FPs are known to flatten front curvature, prevent instabilities and to increase yield.[14] In the system studied here we observed higher conversions relative to that in the published literature; however, there was no trend. Generally, maximum conversions were observed at higher CLD (Table 6.2). This may be attributed to the fact that increasing concentration of EGDM, that has reactive two double bonds, reduces transfer reactions.

6.3.4 Solvent Effect

High boiling point solvents are needed to produce a propagating front, at the same time, temperature should reach to a high value in order to produce a sufficiently rapid decomposition of free radical initiator. A front can sustain itself only when the volumetric rate of heat exceeds the volumetric rate of heat loss incurred by heat dissipation due to solvent and convective losses. While the conduction heat loss rate increases linearly with temperature, the free radical initiator decomposition is a high activation energy process whose rate increases much more rapidly than linearly with temperature. Thus, as the temperature decreases, the ratio of heat loss to heat generation increases, eventually leading to extinction of the front, if temperature is too low. We conducted our experiments by taking dimethyl sulfoxide (DMSO), paraffin, dichloroethane, dodocane, cyclohexanol, cyclohexane and 2-ethoxy ethyl acetate (EEA) at 1:0.4 and 1:0.8 (vol/vol monomer:solvent) proportions at 2 and 4 % initiator concentration (AIBN and BPO) in both sets. Amongst all, the front could be sustained only with EEA (Table 6.3) in HEMA-EGDM system. In presence of low boiling point solvents front could not start and only boiling of monomer mixture was observed and in others fronts were extinguished at lower conversions (10-30 % of the column length).

Table 6.3. Experimental variables used for copolymerization of HEMA-EGDM and GMA-EGDM: Effect of variation in solvent volume

Code No.	Crosslink density %	AIBN mol %	BPO mol %	EEA mL	Code No.
H21	25	-	2	2.36	G21
H22	400	-	2	2.36	G22
H23	25	2	-	2.36	G23

H24	400	2	-	2.36	G24
H25	25	-	4	2.36	G25
H26	50	-	4	2.36	G26
H27	100	-	4	2.36	G27
H28	200	-	4	2.36	G28
H29	400	-	4	2.36	G29
H30	25	-	4	3.67	G30
H31	50	-	4	3.67	G31
H32	100	-	4	3.67	G32
H33	200	-	4	3.67	G33
H34	400	-	4	3.67	G34
H35	25	4	-	2.36	G35
H36	50	4	-	2.36	G36
H37	100	4	-	2.36	G37
H38	200	4	-	2.36	G38
H39	400	4	-	2.36	G39
H40	25	4	-	3.67	G40
H41	50	4	-	3.67	G41
H43	100	4	-	3.67	G42
H43	200	4	-	3.67	G43
H44	400	4	-	3.67	G44

[a] H1-21 & G1-44: Frontal copolymerization reactions using 2-hydroxyethyl methacrylate (HEMA)-ethylene dimethacrylate (EGDM) and glycidyl methacrylate (GMA)-ethylene dimethacrylate (EGDM) respectively; [b] CLD: crosslink density {mol of EGDM/[mol of HEMA/GMA + mol of EGDM] x 100}; [c] AIBN: Azobisisobutyronitrile; [d] BPO: benzoyl peroxide; [e] EEA:2-ethoxy ethyl acetate; [f] For FP: heating time: ~60 sec. Total reactants volume was 8.2 mL; [g] Identical compositions of HEMA-EGDM (H25-H44) were synthesized by suspension polymerization (SP); [h] For SP: temperature- 70^{o}C, stirring speed- 300 rpm, reaction time- 3 h.

Table 6.4. Front velocity, front temperature and percent yield data of the reactions presented in Table 6.2

Code No.	FV cm/min	FT ^{o}C	Yield %
H21-24	No Reaction		
H25	0.64	169	66.78
H26	0.68	163	75.34
H27	0.78	186	93.12
H28	0.82	189	92.44
H29	0.80	175	91.9
H30	0.75	172	67.11
H31	0.44	187	71.96
H32	0.40	181	83.66
H33	0.24	185	96.00
H34	0.20	179	96.03
H35	0.27	141	81.49
H36	0.37	147	85.86
H37	0.47	145	81.73
H38	0.74	154	95.89
H39	0.43	166	87.67
H40	0.22	86	76.21
H41	0.32	105	75.54
H42	0.26	121	80.24
H43	0.48	115	72.62
H44	0.22	122	72.98

[a] FV: front velocity; [b] FT: front temperature; [c] yield: percent yield of the polymer.

Porogens (synonym used for solvent) are solvating or non-solvating inert reagents used to generate 'tailor-made' porous structure in crosslinked polymer networks synthesized by suspension polymerization.[133] In GMA-EGDM set, the polymer formed immediately after the initial ignition and the front propagation was started. At all compositions, although the front propagation was initiated, it extinguished after propagating approximately 50 % of the column length. Porogen dissipates the threshold heat required to sustain the front. Front temperature was considerably low (130-140^{o}C). We then performed few reactions using a diluent. Diluents are inert materials which act as filler and are added to inhibit buoyancy-induced convection in the solutions.[14] Frontal polymerization carried using silica gel as diluent went through to completion only at 400 % CLD.

In HEMA-EGDM polymerization, however, front could be sustained in EEA at 4 mol % initiator concentration. At 2 mol % of AIBN and BPO, front ceased after the initial burst and little propagation (Table 6.3; H21-H24). The type of porogen has marginal influence on rate of polymerization in suspension polymerization, while the same has strong favourable effect in frontal polymerization. Cyclohexane, DMSO etc., as porogen, quenched the front due to extensive heat loss, while EEA sustained the front with both AIBN and BPO. The main rationale for EEA sustaining the front in HEMA-EGDM set, but not in GMA-EGDM system, is the slow phase separation of EEA in HEMA-EGDM due to solvation. In HEMA-EGDM set, there was a marked difference in front velocities and temperatures with AIBN and BPO. BPO produced higher rates of polymerization (Table 6.4). In both systems, front velocity and temperature increased with crosslink density. The rate of polymerization in monomer-porogen system was also

found to be dependent on CLD. With AIBN, at higher volume of porogen (1/0.8 v/v; Table 6.3; H40-H44), bulk polymerization competed with FP. AIBN, with low activation energy, decomposes rapidly and the porogen transferred the heat to the subsequent layers causing bulk polymerization to occur. However, no bulk polymerization was observed with BPO and reactions were completed by true FP. All reactions with DCP ceased due to extensive heat loss.

6.3.5 Complex initiation

High front temperature depletes of initiator which in turn lowers the percent conversion in FP. A mixed initiation system comprised of AIBN and DCP was used with a strategy that the lower activation energy initiator will increase the rate of polymerization while higher activation energy initiator will increase conversion.[42,49] It was indeed observed that the front was stabilized and that yields were much higher (>96 %). The nature of front was flat after the initial uneven propagation (Fig. 6.1). When the reaction is triggered, AIBN, having lower activation energy, is decomposed more rapidly while DCP, with higher activation energy, stabilizes the front. Thus, AIBN ensures moderate velocity while DCP polymerizes the final traces of unreacted monomers before the front moves, ensuring thereby a higher conversion. At 2 mol % (without solvent), AIBN:DCP (2:1 mol/mol) generated higher front velocities in both HEMA-EGDM and GMA-EGDM relative to DCP alone at 4 mol % concentration. Fig. 6.5 presents the front velocity data of HEMA-EGDM system. Front velocities were almost constant (0.93±0.02 cm/min except CLD 25 %). Front temperature was on a lower side (151-172^{o}C), and as per expectation, yields were high (97±2 %). Similarly, in GMA-EGDM system, front velocities were almost constant and relatively faster than that in HEMA-EGDM system

(Fig. 6.5). Front temperatures and percent yield were comparable with HEMA-EGDM system, in the range 160-180^{o}C and 98±2 %, respectively.

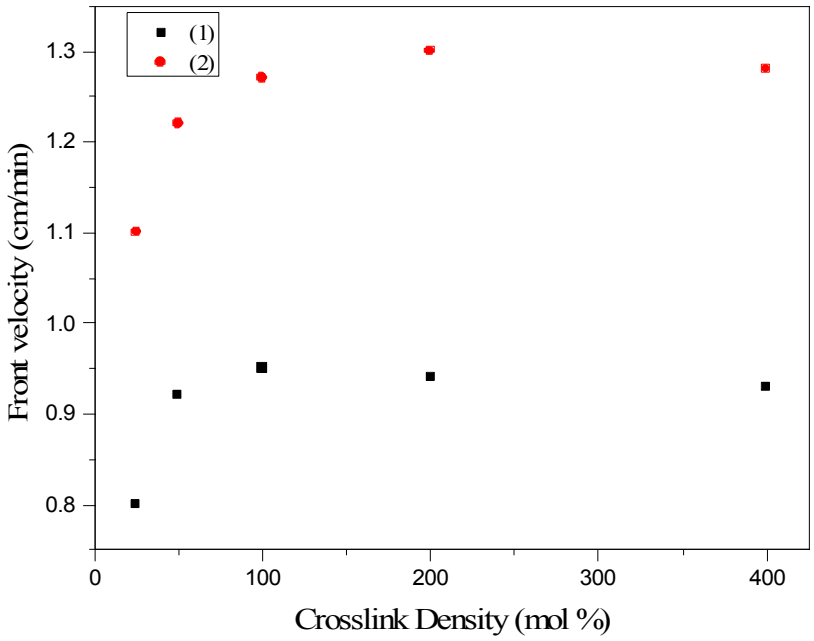

Figure 6.5. Front velocity *Vs* Crosslink density graph of complex initiatiator system (2 mol % AIBN:DCP); (1) poly(HEMA-EGDM) and (2) poly(GMA-EGDM)

6.3.6 Ascending polymerization

To understand front propagation behavior, we conducted selected reactions in both HEMA-EGDM and GMA-EGDM systems with and without solvent at 25 and 100 % CLD by giving heat impetus at the bottom of the reactor. Ascending fronts are, generally, not stable due to convective motions, which causes an extensive amount of dispersed heat.[84,85] In our method, when reaction was performed without solvent, ascending front went through in both sets proceeded in a nonplanar mode. Front

propagated in upward direction and yielded a polymer gel. The propagation was along the walls of the reactor first and was clubbing at the center. DMSO ceased descending polymerization, but ascending polymerization proceeded to completion when performed with monomer:DMSO (1:0.4 vol/vol) in presence of diluent (silica gel) in both sets. All other solvents studied could not produce stable fronts.

6.3.7 Comparison with suspension polymerization

6.3.7.1 Theory and mechanism

We also conducted reactions comprising of monomer(s), mixed initiators (2 mol %), EEA (porogen) and diluent (silica gel; 5 % of monomer). At 1:0.4 monomer:porogen (vol/vol) ratio, it was observed that additional heat impetus was needed for 5 sec for reaction to be completed. The shape of front was flat and products obtained were opaque. In both sets, at higher CLDs (200 and 400 %) front propagation did not go through to completion. All reactions carried at monomer:porogen ratio, 1:0.8 (vol/vol) ceased, even in presence of diluent. The reason being that front temperature was not sufficient to sustain front propagation.

We present a detailed analysis followed by a comparison between frontal and suspension polymerization methodologies. We compared GMA-EGDM and HEMA-EGDM polymerizations at 4 mol % AIBN and BPO concentrations. As solvents ceased the reactions in GMA-EGDM system, we will evaluate and compare HEMA-EGDM system with porogen (2-ethoxyethyl acetate) at 1:0.4 and 1:0.8 monomer:porogen (vol/vol) ratio using 4 mol % AIBN and BPO (Table 6.3) with identical compositions of SP. All polymers were characterized for IR, epoxy/hydroxy number, surface area, pore volume, porosity, solvent/nonsolvent regain and SEM.

Suspension polymerization is widely used in synthesizing macroporous beaded polymers. Beads have internal porosity in both swollen and dry states. The macroporous structure results from phase separation of an inert organic solvent (porogen)[125,133] from the discontinuous polymerizing droplet. For the production of macroporous copolymers, typical recipe comprises of a monovinyl monomer, a divinyl monomer (crosslinker), an initiator, and an inert porogen (diluent). The decomposition of the initiator produces free-radicals which initiate the polymerization and crosslinking reactions. Initiation occurs evenly throughout the layers (propagating reaction zones) and chains grow by addition of monomer units. When EGDM molecule is added to a growing chain, the chain carries a pendent double bond, which may be incorporated in another growing chain. Contribution to chain growth will occur more frequently at the EGDM end, resulting in 'nuclei' whose central portion is high in EGDM content and which possesses a number of outward growing chains with free radical ends. The nuclei are swollen with the surrounding medium to an extent governed by their effective crosslinking and the nature of the medium. When surrounding medium is a good solvent for the polymer, the growing chains will be appreciably extended and will tend not to become entangled inside the nucleus. The monomer mixture is as such a solvent, but as polymerization proceeds in the absence of added diluent and the monomer is used up, the growing chains become less solvated and the nuclei approach progressively closer to each other, with increased penetration opportunities for a second nucleus by a growing chain from the first.

The effect on structure of increased divinyl monomer (EGDM) content in the monomer mixture (increase in % CLD) is thus to increase the size of the nucleus at the expense of growing chains. The product at high conversion of monomer mixture, of high

divinyl monomer content, is therefore a compact and rigid structure with marked network entanglement in the nuclei. In presence of noncompeting solvent (porogen), after a certain reaction time, a three-dimensional network of infinitely large size starts to form. At this point (the gel point) the system (monomer–diluent mixture) changes from liquid to solid-like state. Continuing polymerization and crosslinking reactions decrease the amount of soluble reaction components. After complete conversion of monomers to polymer, only the network and the diluent remain in the system. Crosslinked copolymers prepared by free radical copolymerization exhibit differing pore structures and surface properties (within the pores) depending on the amounts of the crosslinker and the diluent present during the reaction as well as on the solvating power of the diluent. Fig. 6.6 demonstrates typical crosslinking mechanism and formation of porous bead in suspension polymerization.

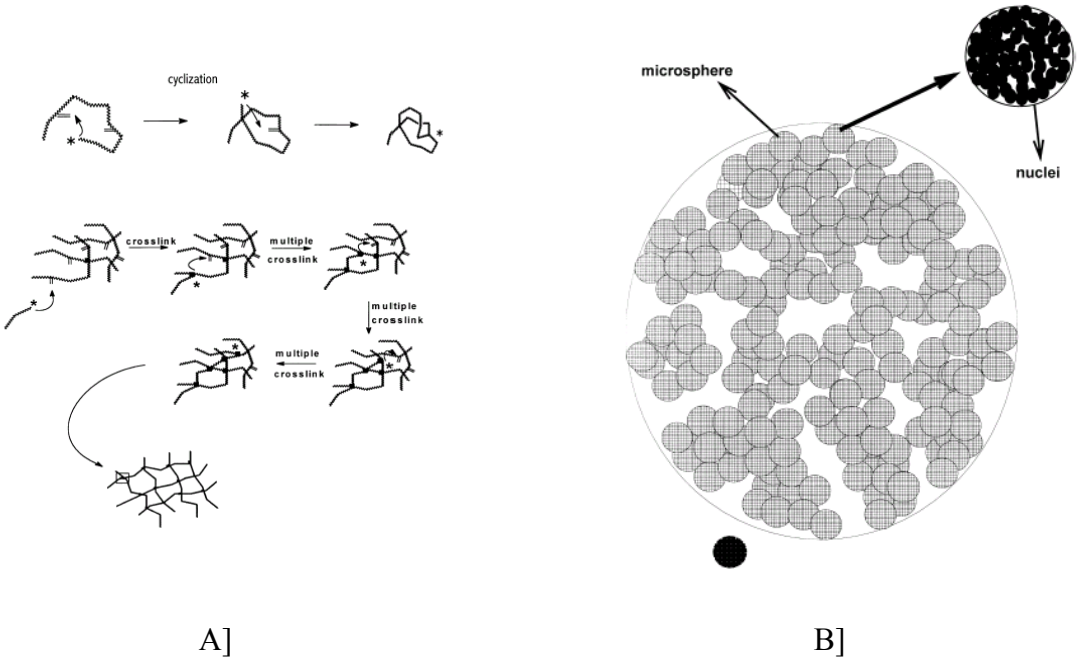

A] B]

Figure 6.6. Schematic representation of A] crosslinking and B] bead formation in suspension polymerization[133]

There are no reports of FP of such systems. We propose the following explanation of the process: In FP, there is a rapid crosslinking due to high front temperature. Phase separation occurs instantaneously and polymerization propagates as a phase separated polymer front. Gel is continuously formed as front propagates. Initiation occurs evenly throughout the layers (propagating reaction zones) and chains grow by addition of monomer units. We conceive no drift in the final composition, as the polymerization process is stochastic at the narrow reaction zone. We believe that porosity is independent of divinyl monomer but dependent on solvent. When EGDM molecule is added to a growing chain, the chain carries a pendent double bond, which may be incorporated in another growing chain. Unlike SP, there is no formation of nuclei in FP. Polymer chains are less solvated. Porosity in FP is due to the gases, monomer, solvent vapors releasing out during the reaction. This porosity is discontinuous in absence of solvent (see later). Solvent (porogen) develops higher porosity in the matrix. As we have seen above, all our reactions excepting EEA failed. EEA is a high boiling liquid and probably solvates the polymer chains more. So partial phase separation takes place at the front temperature and on removal of solvent creates higher pore volume and porosity.

6.3.7.2 Functional group characterization

Formation of copolymer network is confirmed by IR spectroscopy (Fig. 6.7).

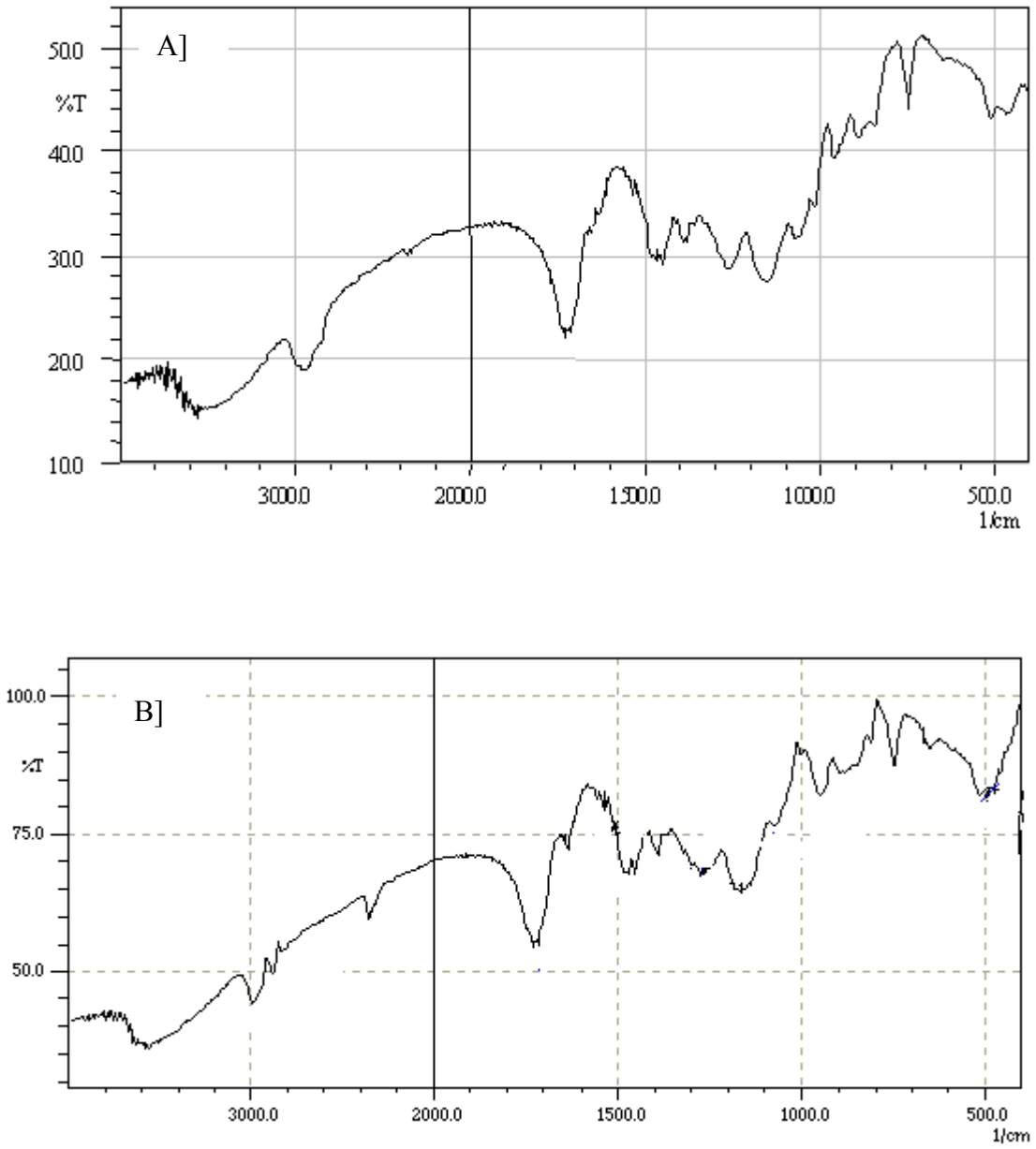

Figure 6.7. Infra-red spectra of copolymer H13 (with 100 % crosslinking density) prepared by a] suspension polymerization and B] frontal polymerization

Table 6.5. Comparison of poly(HEMA-EGDM) by frontal (FP) and suspension polymerizations (SP) for IR absorption

Functional Groups	IR peaks of FP (cm^{-1})	IR peaks of SP (cm^{-1})
-OH	3390	3415

-C=O	1708	1718
-C-O of COH	1070	1072
-C-O-C-	1148	1159

Table 6.6. Typical infra-red absorption bands in poly(GMA-EGDM) prepared by frontal (FP) and suspension polymerization (SP)

Vibrations/ stretching	IR peaks of FP (cm^{-1})	IR peaks of SP (cm^{-1})
C=O carbonyl carbon	1730	1726
Epoxy group	801, 909, 1195	807, 900, 1202
C-O-C stretching	1091	1093

IR spectra of poly(HEMA-EGDM) (CLD 100 %) and poly(GMA-EGDM) synthesized by FP and SP are shown (Fig. 6.7) and tabulated (Tables 6.5 and 6.6). Both methodologies showed no significant difference between copolymers of the two sets. Both poly(HEMA-EGDM) (CLD 100 %) and poly(GMA-EGDM) systems revealed absence of C=C peak at 1600 and 1500 cm^{-1}, indicating complete reaction of vinyl double bond. Additionally characteristic broad peak of –OH vibration around 3400 cm^{-1}, carbonyl carbon peak around 1708 to 1718 cm^{-1} for HEMA-EGDM and carbonyl carbon around (vs C=O) 1725-1730 cm^{-1}, epoxide group (vs C-O-C) at 1200, 900 and 800 cm^{-1} were observed GMA-EGDM systems for both methodologies, respectively.

Epoxy/hydroxy numbers for all polymers were lower than the theoretical value indicating possible intramolecular reactions as observed in HEMA homopolymerization (Chapter III) and also due to disproportionate termination reactions and partial opening of epoxy ring at high temperature (front temperature) through etherification reaction. At high crosslink density, the probability of side reactions reduces due to high reactivity of bifunctional monomer (ethylene dimethacrylate) which yields simultaneous crosslinking

reactions predominantly than side reactions, and thus loss of functionalities can be considerably refrained. For example, experimentally the observed surface epoxy value of FP at 200 % CLD is 1.79 mmol/g which is very close to theoretical value (2.01 mmol/g). Instead, in SP at identical CLD, observed value was 1.36 mmol/g (Table 6.7). At high CLD, in suspension polymerization, at the beginning of the reaction, the reactivity of bifunctional monomer is high which forms compact nuclei, surface epoxy group of the monovinyl monomer (glycidyl methacrylate) reacted at this time, shielded in the compact nuclei and thus are not available for the determination.

Table 6.7. Comparison of poly(GMA-EGDM) prepared by frontal (FP) and suspension polymerizations for epoxy number (data is shown for the reactions carried without porogen; G1-G5)

CLD %	25	50	100	200
Epoxy number FP (mmol/g)	3.92	2.61	2.12	1.79
Epoxy number SP (mmol/g)	4.74	3.59	2.83	1.36

6.3.7.3 Porosity, surface area and morphology

It was observed that copolymers prepared by FP and SP without porogen show low pore volume (H1-H20 and G1-G20). Amongst AIBN and BPO, BPO produced the larger pore volume in both sets. Maximum pore volume was found in G8 (CLD 100%, BPO initiator) i. e. 0.20 cm^3/g (Fig. 6.8), all other samples were in the range 0.03 to 0.20 cm^3/g. Suspension polymerization of identical compositions did not show any porosity, and pore volume and surface area were as less as 0.03 to 0.09 cm^3/g and 5 to 15 cm^2/g respectively. Macroporous morphology and formation of porous texture is dictated by presence of a porogen, its type and relative volume.[133] In absence of a porogen, the pore

volume due to meso and macropores is very low. Total porosity in these matrices was also very low and varied only within 5-15 % in both methodologies and in both sets. At front temperature, a larger number of free radicals are produced and simultaneous front propagation occurs. At higher initiator concentration, more free radicals are generated per unit time which lower the internal pore volume by favouring intramolecular cyclization reactions, resulting in compact nonporous or less porous nuclei. Fig. 6.8 clearly demonstrates the presence of large number of pores in the range below 10 nm.

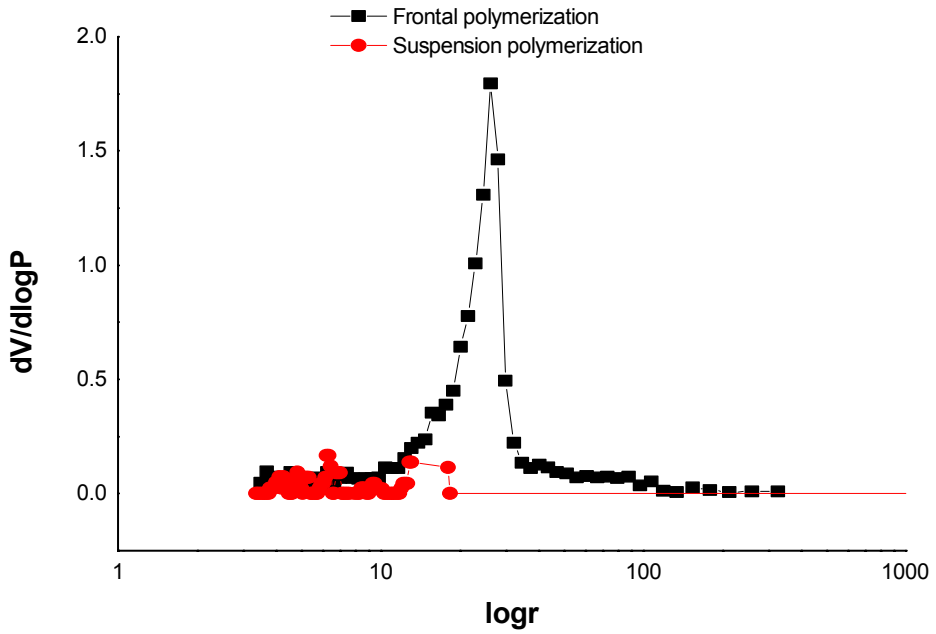

Figure 6.8. Differential pore size distribution of poly(GMA-EGDM) prepared by frontal (FP) and suspension polymerization (SP) at 100% CLD (r is in nm)

Table 6.8. Comparison of FP and SP methodologies in terms of pore volume, surface area and porosity

Code No.	PV mLg^{-1}	SA m^2g^{-1}	Porosity %	Code No.	PV mLg^{-1}	SA m^2g^{-1}	Porosity %
H25	0.1050	21.1739	24.12	SH25	0.0562	12.36	4.51
H26	0.0673	19.4125	21.36	SH26	0.0654	8.695	6.25
H27	0.1750	43.6012	45.62	SH27	0.0699	14.2561	5.14
H28	0.1885	42.8352	41.32	SH28	0.0812	15.351	9.12
H29	0.2816	58.6460	48.65	SH29	0.122	21.354	15.23
H30	0.1462	21.2380	29.42	H30	0.0697	21.1561	4.21
H31	0.2639	50.8644	44.56	H31	0.075	26.2130	6.38
H32	0.3273	69.8643	51.20	H32	0.0915	30.0170	8.54
H33	0.2743	15.9686	8.90	H33	0.0855	25.7916	7.89
H34	0.5250	89.6733	57.14	SH34	0.1690	37.5630	17.89
H35	0.0691	17.1643	16.79	SH35	0.0689	18.124	24.31
H36	0.1406	33.8812	35.12	SH36	0.0455	6.564	6.51
H37	0.1601	36.2511	48.12	SH37	0.0841	9.125	8.12
H38	0.1658	40.3360	39.21	SH38	0.0955	29.46	14.56
H39	0.2098	52.4775	44.23	SH39	0.0678	12.356	11.25
H40	0.1682	28.4016	28.45	SH40	0.1497	25.231	28.36
H41	0.0238	5.3473	12.21	SH41	0.0688	8.5612	11.23
H43	0.3072	89.8048	45.12	SH43	0.0989	14.265	19.65
H43	0.6463	94.3199	61.51	SH43	0.1204	18.3265	21.12
H44	0.3871	72.8557	59.12	SH44	0.1501	24.235	25.64

SH series: polymers prepared by suspension polymerization, compositions identical with FP.; PV: pore volume; SA: surface area

Poly(HEMA-EGDM) system using EEA as porogen for both FP and SP systems were compared (Table 6.8). Monomer to porogen ratio was varied (1:0.4 v/v and 1:0.8

v/v). More than three fold increase in intruded pore volume was obtained in porogenic system in FP. At 1:0.4 (v/v) monomer:porogen ratio, maximum pore volume was obtained with CLD 400 % in both initiation system (Fig. 6.9). At 1:0.8 monomer:porogen (vol/vol) ratio, higher pore volume was obtained with AIBN but this value may not be a true as bulk polymerization competed during the reaction. In general BPO produced stable front and higher pore volumes. Representative porous structured SEM image is shown in Fig. 6.10. BET surface area measurement data also revealed moderate surface areas of FP polymers in the range of 30-95 cm^2/g suitable for chromatographic applications. Maximum surface area was obtained at monomer:porogen (1:0.8 v/v) ratio at 200 and 400 % CLD with AIBN and BPO, respectively. FP produced narrow pore size distribution and higher % porosities (30-65 %) in the matrix. Fig. 6.11 represents typical pore size distribution diagram of FP product which shows the generation of micropores and majority of the pores are within 10-15 nm radius. Identical compositions using SP did not yield porosity due to the solvating nature of EEA and absence of phase separation. Network formed collapsed to form a glassy amorphous gel-type resin on drying. Moreover, bead formation could not take place in SP with monomer:porogen 1:0.8 vol/vol ratio at 4 mol % BPO. Only agglomerated mass was formed. SEM micrographs of the beads obtained SP products showed beaded structure but it contained no/lower porosity (Fig. 6.12).

Additionally, at similar monomer feed ratios, the two copolymerizations differed markedly in the relative yields of the copolymers and the rate of copolymerization. The conversion in FP was in the 70-95 % range in a reaction time lasting 10-15 min depending upon the reaction conditions as shown in Table 6.4. In SP the conversions

were 50-69 % in 3 h. This marked difference is because reaction in FP is initiated by the complete decomposition of the initiator which proceeds rapidly and locally, picking up most neighbouring reactive monomeric species. In SP, reaction is triggered by decomposition of a minute fraction of initiator present (10^{-5} to 10^{-3} /s) and very rapidly reaches a slow but a steady rate. The reaction needs to be conducted for a long time to reach near quantitative conversions. Maximum yield of 68.9 % was obtained by SP at 200 % CLD.

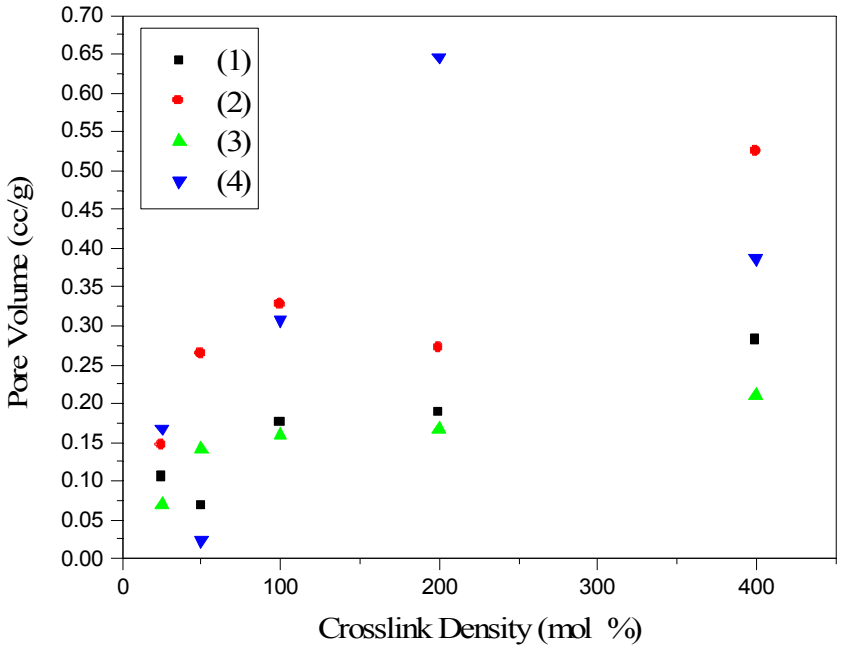

Figure 6.9. HEMA-EGDM FP carried using 2-ethoxyethyl acetate (porogen). (1): FP carried using monomer:porogen (1:0.4 vol/vol) ratio using 4 mol % BPO; (2) FP carried using monomer:porogen (1:0.8vol/vol) ratio using 4 mol % BPO; (3) FP carried using monomer:porogen (1:0.4 vol/vol) ratio using 4 mol % AIBN; (4) FP carried using monomer:porogen (1:0.8 vol/vol) ratio using 4 mol % AIBN.

a]

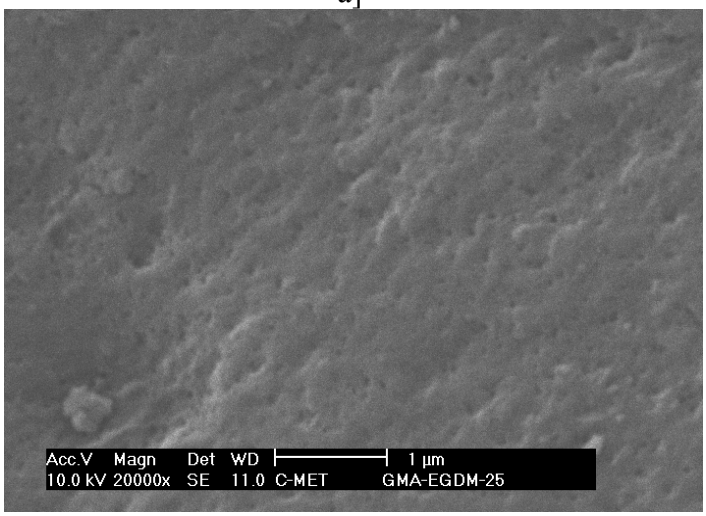

b]

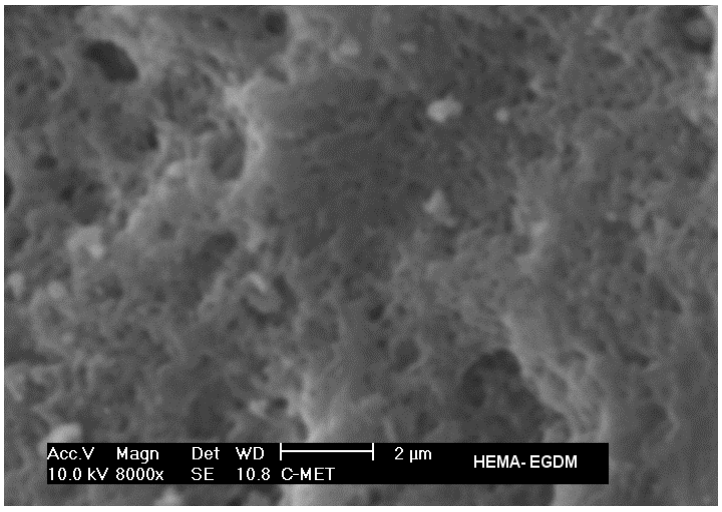

Figure 6.10. SEM microgram showing the porous structure of polymer matrix (a: poly(GMA-EGDM) 25 % CLD at 4 mol % BPO; b] poly(HEMA-EGDM) 25 % CLD and 1:0.4 (vol/vol) monomer:EEA

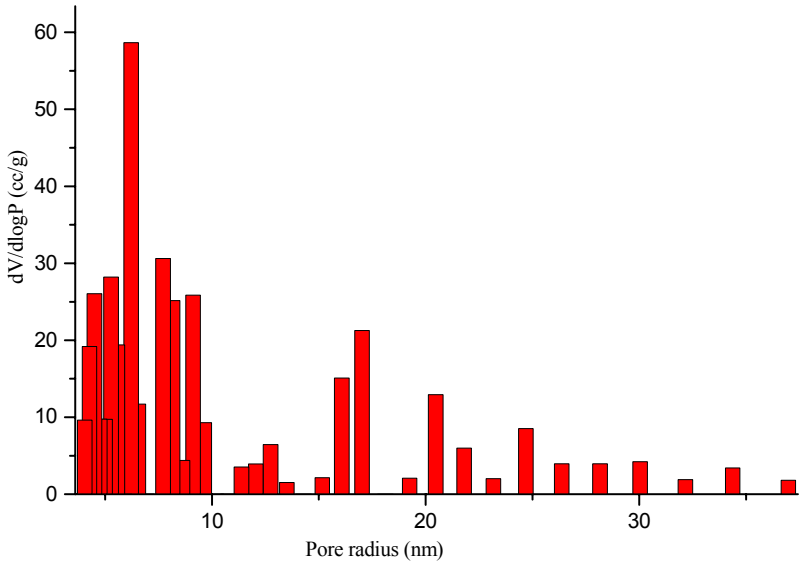

Figure 6.11. Pore size distribution of poly(HEMA-EGDM) representative sample by FP (FP carried using monomer:porogen (1:0.4 vol/vol) ratio using 4 mol % BPO at 100 % CLD)

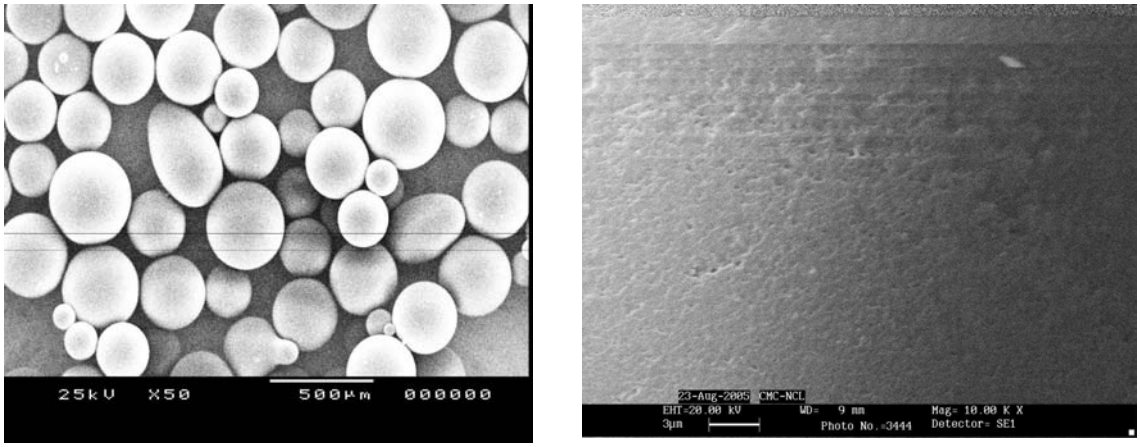

A] B]

Figure 6.12. Beads obtained by suspension polymerization methodology. Beads are homogeneous and there is no porosity. (sample code: SH28)

6.3.8 Solvent-non-solvent regain

Porosity in the matrix is also detected by the solvent and non-solvent regain by the gel. It is also important to know the behavior of the gels in solvents for biological applications. Four representative samples, two from each set, poly(GMA-EGDM) of 25 and 100 % CLD synthesized using 4 mol% AIBN (code no.: G16 and G18) and poly(HEMA-EGDM) synthesized using 4 mol % BPO with 1:0.4 and 1:0.8 monomer:porogen (v/v) ratio at 100 % CLD (code no.:H27 and H32)) were selected for dimethyl formamide (DMF) and water regain studies. The observations are presented in Table 6.9.

Polymers were not swellable. Swelling is a diffusion phenomenon driven by the affinity of the molecules of the swelling material for the molecules of the contracting fluid. The swelling equilibria are determined by a balance of three main forces,[223,224] as follows: 1. The free energy of mixing of the network chains with solvent, 2. The net osmotic pressure within the network, resulting from the mobile counterions surrounding the fixed-charge groups (ion swelling pressure), and 3. The elastic retractile response of the network (elastic swelling pressure). Forces (1) and (2) favour swelling, while force (3) opposes it. A classical crosslinked network has a swelling limit controlled by a balance between the thermodynamic forces due to polymer–solvent interactions and the entropic force of coiled polymer chains. The swelling equilibrium is dependent on the entropy of dilution, the heat of dilution, and the entropy of the polymer network. For a given polymer–solvent system, the equilibrium swelling is a function of the crosslink density.[232] Crosslink density is also related to interstitial chains i.e. the molecular weight between the crosslinks. The equilibrium swelling ratio Q is inversely related to the

crosslink density.[225] Basically, increasing the molar percent of the crosslinking agent to the monomer, interstitial chain molecular weight increases. This in turn reduces the *Q* values.

Polymers prepared using porogen showed higher regains than those prepared without porogen. When synthesized in absence of a porogen, only the spaces between the macromolecular chains are available for the transfer of solutes, therefore the pore diameter is within the range of molecular dimensions, no larger than several nanometers. These gels allow the transfer of low molecular weight solutes, and even of large molecules. We observed no change in the diameter of the particle during the solvent regain process. In addition to what is described above, higher crosslinking led to lowering of the chain flexibility and restricted the solvation of the chains by solvent leading to non-swelling polymer. The increase in the production of radicals increases the rate of polymerization, thereby decreasing the crosslinking density, and is further responsible for a decrease in the swelling capacity. The increasing weight of the copolymer particle in DMF and water was thus predominantly due to penetration of solvents into the open pores.

The solvation depends on interaction between DMF molecules and segments in the polymer network.[221] The kinetic curve generally consists of three stages viz. initial high absorption rate, a slow and constant penetration and plateau value. In the present study it was observed that initial penetration rate of DMF was very rapid and the gel reached plateau within 120 min. From the representative kinetic plot (Fig. 6.13), it is revealed that all copolymers behave in a similar way and equilibrium DMF content (EDC) is attained within 120 min. The relatively lower EDC content is due to the fact

that higher crosslink density polymers possess a compact, rigid structure with marked network entanglement in the nuclei.

Table 6.9. Solvent-non-solvent regain studies of polymers

Polymer code No.	DMF regain mL/g	Water regain mL/g	EDC %
G16	0.035	0.056	24.64
G18	0.043	0.055	29.05
H27	0.08	0.093	40.13
H32	0.091	0.101	41.2

EDC=equilibrium DMF content

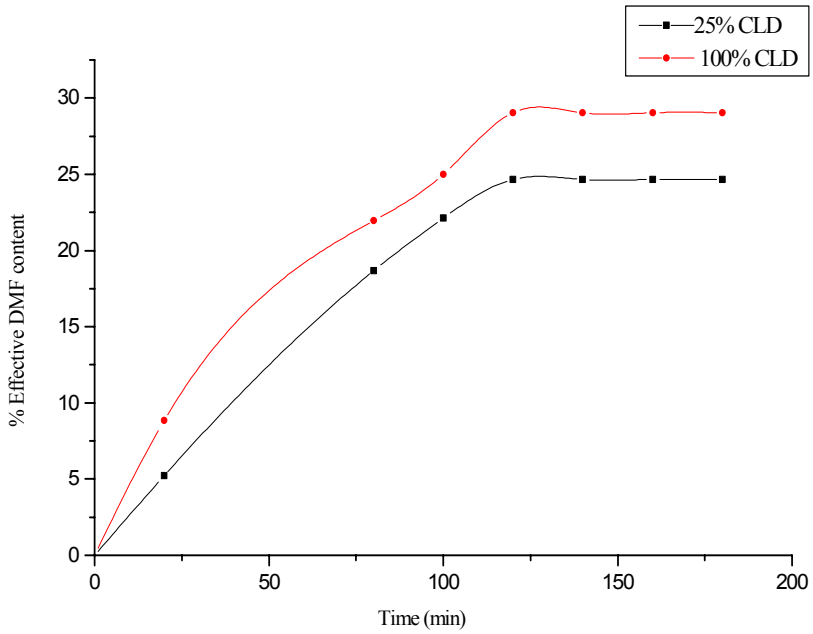

Figure 6.13. Kinetics of percent effective DMF content absorption with time (H27 and H32)

6.3.9 Pattern formation

a] b]

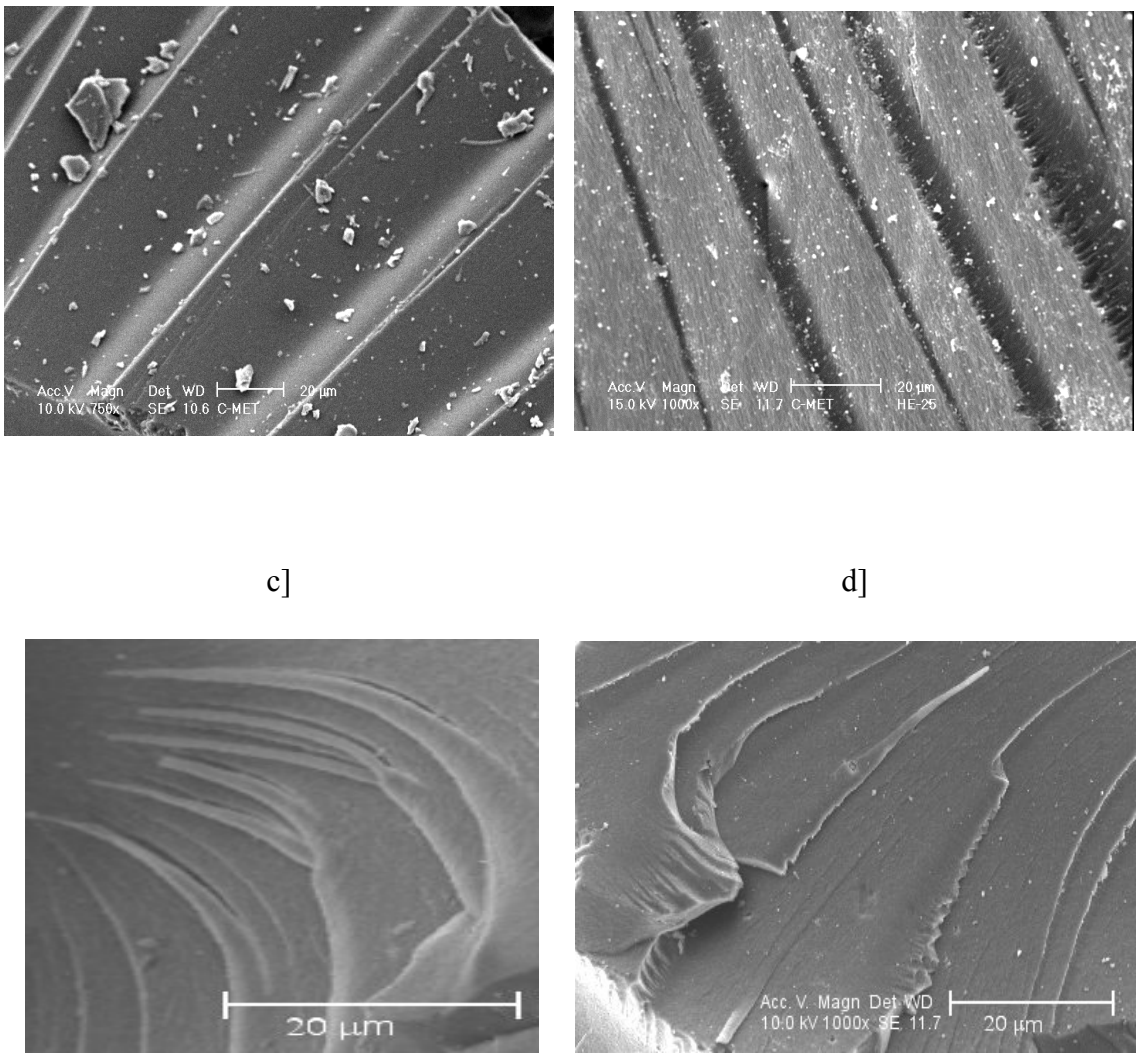

c] d]

Figure 6.14. SEM micrograms showing exotic patterns: Planner patterns of poly(HEMA-EGDM) at a] 25 % CLD synthesized using BPO (H16) and b] 25 % CLD synthesized using 2 mol % AIBN (H11). Poly(GMA-EGDM) synthesized at c] 50 % CLD synthesized by 4 mol % AIBN (G17); d] 25 % CLD synthesized using complex initiation system (AIBN + DCP)

We observed two basic types of spatial patterns viz. planar and non-planar patterns. The type of planar pattern observed under SEM was one with a spatial impulse appearing as a loop followed with regular periodic motion in radial and axial direction (Fig. 6.13 a and b). This gives rise to a repeating pattern thickness of a few micron. Also non-planar patterns viz. layered concentric rings and winding staircase patterns were observed in SEM (Fig. 6.13 c and d). We present, explain and discuss at length these first time observations of the exotic patterns observed under the microscope in Chapter VII.

6.4 Conclusion

A series of copolymers of 2-hydroxyethyl methacrylate (HEMA)/glycidyl metharylate (GMA) and ethylene dimethacrylate (EGDM) were synthesized by frontal polymerization. It was predominantly observed that initially front propagates in the form of bubbles which try to escape along the walls of the reactor tube. After the initial uneven movement the front stabilizes and propagates smoothly. AIBN and BPO produced stable fronts while higher activation energy initiator, DCP could not sustain front due to extensive heat losses. As a general observation, front velocity increased with increasing % CLD. AIBN produced faster fronts than BPO. Dual initiator system (AIBN + DCP) was found to be effective in stabilizing front propagation and resulted in higher yields. At lower initiator concentration, front ceased when reactions were carried in presence of solvents. Amongst several solvents evaluated, 2-ethoxyethyl acetate was found to sustain the front in HEMA-EGDM system. All reactions in GMA-EGDM systems were extinguished in presence of a solvent. These reactions were sustainable only when diluents like silica gel was added and at higher CLD. In HEMA-EGDM system, at higher monomer:solvent ratio (1:0.8) bulk polymerization competed with pure FP. In ascending

polymerization, convective instabilities were observed and front propagation was in nonplanar mode. Interestingly, we could perform reactions in DMSO which was otherwise not possible in descending polymerization.

Polymers synthesized were also compared with suspension polymerization as the functionalized polymers are prepared by SP for chromatographic and enzyme binding applications. When reactions were carried without solvent (porogen), pore volume were lower and discontinuous. EEA was evaluated as a porogen for the first time and it was observed that it produces sufficient pore volume and specific surface area. Pore volume and specific surface area in FP was found to be independent of crosslinker but dependent on type and volume of solvent. At higher volumes of EEA, higher pore volumes were generated. Pore size distribution in FP was also narrow and within a range of 10-50 nm. With porogen, porosity was continuous. With identical compositions, SP could not produce porosity in the matrix due to lack of incipient phase separation. Suspension polymerized beads were glassy and nonporous. Thus, FP was found to be superior over SP in terms of producing higher pore volume with or without solvent, higher yields and less reaction time.

We also evaluated few copolymer networks for solvent non-solvent regain (DMF and water). It was observed that all polymers attain equilibrium volume swelling in 120 min. There was no change in particle diameter due to rigid structure. Increase in mass was the outcome of filling of solvent in open pores.

The presence of exotic patterns is an important finding of this work. Polymers possessed spatial patterns along radial direction, observable under SEM. These patterns

were of two basic types, planar and non-planar. The physico chemical understanding of the process is explained in chapter VII.

Chapter VII

PATTERN FORMATION

7 Pattern Formation

7.1 Introduction

Exotic patterns formed in FP can be investigated as nonlinear phenomena. Spin modes and pattern formation in FP is well reported.[14,22,78] The heat given out during the highly exothermic polymerization reactions is the cause of propagation of thermal polymerization waves. In reality it is the interplay between thermal diffusion and reaction kinetics which gives rise to pattern formation.[65] The associated wave dynamics is in many ways similar to dynamics of combustion waves. The dimensionless parameters such as Zeldovich number that determine spatial structure of these heat waves are of same order in many polymerization reactions as in combustion processes. That is why combustion waves and thermal polymerization waves have similar spatial structures. This thermal wave consists of a narrow reaction zone which separates the initial reactants from high temperature reaction products. During the reaction, the heat released diffuses to adjacent layers of reaction mixture and intensifies reaction there. This process repeats and a self-sustained wave propagates in the reactor tube.

Experimental observations indicate that in addition to uniformly propagating polymerization waves, more complex patterns do appear and an example of such a pattern is spinning wave motion, which is akin to wave propagation of combustion waves.[226-228] The stability of these combustion waves has been studied in detail.[226] The instability of reaction interface was first reported by Begishev et al.[22] for ε-caprolactum ring opening FP. Pojman et al.[78] subsequently reported the spinning head motion in methacrylic acid frontal polymerization. A number of reports then followed explaining dynamics of frontal polymerization and steady state bifurcation analysis.[14,61-71,78] In

chapter I, we have reviewed this phenomenon in detail (section 1.3.4). In mathematical terminology, spirals and spins are formed due to operator singularity. Since the reaction zone is narrow, we say that motion of spiral is planar and we assume that only when this cross section turns into gel, the front moves ahead. Spin modes are formed due to a rotation along theta coordinate from 0 to 2π completing a circle, and heat wave instantaneously converts it into gel. Hot spots, on the other hand, is a different phenomena, occurs at the tip of spiral, and requires more analytical results to predict its occurrence.

In our experimental systems, two types of patterns were observed: (i) clearly visible helical pattern along axial direction, and (ii) the layered pattern, observed predominantly along radial direction under scanning electron microscope (SEM). Helical patterns are formed due to nonplanar front propagation (spin modes). Experimental evidence and a number of rigorous mathematical analysis of causes and occurrences of helical patterns and factors affecting on it, which have been well recorded in literature was reviewed in Chapter I. Volpert and Spade[64] have explained the stability of steady state reaction front propagation. They discussed the bifurcations of stable and unstable solutions, which can occur if interface dynamics is analyzed to determine stability of steady state spatial propagation.[62,64] On the other hand, we are the first to report the layered pattern formation in FP. In reaction diffusion system, Winfree[160] explained the spiral pattern formation as self-organization phenomena. Clearly, variations in reaction chemistry, that is, rate and transport parameters give rise to differing modes of spatio-temporal spin motion.

In first part we deal with pattern formation phenomenon in water triggered polymerization. We will explain mechanism of helical and layered pattern formation in water triggered FP and later we will present the patterns in liquid monomer polymerization i.e. functionalized crosslinked system. We will develop a mathematical model using model reactions and validate with experimental results. The model will give an insight into the physico-chemical process of the spinning wave motion in frontal polymerization.

7.2 Pattern formation in water triggered frontal polymerization

Fronts do not have to propagate as simple planar fronts. As seen in Chapter IV, in Set I, for potassium peroxydisulfate: oxyacids of sulfur redox system, we observed the helical and layered patterns. Analogously to oscillating reactions, a steady state can lose its stability as a parameter is varied and exhibit periodic behavior, either as pulsations or as ‘spin modes’ in which a hot spot propagates around the reactor as the front propagates, leaving a helical pattern. This mode was first observed in SHS. SHS fronts demonstrate a rich variety of dynamical behavior, including planar fronts, spin modes and chaotic reaction waves.

As seen in Chapter IV, the helical and layered patterns were observed in Set I polymerization system (section 4.3.6). The existence of the single-head spin mode requires a physical explanation, especially because of a common opinion about the stabilizing role of thermal conductivity in the preheating zone. The qualitative concept and discussion of thermo-diffusional stability of combustion waves has its origin in the works of Zeldovich. The stability of a thermal front with a one-step reaction, with energy

of activation, E_{eff} and front temperature, T_m is determined by Zeldovich number, Z (Eqn. 1.3):

$$Z = \frac{T_m - T_0}{T_m} \frac{E_{eff}}{RT_m}$$

The planar mode is stable if $Z < Z_{cr} = 8.4$ and unstable if $Z > Z_{cr}$.[65] For our system, using Eqn. 1.3, we get Z = 6.8. This value is very close to the stability boundary. Even though it is under the stability region, we obtained the spin modes. The reason is that the polymerization is not a one-step reaction. Therefore above form of the equation is not directly applied. Moreover, the reaction chemistry is complex and correct estimates of Z_{cr} can be obtained only by fitting the experimental data to formulas derived under the assumption of single-step Arrhenius kinetics.

Recalling what is shown in Fig. 4.10, we can see the formation of helical patterns in the polyacrylamide rods. Due to the simultaneous formation of skin (see section 4.3.4), helical pattern was not clearly visible and sometimes it was buried inside the skin layer on every product from Set I. But pattern formation was inevitable in this system due to high front temperature and reactor geometry. Patterns indicate loss of steadiness during polymerization by spatial and temporal periodic modes, due to competition between heat generated in the reaction zone and its diffusion to the cold reactants.[84,229] The helical patterns observed with naked eyes are ones which form in axial direction (Fig. 4.10). From this Fig., it is clear that both clockwise and anticlockwise motion of spiral occurs and therefore the patterns are formed accordingly and reveal the motion of spinning wave. The qualitative analysis of temperature profile given by dynamics even for the one-dimensional case, which is merely a projection of a spin mode, is helpful to understand

how fronts lose their stability under critical conditions. The temperature profile of the stationary propagating reaction front reflects the heat balance between the heat production caused by the chemical reaction and the heat conductivity sink in each point of the reactive medium. Such a balance can be cited theoretically for systems under critical conditions too. However, any positive temperature perturbation in the reaction zone irreversibly destroys that balance because it leads to the additional reaction heat release exceeding the intensity of the growing heat conductivity flux. In other words, the temperature fluctuation increases both terms of the heat balance mentioned above. Beyond the critical conditions, however, the Arrhenius reaction heat term in the reaction zone becomes quite sensitive and grows more rapidly as the temperature increases than do losses from heat conductivity. Finally, the reaction zone undergoes a thermal runaway with a subsequent relaxation period. Then, again, the temperature profile sharpens and explodes, reaching the imaginary stationary temperature profile. Gradually the system develops new nonstationary regimes. It is interesting that the thermal propagating fronts themselves can be considered as localized thermal runaways restricted by cold reactants on one side and by hot product from another.

Layered patterns (spin mode) can now be explained as follows: the locus of points, from which spirals tilted at a small angle emanate around the core of spiral, follows a helical path. In simple terms it can be related to ratios of velocities in axial and radial directions and the basic transformation can be obtained using the neglected term as for planar patterns (see later). Its wave motion can be related using a mathematical expression to exothermicity and heat diffusion so the competition between the two is able to give us a limit within which we can determine occurrence of planar or non-planar

wave propagation. The pitch along radial direction, as seen from a SEM photograph (Fig. 4.11) between two helical turns, is about 40 microns and the vertical distance between two layers is about 5 microns. These spirals propagate until they reach the tube wall, while the decoupled motion of helical front, from which these spirals originate, descends towards the bottom of tube. The thermal balance, including exothermicity of reaction, is satisfied at tip of helix, the origin of spirals (or spin waves). The motion of the tip of helix, descending downwards, follows a helical path and together with the planar spiral propagation gives rise to a layered or winding staircase pattern.

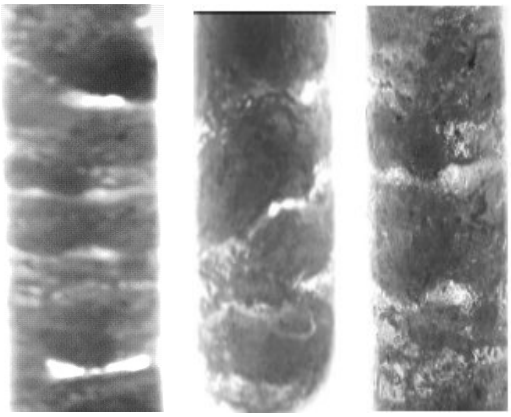

Figure 4.10. Snapshots showing helical patterns on the polyacrylamide surface (dimensions: 12 x 50 mm) in Set I redox systems (c.a. Chapter IV)

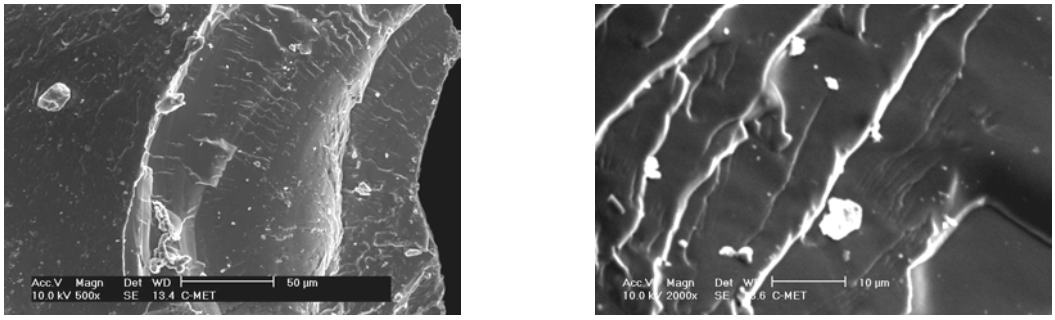

Figure 4.11. SEM surface morphology showing layered patterns on the polyacrylamide surface (dimensions: 12 x 50 mm) in Set I redox systems (c.a. Chapter IV)

7.3 Layered patterns in functionalized crosslinked networks

7.3.1 Mathematical model

7.3.1.1 Background

The generally considered geometry for large-scale production of polymeric material via frontal polymerization reaction is a tubular reactor. Hence, we consider a cylindrical coordinate system, which also applies to a reactor tube in a laboratory in which we carry out the frontal polymerization. Although it is a well-known fact that pattern formation does occur in dynamics of frontal polymerization and have diverse kind of waveforms,[64,78] the spatial patterns formed in laboratory reactor tube cannot be seen with naked eyes. We therefore believe that the imprints of traces of spatial patterns could be visible under microscope on a polymer wake (which solidifies later) left behind by front. Hence, our primary objective is to derive a mathematical model explaining the occurrence of these patterns and analyze the nonlinear phenomena governing this wave motion. Later, we compare the simulation results with experimentally observed patterns.

This pattern formation is motivation for further study using established theory and obtained experimental results.

7.3.1.2 Dynamics of polymerization waves

In this work, we report the occurrence of spinning wave motion due to the propagation of heat as a spiral on the moving front interface. This traveling wave motion is along axis of motion and perpendicular to it for a polymerization scheme used by Spade and Volpert.[64] We develop a basic mathematical model on moving reaction interface and carry out a linear stability analysis and derive a dispersion relation. Also, an equation is derived to describe the motion of radial ordinate along which heat wave traverses. After the needed analytical results are obtained, we use a standard form of wave solution and simulate the spinning wave motion to compare with experimental results. We will analyze this spinning motion in ensuing sections.

7.3.1.3 Model experimental reaction

2-Hydroxyethyl methacrylate (HEMA) (20 g, 0.15 mol) was mixed with azobisisobutyronitrile (AIBN) (1 mol %) in a 12 i. d. x 125 mm thick walled test tube marked in 1 mm units. Reaction mixture was frozen to solid matrix using liquid nitrogen and polymerization was triggered by means of solder iron. Another experiment was carried by adding crosslinker, ethylene dimethacrylate (EGDM) (25 mol %) at ambient initial temperature. The detailed procedure is given in Chapter III and VI. The temperature profile was obtained by inserting a thermocouple (0.125 mm diameter) attached to a temperature recorder (Hi-Tech scientific, India) in to the reaction mixture from the top. Cut sections of the formed polymers were taken carefully and particles were mounted on stubs and sputter-coated with thin gold film. Surface morphology of the

particles were obtained using JEOL JSM-5200 SEM. Experiments and SEM analysis were performed at least three times for each sample to check the reproducibility.

7.3.1.4 Model

The polymerization reaction is described using a steady-state assumption (SSA) that includes rate equations for initiator and monomer concentration, and heat balance equation for overall reaction (Fig. 7.1). The governing equations are written for the sum of concentrations of primary and polymer radicals (see section 1.3.3 for detailed kinetic scheme and reduction of rate equations under SSA). Thus, we remain with two mass balance equations for initiator decomposition and monomer consumption and one equation for heat balance.

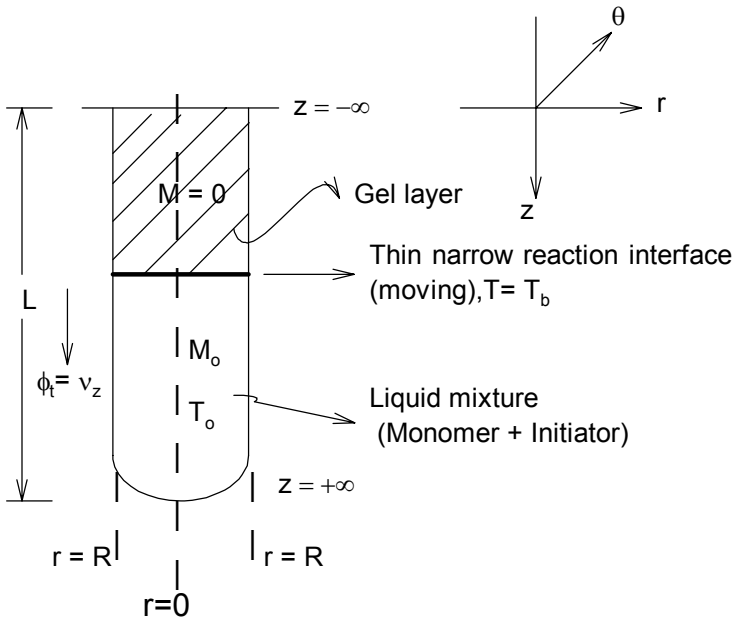

Figure 7.1. Schematic diagram showing propagation of spinning waves

Considering cylindrical geometry of reactor tube, the equations are:[64,230]

$$\frac{\partial M(r,\theta,z,t)}{\partial t} = -K[T]M(r,\theta,z,t)$$

$$\frac{\partial T(r,\theta,z,t)}{\partial t} + \frac{1}{\rho c_p}\left(v_r\frac{\partial}{\partial r} + \frac{v_\theta}{r}\frac{\partial}{\partial \theta} + v_z\frac{\partial}{\partial z}\right)T(r,\theta,z,t) = \kappa\tilde{\nabla}^2 T(r,\theta,z,t) + (-qK[T]M(r,\theta,z,t) + \delta(T(r,\theta,z,t) - T_0)) \quad 7.1$$

where, $q = \frac{(-\Delta H_R)}{\rho c_p}$, $\delta = \frac{hA_H}{\rho c_p}$. Here the Laplacian for cylindrical coordinate is given by:

$$\tilde{\nabla}^2 = \left(\frac{1}{r}\frac{\partial}{\partial r}\left(r\frac{\partial}{\partial r}\right) + \frac{1}{r^2}\frac{\partial^2}{\partial \theta^2} + \frac{\partial^2}{\partial z^2}\right) \quad 7.2$$

We have taken into account only heat-related factors, such as heat release, internal heat transfer, and heat loss through the sample surface. The reason for not considering diffusional process is that the extent of mass transfer in condensed phase is negligible compared to heat effects.[66] Following Spade and Volpert,[64] the limiting situation is considered when appreciable consumption of initiator occurs in the wake of propagation. In this case, the decomposition rate constant is sufficiently small. So we disregarded the equation for initiator and analyzed the kinetics as a two variable system.

Now we assume a moving coordinate system transformation given as:

$$\xi = z - \phi(r,\theta,t) \quad 7.3$$

where $\phi(r, \theta, t)$ gives the location of reaction front in the tube, and ϕ_t is the front propagation velocity. Here, front velocity ϕ_t is assumed to be constant, as seen from experimental observations for many frontal polymerization systems. We further find that $v_z = \phi_t$, $v_r = \phi_r$, $v_\theta = \phi_\theta$. We explain this later when we analyze the motion of spirals on

reaction interface. Substitution of this moving coordinate results in the following Laplacian expression:

$$\begin{aligned}\nabla^2=&\frac{1}{r}\frac{\partial}{\partial r}\left(r\frac{\partial}{\partial r}\right)+\frac{\partial^2}{\partial\xi^2}+\frac{1}{r^2}\frac{\partial^2}{\partial\theta^2}\\&+\left\{\frac{\partial^2}{\partial\xi^2}\phi_r^2+2\frac{\partial^2}{\partial\xi\partial\theta}(-\phi_r)+\frac{\partial}{\partial\xi}(-\phi_{rr})\right\}\\&+\frac{1}{r^2}\left\{\frac{\partial^2}{\partial\xi^2}\phi_\theta^2+2\frac{\partial^2}{\partial\xi\partial\theta}(-\phi_\theta)+\frac{\partial}{\partial\xi}(-\phi_{\theta\theta})\right\}\end{aligned} \tag{7.4}$$

We further assume that the velocities v_r, v_θ are constant, and set $\phi_{rr} = \phi_{\theta\theta} = 0$. Then Eqn. (7.4) becomes:

$$\begin{aligned}\nabla^2=&\frac{1}{r}\frac{\partial}{\partial r}\left(r\frac{\partial}{\partial r}\right)+\frac{\partial^2}{\partial\xi^2}+\frac{1}{r^2}\frac{\partial^2}{\partial\theta^2}\\&+\left\{\frac{\partial^2}{\partial\xi^2}\phi_r^2+2\frac{\partial^2}{\partial\xi\partial\theta}(-\phi_r)\right\}\\&+\frac{1}{r^2}\left\{\frac{\partial^2}{\partial\xi^2}\phi_\theta^2+2\frac{\partial^2}{\partial\xi\partial\theta}(-\phi_\theta)\right\}\end{aligned} \tag{7.5}$$

Now we derive dynamical equations for waves propagating radially on reaction interface. Using Eqns. (7.3) and (7.5), the reduced set of equations Eqn. (7.1) describing polymerization wave dynamics are given as:

$$\begin{aligned}&\frac{\partial M(r,\theta,\xi,t)}{\partial t}=\phi_t\frac{\partial M(r,\theta,\xi,t)}{\partial\xi}-M(r,\theta,\xi,t)K(T)\\&\frac{\partial T(r,\theta,\xi,t)}{\partial t}+\left(\frac{1}{\rho c_p}\right)\left(v_r\frac{\partial}{\partial r}+\frac{v_\theta}{r}\frac{\partial}{\partial\theta}\right)T(r,\theta,\xi,t)=\kappa\nabla^2T(r,\theta,\xi,t)\\&\qquad+(-qK[T]M(r,\theta,\xi,t)+\delta(T(r,\theta,\xi,t)-T_0))\end{aligned} \tag{7.6}$$

where $K(T)$ is a heavyside function defined on either side of moving reaction interface as:

$$K(T) = \left\{ \begin{array}{ll} 0, & \xi < 0 \\ k_0 \exp[-(E/(R_g T_b))], & \xi > 0 \end{array} \right\} \qquad 7.7$$

where $\xi = 0$ i.e. $z = \phi(r, \theta, t)$ gives location of moving interface (this will become clear when we analyze motion on reaction front). Here. for a descending front $\xi = -\infty$ implies top of tube, while $\xi = +\infty$ means bottom of tube and the boundary conditions for moving boundary coordinate ξ are given as:

$$\left. \begin{array}{ll} \xi \to +\infty, & T = T_0, \quad M = M_0 \\ \xi \to -\infty, & \frac{\partial T}{\partial \xi} = 0 \end{array} \right\} \qquad 7.8$$

This is the basic model which we will use in further analysis to study pattern formation on reaction interface.

7.3.1.5 Motion on domain of interface

We have stated earlier that spinning motion observed in combustion processes and in frontal polymerization process is similar to it in many ways. Since we are interested in study of pattern formation, we focus upon the interplay between thermal diffusion and reaction kinetics that results into self-organization of spatio-temporal structures.[160,231,232] Further, we observed during experiments that the reaction front descends at a constant velocity; the front surface was sharp and was perpendicular to axis of motion. So we assume that spinning motion of heat wave takes place on the interface as the exothermic reaction occurs instantaneously and that the front interface is a narrow reaction zone. The traveling wave solution along axis of motion together with spinning

motion, on interface, gives rise to spinning wave. We assume that this reaction interface thus is a planar surface, and it is only a few micron thick (as we will see later in a micrograph). Further, to describe the motion on interface (neglecting derivatives w.r.t. ξ[64] Eqn. (7.6) reduces to:

$$\frac{\partial M(r,\theta,\xi,t)}{\partial t} = -M(r,\theta,\xi,t)K(T)$$

$$\frac{\partial T(r,\theta,\xi,t)}{\partial t} + \left(\frac{1}{\rho c_p}\right)\left(v_r\frac{\partial}{\partial r} + \frac{v_\theta}{r}\frac{\partial}{\partial \theta}\right)T(r,\theta,\xi,t) = \kappa\hat{\nabla}^2 T(r,\theta,\xi,t) + (-qK[T]M(r,\theta,\xi,t) + \delta(T(r,\theta,\xi,t) - T_0)) \quad 7.9$$

and for motion on interface the Laplacian operator in Eqn. (7.5) reduces to

$$\hat{\nabla}^2 = \frac{1}{r}\frac{\partial}{\partial r}\left(r\frac{\partial}{\partial r}\right) + \frac{1}{r^2}\frac{\partial^2}{\partial \theta^2} \quad 7.10$$

In order to study the pattern formation, we face following problem. The actual pattern is few micron thick (as we will see in SEM photographs later) and it is a very tedious and time-consuming process to obtain the same numerically and then give a three-dimensional polar plot. We make an approximation that the basic feature across the few micron thick narrow reaction zone retains its shape as it grows beginning at $\xi = 0$ towards liquid side. This pattern growing in the narrow reaction zone repeats itself to give rise to a self-sustaining propagation of spinning wave. Since the cross-section anywhere in this region gives all qualitative features of the spatio-temporal pattern, we consider only a planar cross section in our model and study it. Thus, we need to study the spiral motion that occurs across the planar cross section. We now discuss this pattern formation.

Following the analysis of spiral motion explained by Winfree,[160] we see that the core of spiral, which is a stationary point in space having a phase discontinuity[233] lies along axis of motion and since the concentration gradient is infinitely steep near core self-organization cannot begin at this point. After a certain radial distance from core (equal to $\tilde{}\lambda_0/2\pi$, where $\tilde{}\lambda_0$ is spacing between adjacent spiral turns) on the outside of the first spiral turn around core spatio-temporal motion will begin. Here the dynamical system is at a Hopf point. According to theory given by Winfree, each spiral outside first turn around core will usually have two opposite arms simultaneously rotating around the core and propagating in radial direction. This spiral pattern can be approximated by equally spaced concentric rings propagating towards wall of tube. Hence, for this wave motion occurring in neighbourhood of a Hopf point, we will approximate the wave on planar interface as concentric rings, and the phase can be expressed as, $\phi = \omega t + \theta$. In reality, this phase ϕ is a function of radial distance r and is expressed as $\phi = \varsigma_0(r)$.[231] Therefore, the deviation between phase of rotating coordinate and radial coordinate denoted as α can be given as:

$$\alpha = \omega t + m\theta - \varsigma_0(r) \qquad 7.11$$

Where, m is termed as a winding number, implying the number of arms of spiral turn around the core at a given radial distance. The winding number m can take integer values as ±1,±2,±3,…. Thus, the wave motion originating from core of spiral is a disturbance propagating in radial direction. Now, we will use phase averaging operator[232] to define deviation from average value. Thus, for any given arbitrary function $\sigma(\cdot)$, we have:

$$< \sigma(\cdot) >= \frac{1}{2\pi} \int_0^{2\pi} \sigma(\alpha) d\alpha$$

and obtain deviational equations of polymerization dynamics occurring on front interface which will tell us about pattern formation. We use an averaged value of state variables < **X**(*r, t*) > and define a deviation vector **x**(*r, t*) as:

$$\mathbf{X}(r,t) =< \mathbf{X}(r,t) > +\mathbf{x}(r,t) \qquad 7.12$$

Furthermore, it has been found that the winding wave breaks into almost concentric rings soon after traversing some radial distance. Then, to apply the approximation of concentric rings (which are rotating waves), we require that:[232]

$$\mathbf{X}(r,\alpha) = \mathbf{X}(r,\alpha + 2\pi) \qquad 7.13$$

Thus, for a given *r* and respective concentric ring contour of wave at that *r*, we see that θ varies between 0 to 2π and takes $\tau 0$ time to complete the revolution. This clearly explains why location of moving interface is expressed as $\phi(r, \theta, t)$. Using above relations in Eqns. (7.12), (7.13) and following Greenberg[231] we will derive a fundamental relation giving equation of motion of radial coordinate. First we assume that the reaction is instantaneous and converts available liquid monomer into polymer gel in the narrow reaction zone or the moving reaction interface; hence the steady state concentration of monomer is zero. Further, the wave motion occurs as a deviation outside the circle around core and the global nonuniform pattern grows or develops in small local neighborhood of this Hopf point. Before we derive a dispersion relation, we find an expression for steady state temperature T_b to define deviation. Here the expression for

steady state interface temperature T_b which has been derived by Spade and Volpert (2001)[64] remains the same in our case as well. The transcendental relation for T_b is given as:

$$T_b^2 - \frac{M_0 q E \phi_t^2}{\kappa k_0 R_g} \exp\left(\frac{E}{R_g T_b}\right) = 0 \qquad 7.14$$

We consider deviation from this steady state temperature T_b given in Eqn. (7.14), which is attained at the instance of instantaneous reaction, and later causes motion of a disturbance resulting into propagation of spinning wave outside the first circle traversed by wave around the core. Thus, the deviations for motion on interface are defined as, $\mathbf{x} \equiv (x_1, x_2) = (M(t, \cdot) - 0,\ T(t, \cdot) - T_b)$, which exist on the side of liquid mixture of monomer and initiator. These deviational equations using Eqn. (7.9) come out as:

$$\frac{\partial x_1(r,\theta,\xi,t)}{\partial t} = -x_1(r,\theta,\xi,t)K(T) \qquad 7.15$$

$$\frac{\partial x_2(r,\theta,\xi,t)}{\partial t} = \kappa \hat{\nabla}^2 x_2(r,\theta,\xi,t) + (-qK[T]x_1(r,\theta,\xi,t) + \delta x_2(r,\theta,\xi,t))$$

Here, for a given r, we have neglected the gradient term, $\left(v_r \frac{\partial}{\partial r} + \frac{v_\theta}{r}\frac{\partial}{\partial \theta}\right) x_2(r,\theta,\xi,t)$ (as convective effects during heat wave traversal along radial coordinate are absent). Solving this equation using symbolic manipulator gives the coordinate transformation as, $r = \exp[(v_r/v_\theta)\theta]$ which we use to compute the polar plot. Further the boundary conditions come out as:

$$\mathbf{x}(r,\alpha)=\mathbf{x}(r,\alpha+2\pi)$$
$$\frac{\partial x_1}{\partial r}=\frac{\partial x_2}{\partial r}=0,\quad \frac{\partial x_j(r,m\theta)}{\partial\theta}=\frac{\partial x_j(r,m\theta+2\pi)}{\partial\theta},\quad j=1,2$$

To obtain motion around core of spiral, we consider a disturbance having a form,

$$\mathbf{x}(t)\sim\exp[\omega t+m\theta+\imath(\varphi t-\varsigma_0(r))]+c.c. \tag{7.16}$$

where φ is variation in growth rate ω as pattern evolves from first turn around core to reach the wall of cylindrical tube. Now note that the heat wave travels along $\varsigma_0(r)$. Therefore to derive its equation of motion (similar to that obtained by Greenberg,[231] we neglect the reaction term and heat losses in temperature balance equation (15) and substitute disturbance in Eqn. (7.16) into it. Separating real and imaginary parts and upon rearrangement gives the fundamental identity for radial motion of spirals as:

$$\left(\frac{1}{r}\frac{\partial}{\partial r}\left(r\frac{\partial\varsigma_0(r)}{\partial r}\right)\right)=\Omega\left[\frac{1}{\omega}\left(\frac{m^2}{r^2}+\left(\frac{\partial\varsigma_0(r)}{\partial r}\right)^2\right)\right]-\Omega[r] \tag{7.17}$$

This is the fundamental relation for motion of radial coordinate along which spinning wave motion occurs. Now, we can carry out the linear stability analysis of these waves appearing upon moving reaction interface.

7.3.1.6 Linear stability analysis

Since the disturbance in phase is giving rise to pattern formation, we consider a deviation in spatio-temporal solution near the core using $\omega(r)t + m_\theta$ as growth term and determine linear stability of spatial structure that forms as a spatial pattern. We thus use a standard wave solution form at a given r as:

$$x_i(r,\theta,\xi,t) \sim \exp[\omega t + m\theta - \imath\varsigma_0(r)], \qquad i = 1,2 \tag{7.18}$$

Here we see that for the approximation of propagating concentric rings, at a given radial distance *r*, the critical point relation is independent of variable *r*, although it appears in the actual expression. Note that here we do not consider variation φ in growth rate ω in Eqn. (7.18), as the critical point relation holds for a given radial position *r*. Now we substitute Eqn. (7.18) into Eqn. (7.15) and obtain a determinant equation giving us the critical point relation as:

$$\mathrm{Det}\left(\begin{pmatrix} \omega & 0 \\ 0 & -\delta - \omega + \kappa\left(\frac{m^2}{r^2} + \frac{1}{r}\left(-\imath\varsigma_0'(r) - r\varsigma_0'(r)^2 - \imath r\varsigma_0''(r)\right)\right) \end{pmatrix}\right) = 0 \tag{7.19}$$

Separating real and imaginary parts of Eqn. (7.19), and solving the differential equation in imaginary part we obtain a solution for $\varsigma_0(r)$ as:

$$\varsigma_0(r) = c[2] + c[1]\log[r] \tag{7.20}$$

Using Eqn. (7.20) and from real part of determinant expression, we obtain an expression for $\omega(r)$ as,

$$\omega = \Omega(r) = 0, \quad \frac{-r^2\delta + \kappa\left(m^2 - c[1]^2\right)}{r^2} \tag{7.21}$$

7.3.1.7 Results and Discussion

We performed HEMA polymerization in two sets. In first, we lowered the initial reaction temperature and in other, added a crosslinker. We could not observe the imprints of spiral traces with naked eyes. However, both sets produced similar patterns when

observed under the scanning electron microscope (SEM). The representative micrographs are shown in Figs. 7.2 and 7.3. We began the simulation with the standard wave solution given in Eqn. (7.18) and that for radial motion (Eqn. (7.20)) and obtain the patterns on interface near a critical point (Hopf point).

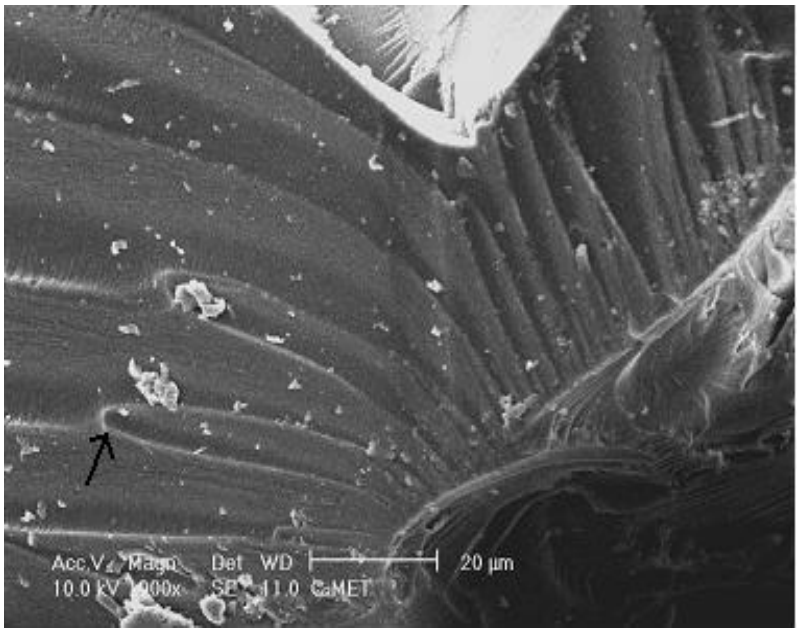

Figure 7.2. SEM photograph of poly(HEMA) (prepared by adding 25 mol % EGDM) showing wave motion on moving reaction interface. The motion begins after a distance of about 21 μm and loops emerge (marked by arrow) around the core of spiral, which finally break into impulses when spiral motion breaks into rotating coordinates

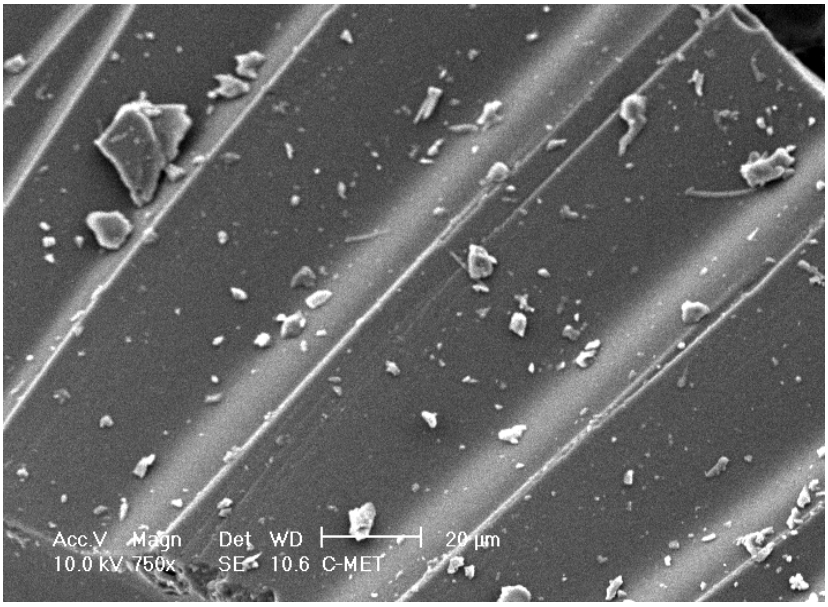

Figure 7.3. SEM photograph showing a cut section of polymer whose average distance between the two ramps is equal to distance between adjacent spiral turns (49.0 µm)

The coordinate transformation needed to produce a polar plot using a symbolic manipulator (MATHEMATICA) was obtained from solution of the equation $\left(v_r \frac{\partial}{\partial r} + \frac{v_\theta}{r}\frac{\partial}{\partial \theta}\right) x_2(r,\theta,t) = 0,$ we had set to zero. The transformation comes out as $\theta = v_\theta/v_r \log[r]$. Fig. 7.2 shows that the motion does not begin until a radial distance of about 21 µm is reached. We use this data to simulate pattern formation. Also from Fig. 7.3 we find that the waves formed on radial mesh has periodicity of an average of 49.0 µm. We will verify this periodicity using our model calculations. Here the periodicity in $z-$direction is neglected as it does not affect that in r direction and that we have considered a planar cross section perpendicular to axis of motion. Further we put parameter values for our simulation (from experimental run) as $\kappa = 0.0014$, $\varepsilon = 21$ µm, $\delta = 0.016$, $\eta = 0.04$ (values obtained from ref 178), and $m = 2$. The value of winding number m has been taken as two as spirals may appear in pair for a two dimensional system.[160] We find that the numerical values of constants of integration come out as: $c[1]$

= ±9.2002, ±400883.0 and corresponding numerical values are $c[2]$ = ±49.0102, ±1.22×106.

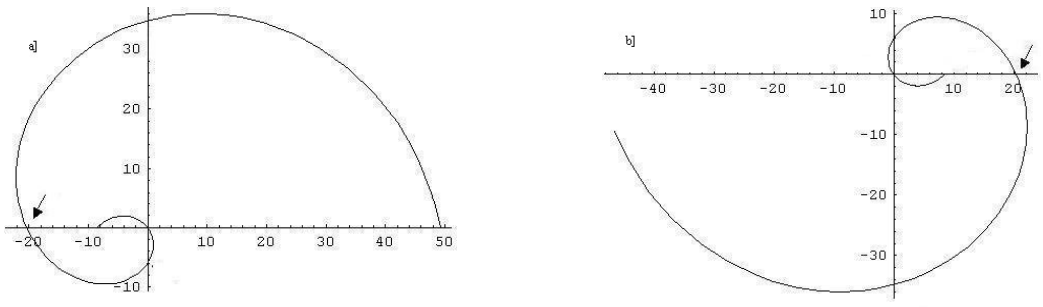

Figure 7.4. The opposite arms of a spiral around the core as plotted using Eqn. (7.20). The arms of a spiral appear around the core. These are opposite arms and turn around and cut x-axis at about 21 μm (shown by arrows)

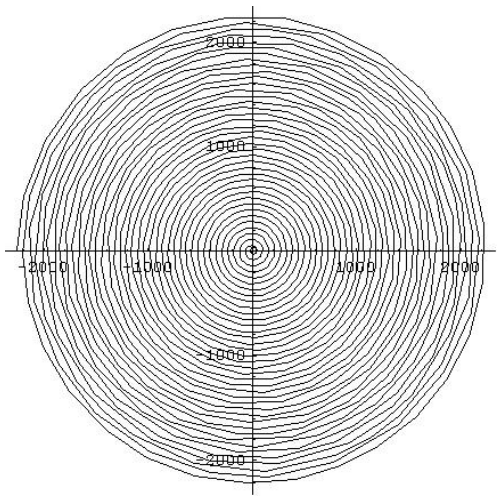

Figure 7.5. The spiral motion of radial coordinate, which can be approximated by concentric rings

This confirms that spirals have appeared in pairs. Thus, the winding number for each pair of spirals is two (m = 2). The first pair appears at around 21 μm along x-axis (see Figs. 7.4a,b), while second pair appears at around ~ 600000 μm, which is not shown in figure. This solution is discarded. Since they are solutions of a differential equation,

for a selected value of $\omega(r)$, only one pair would get selected for motion to occur. Clearly, the selected values are $c[1] = \pm 9.2002$, $c[2] = \pm 49.0102$. The motion near the core cannot begin below a radial distance of $44.5/(2\pi) = 7.8$ μm. This is confirmed from Fig. 7.4a,b. We will explain soon how the velocity ratio needed to produce polar plots is calculated. The radial coordinate motion as given by Eqn. (7.20) is simulated for both the arms of spiral and plotted together in Figure 7.5. Therefore motion cannot begin closer than a distance of $\tilde{\lambda}_0/2\pi$ from the core of spiral i.e. about 8.2. This hollow region around the core extends till ~ 21 μm (see along y-axis in Fig. 7.4a or 7.4b) as observed from SEM photograph in Fig. 7.2 and is greater than 8.2 μm along x-axis in Fig. 7.4a or 7.4b. This confirms discussion on spirals by Winfree.[160]

Now we plot more turns of radial coordinate giving spiral motion for one spiral arm in Fig. 7.6. We measure the distance of second turn around core, where first turn implies that self-organization is initiated for the spatio-temporal structure to begin wave motion at this point. This occurs at a distance of ~49 μm along x-axis and ~51 μm along y-axis as is seen from Fig. 7.6. The second turn occurs at around ~93 μm along x-axis and ~110 μm along y-axis. This distance between second and first turns is denoted by $\tilde{\lambda}_0$ (i.e. spacing between adjacent spirals) and is about ~51 μm. This matches closely with average pitch which is seen in Fig. 7.3 (~49 μm). For this distance the velocity ratio $(v_r/v_\theta) = 0.946342$, as calculated using Eqn. (7.20). As these velocities are assumed to be constant in our two-dimensional (2D) model, this value can be used in coordinate transformation to compute the polar plots for simulation.

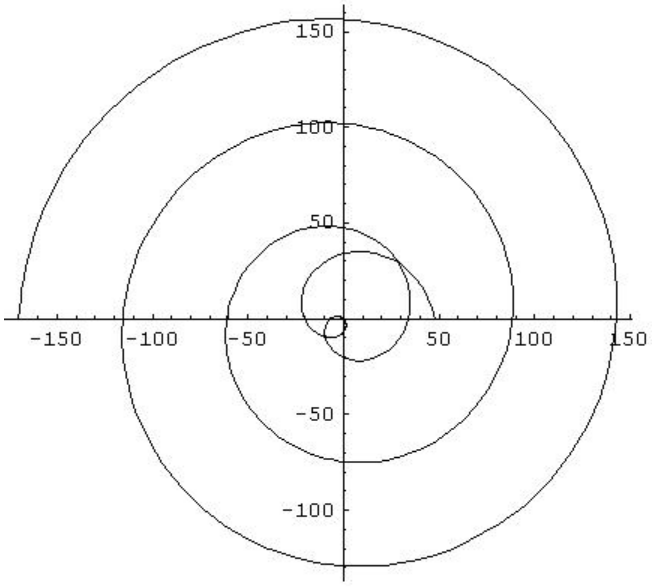

Figure 7.6. A few turns of motion of a single arm of spiral. The distance between the adjacent (first two turns) spiral turns is 51 μm (shown by double-headed arrow)

We further note that the approximate distance between ramps observed on radial mesh should have same periodicity as adjacent spirals turns in motion of radial coordinate. The measurement marks seen in Fig. 7.3, indicate average distance between two ramps to be of the order of ~49.0 μm, which compares well with simulation results in Fig. 7.6. We also note that on radial mesh the average distance between two ramps is slightly diverging; this is clearly indicated by Fig. 7.6 where distance between adjacent turns of radial coordinate motion is seen to diverge marginally.

Our analysis further reveals that the cosine term in perturbation solution in Eqn. (7.18) consists of three terms as a sum viz. $\omega(r)t$, 2θ and $c[2] + c[1]Log[r]$. For $m = 1$ concentric rings will appear while for $m > 1$ loops will appear. The spatial structure gets further modified due to presence of other two terms.

Eqn. (7.18) has been now used to plot spinning wave motion for one arm of spiral and is shown in Fig. 7.7. The standard wave solution in Eqn. (7.18) produces patterns

near the core of spiral qualitatively as shown in Fig. 7.7 and compares well with loops emanating radially from first turn around the core as seen from SEM photograph in Fig. 7.3. After traversing this distance the phase of spiral becomes almost equal to rotating coordinates and loops disappear and ramps appear (see Fig. 7.1). This breaking of spiral into rotating coordinates is as discussed by Koga[232] in the analysis of spiral motion. Lastly we see that before continuous smooth periodic motion begins, loops are formed for first two turns and then ramps appear. This is confirmed by simulation (see loops in Fig. 7.7, the other part is not shown in figure).

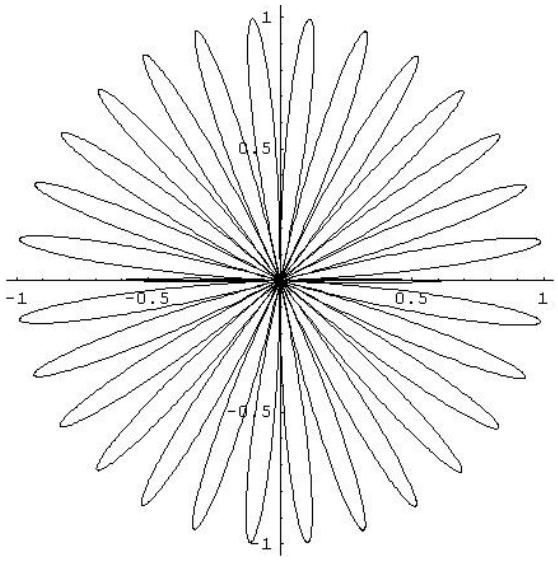

Figure 7.7. Spatio-temporal pattern (loops) which appear before smooth periodic motion begins as obtained using Eqn. (7.18) that is formed upon moving reaction interface

We also note that the samples near tube wall give only solid polymeric material with any imprints of wave motion being absent. This is because by the time ramps could reach the wall reaction is triggered in the upper layer as well and fuses the imprints due to spiral motion, if any, with the gel formed. The ramps, which appear along a radial mesh, as seen in polar plot travel only a short distance. Later as this wave propagates in space the localized patterns are destroyed to give rise to more complex patterns. Near the tube

wall they vanish and patterns disappear. Hence under SEM we do not observe any pattern formation in some particles. At some distance from core of spirals when ramps have developed (Figure 7.2b), the co-existing spirals superimpose and give rise to a complex pattern, as shown in Figure 7.8.

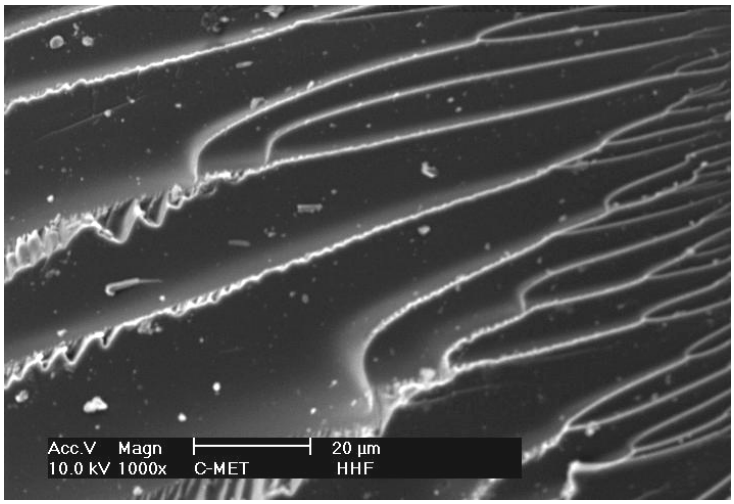

Figure 7.8. Superposed co-existing spirals forming a complex pattern

7.3.2 Physico-chemical explanation to pattern formation in functionalized crosslinked copolymer networks

After developing and validating the mathematical model, we are ready to build up evolved physico-chemical explanation of the phenomenon. We will analyze and explain the patterns formed in functionalized crosslinked system.

Although degree of crosslinking is a measure as a bifurcation parameter,[81] we did not observe the visible helical patterns in any of the HEMA-EGDM or GMA-EGDM copolymerization system. We observed that during the polymerization, along with gases, monomer vapors also escape along the walls of reactor tube. These vapors polymerize as they go in upward direction and form a skin layer upon the already formed polymer. Therefore, it is highly probable that skin layer is one of the reasons for absence of helical patterns. When observed carefully in sunlight we could see the weak helical patterns

buried inside the skin layer (Fig. 7.9). These patterns were not regular. When polymer rods (prepared without using solvent) were broken along its axis, translucent and pale sections were observed. This shows that hot spot(s) must be the present and a pattern must have formed only because of the spinning wave motion of the reaction zone. A similar experiment has been reported by Manz et al. for FP of 1,6-hexanediol diacrylate.[81] They showed the presence of a single head hot spot by slicing the gels and performing an MRI analysis of each slice followed by a computer-aided reconstruction. In our system, although the helical patterns were invisible, the traversal of heat wave along radical direction resulted in planar/nonplanar spatial patterns. The radial pitch of these patterns was very small and therefore was observable only under SEM. The detailed pattern formation (both planar and helical) based on our mathematical model is explained below.

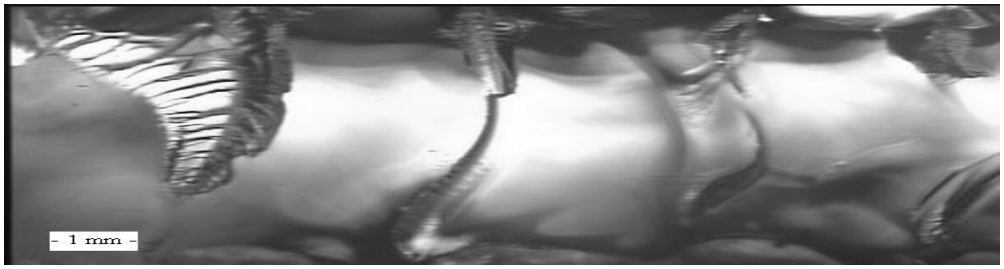

Figure 7.9. Weak helical pattern observed in poly(GMA-EGDM) (sample code G3) when observed under a optical microscope which was buried inside the polymer skin

The interplay of thermal diffusion and chemical kinetics during the frontal polymerization reaction gives rise to pattern formation.[65] The pattern formation occurring during the axial motion of moving reaction interface is a complex phenomena. This arises due to occurrence of chemical instability when plane waves appear on both sides of reaction interface forming a continuous motion. Further, there exists a difference in concentration gradients across the interface indicating presence of a narrow reaction zone

separating gel and liquid phases.[84] Also, the planar reaction interface is at an uniform temperature which is a front temperature describing the steady state of moving front. As investigated in the mathematical model above, pattern formation is identified as the self-organization of wave motion in the vicinity of core of spiral. This core of spiral forms around the center of reactor tube along radial-axis. The spiral wave motion occurs along a radial coordinate[84] along which the temperature or heat wave traverses and due to interaction with the chemical kinetics gives rise to a characteristic spatial waveform. The moving reaction front descends at a constant speed of propagation and the spatial pattern repeats itself. This is still a planar motion of moving reaction front and since this occurs at a critical point as a self-organizing phenomena is termed as an instability. These spatial planar patterns are of two types, i. either a concentric ring pattern, Or ii. a characteristic pattern appears with an impulse, followed with a smooth regular motion. In the mathematical model, we have extended Koga's[232] conditions for occurrence of such patterns for planar spiral motion, to a case of moving reaction interface. In our experimental conditions, both types of patterns were observed. Fig. 7.10 shows concentric rings traveling up to a distance before they vanish due to heat diffusion from the upper gel layer. When reaction velocity is comparable to that of traversal of heat wave, we see ramps being formed. The bifurcation of this type has been explained by Koga on his analysis of spiral waves appearing in reaction-diffusion system. Fig. 7.11 presents different types of photograph of ramp type radial pattern.

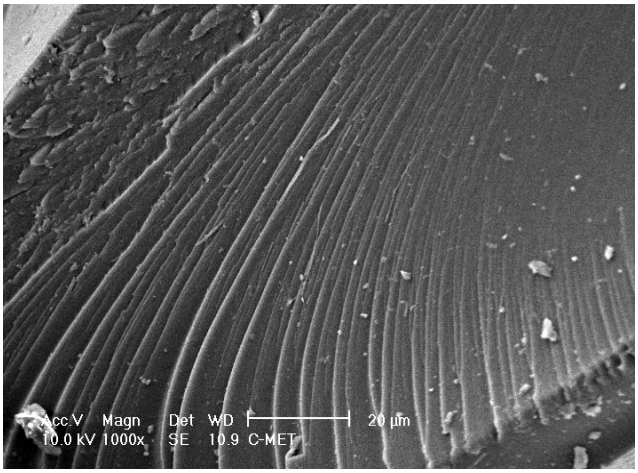

Figure 7.10. Concentric rings formed in poly(GMA-EGDM) synthesized at 100 mol % CLD using 4 mol % AIBN (H18)

A] B]

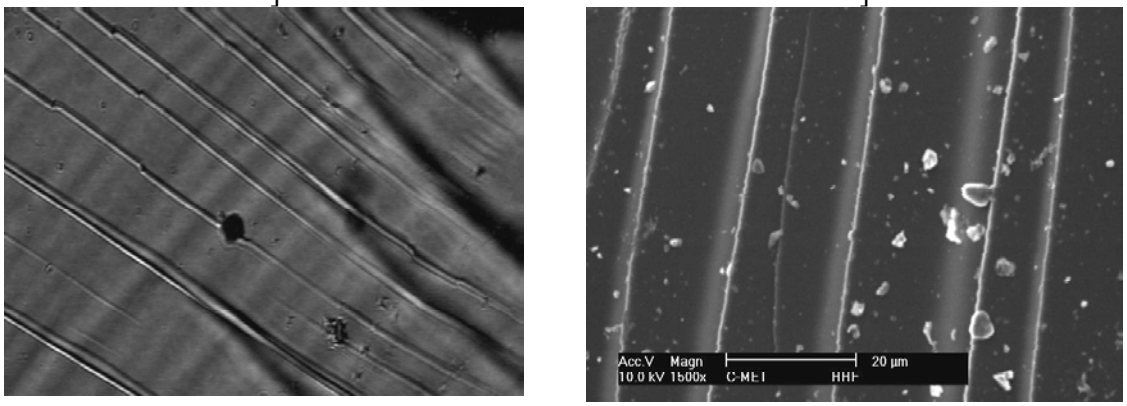

Figure 7.11. Ramps formed in HEMA homopolymerization carried using freeze-thaw technique A] optical microscope image and B] SEM picture

SEM micrograms show the spatial patterns along radial direction perpendicular to axial motion (Fig. 6.14a & b). In this case the reaction is narrow and results in a planar front propagation. When the thermal diffusion spreads itself to adjacent monomer and initiator mixture the motion of moving reaction interface becomes a non-planar front propagation and still repeats itself as a steady characteristic spatial pattern.

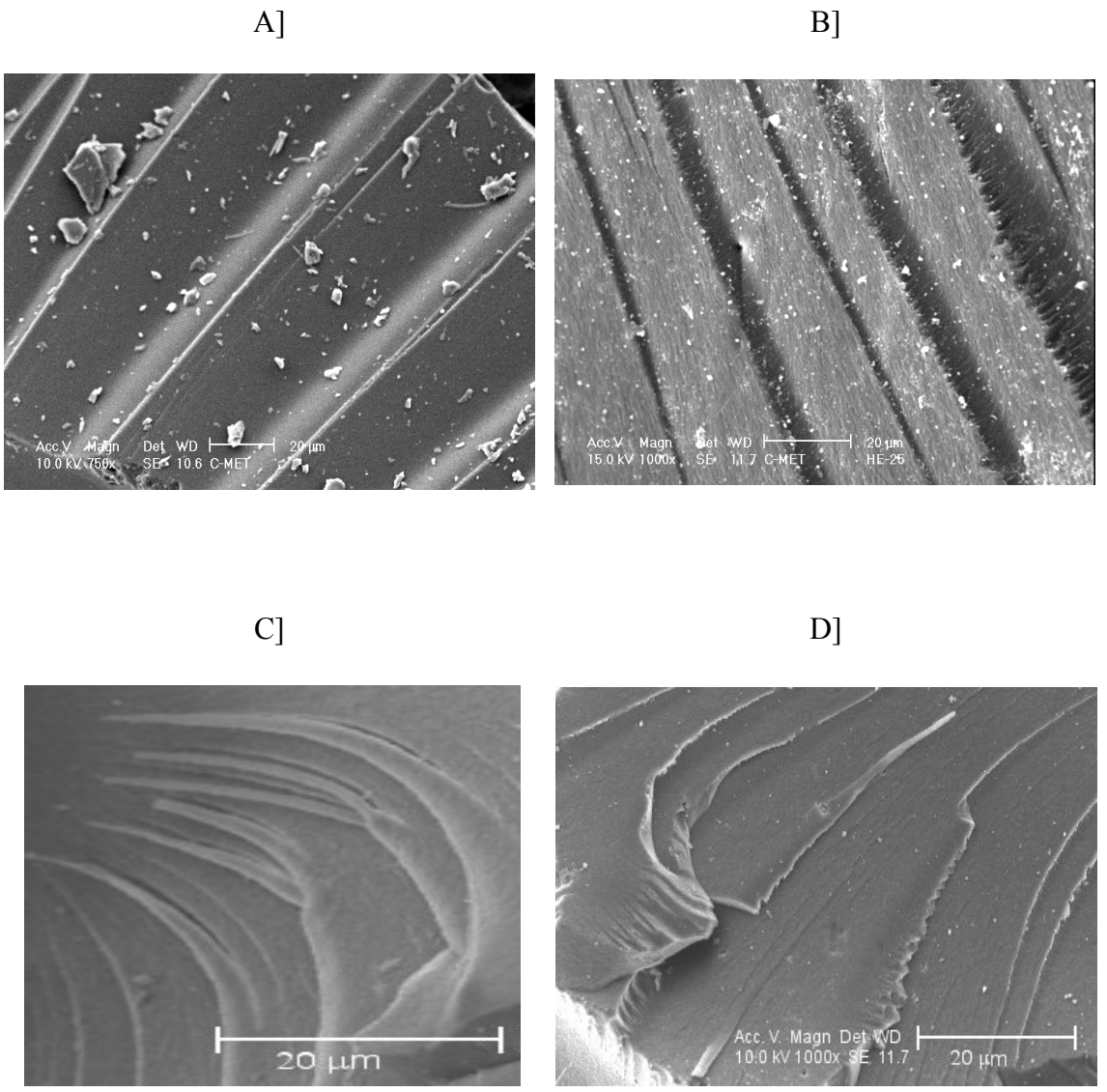

Figure 6.14. SEM pictures showing exotic patterns: Planner patterns of poly(HEMA-EGDM) at a] 25 % CLD synthesized using BPO (H16) and b] 25 % CLD synthesized using 2 mol % AIBN (H11). Poly(GMA-EGDM) synthesized at c] 50 % CLD synthesized by 4 mol % AIBN (G17); d] 25 % CLD synthesized using complex initiation system (AIBN + DCP)

Again, these patterns are of two types: layered concentric rings and winding staircase patterns. SEM picture in Fig. 6.14c shows the winding staircase pattern while Fig. 6.14d shows layered concentric rings. These layered patterns are formed during the front motion and are a self-organizing phenomenon.[160] We also observed some

intermediate spatial patterns (Fig. 7.9) which are planar and non-planar but not a clearly identifiable pattern discussed above.

In presence of solvent, the front temperature comes down drastically. Therefore, we did not observe traces of spiral motion when we carry the reactions in porogen. We may conclude therefore that occurrence of hot spots are controlled by temperature and as solvent controls front temperature, the instabilities are absent in the system or the patterns might be very weak and unobservable. However, it is not true that spirals do not appear. The truth is that they cannot be seen with naked eye/SEM. Mathematically, when spirals asymptotically reach a limit which is too small and stochastically perturbed in that spiral traces may not continue to be remain present. But as a principle, due to operator singularity they are present at some micro or nano level in that their occurrence can be neglected.

7.4 Conclusion

Helical and layered patterns formed during the FP of various systems were analyzed. Helical patterns are generated due to the imbalance in the heat generated in the reaction zone and the heat diffused in the next layer. In water triggered FP clear helical patterns were observed while in crosslinked system it is suspected that the patterns are buried inside the skin. Layered patterns were also observed in both the systems due to the traversal of heat wave in radial direction. A mathematical model to describe the phenomenon was developed.

A two-dimensional approximation of wave motion in (r, θ, z, t) co-ordinates is useful in determining characteristic features of spatio-temporal patterns and in predicting homogeneity of material. Now we will discuss the utility of this model. We find that our

model uses the distance from which motion begins around core of spiral (21 μm) and calculates pitch of the spiral which matches closely with experimental observation in micrograph. The model also predicts qualitatively the ramp wave and spiral wave motion as observed under scanning electron microscope (SEM). Both the results are reported in open literature for the first time to the best of our knowledge. This 2D version of model can be extended to obtain results for 3D model, which will be useful in devising numerical methods to study pattern formation in detail. The 3D model so developed can also be useful in studying formation of helical patterns which is a non-planar motion. The analysis of non-planar motion becoming unstable will be helpful in understanding the causes of polymer matrix becoming porous.

The interplay between thermal diffusion and kinetics gives rise to spin mode patterns in solidified polymer as heat wave propagates on planar moving interface and front descends. Although this is an instability, the regularity of structure maintains uniform microstructure and morphology. An unstable motion otherwise ends up in formation of poor grade material which does not perform well in applications. The model can predict the pattern and its regularity and is useful in determining quality of polymer.

Chapter VIII

SUMMARY & CONCLUSION

8 Summary and conclusion

8.1 Summary and conclusion

Free radical frontal polymerization (FP) is a process wherein the localized reaction zone propagates into mixture of monomer(s) and initiator in the form of narrow reaction front. The task consisted of the investigation of FP technique by means of synthesizing materials by new technique and understanding fundamentals of the process.

In chapter one, we reviewed the work of free radical or thermal frontal polymerization. It was revealed that significant advances in FP technique have opened the way to the development of polymers with tailored molecular architectures and physical properties. We also reviewed the rich nonlinear dynamics associated with the FP technique and studied the various instabilities and the mathematical models to study them.

In chapter two, aims and objectives of the task were outlined.

In third chapter, the investigation on the traveling fronts of 2-hydroxyethyl methacrylate homopolymerization is presented. The effect of various input parameters (type of initiators and their concentration, solvent, type of diluents and their concentration etc.) on. front velocity, front temperature and conversion were investigated. It was observed that facile gelation takes place due to inter/intramolecular reaction in HEMA frontal homopolymerization. In presence of solvents, front was not stable and collapsed due to double diffusive instabilities. Water regain was significantly higher than cyclohexane regain or pore volume as measured by mercury porosimetry. The effective water content (EWC) was much higher than that observed hitherto for PHEMA by conventional polymerization, which is advantageous in

applications like contact lens. The study also revealed the first time observations of patterns at granular level. Additionally, the divinyl monomer, ethylene dimethacrylate was frontally polymerized. Detailed study similar to HEMA polymerization was conducted. Flat front propagation with less formation of bubble was observed in this case.

We could start a new sub-branch in FP, water triggered FP. Fourth chapter was about a detailed understanding of this process. New redox pairs were investigated and the mechanism of the water triggered polymerization was proposed. Conditions under which reaction could be triggered and effect of various parameters, as mentioned above, as well as reaction variables such as type and concentration of redox couple and volume of water on measurable parameters of FP such as front velocity, front temperature, shape of front and yield were investigated.

The methodology also yielded a rich dynamics. Some unique features like breath structures with "weak redox couple" and nonplanar frontal regime with "strong redox couples" were observed. For the first time helical and layered patterns were obtained. Possibility of the scaling up of the process was also investigated. For this, effect of reactor length and geometry was investigated on rate of polymerization and induction period. A detailed mechanism of the water triggered frontal polymerization was modeled and empirical equations were derived for rate of polymerization and induction period. The expressions were validated using experimental data. It was found that FP method is rapid and can be scaled-up easily and effectively.

The possibility of using frontal polymerization to produce copolymers has been investigated. Amongst several pairs tested, solid-solid monomer pairs yielded clear front

propagation. With liquid-liquid monomer pairs, fronts were extinguished due to various instabilities. With solid-liquid pairs, front propagation was possible only at low concentration of liquid monomer. An exhaustive analysis of four pairs viz. acrylamide-potassium acrylate, acrylamide-potassium methacrylate, acrylamide-ammonium acrylate and acrylamide-ammonium methacrylate was carried out. It was observed that with acrylate salts the rate of polymerization was always higher than respective methacrylate salts. In methacrylate salts, the rate of polymerization was relatively unaffected by the molar composition in the feed. Front temperature was also higher in acrylates. Potassium acrylate based systems imidized due to very high front temperature.

The reactivity ratio values of comonomers indicate that even at higher front temperature, the process is not completely stochastic and acrylamide always react rapidly than carboxylate salts. Fineman-Ross and Kelen-Tudos models were used to estimate the reactivity ratios. It was found that the values differ drastically in two sets and for a given data, which seems to be well behaved with Fineman-Ross method does not behave properly in Kelen-Tudos method and vice versa. We concluded that the system may not be behaving as per the assumptions of the models on more than one point. Hence, the simple models and their estimation procedures may not be applicable to the frontal copolymerizations studied here. One of the unique outcomings of this process was, successful copolymerization of carboxylate salts, homopolymerization of which otherwise is not possible by FP.

In sixth chapter, a series of copolymers of 2-hydroxyethyl methacrylate (HEMA)/glycidyl metharylate (GMA) and ethylene dimethacrylate (EGDM) were synthesized by frontal polymerization. It was observed that AIBN and BPO produced

stable fronts while higher activation energy initiator, DCP could not sustain front due to extensive heat losses. As a general observation, front velocity increased with increasing % CLD. Amongst several solvents evaluated, 2-ethoxyethyl acetate was found to sustain the front in HEMA-EGDM system. All reactions in GMA-EGDM systems were extinguished in presence of a solvent. In ascending polymerization, convective instabilities were observed and front propagation was in nonplanar mode.

Polymers synthesized were also compared with suspension polymerization. When reactions were carried without solvent (porogen), pore volume were lower and discontinuous. EEA was evaluated as a porogen for the first time and it was observed that it produces sufficient pore volume and specific surface area. Pore volume and specific surface area in FP was found to be independent of crosslinker but dependent on type and volume of solvent. At higher volumes of EEA, higher pore volumes were generated. Pore size distribution in FP was also narrow and within a range of 10-50 nm. With identical compositions, SP could not produce porosity in the matrix. Thus, FP was found to be superior over SP in terms of producing higher pore volume with or without solvent, higher yields and less reaction time. We also evaluated some of our polymers for solvent non-solvent regain (DMF and water). It was observed that all polymers attain equilibrium volume swelling in 120 min. There was no change in particle diameter due to rigid structure.

The presence of exotic patterns is an important finding of this work. Polymers possessed spatial patterns along radial direction, observable under SEM. These patterns were of two basic types viz. planar and non-planar.

Helical and layered patterns formed during the FP of various systems were analyzed in chapter seven. Helical patterns are generated due to the imbalance in the heat generated in the reaction zone and the heat diffused in the next layer. In water triggered FP clear helical patterns were observed while in crosslinked system it is suspected that the patterns are buried inside the skin. Layered patterns were also observed in both systems due to the traversal of heat wave in radial direction. A mathematical model to describe the phenomenon was developed. The interplay between thermal diffusion and kinetics gives rise to spinmode patterns in solidified polymer as heat wave propagates on planar moving interface and front descends. Although this is an instability, the regularity of structure maintains uniform microstructure and morphology. An unstable motion otherwise ends up in formation of material with lower quality which does not perform properly on application. The model can predict the pattern and its regularity and is useful in determining quality of polymer.

8.2 Future prospects

Frontal polymerizations are conducted in absence of solvent and hence the product need not be separated from the solvent and there is no contaminated solvent requiring disposal. Bulk polymerization of reactive monomers like acrylates cannot normally be accomplished safely because of the large exothermicity associated with it. Frontal polymerization of highly reactive monomers can be performed safely because the reaction is localized in a narrow zone. Very high molecular weights, of the order of 10^6, can be reached in time scales of few minutes with only initial energy input for a few seconds, thus making the process cost and energy efficient. The products are of superior quality in terms of molecular weight and morphology due to high reaction

rates and low reaction times. These polymers are of technological importance in flocculation.

Search for newer monomers which can undergo frontal polymerization is still on. 2-Hydroxyethyl methacrylate, monomer studied extensively in this task, can be derivatized to produce a wide range of polymeric reagents suited to pharmaceutical, chromatographic applications as well as to immobilize biopolymers (enzymes, antibodies, cells), encapsulate mammalian cells and other sensitive compounds. Transparent PHEMA, prepared by bulk polymerization, forms gels by entrapping water or other liquids. If we get similar properties by FP in short reaction time and with unique microstructure it would be a tremendous advantage.

Water triggered frontal polymerization does not even require energy input. 1-2 Drops of water initiates the reaction. This opened up a new way to synthesize polymers. Various homo and copolymers (e.g. acrylamide-N,N-methylenebisacrylamide) can be synthesized and studied. A new set of redox pairs can be investigated and process can be further tailor-made. It is important to have an effect of reactor geometry and the theoretical understanding of the process as scale-up criterion to make the system commercially viable. The method has an industrial application as we have showed that process can be scaled-up to semi-pilot level. We also have derived the empirical derivations and validated them using the experimental data. A more fundamental understanding of the process and development of fundamental mathematical model is still an open area. Water triggered frontal polymerization also had illustrated the dynamic behaviour. There is a lot of scope to study the phenomenon like “breath figures” observed in the methodology.

There are very few reports on copolymerization in FP. Our study demonstrates the anomalous behaviour in solid-solid copolymerizing system. The nonlinearity observed can be better explained by newer models. There is a need to develop an evolved mathematical model. Small comonomer blocks if packed alternatively, it would be interesting to see the microstructure of the formed copolymer. We may conjecture formation of block copolymers.

Functionalized crosslinked network formation by FP technique has not been reported as yet. The study gave us the unique opportunity to have a better understanding of a simultaneous crosslinking process. Effect of various input parameters were investigated which aided in maturating the area as well enrich our knowledge. Our observations showed that frontal polymerization produces porosity in the matrix even in the absence of a porogen and that the process depends upon fewer parameters as compared to the suspension polymerization. A proper understanding and optimization of the conditions for FP to yield functionalized copolymer networks will be of great technological interest as these products have greater surface area and intruded pore volume. They are superior in terms of percent yields as well as reaction rates. New functionalized networks using monomers pairs like like allyl glycidyl methacrylate: ethylene dimethacrylate, 2-hydroxy ethyl methacrylate:pentaerythritol tetraacrylate, etc. can be synthesized for various applications. There is also a scope of *in situ* modification reactions. Dibenzoyl tartarate like moiety can be *in situ* attached to the monovinyl monomer which can be used as chiral resolving agent.

Pattern formation is a complex phenomenon in FP. We have been able to observe for the first time helical patterns in acrylamide polymerization. We also

observed the layered patterns in few systems under a microscope. Although the phenomenon has been studied significantly, in dynamics several questions remain to answered:[14]

i. What is the exact relationship between the heat loss and the mode of propagation?
ii. What is the experimental relationship between test tube size and number of spin heads? Numerical analysis of hot-spot generation is not known.
iii. Can multiplicity of spin modes be observed experimentally? In other words, can more than one propagation mode exist under the same experimental conditions?
iv. What is the effect of complex reaction kinetics (like in crosslinked copolymer synthesis) on the front stability?

Nevertheless, there are not many reports in literature concerning bifurcation theory and breaking of singularity in FP dynamics. Determining the conditions for occurrence of instabilities to identification of regions in parameter space where inhomogeneities can be present will make frontal polymerization more technological faced. Understanding the causes of the same will aid in the synthesis of FP products with uniform microstructure, in a reproducible manner.

REFERENCES

1. Merzhanov, A. G.; Borovinskaya, I. P. *Dokl. Nauk. SSSR* **1972**, *204*, 336.

2. Merzhanov, A. G. *Internat. Chem. Eng.* **1980,** *20*, 150.

3. Shkadinsky, K. G.; Khaikin, B. I.; Merzhanov, A. G. *Combust. Explos. Shocks Waves* **1971**, *1*, 15.

4. Anselm-Tambureni, U.; Munir, Z. *J. Appl. Phys.* **1989**, *66*, 5039.

5. Moore, J. J. *Prog. Mat. Sci.* **1995**, *39*, 243.

6. Merzhanov, A. G. *Archiv. Comb.* **1981**, *1*, 23.

7. Merzhanov, A. G. *Combust. Sci. Technol.* **1994**, *98*, 307.

8. Puszynski, J.; Degreve J.; Hlavacek, V. *Ind. Eng. Chem. Res.* **1987**, *26*, 1424.

9. Verma, A.; Lebert, J. P. *Chem. Eng. Sci.* **1992**, *47*, 21779.

10. Hlavacek, V. *Am. Ceram. Soc. Bull.* **1991**, *70*, 240.

11. Merzhanov, A. G. *Int. J. Self-Propagating High Temp. Synth.* **1993**, *2*, 113.

12. Chechilo, N. M.; Khvilivitskii, R. J.; Enikolopyan, N. S. *Dokl. Akad. Nauk. SSSR* **1972**, *204*, 1180.

13. Chechilo, N. M.; Enikolopyan, N. S. *Dokl. Phys. Chem.* **1975**, *221,* 392.

14. Pojman, J. A.; Ilyashenko, V. M.; Khan, A. M. *J. Chem. Soc. Faraday Trans.* **1996**, *92,* 2824.

15. Novozhilov, B. V. *Pure & Appl. Chem.* **1992**, *64*, 955.

16. Davtyan, S. P.; Zhirkov, P. V.; Volfson, S. A. *Russian Chem. Rev.* **1984**, *53*, 150.

17. Enikolopyan, N. S.; Kozhushner, M. A.; Khanukaev, B. B. *Doklady Phys. Chem.* **1974**, *217,* 676.

18. Chechilo, N. M.; Enikolopyan, N. S. *Dokl. Phys. Chem.* **1976**, *230*, 160.

19. Davtyan, S. P.; Sukrov, N. F.; Rozenberge, B. A.; Enikolopyan, N. S. *Dokl. Phys. Chem.* **1977**, *232*, 64.

20. Surkov, N. F.; Davtyan, S. P.; Rozenberg, B. A.; Enikolopyan, N. S. *Dokl. Phys. Chem.* **1976**, *228,* 435.

21. Begishev, V. P.; Volpert, V. A.; Davtyan, S. P.; Malkin, A. Y. *Dokl. Akad. Nauk SSSR* **1973**, *208,* 892.

22 Begishev, V. P.; Volpert, V. A.; Davtyan, S. P.; Malkin, A. Y. *Dokl. Phys. Chem.* **1985**, *279*, 1075.

23 Volpert, V. A.; Mergabova, I. N.; Davtyan, S. P.; Begishev, V. P. *Combust. Explos. Shock Waves* **1986**, *21,* 443.

24. Karger-Kocsis, J.; Szafner, A. *Macrmol. Chem.* **1978**, *179*, 519.

25. Frunz, T. M.; Kurashev, V. V.; Kotelnikov, V. A.; Davtyan, S. P.; Volkova, T. V. *Vysokomol. Soed.* **1978**, *20B*, 206.

26. Arutyunyan, K. A.; Davtyan, S. P.; Rozenberg, B. A.; Enikolopyan, N. S. *Vysokomol. Soed.* **1974**, *16A*, 2115.

27 Arutyunyan, K. A.; Davtyan, S. P.; Rozenberg, B. A.; Enikolopyan, N. S. *Dokl. Akad. Nauk. USSR* **1975**, *223*, 687.

28. Aleksanyan, G. G.; Arutyunyan, K. A.; Bodneva, V. L.; Davtyan, S. P.; Prut, E. V.; Rozenberg, B. A.; Shkadinskii, K. G.; Yenikolopyan, N. S. *Polym. Sci. USSR* **1975**, *A17,* 1052.

29. Enikolopyan, N. S.; Kozhushner, M. A.; Khanukaev, B. B. *Doklady Phys. Chem.* **1974**, *217,* 676.

30. Khanukaev, B. B.; Kozhushner, M. A.; Enikolopyan, N. S. *Dokl. Phys. Chem.* **1974**, *214,* 84.

31. Zhizhin, G. V.; Segal, A. S.; Babadzhanyan, A. S.; Volpert, V. A.; Davtyan, S. P. *Kinet. Kataliz* **1986**, *27*, 1310.

32. Zhizhin, G. V. In *Mackrokinetics of frontal polymerization reactors* **1988**, Politehnika, St. Petersburg, (in Russian).

33. Odian, G. *In Principles of Polymerization* **2004**, 4th Edition, Wiley Inter sciences, A John Wiley & Sons, INC., USA.

34. Pojman, J. A. *J. Am. Chem. Soc*. **1991**, *113*, 6284.

35. Pojman, J. A.; Khan, A. M.; Mathias, L. *Microgr. Sci. Tech.* **1997**, *X*, 36.

36. Pojman, J. A.; Curtis, G.; Ilyashenko, V. *J. Am. Chem. Soc.* **1997,** *115*, 3783.

37. Pojman, J. A.; Nagy, I. P.; Salter, C. *J. Am. Chem. Soc.* **1993**, *115*, 11044.

38. Fortenberry, D. I.; Pojman, J. A. *J. Polym. Sci. Part A: Polym Chem.* **2000**, *38*, 1129.

39. Nagy, I. P.; Pojman, J. A. *J. Phys. Chem.* **1996**, *100*, 3299.

40. Pojman, J. A.; Fortenberry, D.; Khan, A.; Ilyashenko, V. In *Synthesis Characterization of Advanced Materials* **1998**, Serio, M. A.; Gruen, D. M.; Malhotra, R. Eds., American Chemical Society: Washington, DC, *681*, pp. 220.

41. Washington, R. P.; Steinbock, O. *Polymer News* **2003**, *28*, 303.

42. Pojman, J. A.; Willis, J.; Fortenberry, D.; Ilyashenko, V.; Khan, A. *J. Polym. Sci. Part A: Polym Chem.* **1995**, *33,* 643.

43. Nagy I. P.; Pojman, J. A. *J. Phys. Chem.* **1996**, *100*, 3299.

44. Khan A. M. *Ph. D. thesis* **1997**.

45. Pojman, J. A.; Craven, R.; Khan, A.; West, W. *J. Phys. Chem.* **1992**, *96*, 7466.

46. Novozhilov, B. V. *Dokl. Akad. Nauk SSSR* **1961**, *141*, 151.

47. Masere, J.; Chekanov, Y.; Warren, J. R.; Stewart, F.; Al-Kaysi, R.; Rasmussen, J. K.; Pojman, J. A. *J. Poly. Sci. Part A. Polym. Chem.* **2000**, *38,* 3984.

48. Bazile Jr., M.; Nichols, H. A.; Pojman, J. A.; Volpert, V. *J. Polym. Sci. Part A: Polym Chem.* **2002**, *40*, 3504.

49. Goldfeder, P. M.; Volpert, V. A. *Math. Problems in Enginering* **1999**, *5,* 139.

50. Pojman, J. A.; Willis, J.; Fortenberry, D.; Ilyashenko, V.; Khan, A. *J. Polym. Sci. Part A: Polym Chem.* **1995**, *33,* 643.

51. Pojman, J. A.; Willis, J. R.; Khan , A. M.; West, W. W. *J. Polym. Sci. Part A: Polym Chem.* **1996**, *34*, 991.

52. Szalay, J.; Nagy, I. P.; Barkai, I.; Zsuga, M. *Die Angew. Makomol. Chem.* **1996**, *236,* 97.

53. Gill, N.; Pojman, J. A.; Willis, J.; Whitehead, J. B. *J. Poly. Sci. Part A. Polym. Chem*. **2003**, *41*, 204.

54. Volpert, V. A.; Volpert, V. A.; Ilyashenko, V. M.; Pojman, J. A. *Chem. Eng. Sci.* **1998**, *53,* 1655.

55. White, S. R.; Kim, C. *37th Int. SAMPE Symp. Exhib.* **1992**, 240.

56. White, S. R.; Kim, C. *J. Reinforced Plastics and Comp.* **1993**, *12*, 520.

57. Khan, A. M.; Pojman, J. A. *Trends Polym. Sci.* **1996**, *4*, 253.

58. Masere, J.; Stewart, F.; Meehan, T.; Pojman, J. A. *Chaos*, **1999**, *9*, 315.

59. Balcom, B. J.; Carpenter, T. A.; Hall, L. D. *Macromolecules* **1992**, *25*, 6818.

60. Masere, J.; Pojman, J. A. *J. Chem. Soc. Faraday Trans.* **1998**, *94*, 919.

61. Pojman, J. A.; Masere, J.; Petretto, E.; Rustici, M.; Huh, D.-S.; Kim, M. S.; Volpert, V. *Chaos* **2002**, *12*, 56.

62. Volpert, V.; Volpert, V. *Eur. J. Appl. Math.* **1994**, *5*, 201.

63. Goldfeder, P. M.; Volpert, V. A.; Ilyashenko, V. M.; Khan, A. M.; Pojman, J. A.; Solovyov, S. E. *J. Phys. Chem. B* **1997**, *101*, 3474.

64. Spade, C. A.; Volpert, V. A. *Combustion Theory and Modeling* **2001**, *5*, 21.

65. Solovyov, S. E.; Ilyashenko, V. M.; Pojman, J. A. *Chaos* **1997**, *7*, 331.

66. Goldfeder, P. M.; Volpert, V. A. *J. Eng. Math.* **1998**, *34*, 301.

67. Spade, C. A.; Volpert, V. A. *Chem. Eng. Sci.* **2000**, *55*, 641.

68. Goldfeder, P. M.; Volpert, V. A. *Math. Problems in Eng.* **1998**, *4,* 377.

69. Commissiong, D. M. G.; Gross, L. K.; Volpert, V. A. *J. Eng. Math*. **2006**, *54*, 389.

70. Apostolo, M.; Tredici, A.; Morbidelli, M.; Varma, A. *J. Polym. Sci. Part A: Polym Chem.* **1997**, *35,* 1047.

71. Golovaty, .D. In *On Step Function Kinetics Model of Frontal Polymerization in the Absence of Monomer Diffusion,* Communicated to SIAP **2006**.

72. Cardarelli, S. A.; Golovaty, .D; Gross, L. K.; Gyrya, V. T.; Zhu, J. *Physica D*, **2005**, *206*, 145.

73. Aldushin, A. P.; Martemyanova, T. M.; Merzhanov, A. G.; Khaikin, B. I.; Shkadinskii, K. G. *Combust., Explos. Shock Waves* **1973**, *9*, 531.

74. Ivleva, T. P.; Merzhanov, A. G.; Shkadinskii, K. G. *Combust., Explos. Shock Waves* **1980**, *16*, 133.

75. Ivleva, T. P.; Merzhanov, A. G.; *Dokl. Phys.* **1999**, *44*, 739.

76. Aldushin, A. P.; Kasparyan, S. G. *Dokl. Akad. Nauk SSSR* **1979**, *244*, 67.

77. Matkowsky, B. J.; Sivashinsky, G. I. *SIAM Soc. Ind. Appl. Math. J. Appl. Math.* **1978**, *35*, 465.

78. Pojman, J. A.; Ilyashenko, V. M.; Khan, A. M. *Physica D* **1995**, *84*, 260.

79. Huh, D. S.; Kim, H. S. *Polym. Int.* **2003**, *52*, 1900.

80. Huh, D. S.; Choe, S. J., Lee, B. J. *Bull. Korean Chem. Soc.* **2002**, *23*, 325.

81. Manz, B.; Masere, J.; Pojman, J. A.; Volke, F. *J. Poly. Sci. Part A. Polym. Chem.* **2001**, *39,* 1075.

82. Davtyan, S. P.; Hambartsumyan, A. F.; Davtyan, D. S.; Tonoyan, A. O.; Hayrapetyan, S.; Bagyan, S. H.; Manukyan, L. S. *Eur. Polym. J.* **2002**, *38*, 2423.

83. Binici, B.; Fortenberry, D. I.; Leard, K. C.; Molden, M.; Olten, N.; Popwell, S.; Pojman, J. A. *J. Polym. Sci. Part A: Polym. Chem.* **2006**, *44*, 1387.

84. McCaughey, B., Pojman, J. A., Simmons, C., Volpert, V. A. *Chaos* **1998**, *8*, 520.

85. Bowden, G., Garbey, M., Ilyashenko, V. M., Pojman, J. A., Solovyov, S. E., Taik, A., Volpert, V. A., J. Phys. Chem. B **1997**, *101*, 678.

86. Allali, K.; Pojman, J.; Volpert, V. *J. Eng. Math.* **2001**, *41,* 13.

87. Volpert, Vit. A.; Volpert, V. A.; Pojman, J. A. *Chem. Eng. Sci.* **1994**, *14*, 2385.

88. Volpert, V.; Volpert, V. A.; Pojman, J. A.; Solovyov, S. E. *Eur. J. Appl. Math.* **1996**, *7,* 303.

89. Davtyan, D. S.; Bagdasaryan, A. E.; Tonoyan, A. O.; Davtyan, S. P. *Chem. Phys. Reports* **2001**, *19*, 1757.

90. Pojman, J. A.; Volpert, V. A.; Volpert, V. A. In *Self-Propagating High-Temperature Synthesis of Materials* **2002**; Borisov, A. A.; De Luca., L. T.; Merzhanov, A. G. Eds.; Taylor and Francis: New York, 99.

91. Pojman, J. A.; Elcan, W.; Khan, A. M.; Mathias, L. *J. Polym. Sci. Part A: Polym Chem.* **1997**, *35*, 227.

92. Pojman, J. A.; Griffith, J.; Nichols, H. A. *e-Polymers* **2004**, *13*, 1.

93. Fiori, S.; Mariani, A.; Ricco, L.; Russo, S. *e-Polymers* **2002**, *29*, 1.

94. Tredici, A.; Pecchini, R.; Morbidelli, M. *J. Polym. Sci. Part A: Polym Chem.* **1998**, *36*, 1117.

95. Szalay, J.; Nagy, I.; Bayai, I.; Deak, G.; Bazsa, G.; Zsuga, M. *Macromol. Rapid Comm.* **1999**, *20*, 315.

96. Fiori, S.; Malucelli, G.; Mariani, A.; Ricco, L.; Casazza, E. *e-Polymers* **2002**, *57*, 1.

97. Mariani, A. F. S.; Bidali, S.; Fiori, S.; Malucelli, G.; Ricco, L. *Macromol. Symp*. **2004**, 218, 1.

98. Hu, T.; Chen, S.; Tian, Y.; Pojman, J. A.; Chen, L. *J. Poly. Sci. Part A. Polym. Chem.* **2006**, *44*, 3018.

99. Pujari, N. S.; Vaidya, B. K.; Bagalkote, S.; Ponrathnam, S.; Nene, S. N. *J. Membr. Sci.* **2006**, *285*, 395.

100. Yu, X. H.; Grady, B. P.; Reiner, R. S.; Cooper, S. L. *J Appl Polym Sci* **1993**, *49*, 1943.

101. Valet, A. *Prog. Org. Coat.* **1999**, *35*, 223.

102. Perry, M. F.; Volpert, V. A.; Lewis, L. L.; Nichols, H. A.; Pojman, J. A. *Macromolecular Theory and Simulations* **2003**, *12*, 276.

103. Washington, R. P.; Steinbock, O. *J. Am. Chem. Soc.* **2001**, *123,* 7933.

104. Yan, Q.; Zhang, W. F.; Lu, G. D.; Su, X. T.; Ge, C. C. *Chem. Eur. J.* **2005**, *11*, 1609.

105. Yan, Q. Z.; Su, X. T.; Zhang, W. F.; Ge, C. C. *Chemical Journal of Chinese Universitie*s **2005**, *26*, 1363.

106. Yan, Q.; Zhang, W. F.; Lu, G. D.; Su, X. T.; Ge, C. C. *Chem., Eur. J.* **2006**, *12*, 3303.

107. Schmidt, H.; Krug, H. *ACS Symp. Ser.* **1994**, *572*, 183.

108. Schmidt, H. K. *Macromol. Symp*. **1996**, *101*, 333.

109. Nagy, I. P.; Sike, L.; Pojman, J. A. *J. Am. Chem. Soc.* **1995**, *117*, 3611.

110. Nagy, I. P.; Sike, L.; Pojman, J. A. *Adv. Mat.* **1995**, *7*, 1038.

111. Vicini, S.; Mariani, A.; Princi, E.; Bidali, S.; Pincin, S.; Fiori, S.; Pedemonte, S.; Brunetti, A. *Polym. Adv. Technol*. **2005**, *16*, 293.

112. Davtyan, S. P.; Tonoyan, A. O.; Tataryan, A. A.; Schick, C. *Composite Interface*s **2006**, *13*, 535.

113. Paul, D. R.; Newman, S. (Eds.) In *Polymer Blends V 1*, Academic press, San Diego., **1978**.

114. Martuscllie, E.; Palumbo, R.; Kryszewski, M. (Eds.) In *Polymer Blends: Processing, Morphology, and Properties*, Platimum Publication Corp.; Newyork, **1980**.

115. Paul, D. R.; Newman, S., *Polymer Blends*, V1, Academic Press, San Diego, **1978**.

116. Tredici, A.; Pechhini, R.; Sliepcevich, A.; Morbidelli, M. *J. Appl. Polym. Sci.* **1998**, *70,* 2695.

117. Chen, S.; Tian, Y.; Chen, L.; Hu, T. *Chem. Mater*. **2006**, *18*, 2159.

118. Mariani, A.; Fiori, S.; Chekanov, Y.; Pojman, J. A. *Macromolecules* **2001**, *34*, 6539.

119. Fiori, S.; Mariani, A.; Ricco, L.; Russo, S. *Macromolecules* **2003**, *36*, 2674.

120. Mariani, A.; Bidali, S.; Fiori, S.; Malucelli, G.; Sanna, E. *e-Polymers* **2003**, *44*, 1.

121. Fiori, S.; Mariani, A.; Ricco, L.; Russo, S. *e-Polymers* **2002**, *29*, 1.

122. Bidali, S.; Fiori, S.; Malucelli, G.; Mariani, A. *e-Polymers* **2003**, *60*, 1.

123. Chen, S.; Sui, J.; Chen, L.; Pojman, J. A. *J. Polym. Sci. Part A Polym. Chem.* **2005**, *43*, 1670.

124. Chen, S.; Feng, C.; Sui, J. *Acta Polymerica Sinica* **2005**, *1*, 1.

125. Guyot, A.; Bartholin, M. *Prog. Polym. Sci.* **1982**, *8*, 277.

126. Kahovec, J.; Jelinkova, M.; Coupek, J. *Polym. Bull.* **1987**, *18*, 495.

127. Hodge, P.; Sherrington, D. C. In *Syntheses and Separations Using Functional Polymers*, Wiley: New York **1989**.

128. Piskin, E. *Int. J. Artif. Organs* **1986**, *9*, 289.

129. Horak, D.; Svec, F.; Kalal, J.; Adamyan, A.; Volynskii, O.; Voronkova, L. K.; Gumargalieva, K. *Biomaterials* **1986**, *7*, 467.

130. Robert, C.; Buri, P. A.; Peppas, N. A. *J. Controlled Release* **1987**, *5*, 151.

131. Kamei, S.; Okubu, M.; Matsumoto, T. *J. Appl. Polym. Sci.* **1987**, *34*, 1439.

132. Stevenson, W. K. T.; Sefton, N. O. *Biomaterials* **1987**, *8*, 449.

133. Okay, O. *Prog. Polym. Sci.* **2000**, *25*, 711.

134. Naghash, H. J.; Okay, O.; Yildirim, H. *J. Appl. Polym. Sci.* **1995**, *56*, 477.

135. Gowarikar, V. R.; Viswanathan, N. V.; Sreedhar, J. In *Polymer Science*, Wiley Eastern Ltd., New Delhi; **1995**; p 30.

136. Volpert, V. A. *Appl. Math. Lett.* **1997**, *10*, 59.

137. Bennett, D. J.; Burford, R. P.; Davis, T. P.; Tilley, H. J. *Polym. Int.* **1995**, *36*, 219.

138. Okay, O.; Gurun, C. *J. Appl. Polym. Sci.* **1992**, *46*, 421.

139. Stamberg, J.; Sevcik, S. *Collect. Czech. Chem. Commun.* **1966**, *31*, 1009.

140. Pojman, J. A.; Epstein, I. R. *J. Phys. Chem.* **1990,** *94*, 4966.

141 Svec, F.; Hradil, J.; Coupek, J.; Kilal, J. *Die Angew. Makromol. Chemie* **1975**, *48(I 975)*, 135.

142. Tuncel, A.; Poskin, E. *J.Appl. Polym. Sci.* **1996**, *62*, 789.

143. Kern, W. *Angew. Chem*. **1949**, *61*, 471.

144. House, D. A. *Chem. Rev.* **1962**, *62*, 185.

145. Sarac, A. S. *Prog. Polym. Sci.* **1999**, *24*, 1149.

146. Misra, G. S.; Bajpai, U. D. *Prog. Polym. Sci.* **1982**, *8,* 61.

147. Berry, K. L.; Person, J. H. *J. Am. Chem. Soc.* **1951**, *73*, 5195.

148. Finch, A. In *Chemistry, technology of water soluble polymers*, 2nd edition, Plenum press, New York, **1983**.

149. Riggs, J. P.; Rodriguez, F. *J. polym. Sci.* **1967**, *A1(5)*, 3161.

150. Braun, H. B.; Chadron, C. In *Techniques of Polymer synthesis and characterization*, John Wiley and sons, Inc., New York, **1971**.

151. Harmon, L.; Betzel, C. *Ann.* **1950**, *69*, 566.

152. Harmon, L.; Betzel, C. *J. Polym. Sci.* **1955**, *18*, 438.

153. Meltzer, T. H.; Tobolsky, A. V. *J. Am. Chem. Soc.* **1954**, *76*, 5178.

154. Imoto, M.; Takemoto, K. *J. Polym. Sci.* **1955**, *18*, 377.

155. Horner, L.; Schwenk, E. *Angew. Chem.* **1949**, *61*, 411.

156. Orr, R. J.; Williams, H. L. *Disc. Faraday Soc.* **1953**, *14*, 237.

157. Whitby, G. S.; Wellman, N.; Floutz, V. W.; Stephans, H. L. *Ind. Eng. Chem.* **1950**, *42*, 445.

158. Embree, W. H.; Splosky, R.; Williams, H. L. *Ind. Eng. Chem.* **1951**, *43*, 2553.

159. Narain, H.; Jagdale, S. M.; Ghatge, N. D.; *J. Polym. Sci. Polym. Chem. Ed.* **1981**, *19*, 1225.

160. Winfree, A. *Scientific American* **1974**, *June*, 84.

161. Nakano, A.; Minoura, Y. *Polymer* **1968**, *10*, 1.

162. Srivastava, S.; Ghosh, S. *Z. Physik. Chem. **1957**, 207,* 161.

163. Kapanna, A. N. *Z. Physik. Chem.* **1956**, *205,* 47.

164. Varma, A. J.; Mukasyan, A.; Hwang, S. *Chem. Eng. Sci.* **2001**, *56*, 1459.

165. Srinivasarao, M.; Collings, D.; Philips, A.; Patel, S. *Science* **2001,** *292(*6), 79.

166. Rayleigh, L. *Nature* **1911**, *86*, 416.

167. Rayleigh, L. *Nature* **1912,** *90*, 436.

168. Baker, J. T. *Philos. Mag*. **1922,** *56*, 752.

169. Aitken, J.; Rayleigh, L. *Nature* **1911***, 86*, 516.

170. Beysens, D.; Steyer, A.; Guenoun, P.; Fritter, D.; Knobler, C. M. *Phase Transitions* **1991***, 31,* 219.

171. Briscoe, B. J.; Galvin, B. J. *J. Phys. D* **1990,** *23*, 422.

172. Beysens, D.; Knobler, C. M. *Phys. Rev. Lett*. **1986**, *57*, 1433.

173. Widawski, G.; Rawiso, M.; Francois, B. *Nature* **1994**, *369*, 387.

174. Erdogan, B.; Song, L.; Wilson, J. N.; Park, J. O.; Srinivasarao, M.; Bunz, U. H. F. *J. Am. Chem. Soc.* **2004**, *126*, 3678.

175. Xu, Y.; Zhu, B.; Xu, Y. *Polymer* **2005**, *46*, 713.

176. Saunders, A. E.; Dickson, J.; Shah, P. S.; Lee, M. Y.; Lim, K. T.; Johnston, K. P.; Korgel1, B. A. *Phyisic. Rev. E*. **2006**, *73*, 31608.

177. Himmelblau, D. M.; Bischoff, K. B.; In *Process Analysis and simulation,* John Wiley and sons, New York, **1968**.

178. Brandrup, J.; Immergut, E. In *Polymer Handbook*, John Wiley and sons, New York, **1989**.

179. Schoonover, I. C; Brauer, G. M.; Sweeney, W. T. *Journal of Research of the National Bureau of Standards*, **1952**, 49(6), 2372.

180. Basio, A.; Kabel, R. L. In *Scale-up of chemical process*, John Wiley and sons, New York, **1985**.

181. Chanda, M. In *Advanced Polymer Chemistry: A problem solving guide,* Marcel Dekker Inc. New York, **2000**.

182. Ponrathnam, S. *Ph. D. Thesis* **1976**.

183. Gadgil, J. M. *Ph. D. Thesis* **1993**.

184. Mayo, F. R.; Lewis, F. M. *J. Am. Chem. Soc.* **1944**, *66*, 1594.

185. Joshi, R. M.; Joshi, S. G. *J. Macromol. Sci.-Chem*. **1971**, *A5*, 1329.

186. Joshi, R. M. *J. Macromol. Sci.-Chem*. **1973**, *A7*, 1231.

187. Fineman, M.; Ross, S. D. *J. Polym. Sci.* **1950**, *5*, 249.

188. Tidwell, P. W.; Mortimer, G. A. *J. Polym. Sci.* **1965**, *A3*, 369.

189. Tidwell, P. W.; Mortimer, G. A. *J. Macromol. Sci.-Rev. Macromol. Chem.* **1970**, *C4*, 281.

190. Kelen, T.; Tudos, F. *J. Macromol. Sci.-Chem*. **1975**, *A9*, 1.

191 Kennedy, J. P.; Kelen, T.; Tudos, F. *J. Macromol. Sci.-Chem*. **1975**, *A13*, 2277.

192. Fukuda, T.; Ma, Y-D.; Inagaki, H. *Macromolecules* **1985**, *18*, 17.

193. Sandler, S. R.; Karo, W. In *Polymer Syntheses*, 2nd Ed.; Academic Press: New York, **1992**; *Vol. 1*, p 420.

194. Nikolaev, A. F.; Okhrimenko, G. I. In *Water-Soluble Polymers*, Moscow: Khimiya, **1979**.

195. Krentsel, L. B.; Kudryavtsev, Y. V.; Rebrov, A. I.; Litmanovich, A. D.; Plate, N. A. *Macromolecules* **2001**, *34*, 5607.

196. Martinovich, V. I.; Elinson, I. S.; Soldatov, V. S. *Izv. Nats. Akad. Nauk Belarusi, Ser. Khim. Nauk* **2001**, *4*, 90.

197. Krul, L. P.; Nareiko, E. I.; Matusevich, Yu. I.; Yakimtsova, L. B. *Polym. Bull.* **2000**, *45*, 159.

198. Raju, M.; Padmanabhara-Raju, M. *Adv. Polym. Tech.* **2001**, *20(2)*, 146.

199. Dassanayake, N. L.; Phillips, R. W. *Anal. Chem.* **1984**, *56*, 1753.

200. Vandyke, J. D.; Kasperski, K. L. *J. Polym. Sci. Pt A: Polym. Chem.* **1993**, *31*, 1807.

201. Shaglayeva, N. S.; Brodskaya, E. I.; Rzhepka, A. V.; Lopyrev, V. A.; Voronkov, M. G. *Polymer science USSR* **1979**, *21*,1944.

202. Kenyeres, J. S.; Ursu, V. *J. Polym. Sci.Polym. Chem. Ed.* **1980**, *18*, 275.

203. Leyte, J. C.; Mandel, M. ***J.*** *Polyrn. Sci. A* **1964**, *2*, 1879.

204. Okay, O.; Gurun, C. *J. Appl. Polym. Sci*. **1992**, *46*, 1807.

205. Nagahash, H.; Okay, O.; Yildirim, H. *J. Appl. Polym. Sci.* **1995**, *56*, 477.

206. Wijnhoven, J. E.; Vos, G. J. *Science* **1998**, *281*, 802.

207. Tanev, P.T.; Chibwe, M.; Pinnavaia, T. J. *Nature* **1994**, *368*, 321.

208. Maquet, V.; Jerome, R. *Mater. Sci. Forum* **1997**, *250*, 15.

209. Peters, M. C.; Mooney, D. J. *Mater. Sci. Forum* **1997**, *250*, 43.

210. Bancel, S.; Hu, W.S. *Biotechnol. Prog.* **1996**, *12*, 398.

211. Camilla, V.; Frantisek, S.; Jean Frechet, M. J. *Chem. mater.* **1996**, *8*, 744.

212. Glass, E. *Adv Chem. Series* (Hydrophilic Polymers**) 1996**, *248*.

213. Fishman, M.; Friedman, R.; Huang, S. *ACS Symp. Ser. (Polymers from Agricultural Coproducts)* **1994**, *575*.

214. Johnson, P.; Lloyd-Jones, G.; In *Drug Delivery Systems. Fundamentals and Techniques*, (Ellis Horwood Serires in Biomedicine), VCH Verlagsgesellschaft: Weinheim, Federal Republic of Germany, **1987**.

215. Kenawy, E.; Sherrington, D. *Eur. Polym. J.* **1992**, *28*, 841.

216. Galia, M.; Svec, F.; Frechet, J. *J. Polym. Sci. Polym. Chem. Ed.* **1994**, *32*, 2169.

217. Sederal, W. I.; DeJong, G.J.; *J. Appl. Polym. Sci.* **1973**, *17*, 2385.

218. Horak, D.; Svec, F.; Ilavsky, M.; Bleha, M.; Baldrian, J.; Kalal, J.; *Angew. Makromol. Chem.* **1992**, *192*, 113.

219. Rosenberg, J. E.; Flodin, P. *Macromolecules* **1987**, *20*, 1518.

220. Lee, H. K. In *Handbook of epoxy resins*, McGraw-Hill Book Company, New York **1967**, p. 4.

221. Pujari, N. S., Trivedi, J.; Ingavle, G.; Ponrathnam, S. *React. Fuct. Polym.* **2006**, *66*, 1087.

222. Ajzenberg, N.; Ricard, A. *J. Appl. Polym. Sci.* **2001**, *80*, 1220.

223. Siegel, R. A.; Firestone, B. A. *Macromolecules* **1988**, *21*, 3254.

224. Park, T. G.; Hoffman, A. S. *J. Appl. Polym. Sci.* **1992**, *46*, 659.

225. Kiatkamjornwong, S.; Phunchareon, P. *J. Appl. Polym. Sci.* **1999**, *72*, 1349.

226. Sivashinsky, G. I. *S.I.A.M. J. Appl. Math.* **1981**, *40(3)*, 432.

227. Ivleva, T. P.; Merzhanov, A. G. *Doklady Physics* **2000**, *45(4),* 136.

228. Ivleva, T. P. *Doklady Physics* **2001**, *46(5),* 299.

229. Ilyashenko, V. M.; Pojman, J. A. *Chaos* **1998**, *8*, 285.

230. Bird, S.; Stewart, W.; Lightfoot, E. N. In *Transport Phenomenon*, John Wiley & Sons Inc.; New York **1960**.

231. Greenberg, J. M. *S.I.A.M. J. Appl. Math.* **1976**, *30(2)*, 199.

232. Koga, S. *Prog. Theor. Phy.* **1982**, *67*, 164.

233. Kuramoto, Y. In *Chemical Oscillations, waves and turbulence*, Springer Verlag, Berlin **1984**.

List of publications/patents

1] **N. S. Pujari**, A. R. Vishwakarma, M. R. Kelkar and S. Ponrathnam, "Gel formation in frontal polymerization of 2-hydroxyethyl methacrylate", *e-Polymers* **2004**, *49,* 1.

2] **N. S. Pujari**, A. R. Vishwakarma, T. S. Pathak, S. Mule and S. Ponrathnam, "Frontal copolymerization of 2-hydroxy ethyl methacrylate and ethylene glycol dimethacrylate without porogen: Comparison with suspension polymerization", *Polym. Int.* **2004**, *53*, 2045.

3] **N. S. Pujari**, A. R. Vishwakarma, T. S. Pathak, A. M. Kotha and S. Ponrathnam, "Functionalized Polymer Networks: Synthesis of microporous polymers by frontal polymerization", *Bull Mat. Sci.* **2004***, 27*, 529.

4] **N. S. Pujari**, A. R. Vishwakarma, C. R. Rajan and S. Ponrathnam, "An improved process for the preparation of the functionalized acrylamide copolymers", *Indian Patent No*. 1097/DEL/2004, **2006.**

5] **N. S. Pujari**, S. R. Inamdar, B. D. Kulkarni and S. Ponrathnam, "Water Triggered Frontal Polymerization", *Macromol. Rapid Commun.* **2007,** *28*, 109.

6] S. R. Inamdar, **N. S. Pujari**, I. A. karimi, B. D. Kulkarni, S. Ponrathnam and R. K. Tayal, "Spinning Wave Motion in Frontal Polymerization", *Chem. Eng. Sci.* **2007,** DOI 10.1016/j.ces.2006.11.037.

7] **N. S. Pujar**i, S. R. Inamdar, J. A. Ambekar, B. D. Kulkarni and S. Ponrathnam, "A complete analysis of frontal copolymerization of mono and divinyl monomers", *Chem. Eur. J.* **2007**, *published online.*

8] **N. S. Pujari,** S. R. Inamdar, B. D. Kulkarni and S. Ponrathnam, "On Scale Up Criterion of Water Triggered Frontal Polymerization", *Communicated.*

9] **N. S. Pujari,** J. M. Gadgil, E. J. Dayakaran and S. Ponrathnam, "About Copolymer Reactivity Ratio in Frontal Copolymerization", *draft ready for communication*

10] **N. S. Pujari,** S. R. Inamdar and S. Ponrathnam, "Frontal Polymerization" *(Review Article), MS under preparation.*

Conference papers

1] **N. S. Pujari**, A. R. Vishwakarma, S. Ponrathnam, "Frontal copolymerization of 2-

hydroxyethyl methacrylate and ethyleneglycol dimethacrylate", International Conference on polymers (Macro2004), 2004, 14-17 December, Thiruvananthpuram, India.

2] **N. S. Pujari**, S. R. Inamdar, R. K. Tayal and S. Ponrathnam, "Frontal Polymerization: Opportunities and Challenges", National Conference on Frontiers in Polymer Science & Technology (Polymer 2006), *Invited,* 2006, 10-12 February, Kolkata, India.

Other

a] Presented posters at various national/international conferences

b] Cover Page article of investigation in frontal polymerization in Bulletin of Material Science, December 2004 issue.

Awards

1] Best poster award for the poster "Instabilities in Frontal Polymerization" on the occasion of National Science Day, National Chemical Laboratory Symposium, February 2005.